



**Universidade Federal do Rio
Grande – FURG**

Instituto de Oceanografia

Programa de Pós-Graduação em
Oceanologia



**Université de Perpignan Via
Domitia - UPVD**

**Collège Doctoral Languedoc-
Roussillon**

École Doctorale Energie et
Environnement

On the role of Agulhas eddies to anthropogenic carbon absorption and acidification state in the South Atlantic Ocean

Iole Beatriz Marques Orselli

Supervisor: *Prof. Dr. Rodrigo Kerr Duarte Pereira*
Universidade Federal do Rio Grande (FURG), Brazil

Supervisor: *Prof. Dr. Catherine Goyet*
Université de Perpignan Via Domitia (UPVD), France

Co-supervisor: *Prof. Dr. José Luiz Lima de Azevedo*
Universidade Federal do Rio Grande (FURG), Brazil

Rio Grande, RS, Brazil

March 2020



**Universidade Federal do Rio
Grande – FURG**

Instituto de Oceanografia

Programa de Pós-Graduação em
Oceanologia



**Université de Perpignan Via
Domitia - UPVD**

**Collège Doctoral Languedoc-
Roussillon**

École Doctorale Energie et
Environment

On the role of Agulhas eddies to anthropogenic carbon absorption and acidification state in the South Atlantic Ocean

Iole Beatriz Marques Orselli

PhD Thesis presented to the graduation
program in Oceanology, as part of the
requirements for obtaining a Doctorate
Degree.

Supervisor: *Prof. Dr. Rodrigo Kerr Duarte Pereira*
Universidade Federal do Rio Grande (FURG), Brazil

Supervisor: *Prof. Dr. Catherine Goyet*
Université de Perpignan Via Domitia (UPVD), France

Co-supervisor: *Prof. Dr. José Luiz Lima de Azevedo*
Universidade Federal do Rio Grande (FURG), Brazil

Rio Grande, RS, Brazil

March 2020

On the role of Agulhas eddies to anthropogenic carbon absorption and acidification state in the South Atlantic Ocean

PhD Thesis presented to the Graduation program in Oceanology, as part of the requirements for obtaining a Doctorate Degree.

by

Iole Beatriz Marques Orselli

Rio Grande, RS, Brazil

March 2020

© A cópia parcial e a citação de trechos desta tese são permitidas sobre a condição de que qualquer pessoa que a consulte reconheça os direitos autorais do autor. Nenhuma informação derivada direta ou indiretamente desta obra deve ser publicada sem o consentimento prévio e por escrito do autor.

ORSELLI, IOLE BEATRIZ MARQUES

On the role of Agulhas eddies to anthropogenic carbon absorption and acidification state in the South Atlantic Ocean / Iole Beatriz Marques Orselli. – Rio Grande: FURG, 2020.

Número de páginas p. 221

Tese (Doutorado) – Universidade Federal do Rio Grande. Doutorado em Oceanografia Física, Química e Geológica.

Keywords: Agulhas eddies; CO₂ fluxes; Carbonate system; Anthropogenic carbon; South Atlantic Ocean.

Palavras-chave: Vórtices das Agulhas, Fluxos de CO₂; Sistema carbonato; Carbono antropogênico; Oceano Atlântico Sul.

Mots-clés : tourbillons des Aiguilles ; flux de CO₂ ; Système du carbone ; Carbone anthropique ; Océan Atlantique Sud.

Title: On the role of Agulhas eddies to anthropogenic carbon absorption and acidification state in the South Atlantic Ocean.

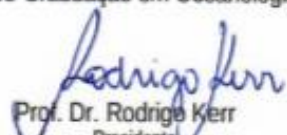


ATA ESPECIAL DE DEFESA DE TESE DE DOUTORADO – 04/2020
1ª TESE em COTUTELA ENTRE FURG E UNIVERSITÉ DE PERPIGNAN VIA
DOMITIA (UPDV-FRANÇA)

Às nove horas do dia dezessete de março do ano de dois mil e vinte, no Auditório SEAD - FURG/Carreiros, reuniu-se a Comissão Examinadora da Tese de **DOUTORADO** intitulada "**ON THE ROLE OF AGULHAS EDDIES TO ANTHROPOGENIC CARBON ABSORPTION AND ACIDIFICATION STATE IN THE SOUTH ATLANTIC OCEAN**", da **Acad. Iole Beatriz Marques Orselli**. A Comissão Examinadora foi composta pelos seguintes membros: Prof. Dr. Rodrigo Kerr - Orientador/Presidente – (IO/FURG), Prof. Dr. José Luiz Lima de Azevedo - (Co-orientador - IO/FURG), Profa. Dra. Catherine Goyet – (Orientadora – UPDV/FRANÇA), Prof. Dr. Franck Touratier – (UPDV/FRANÇA), Profa. Dra. Olga Sato (IO/USP), Prof. Dr. Moacy Araújo – (UFPE), Profa. Dra. Leticia C. Da Cunha (UFRJ), Profa. Dra. Eunice Machado (IO/FURG) e Prof. Dr. Carlos Alberto Eiras Garcia (IO/FURG). Dando início à reunião, o Orientador e Presidente da sessão, Prof. Dr. Rodrigo Kerr, agradeceu a presença de todos e fez a apresentação da Comissão Examinadora, destacando que esta é a 1ª Tese de Doutorado realizado pelo Programa em Cotutela entre a FURG e a Université de Perpignan Via Domitia (UPDV-FRANÇA). Logo após esclareceu que o Candidato teria um tempo de 45 a 60 min para explanação do tema, e cada membro da Comissão Examinadora, um tempo máximo de 30 min para perguntas. A seguir, passou à palavra a Candidata que apresentou o tema e respondeu às perguntas formuladas. Após ampla explanação, a Comissão Examinadora reuniu-se em reservado para discussão do conceito a ser atribuído a Candidata. Foi estabelecido que as sugestões de todos os membros da Comissão Examinadora, que seguem em pareceres em anexo, foram aceitas pelo Orientador/Candidata para incorporação na versão final da Tese. Finalmente, a Comissão Examinadora considerou a candidata **APROVADA**, por unanimidade. Nada mais havendo a tratar, foi lavrada a presente ATA que após lida e aprovada, será assinada pela Comissão Examinadora, pela Candidata e pelo Coordenador do Programa de Pós-Graduação em Oceanologia.



Prof. Dr. José Luiz Lima de Azevedo



Prof. Dr. Rodrigo Kerr
Presidente



Profa. Dra. Catherine Goyet

1/2



Prof. Dr. Franck Touratier



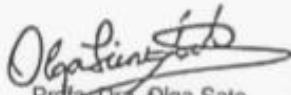
Prof. Dr. Mécyr Araújo



Profa. Dra. Eunice Machado



Prof. Dr. Carlos Alberto E. Garcia



Profa. Dra. Olga Sato



Profa. Dra. Leticia C. da Cunha



Acad. Iole Beatriz M. Orselli

*“Navegar é preciso
pelos oceanos da consciência
e aportar na terra
do amor sem fim”*

Anjo da busca

*“Gente que vem do mar é como é.
Deve ser essa coisa de andar meio nua e não,
essa liberdade de não ter que vestir completamente.
Essa coisa de caminhar, caminhar, caminhar...
Como que sem rumo,
ajeitando o prumo e o vento na vela,
seja para onde for.
Gente que vem do mar é como é.
Vive o que tem.
Preza o que tem.
Come o que tem.
E tem, talvez por isso,
sempre mais.
Acredita no sol e no sal.
Prefere o bem ao mal.
É feliz com cada grão de areia.
Gente que vem do mar se derrama: é oceano.
Gente que vem do mar corre o mar na veia.”*

Eulíricas

To my mom and my dad (*in memoriam*)

Summary / Table of contents

Acknowledgements.....	xii
List of figures	xix
List of tables.....	xxxii
List of acronyms and abbreviations	xxxviii
Abstract.....	xl
Resumo	xli
Résumé	xlii
Preface.....	43
Chapter I. Introduction	45
1.1 Introduction: English version.....	45
1.2 Introdução: versão em português	59
1.3 Introduction: version en français	74

Chapter II. Hypothesis	89
Chapter III. Objectives.....	90
3.1 Main objective:	90
3.2 Specific objectives:	91
Chapter IV. Methods	92
4.1. Oceanographic cruises	92
4.2. First article - PhD 01:.....	96
4.3. Second article - PhD 02:	110
Chapter V. Articles	124
5.1 First article – PhD 01:.....	127
Article – PhD 01: supporting information	141
5.2 Second article – PhD 02:	151

Chapter VI. Synthesis of the discussion and conclusions..... 177

4.1 Synthesis of the discussion and conclusions.....177

4.2 Síntese da discussão e conclusões 183

4.3 Synthèse de la discussion et conclusions 189

Chapter VII. Associated/related production 195

7.1. Scientific collaborations..... 195

7.2. Undergraduate student co-supervision..... 198

7.3. Training course on CO₂ measurements 198

7.4. Conferences..... 199

7.5. Relevant courses 201

7.6. Received grants 202

7.7. Ship-based fieldwork 202

7.8. Relevant laboratory activities 202

Chapter VIII. References 204

Acknowledgements

I would like to start this section by acknowledging my supervisors: you are best team someone could ask for! Rodrigo, Zé and Catherine, you were always there for me to help me seek all the craziness I dreamed about, and to pull me back down to earth when necessary 😊

Rodrigo, primeiro quero agradecer por você ter aceitado ser meu orientador lá nos tempos longínquos do mestrado. Também por ter me persuadido a fazer o doutorado, afinal eu tava precisando só do seu empurrãozinho. Agora, principalmente, obrigada por ser tão compreensivo e paciente comigo. Você é muito especial pra mim.

Zé, obrigada por aceitar entrar nessa loucura de projeto de CO₂ e vórtices e por me motivar sempre que eu fiquei desanimada. Pode ter certeza que ouvir aquele “enfadonho” uma vez, me instiga a querer fazer sempre as melhores apresentações que eu poderia imaginar hehe

À toi, Catherine, pour me montre que tu es une personne avec une vie normal, avec les jours réservés pour faire de la natation, pour les fois dans les queles j'ai vû Frank et toi à discuter normalement les resultats d'un papier. Pour se assoir avec moi devant mon ordi et me faire comprendre que l'oportunité de travailler avec toi a été plus important que quelque moment de tristesse que j'ai vivre pendant le periode de la cotutele. Pour me montre que je ne dois pas avoir peur de parler avec un spécialiste, parce que vous etes personnes normales (ou presque, comme les fois dans les quelles on a travailler ensemble dans l'Antartique et toi a faite des blagues avec Jannine et moi hahaha). Je suis très contente et heureux d'avoir été ta élève. Merci beaucoup!

Mauricio, obrigada por tudo que você sempre fez por mim, por todas as super oportunidades que me proporcionou e também pelas vezes que me fez pensar de formas completamente diferentes, deixando as pessoas ouvirem as engrenagens do meu cérebro funcionando.

Papi, você vai ser sempre a maior e mais dolorida saudade que habita em mim. Todas as lembranças nossas me fazem ser a mulher que sou hoje e sou muito grata por tudo que você e a Mami sempre fizeram por mim. Lembro muito de uma das nossas últimas conversas pessoalmente em que você me disse que era um homem realizado por ter me criado como fez, orgulhoso da menina que você criou e cresceu pra se tornar aquela menina com quem você conversava aquela tarde... Eu me referi a essa nossa conversa como sendo "pessoalmente" porque continuo conversando com você... uma parte sua que vai sempre habitar em mim. E escrevi "aquela menina", porque ela deixou de ser daquela forma quando ela deixou de ter você todos os dias levando o café na cama... Porque ela era um brotinho... ela mudou muito e agora acho que ela só existe em você... porque em mim ela é uma lembrança muito distante. Obrigada por plantar aquele brotinho, adubar e regar diariamente! Ela é a base, minha raiz, meu centro... cresci ao redor dela, me tornando cada vez mais parecida com você. Obrigada por ter sido o melhor pai do mundo!

Mami, começo dizendo que eu te amo, que te admiro, te respeito e te agradeço por ter plantado aquele brotinho que eu fui um dia.... por ter me regado e adubado com meu pai, que foi o melhor pai que você poderia ter escolhido pra mim! Agora quero aproveitar pra pedir desculpas... você, mais do que ninguém, sabe que eu não sou uma pessoa nada fácil de lidar... afinal, se tem alguém com quem eu fiquei parecida acho que com meu pai, né... Você me mostrou como é importante a gente ser bom, carinhoso e demonstrar nosso amor. Isso porque todas as vezes que eu brigava com você, eu sentia um desespero absurdo e um medo de aquela ter sido a última oportunidade de dizer o quanto eu te amo. Você me mostrou que eu tenho que deixar de ser tão igual ao meu pai, não guardar tanto rancor e nem ser tão explosiva, porque eu não queria, de forma nenhuma, que essa fosse nossa última conversa. Então, por mais que eu tivesse maluca de raiva, eu tinha que engolir meu ego, meu mau humor e ir lá te escrever que eu não queria ficar brigada com você... eu to escrevendo isso cheia de lágrimas aqui... porque eu sei que nunca disse isso pessoalmente mas você sabe que eu sou fechada e que sempre foi muito difícil pra mim conversar sobre meus sentimentos. Agora vou parar porque isso é um agradecimento, não uma carta de desabafo (apesar de que pra tese acho que essas coisas se fundem)....

Aos meus amigos que seguraram muito minha onda, mesmo enquanto eu tava na França, mesmo quando o esforço pra manter contato fosse tão cansativo, mas que a gente sabia que não podia deixar de se fazer presentes.

Lela, você não tem ideia de quantas vezes eu quis que você estivesse na França comigo... você é minha irmã loira, a irmã que me acompanha desde os 2 aninhos, desde quando a gente nem tinha lembranças... Obrigada por sempre cuidar de mim, mesmo com toda a distância dos últimos anos.

Todo mundo pensa que o período do sanduíche é maravilhoso e blablabla, mas não é sempre assim... enfim, agradeço as mulheres mais sensacionais que eu poderia ter como companhia nessa jornada:

Nic, você é uma irmã pra mim! Todo tempo que moramos juntas me fez crescer infinitamente, com certeza, desde quando nos conhecemos, num navio, não imaginávamos quantas águas iríamos navegar juntas... quero que vc leia (porque sei que já imagina), pra que tenha certeza de tudo que sua amizade significa pra mim.

Maluzita, musa da calmaria, rainha da tranquilidade e dos xingamentos em Alemão: você é sensacional! Ainda sinto falta dos finais de semana que o telefone (fixo! ahahaha só nós duas, né?!) tocava e a gente combinava uma prainha, seguida de uma feira e um super almoço família... dos dias que eu chegava em casa e você tava em paz tocando seu violão... Obrigada por sempre me acalmar com um olhar, um abraço, ou mesmo em silêncio, sentada no outro sofá. Obrigada por todo carinho que sempre me deu! Saiba que eu sempre penso em você!

Camila, Mariah, Gis e Nina: vocês foram as mulheres super empoderadas que me mais me ajudaram a chegar nessa liberdade que tenho hoje. Não falo de liberdade de coisas mundanas, mas de liberdade de pensamento mesmo... de me sentir em paz com o que eu sinto em relação à minha feminilidade, aos meus sentimentos, enfim, à minha vida. Vocês são minhas bruxinhas, meus 4 coraçõezinhos verdes...

Gis e Mariah, morar com vocês têm sido o melhor presente de retorno ao Brasil. Vocês são minhas companheiras de dia-a-dia, minhas irmãs escolhidas e as melhores tias dos cachorros! Amo vocês!

Ellinha, minha flor: você é a mulher mais forte que cruzou meu caminho desde que saí da minha tão amada São Paulo, do colo da minha mãe... com isso você sabe que se tornou minha mãe em Rio Grande. A mãe pra quem eu pedia colo quando a gente tava no mar, em Punta Arenas, ou mesmo em Rio Grande mesmo.... todas as vezes que você

segurou minha onda, me mostrou que tinha muito o que eu ver além das minhas tempestades e também me mostrou como a gente tem que fazer pra superar todas as adversidades que a vida insiste em colocar no nosso caminho.

Wiltinho, você é a pessoa mais igual a mim que eu conheço (não sei se isso é bom pra nós, porque vai ser difícil assim lá longe, né?! ahaha), mas com certeza você é especial. Obrigada por sempre concordar em não discordar, afinal, se a gente teimasse um com o outro, como ia fazer?!?! ahaha

Pedrito, seu nariz mole! É pra eu agradecer, né... então vou começar agradecendo pelas aulas de geopolítica! Hahahah agora, obrigada também por todas as conversas, poemas e brincadeiras!

Martim, você com certeza merece um spacinho especial aqui. Fico muito feliz por ter vc sempre próximo e saber que você sempre estaria a um skype de distância, em qualquer momento que eu precisasse (nem que fosse pra ver se a luz tá boa pra entrevista hehe). Fico feliz em ter acompanhado sua carreira, em ver aquele menino que eu entrevistei um dia pra entrar na Jr, no primeiro ano de graduação, tenha se tornado oceanógrafo, mestre e aspirante a doutor. Fico feliz em termos dividido tantos momentos importantes, em ter estado com você na sua primeira Antártica, em saber que eu sempre tinha você lá naquele ano caótico. Como você já disse uma vez, obrigada por todos os skypes doidos, com chá, cerveja ou Jack! hehe Enfim, obrigada por ser tão próximo, mesmo com toda a distância que teve entre a gente.

Aos LEOCers todos!

Aos meus companheiros de sala, desde a época da "Sala simpatia", da "Sala do Fujita" e da "Sala 18", que me aguentaram por todos esses anos, durante os surtos pré-seminários e, principalmente, pré-qualificação.

Lolozinha, minha rainha, primeiro quero te agradecer por me eleger a princesa no seu reinado! Pode ter certeza que ser sua princesinha me mostrou quanto carinho eu tinha nessa família que a gente desenvolveu aí no lab. Também quero agradecer por me mostrar que eu já estive completamente errada, por me ensinar que posso desenvolver um carinho enorme por alguém tão diferente de mim, em todos os sentidos possíveis. Por me mostrar

que eu também posso me impor sempre que sentir meus limites sendo ultrapassados e que nunca eu devo me submeter a algo que discordo.

Fuji, obrigada por ser meu malvado favorito! Obrigada por todas as conversas em terra e no mar, pelos infinitos ensinamentos e também pelas discussões. É sempre um prazer ter você por perto, mesmo quando você quer me explodir! Ah, não podia esquecer de agradecer pelas laranjas descascadas e pelos cheesecakes!

Rubio, obrigada pelas conversas e pela companhia nos cafezinhos, tanto em terra quanto no mar!

Marília, obrigada pelas conversas, pela calma que você transparece e pelo agrião!

Elianinha, obrigada pelas conversas, pelos cafés, pelas jantinhas e pela companhia também na academia! Agradece aos seus pais pelas cachaças de butiá!

Chris, obrigada pelo carinho, pela companhia, pelas conversas, pelos passeios e até pelo brigadeiro com óleo de coco e aveia que eu nunca vou esquecer! hahahaha

Cirino, obrigada por ser tão carinhoso, com esse seu jeitinho de filhote, e por cuidar de mim e me dar colo sempre que precisei.

Cíntia, você foi a última aquisição pra nossa família, mas já chegou sendo fundamental no pacote! Obrigada aceitar experimentar novos passeios comigo (paga a língua! Hahaha), por todas as noites de comilança e por todas as conversas, Tintiazinha!

Nine, obrigada por me apoiar no desenvolvimento da tese e, principalmente, por toda ajuda que me deu quando tava indo e quando já tava morando na França. Você foi fundamental pra eu ter conseguido me instalar e me ajeitar por lá. Obrigada pelos passeios, voltinhas, cafés e pelo pique-nique de aniversário na praia!

Juju, seu apoio foi muito importante pra mim! Cada vez que eu lia alguma das suas mensagens me dando força, ou mesmo quando o Gus me disse um dia que te ouviu falando de mim no sushi... Obrigada, lindinha!! Te desejo todo sucesso desses mares! Vai fundo que o oceano é o limite! E, se vc precisar pegar um fôlego pra continuar nadando, pode ter certeza que eu vou estar lá pra te apoiar. Ser sua co-orientadora foi um prazer! ;)

Maurinho, obrigada por ser meu companheiro de doutorado, de sala, de qualificação e de sofrimentos infundados que o doutorado emana!

Brendonzinho, obrigada pelo carinho e pela parceria!

Chicooooo! Obrigada por segurar minha onda nas épocas de cassino que foram mais tensas, por estar sempre presente por mensagens e por seguir sendo parceiro em SP! Obrigada também por ter aceitado colaborar comigo nos artigos! Você foi fundamental pro andamento da minha pesquisa.

Andrea, nossa eterna miss LEOC! Obrigada por todo carinho que você sempre me deu, desde que chegou no Cassino e se juntou à minha família rio-grandina. Também quero agradecer por ser sempre perfeitinha, mostrando que é possível! Parabéns por ser essa menina-mulher inteligente, carinhosa, amável e perfeita!

Josué, Josuel, Zé, Zezito.... tantos nomes pra chamar esse super amigo que o Cassino me deu, nunca seriam suficientes pra representar o quanto você é importante pra mim! É, com certeza, um exemplo a seguir! Obrigada por ter sido 'meu irmão mais velho' quando moramos juntos, e meu mestre Yogui, sempre! Além de muitas lembranças de segundas gastronômicas, sábados de yoga, almocinho, dias de praia, você sempre esteve presente em momentos difíceis, pra me acalmar, enxugar lágrimas, me fazer respirar e seguir em frente. Sinto muita falta dos nossos almoços juntos em casa, regados à chimarrão e música gaúcha! Saiba que eu continuo escutando Pirisca aos domingos... hahaha

Carol, minha neguinha. Obrigada por ter sido minha irmãzinha mais nova, por todas as conversas e por todo carinho!

Belzinha, você sempre foi uma inspiração pra mim, desde pequena!

Lúcia, minha super psicóloga, eu tenho certeza que só to terminando o doutorado, tendo a oportunidade de escrever esses agradecimentos aqui, porque eu tive você por perto. Queria eu ter tido a lucidez de procurar acompanhamento antes, em um estado mais "normal" (se é que ele existe...)

À vous, mes amis français: Moulham, Jordana, Lefteris et Justin. Même avec toute la formalité de la langue française, je peu dire que j'ai des amis! Et je peu le faire parce

que je sais que vous avez été présent toujours dans toutes les fois dans les quelles qui j'ai eu besoin.

Leandra, obrigada por gerenciar nossas viagens, passagens, prestações de contas e nossas bagunças também.

Frank, Virgínia and Eunice, thank you for accepting evaluate the thesis development, by composing my thesis committees in the graduate programs of Brazil and France.

Thank the jury. Especially to Garcia, whose efforts were essential for the development of the Trans-Atlantic and FORSA cruises.

This thesis contributed to the project “*Estudos Avançados de Médias e Altas Latitudes*” (CAPES grant n° 23038.001421/2014–30). I acknowledge CAPES/CMAR2 for the Ph.D. funding (CAPES process n°. 23038.001421/2014–30 and BEX 0077/17–8).

I also thank the INCT-Criosfera, for the support to participate in different courses, conferences and fieldworks.

I would like to thank the staff of the ED 305, IMAGES_ESPACE-DEV for all support.

Agradeço também ao PPGO pelo financiamento para participar de cursos e congressos e seus funcionários (Clabisnei, Elisa, Grasi, Eunice e Rodrigo), sempre gentis e prestativos.

I thank everyone who somehow collaborated with the data collection and the accomplishment of this work.

List of figures

Chapter I. Introduction

1.1 Introduction: English version

Figure 1.1. Left panel: concentrations of carbon dioxide (CO₂, red line; ppm), methane (CH₄, green line; ppb) and nitrous oxide (N₂O, black line; ppb) in the atmosphere over the last 2000 years (IPCC 2007). Right panel: annual global emissions of CO₂ since the Industrial Revolution according to the source (Global Carbon Project).. 46

Figure 1.2. Full record of the carbon dioxide (CO₂) concentration in the atmosphere at the Mauna Loa Observatory (the Keeling curve). The green continuous line indicates the 400 ppm baseline. From: <https://scripps.ucsd.edu/programs/keelingcurve/>..... 47

Figure 1.3. Schematic figure of the air-sea exchange of CO₂. The uptake by the oceans is split in the biological and physical pumps. The figure was created based on Denman et al. (2007)..... 48

Figure 1.4. Schematic flows of water masses in the Southern Ocean in a meridional section: High Saline Shelf Water (HSSW), Antarctic Surface Water (AASW), upwelling of Circumpolar Deep Water (CDW), formation (by deep convection) of Antarctic Bottom Water (AABW), and formation (by subduction) of South Atlantic Mode Water (SAMW) and Antarctic Intermediate Water (AAIW). The last two water masses ventilate the central and intermediate layer of the oceans, as indicated. The colours indicate the C_{ant} content in the water column. From: Pardo et al. (2014)..... 49

Figure 1.5. C_{ant} content in sections of the Atlantic, Indian and Pacific oceans. From: Gruber et al. (2019). 51

Figure 1.6. Schematic circulation of the main ocean currents at the surface South Atlantic Ocean. Red arrows indicate warm water currents and blue arrows indicate cold water currents. Please O'Brien et al (2017) for further details about the ocean circulation in the area..... 53

- Figure 1.7. Agulhas eddies schematic representation. a) Sea surface temperature map, indicating ocean currents and Agulhas eddies at their formation region. From: <http://act.rsmas.miami.edu/science/>. b) An anticyclonic lens eddy, representing an Agulhas eddy structure as soon as it is released at the Agulhas leakage region. c) An anticyclonic non-lens eddy, representing an Agulhas eddy structure along its trajectory through the South Atlantic Ocean. For both panels b and c, each letter represents: h, depth of the eddy; η sea level anomaly caused by the eddy presence; ξ , downward displacement of the thermocline; H height of the fluid carried by the eddy movement. b and c from: Azevedo & Mata (2010). 54
- Figure 1.8. Representation of the Agulhas leakage being affected by the southward displacement of the Subtropical Front caused by the westerlies southward expansion over a 30 years period. From: Beal et al. (2011). 56

1.2 Introdução: versão em Português

- Figura 1.1. Painel esquerdo: concentrações de dióxido de carbono (CO_2 , linha vermelha; ppm), metano (CH_4 , linha verde; ppb) e óxido nitroso (N_2O , linha preta; ppb) na atmosfera nos últimos 2000 anos (IPCC 2007). Painel direito: emissões globais anuais de CO_2 desde a Revolução Industrial, de acordo com a fonte (Global Carbon Project). 60
- Figura 1.2. Registro completo das concentrações de dióxido de carbono (CO_2) na atmosfera no observatório de Mauna Loa (curva de Keeling). A linha verde continua indica o patamar de 400ppm. De: <https://scripps.ucsd.edu/programs/keelingcurve/> 61
- Figura 1.3. Figura esquemática da transferência de CO_2 na interface ar-mar. A captação pelos oceanos é dividida nas bombas biológica e físicas. A figura foi criada com base em Denman et al. (2007). 62
- Figura 1.4. Fluxo esquemático das massas de água no Oceano Austral em uma seção meridional: High Saline Shelf Water (HSSW), Antarctic Surface Water (AASW), ressurgência da Circumpolar Deep Water (CDW), formação (por convecção profunda) de Antarctic Bottom Water (AABW), e formação (por subducção) da South Atlantic Mode Water (SAMW) e da Antarctic Intermediate Water (AAIW). As duas últimas massas de

água ventilam as camadas central e intermediária dos oceanos, conforme indicado. As cores indicam o conteúdo de C_{ant} na coluna de água. De: Pardo et al. (2014).	63
Figura 1.5. Conteúdo de C_{ant} em seções dos oceanos Atlântico, Índico e Pacífico. De: Gruber et al. (2019).	65
Figura 1.6. Circulação esquemática das principais correntes oceânicas na superfície do Oceano Atlântico Sul. As setas vermelhas indicam correntes de água quente e as setas azuis indicam correntes de água fria. Dirija-se a O'Brien et al. (2017) para mais detalhes sobre a circulação oceânica na região.....	67
Figura 1.7. Representação esquemática dos vórtices das Agulhas. a) Mapa da temperatura da superfície do mar, indicando correntes oceânicas e vórtices das Agulhas em sua região de formação. De: http://act.rsmas.miami.edu/science/ . b) Um vórtice anticiclônico do tipo lente, representando um vórtice das Agulhas assim que é liberado na região de vazamento das Agulhas. c) Um vórtice anticiclônicos do tipo não-lente, representando uma estrutura de vórtice das Agulhas ao longo de sua trajetória pelo Oceano Atlântico Sul. Para os painéis b e c, cada letra representa: h, profundidade do vórtice; η anomalia de nível do mar causada pela presença do vórtice; ξ , deslocamento pra baixo da termoclina; H altura do fluido carregado pelo movimento do vórtice. b e c de: Azevedo & Mata (2010).	68
Figura 1.8. A representação do vazamento das Agulhas sendo afetado pelo deslocamento para o sul da Frente Subtropical, causado pela expansão em direção ao sul dos ventos de oeste em um período de 30 anos. De: Beal et al. (2011).	70

1.3 Introduction: version en français

Figure 1.1. Panneau gauche: concentrations de dioxyde de carbone (CO_2 , ligne rouge; ppm), méthane (CH_4 , ligne verte; ppb) et de l'oxyde nitreux (N_2O , ligne noire; ppb) dans l'atmosphère au cours des 2000 dernières années (IPCC 2007). Panneau droite: émissions mondiales annuelles de CO_2 depuis la révolution industrielle selon la source (Global Carbon Project)..... 75

Figure 1.2. Enregistrement complet de la concentration de dioxyde de carbone (CO_2) dans l'atmosphère à l'Observatoire du Mauna Loa (courbe de Keeling). La ligne continue verte indique la ligne de base de 400 ppm. De : <https://scripps.ucsd.edu/programs/keelingcurve/> 76

Figure 1.3 Figure schématique de l'échange air-mer de CO_2 . L'absorption par les océans est divisée en pompes biologiques et physiques. La figure a été créée sur la base de Denman et al. (2007). 77

Figure 1.4. Flux schématiques des masses d'eau dans l'océan Austral dans une section méridionale : High Saline Shelf Water (HSSW), Antarctic Surface Water (AASW), remontée de Circumpolar Deep Water (CDW), formation (par convection profonde) de Antarctic Bottom Water (AABW), et formation (par subduction) de South Atlantic Mode Water (SAMW) et Antarctic Intermediate Water (AAIW). Les deux dernières masses d'eau ventilent la couche centrale et intermédiaire des océans, comme indiqué. Les couleurs indiquent le contenu C_{ant} dans la colonne d'eau. De : Pardo et al. (2014). 78

Figure 1.5. C_{ant} contenu dans des sections des océans Atlantique, Indien et Pacifique. De : Gruber et al. (2019). 80

Figure 1.6. Circulation schématique des principaux courants océaniques à la surface de l'océan Atlantique Sud. Les flèches rouges indiquent les courants d'eau chaude et les flèches bleues indiquent les courants d'eau froide. Veuillez consulter O'Brien et al (2017) pour plus de détails sur la circulation océanique dans la région. 82

Figure 1.7. Représentation schématique des tourbillons des Aiguilles. a) Carte des températures de la surface de la mer, indiquant les courants océaniques et les tourbillons d'Aiguilles dans leur région de formation. De: <http://act.rsmas.miami.edu/science/>. b) Un

tourbillons anticycloniques de type « lens », représentant une structure de tourbillon des Aiguilles dès qu'il est libéré dans la région de prolongement des Aiguilles. c) Un tourbillons anticycloniques de type « non-lens », représentant une structure de tourbillon des Aiguilles le long de sa trajectoire à travers l'océan Atlantique Sud. Pour les panneaux b et c, chaque lettre représente : h, profondeur du tourbillon; η anomalie du niveau de la mer causée par la présence du tourbillon; ξ , déplacement vers le bas de la thermocline; H hauteur du fluide porté par le mouvement des tourbillons. b et c de : Azevedo & Mata (2010). 83

Figure 1.8. Représentation du prolongement du courant des Aiguilles affectée par le déplacement vers le sud du front subtropical causé par l'expansion vers le sud des vents d'ouest sur une période de 30 ans. De : Beal et al. (2011)..... 86

Chapter IV. Methods

4.1. Oceanographic cruises

Figure 4. 1. Map of the sampled region in the South Atlantic Ocean. The yellow crosses correspond to the XBT profiles performed during the FORSA cruise (FORSA_XBT). The CTD stations are indicated by yellow dots (FORSA_2015), green dots (TAII_2011_02), purple dots (TAII_2011_01), blue diamonds (A10_2011), and red squares (A10_2003). The bottom bathymetry is represented by colour shadings. 93

4.2. First article - PhD 01

Figure 4. 2. Scheme presenting the GO-8050 CO₂ analyser. The upper panels present the ‘wet box’ and the ‘dry box’ of the system. The red rectangles highlight the main parts of the system: the seawater inlet region, the main equilibrator and the infrared gas analyser (LI-7000). 97

Figure 4. 3. The main equilibrator. a) An image of the shower equilibrator supplied by General Oceanic®. b) A scheme of a shower-type equilibrator, indicating the seawater inlet (“água do mar”), the connections from (“A”) and to (“B”) the infrared system, the pressure and thermometer sockets and seawater escape. 98

Figure 4. 4. a) Scheme of the LI-7000 operational system, considered the application of the closed system set up for the reference, including the scrubber tube on the reference path. b) The scrubber tube contain chemicals that absorb the CO₂ (Ascarite II) and H₂O (Magnesium Perchlorate). 98

Figure 4. 5. Snapshot of the Video S1. Animation map of the South Atlantic Ocean composed from the sea level anomaly (SLA – m) data. The black continuous line corresponds to the SLA contours of 0.01, 0.02, 0.05, 0.1, 0.15, 0.2 and 0.25 m. The V_n (n = 1 to 6) correspond to each eddy sampled in the FORSA cruise trajectory. Supplementary data to this article and this video can be found online at <https://doi.org/10.1016/j.pocean.2018.10.006> 105

Figure 4. 6. Snapshot of the Video S1 at the moment when V5 and V6 interact with each other. Animation map of the South Atlantic Ocean composed from the sea level anomaly (SLA – m) data. The black continuous line corresponds to the SLA contours of 0.01, 0.02, 0.05, 0.1, 0.15, 0.2 and 0.25 m. The Vn (n = 1 to 6) correspond to each eddy sampled in the FORSA cruise trajectory. Supplementary data to this article and this video can be found online at [https:// doi.org/10.1016/j.pocean.2018.10.006](https://doi.org/10.1016/j.pocean.2018.10.006)..... 105

Figure 4. 7. Snapshots of the Video S1 at the moment when V4 and V5 interact with each other. Animation map of the South Atlantic Ocean composed from the sea level anomaly (SLA – m) data. The black continuous line corresponds to the SLA contours of 0.01, 0.02, 0.05, 0.1, 0.15, 0.2 and 0.25 m. The Vn (n = 1 to 6) correspond to each eddy sampled in the FORSA cruise trajectory. Supplementary data to this article and this video can be found online at [https:// doi.org/10.1016/j.pocean.2018.10.006](https://doi.org/10.1016/j.pocean.2018.10.006)..... 106

Figure 4. 8. Snapshot of the Video S1 at the moment when V2 and V3 interact with each other. Animation map of the South Atlantic Ocean composed from the sea level anomaly (SLA – m) data. The black continuous line corresponds to the SLA contours of 0.01, 0.02, 0.05, 0.1, 0.15, 0.2 and 0.25 m. The Vn (n = 1 to 6) correspond to each eddy sampled in the FORSA cruise trajectory. Supplementary data to this article and this video can be found online at [https:// doi.org/10.1016/j.pocean.2018.10.006](https://doi.org/10.1016/j.pocean.2018.10.006)..... 107

4.3. Second article - PhD 02

Figure 4. 9. Plot of the CTD station position (green circle) in the sea level anomaly field of the day in which the station was performed. The numbers indicate the eddies' IDs in the database..... 111

Figure 4. 10. Plot of the CTD station position (green circle) in the sea level anomaly field of the day in which the station was performed. This is an example of one time that an anticyclonic eddy (positive sea level anomaly) was observed matching the station position. The numbers indicate the eddies' IDs in the database. 111

Figure 4. 11. Plot the back and forward trajectories of the eddies that match the CTD stations positions. The red (blue) dots and lines correspond to anticyclonic (cyclonic)

eddies. This was used to determine whether it could be considered an Agulhas eddy or not. The numbers indicate the eddies' IDs in the database. 112

Figure 4. 12. Map indicating the approximate CTD-sampling position of the 13 Agulhas eddies used in this study: V1, V3, and V5 (FORSA_2015); VT62 (TAII_2011_01); VT85, VT87, and VT93 (TAII_2011_02); VA42, VA63, and VA91 (A10_2011); and VA04, VA55, and VA71 (A10_2003). 113

Chapter V. Articles

5.1 First article – PhD 01

Figure 1. Map of the study region in the South Atlantic Ocean. The black continuous line corresponds to the FORSA cruise section. The schematic flows of the main ocean currents of the subtropical anticyclonic gyre are indicated as: Benguela Current System (BCS, yellow dotted line), southern branch of the South Equatorial Current (sSEC, green dot-dashed line), Brazil Current (BC, magenta dashed line) and South Atlantic Current (SAC, blue dot-dot-dashed line). The Agulhas Current (AC, red continuous line), Agulhas eddies (red continuous circles) and Agulhas Current retroflexion zone (black dotted ellipse) are also indicated in this representative map. Please see Peterson and Stramma (1991) for further details about the ocean circulation in the area. The bottom bathymetry is represented by color shadings..... 129

Figure 2. a) Map of the South Atlantic Ocean composed by a snapshot of the sea level anomaly (SLA – m) data of 4th July, 2015. The black continuous line corresponds to the FORSA trajectory. The colored-dashed lines correspond to each eddy trajectory. The colored circles indicate the position of each eddy when sampled during the FORSA cruise. The colors used to represent each eddy are indicated in the plot. b) The XBT temperature section for the cruise transect. The vertical black-dashed lines indicate the center of the eddies. The white continuous lines show the isotherms splitting each indicated water mass, as following: TW – Tropical Water, SACW – South Atlantic Central Water, AAIW – Antarctic Intermediate Water, NADW – North Atlantic Deep Water. In both subplots V_n ($n = 1$ to 6) indicate the number of each sampled eddy.....131

Figure 3. Longitudinal distribution of: a) $p\text{CO}_2^{\text{atm}}$ (red, μatm), $p\text{CO}_2^{\text{sw}}$ (blue, μatm) and temperature-normalized $p\text{CO}_2^{\text{sw}}$ ($Np\text{CO}_2^{\text{sw}}$, green, μatm). The $Np\text{CO}_2^{\text{sw}}$ calculation considered a mean temperature of 20.39°C . b) Chl-*a* (mg m^{-3}). The black-dashed lines indicate the center of the eddies while the grey-dashed lines indicate their eastern and western limits.....132

Figure 4. Left column: Longitudinal distribution of $\Delta p\text{CO}_2$ (μatm) with sea-air CO_2 net flux ($\text{FCO}_2^{\text{T09}}$, $\text{mmol m}^{-2} \text{d}^{-1}$) calculated using the K_T determined by Takahashi et al. (2009) in colors. Right column: temperature ($^\circ\text{C}$) vs $p\text{CO}_2^{\text{sw}}$ (μatm) diagrams, with salinity in colors. Inside each right panel are inserted the linear correlation coefficients (r) between temperature and salinity vs $p\text{CO}_2^{\text{sw}}$ and the number of data used (n). Significance at 95% confidence level ($p < 0.05$). Panels a and d) encompass all cruise data. Panels b and e) show the eastern basin data. Panels c and f) show the western basin data. Note that the color scales used for both $\text{FCO}_2^{\text{T09}}$ and salinity are in the same range for all panels.133

Figure 5. Measured vs modelled results, where: a) $p\text{CO}_2^{\text{sw}}$ (μatm), b) $f\text{CO}_2^{\text{sw}}$ (μatm), c) $Np\text{CO}_2^{\text{sw}}$ (μatm) and d) $Nf\text{CO}_2^{\text{sw}}$ (μatm). Note that the black dots consider all cruise data and red dots represent only the data inside the eddies. In each diagram are presented the coefficients of determination, the standard error (μatm) and the number of data (N)....134

Article – PhD 01: supporting information

Figure S1. a) Map of the monthly mean wind speed (m s^{-1}) data of July 2015 (at 10 m height) for the South Atlantic Ocean. The black line corresponds to the FORSA section. b) The longitudinal distribution of monthly mean wind speed (m s^{-1}) data of July 2015 (at 10 m height) in the FORSA section. These data were extracted from the ERA-Interim atmospheric reanalysis product of the European Centre for Medium Range Weather Forecast (<http://apps.ecmwf.int/datasets/data/interim-full-moda/levtype=sfc/>).....144

Figure S2. a) Map of the study region in the South Atlantic Ocean. The red continuous line corresponds to the FORSA cruise section. The blue dots indicate the position of the CTD profiles executed during the cruise. The bottom bathymetry is represented by color shadings. b) θ/S pressure diagram. c) θ/S -DO diagram. Isopycnals are indicated by grey lines. Potential temperature (θ) is in $^\circ\text{C}$, pressure is in db and OD is in $\mu\text{mol kg}^{-1}$144

Figure S3. a) Map of the region near the Brazilian coast (western than 39.25°W , shallower than 3000m), at the westernmost part of the occidental basin of the South Atlantic Ocean. The blue continuous line corresponds to the FORSA cruise data considered in this brief zoom of the region (subplot b and Table S2). The bottom bathymetry is represented by color shadings. b) Temperature ($^{\circ}\text{C}$) vs $p\text{CO}_2^{\text{sw}}$ (μatm) diagram, with salinity in colors, considering just the region included in the subplot a). Inside this diagram are inserted the linear correlation coefficients (r) between temperature and salinity vs $p\text{CO}_2^{\text{sw}}$ and the number of data used (n). Significance at 95% confidence level ($p < 0.05$). c) Map of the spatial distribution of $\Delta p\text{CO}_2$ (μatm) at the westernmost part of the occidental basin. d) Map of the sea-air CO_2 net flux ($\text{FCO}_2^{\text{T09}}$, $\text{mmol m}^{-2} \text{d}^{-1}$) calculated using the K_{T} determined by Takahashi et al. (2009) at the westernmost part of the occidental basin. c and d) Encompasses more data than considered for the subplots a and b and Table S2, to highlight the difference between the region near the Brazilian coast and the deeper regions. The bottom bathymetry is also represented in c and d subplots, by grey color shadings.145

Figure S4. a to f) Longitudinal distribution of $\Delta p\text{CO}_2$ (μatm) with sea-air CO_2 net flux ($\text{FCO}_2^{\text{T09}}$, $\text{mmol m}^{-2} \text{d}^{-1}$) calculated using the K_{T} determined by Takahashi et al. (2009) in colors. g to l) Longitudinal distribution of temperature ($^{\circ}\text{C}$) with $p\text{CO}_2^{\text{sw}}$ (μatm) in colors. Inside each diagram are inserted the linear correlation coefficients (r) between temperature and salinity vs $p\text{CO}_2^{\text{sw}}$ and the number of data used (n), for each eddy. Significance at 95% confidence level ($p < 0.05$). The number of the eddy is indicated in the top-north-western side of each subplot. Note that the color scales used for both $\text{FCO}_2^{\text{T09}}$ and $p\text{CO}_2^{\text{sw}}$ are in the same range for all subplots.....146

Figure S5. Longitudinal distribution of temperature ($^{\circ}\text{C}$) with depth (m) in colors. The black-dashed lines indicate the center of the eddies.....147

Figure S6. Measured vs modelled results including the longitude ($^{\circ}\text{E}$) in colors. a) $p\text{CO}_2^{\text{sw}}$ (μatm). b) $f\text{CO}_2^{\text{sw}}$ (μatm). c) $Np\text{CO}_2^{\text{sw}}$ (μatm). d) $Nf\text{CO}_2^{\text{sw}}$ (μatm).....147

Figure S7. Maps of each study considered to compare results of CO_2 -related parameters ($p\text{CO}_2^{\text{sw}}$, $f\text{CO}_2^{\text{sw}}$, $\Delta p\text{CO}_2$, $\Delta f\text{CO}_2$, FCO_2) to the FORSA results, used in Table 5, main text. a) Map of AMT cruises transects studied by Lefèvre and Moore (2000), obtained from SOCAT v5 database (Bakker et al., 2016). b) Map of all FICARAM cruises sections

studied by Padin et al. (2010), obtained from SOCAT v5 database (Bakker et al., 2016). c) Map representing the data used from the Sutherland et al. (2015) report of the R/V Nathaniel B. Palmer cruise 15/8, conducted in 2015, available at www.ldeo.columbia.edu/res/pi/CO2/carbondioxide/Palmer_data/1508SFC.PRT. d) Map representing the data used from the Wanninkhof and Castle (2013) report of the A10 CLIVAR/ WOCE cruise, conducted in 2011, available at cdiac.ornl.gov/ftp/oceans/CLIVAR/A10_2011/. e) Map representing the data used from the Uchida et al. (2005) report of the A10 CLIVAR/ WOCE cruise, conducted in 2003, available at www.nodc.noaa.gov/ocads/oceans/RepeatSections/clivar_a10.html. f) Map representing the cruise conducted in 2011 studied by Lencina-Avila et al. (2016). g) Map representing the data used from the Takahashi et al. (2009) database, available at www.ldeo.columbia.edu/res/pi/CO2/carbondioxide/air_sea_flux/month_flux_2006c.txt. h) Map representing the data used from the Bakker et al. (2016) report of the SOCAT v5 database, available at www.socat.info/index.php/data-access/. The bottom bathymetry is represented by color shadings, as indicated in the color bars.....148

5.2 Second article – PhD 02

Figure 1. Map of the sampled region in the South Atlantic Ocean. The yellow crosses correspond to the XBT profiles performed during the FORSA cruise (FORSA_XBT). The CTD stations are indicated by yellow dots (FORSA_2015), green dots (TAII_2011_02), purple dots (TAII_2011_01), blue diamonds (A10_2011), and red squares (A10_2003). The gray circles indicate the approximate positions at which the eddies were sampled: V1, V3, and V5 (FORSA_2015); VT62 (TAII_2011_01); VT85, VT87, and VT93 (TAII_2011_02); VA42, VA63, and VA91 (A10_2011); and VA04, VA55, and VA71 (A10_2003). The black lines represent the main currents of the surface circulation, which are the Benguela Current System (BCS, dotted line), southern branch of the South Equatorial Current (sSEC, dot-dashed line), Brazil Current (BC, dashed line) and South Atlantic Current (SAC, dot-dot dashed line). The Agulhas Current (AC, continuous line) and Agulhas Current retroflection zone (black dotted ellipse) are also indicated. The bottom bathymetry is represented by color shadings.....155

Figure 2. Map of the cruise sections and sampled eddies (a). For a complete description of this map, please see Figure 1. Left panels show the salinity profiles (b to e), while right panels show potential temperature ($^{\circ}\text{C}$; f to j) profiles. The hydrographic sections are TAII_02 – 2011 (b and g), TAII_01 – 2011(c and h), A10_2011 (d and i) and A10_2003 (e and j). The continuous gray lines or gray dots indicate the position of the CTD stations (at each 1 m for TAII and FORSA cruises). Temperature from XBT of the FORSA – 2015 cruise section and CTD stations indicated by continuous gray lines (f). The sampled eddies are indicated in the hydrographic sections of all cruises by vertical white lines. The water masses positions in the water column are indicated by their achronims in the panels f to j. For details please see the θ/S diagrams (Figure 3) and the water masses properties (Table 3).....160

Figure 3. Map of the cruise sections (a). For a complete description of this map, please see Figure 1. θ/S -longitude diagrams for each section (b to f). θ/S -longitude of the FORSA – 2015 cruise section (b), TAII_02 – 2011 section (c), A10_2011 section (d), TAII_01 – 2011 section (e), and A10_2003 section (f). The continuous gray lines represent the isopycnals. The water masses are indicated by their achronims. For details please see the water masses properties (Table 3).....161

Figure 4. C_T model results considering the A10 section of (a to c) 2003 and (d to f) and 2011. Measured vs. modeled C_T (a and d), including the RMSE of the model equation, measured vs. modeled r^2 , and number of measurements (N). Measured (blue dots) and modeled (red dots) vertical profiles (b and e). Vertical profile of the difference between measured and modeled C_T (c and f). The C_T and C_T -differences units are $\mu\text{mol kg}^{-1}$163

Figure 5. A_T model results considering the A10 section of (a to c) 2003 and (d to f) and 2011. Measured vs. modeled A_T (a and d), including the RMSE of the model equation, measured vs. modeled r^2 , and number of measurements (N). Measured (blue dots) and modeled (red dots) vertical profiles (b and e). Vertical profile of the difference between measured and modeled A_T (c and f). The A_T and A_T -differences units are $\mu\text{mol kg}^{-1}$164

Figure 6. a) Map of the cruise sections and sampled eddies. For a complete description of this map, please see Figure 1. From b to e) anthropogenic carbon ($C_{\text{ant-TrOCA}}$ $\mu\text{mol kg}^{-1}$) content along the cruise sections: b) TAII_02 - 2011 section, c) TAII_01 – 2011 section, d) A10_2011 section, e) A10_2003 section. The continuous gray lines or gray dots

indicate the position of CTD stations. The sampled eddies are indicated by a continuous white line. From f to j) anthropogenic carbon ($C_{\text{ant-TrOCA}}$ mol m kg⁻¹) inventory along the water column. f) FORSA – 2015 section, g) TAII_02 - 2011 section, h) TAII_01 - 2011 section, i) A10_2011 section, j) A10_2003 section. The column inventory were determined by integrating the C_{ant} from 200 m to 500 m for the FORSA cruise and from 200 m to 1500 m for the other cruises. The sampled eddies are indicated by a continuous black line.....165

Figure 7. Vertical profiles of $\Delta C_{\text{ant-TrOCA}}$ (left panels) and ΔC_T (right panels), a and b) FORSA cruise and c and d) TAII cruise, where c and d include an inset panel denoting the entire water column depth below the surface mixed layer (200m).....166

Figure 8. a) Map of the cruise sections and sampled eddies. For a complete description of this map, please see Figure 1. From b to n) section of the anthropogenic carbon ($C_{\text{ant-TrOCA}}$ $\mu\text{mol kg}^{-1}$) content in the studied eddies. From b to d) V1, V3 and V5, sampled in the FORSA cruise (the white portion of these maps correspond to nonsampled depths). From e to g) VA42, VA63 and VA91, sampled in A10_2011 cruise. From h to j) VA04, VA55 and VA71, sampled in A10_2003 cruise. From k to n) VT62 (TAII_01 section), VT85 (TAII_02 section), VT87 (TAII_02 section) and VT93 (TAII_02 section), sampled in TAII cruise. The continuous gray lines or gray dots indicate the position of CTD stations.....167

Figure 9. a) Map of the cruise sections and sampled eddies. For a complete description of this map, please see Figure 1. From b to n) inside-outside eddy anthropogenic carbon ($C_{\text{ant-TrOCA}}$ $\mu\text{mol kg}^{-1}$) content at 500 m and 1000 m depth. From b to d) V1, V3 and V5, sampled in the FORSA cruise (the white part at 1000 m correspond to non-sampled depths outside of these eddies). From e to g) VA42, VA63 and VA91, sampled in A10_2011 cruise. From h to j) VA04, VA55 and VA71, sampled in A10_2003 cruise. From k to n) VT62 (TAII_01 section), VT85 (TAII_02 section), VT87 (TAII_02 section) and VT93 (TAII_02 section), sampled in TAII cruise.....168

List of tables

Chapter IV. Methods

4.1. Oceanographic cruises

Table 4. 1. Table of cruise details presenting each study considered to develop this thesis.	93
---	----

4.2. First article - PhD 01

Table 4. 2. Radius (km), lifetime (d) and sea-air CO ₂ net flux calculated using Takahashi et al. (2009) and Wanninkhof (2014) coefficients – FCO ₂ ^{T09} and FCO ₂ ^{W14} (first and second lines for each FCO ₂ result presented in the table). Results are presented for each eddy (Vn, n=1 to 6), for the ‘Agulhas true’ eddy, the ‘Agulhas evolved’ eddy and the ‘Agulhas typical’. The FCO ₂ reported in this table are in different units, as indicated in the respective line. *indicates that the eddy lifetime accounting was finished with the data availability until the analysis.	104
--	-----

Table 4. 3. Considering Eq. 4.14, this table presents the coefficients determined for each parameter in the multiple linear regression model. CO ₂ -related parameters are: seawater CO ₂ partial pressure/fugacity (pCO ₂ ^{sw} /fCO ₂ ^{sw} , μatm), temperature-normalized pCO ₂ ^{sw} /fCO ₂ ^{sw} (NpCO ₂ ^{sw} /NfCO ₂ ^{sw} μatm, @ 20.39°C). The measured vs. modeled parameter coefficients of determination are referred to as R ² . The units of each determined parameter are: α (μatm), β ₁ (μatm°C ⁻¹), β ₂ (μatm), β ₃ (μatm mg ⁻¹ m ³), standard error (μatm). The number of data points used is 8650.	108
--	-----

4.3. Second article - PhD 02

Table 4. 4. Radius (km) and lifetime (d) of each eddy investigated on this study in the in situ sampling day and life history. Superscript T or E indicates whether the eddy can be considered a true or evolved eddy according to the classification of Orselli et al. (2019a). * indicates that the eddy lifetime accounting was completed together with the data availability in the AVISO product until analysis. # indicates that the eddy was formed during the splitting of a 925-day old Agulhas eddy. 113

Table 4. 5. Results from the C_T multiple linear regression (MLR) tests (at cruise sampling year). Each test was conducted using a different set of input parameters. T is temperature ($^{\circ}\text{C}$), S is salinity, A_T , DO is dissolved oxygen ($\mu\text{mol kg}^{-1}$), AOU is apparent oxygen utilization ($\mu\text{mol kg}^{-1}$), NO_3 is nitrate ($\mu\text{mol kg}^{-1}$), Pres is pressure (dbar), Lon is longitude, Lat is latitude. N indicates the number of measurements used in each test. R^2 is coefficient of determination. The standard error is in $\mu\text{mol kg}^{-1}$ 116

Table 4. 6. Results from the A_T multiple linear regression (MLR) tests (at cruise sampling year). Each test was conducted using a different set of input parameters. T is temperature ($^{\circ}\text{C}$), S is salinity, A_T , DO is dissolved oxygen ($\mu\text{mol kg}^{-1}$), AOU is apparent oxygen utilization ($\mu\text{mol kg}^{-1}$), NO_3 is nitrate ($\mu\text{mol kg}^{-1}$), Pres is pressure (dbar), Lon is longitude, Lat is latitude. N indicates the number of measurements used in each test. R^2 is the coefficient of determination. The standard error is in $\mu\text{mol kg}^{-1}$ 117

Table 4. 7. Limits of the uncertainties required for each carbonate system parameter in the climate and weather conditions, defined by the GOA-ON Requirements and Governance Plan (Newton et al., 2015)..... 118

Table 4. 8. Results from the C_T polynomial model tests (at cruise sampling year). Each test was conducted using a different set of input parameters. θ is potential temperature ($^{\circ}\text{C}$), S is salinity, AOU is apparent oxygen utilization ($\mu\text{mol kg}^{-1}$). N indicates the number of measurements used in each test. R^2 is the coefficient of determination. The RMSE – root mean square error is in $\mu\text{mol kg}^{-1}$ 119

Table 4. 9. Results from the A_T polynomial model tests (at cruise sampling year). Each test was conducted using a different set of input parameters. θ is potential temperature

(°C), S is salinity, Pres is pressure (dbar). N indicates the number of measurements used in each test. R^2 is the coefficient of determination. The RMSE – root mean square error is in $\mu\text{mol kg}^{-1}$ 119

Table 4. 10. The p_{ij} coefficients (with 95% confidence bounds) of the polynomial models developed for C_T and A_T , according to Equation 1. 121

Chapter V. Articles

5.1 First article – PhD 01

Table 1. Average, standard deviation (std), range (min, max) and number of measurements (n) of the results from: temperature (T, °C); salinity (S); and CO₂-related parameters: seawater CO₂ partial pressure ($p\text{CO}_2^{\text{sw}}$, μatm), temperature-normalized $p\text{CO}_2^{\text{sw}}$ ($Np\text{CO}_2^{\text{sw}}$, μatm , @ 20.39°C), sea-air CO₂ difference ($\Delta p\text{CO}_2$, μatm) and sea-air CO₂ net flux calculated using Takahashi et al. (2009) coefficient ($\text{FCO}_2^{\text{T09}}$, $\text{mmol m}^{-2} \text{d}^{-1}$).132

Table 2. Average \pm standard deviation, range (min; max) of the results from: temperature (T, °C); salinity (S); and CO₂-related parameters: seawater CO₂ partial pressure ($p\text{CO}_2^{\text{sw}}$, μatm), temperature-normalized $p\text{CO}_2^{\text{sw}}$ ($Np\text{CO}_2^{\text{sw}}$, μatm , @ 20.39°C), sea-air CO₂ difference ($\Delta p\text{CO}_2$, μatm) and sea-air CO₂ net flux calculated using Takahashi et al. (2009) coefficient ($\text{FCO}_2^{\text{T09}}$, $\text{mmol m}^{-2} \text{d}^{-1}$) for the each sampled eddy.133

Table 3. Radius (km), lifetime (d) and sea-air CO₂ net flux calculated using Takahashi et al. (2009) coefficient ($\text{FCO}_2^{\text{T09}}$). Results are presented for each eddy (Vn, n=1 to 6), for the ‘Agulhas true’ eddy, the ‘Agulhas evolved’ eddy and the ‘Agulhas typical’. The FCO_2 reported in this table are in different units, as indicated in the respective line. *indicates that the eddy lifetime accounting was finished with the data availability until the analysis.134

Table 4. Considering the Eq. 4 ($m\text{CO}_2^{\text{sw}} = \alpha + \beta_1 * T + \beta_2 * S + \beta_3 * \text{chla}$), this table presents the coefficients determined for each parameter in the multiple linear regression model. CO₂-related parameters are: seawater CO₂ partial pressure/fugacity

($p\text{CO}_2^{\text{sw}}/f\text{CO}_2^{\text{sw}}$, μatm), temperature-normalized $p\text{CO}_2^{\text{sw}}/f\text{CO}_2^{\text{sw}}$ ($Np\text{CO}_2^{\text{sw}}/Nf\text{CO}_2^{\text{sw}}$ μatm , @ 20.39°C). The measured vs modelled parameters coefficients of determination are referred to as r^2 . The units of each determined parameter are: α (μatm), β_1 ($\mu\text{atm } ^\circ\text{C}^{-1}$), β_2 (μatm), β_3 ($\mu\text{atm mg}^{-1} \text{ m}^3$), standard error (μatm). The number of data used is 8650.....134

Table 5. Comparative results of CO₂-related parameters: seawater CO₂ partial pressure ($p\text{CO}_2^{\text{sw}}$, μatm), seawater CO₂ fugacity ($f\text{CO}_2^{\text{sw}}$, μatm), sea-air $p\text{CO}_2$ difference ($\Delta p\text{CO}_2$, μatm), sea-air $f\text{CO}_2$ difference ($\Delta f\text{CO}_2$, μatm), sea-air CO₂ net flux (FCO_2 , $\text{mmol m}^{-2} \text{ d}^{-1}$) obtained for the South Atlantic Ocean used to the FORSA results discussion. The sampling season is referred to Sp (spring), Sm (summer), A (autumn) and W (winter). Each transference coefficient used in the FCO_2 estimative, as well as other specificities for each study are indicated. A map of each considered study area was inserted in the Fig. S7.....135

Article – PhD 01: supporting information

Table S1. The linear correlation coefficients for temperature – T ($^\circ\text{C}$), salinity – S and chlorophyll-*a* – Chl-*a* (mg m^{-3}) vs seawater CO₂ partial pressure – $p\text{CO}_2^{\text{sw}}$ (μatm) and/or temperature-normalized $p\text{CO}_2^{\text{sw}}$ – $Np\text{CO}_2^{\text{sw}}$ (μatm) @ 20.39°C for each region. The number of data used is referred to as n. Significance at 95% confidence level ($p < 0.05$).....149

Table S2. Average, standard deviation (std), range (min, max) and number of measurements (n) of the results from hydrographic (temperature – T in $^\circ\text{C}$, salinity – S) and CO₂-related parameters (seawater CO₂ partial pressure – $p\text{CO}_2^{\text{sw}}$ μatm , temperature-normalized $p\text{CO}_2^{\text{sw}}$ – $Np\text{CO}_2^{\text{sw}}$ μatm @ 20.39°C; sea-air CO₂ difference – $\Delta p\text{CO}_2$ μatm ; sea-air CO₂ net flux calculated using Takahashi et al. (2009) coefficient ($\text{FCO}_2^{\text{T09}}$, $\text{mmol m}^{-2} \text{ d}^{-1}$). These results encompasses just the region near the Brazilian coast

(western than 39.25°W , shallower than 3000m), at the westernmost part of the occidental basin of the South Atlantic Ocean (Figure S4a).....149

Table S3. The linear correlation coefficients for temperature – T ($^{\circ}\text{C}$), salinity – S and chlorophyll- a – $\text{Chl-}a$ (mg m^{-3}) vs seawater CO_2 partial pressure – $p\text{CO}_2^{\text{sw}}$ (μatm) and/or temperature-normalized $p\text{CO}_2^{\text{sw}}$ – $Np\text{CO}_2^{\text{sw}}$ (μatm) @ 20.39°C for sampled eddies. Results are presented for each eddy (Vn , $n=1$ to 6). The number of data used is referred to as n . Significance at 95% confidence level ($p<0.05$).....150

5.2 Second article – PhD 02

Table 1. Radius (km) and lifetime (d) of each eddy investigated on this study in the *in situ* sampling day and life history. Superscript T or E indicates whether the eddy can be considered a true or evolved eddy according to the classification of Orselli et al. [35]. * indicates that the eddy lifetime accounting was completed together with the data availability in the AVISO product until analysis. # indicates that the eddy was formed during the splitting of a 925-day old Agulhas eddy.....156

Table 2. The p_{ij} coefficients (with 95% confidence bounds) of the polynomial models developed for C_T and A_T , according to Equation 1.....158

Table 3. Thermohaline ranges used to characterize the water masses observed in this study, including their positions in the water column layer and references.....162

Chapter VI. Synthesis of the discussion and conclusions

6.1 Synthesis of the discussion and conclusions

Table 6. 1. Limits of the uncertainties required for each carbonate system parameter, to achieve the climate and weather conditions (i.e., relative uncertainty of the dissolved carbonate ion calculation of 1% and 10%, respectively), defined by the GOA-ON Requirements and Governance Plan (Newton et al., 2015), including the results from the models introduced in this thesis. 181

6.2 Síntese da discussão e conclusões

Tabela 6.1. Limites das incertezas exigidas para cada parâmetro do sistema de carbonato, para alcançar as condições clima e tempo (i.e., incerteza relativa do cálculo do íon carbonato dissolvido de 1% e 10%, respectivamente), definido pelo Plano de Governança do GOA-ON (Newton et al., 2015), incluindo os resultados dos modelos introduzidos nesta tese..... 187

6.3 Synthèse de la discussion et conclusions

Tableau 6. 1. Limites des incertitudes requises pour chaque paramètre du système carbonaté, pour atteindre les conditions ‘climat’ et ‘temps’ (i.e., incertitude relative du calcul des ions carbonates dissous de 1% et 10%, respectivement), définies par le GOA-ON Requirements and Governance Plan (Newton et al., 2015), y compris les résultats des modèles présentés dans cette thèse..... 194

List of acronyms and abbreviations

A

AABW – Antarctic Bottom Water
AAIW – Antarctic Intermediate Water
 A_T – total alkalinity
A10 – CLIVAR/WOCE Repeat
Hydrography Section A10
AOU apparent oxygen utilization

B

BrOA – Brazilian Ocean Acidification
Network (acronym from Portuguese
*Rede Brasileira de Pesquisa em
Acidificação dos Oceanos*)

C

C_{ant} – anthropogenic carbon
 $C_{\text{ant-TrOCA}}$ – anthropogenic carbon
estimated by the TrOCA method
 CaCO_3 – calcium carbonate
 CO_2 – carbon dioxide
 CH_4 – methane
chl-a – satellite-derived sea surface
chlorophyll-*a*
CRM certified reference material
 C_T – total dissolved inorganic carbon
CTD – conductivity-temperature-depth

F

FCO_2 – sea-air CO_2 net fluxes

$\text{FCO}_2^{\text{T09}}$ – sea-air CO_2 net fluxes
determined with [Takahashi et al. \(2009\)](#)
coefficient

$\text{FCO}_2^{\text{W14}}$ – sea-air CO_2 net fluxes
determined with [Wanninkhof \(2014\)](#)
coefficient

$f\text{CO}_2^{\text{sw}}$ – CO_2 fugacity

FORSA – Following Ocean Rings in the
South Atlantic

G

GOAL – Brazilian High Latitude
Oceanography Group (acronym from
Portuguese *Grupo de Oceanografia de
Altas Latitudes*)

GOA-ON – Global Ocean Acidification-
Observing Network

I

IPCC – Intergovernmental Panel on
Climate Change

K

K_S CO_2 solubility coefficient

K_T CO_2 transfer coefficients

M

MLR – multiple linear regression

N

Na₂CO₃ sodium carbonate
 NaCl sodium chloride
 NADW – North Atlantic Deep Water
 N₂O – nitrous oxide
 $NpCO_2^{sw}$ – temperature-normalized CO₂
 partial pressure
 $NfCO_2^{sw}$ – temperature-normalized CO₂
 fugacity

P

pCO_2 – CO₂ partial pressure
 pCO_2^{eq} – CO₂ partial pressure of the
 equilibrator
 pCO_2^{sw} – CO₂ partial pressure at the *in
 situ* temperature
 pCO_2^{atm} – CO₂ partial pressure of the
 atmosphere
 P_{atm} – atmospheric pressure (atm)
 P_{H₂O^{eq}} – water vapor pressure (atm)
 inside the equilibrator
 P_{H₂O} – water vapor pressure (atm)

S

SACW – South Atlantic Central Water

T

TAII – Trans-Atlantic II
 TW – Tropical Water
 T_{eq} – equilibrator temperature (°C);
 T_{is} – *in situ* temperature (°C)
 TrOCA Tracer combining Oxygen,
 inorganic Carbon, and total Alkalinity

X

XBT –
 xCO_2^{sw} – seawater CO₂ molar fraction
 xCO_2^{atm} – atmospheric CO₂ molar
 fraction

θ

θ – potential temperature

Δ

ΔpCO₂ – difference between sea water
 and atmospheric CO₂ partial pressures
 ΔC_{ant-TrOCA 2011 – 2003} – C_{ant} content
 difference between the cruise years
 ΔC_{T 2011 – 2003} – C_T content difference
 between years was determined

Abstract

Human activities have been releasing large amounts of carbon dioxide (CO₂) into the atmosphere since the Industrial Revolution. Part of this excess CO₂ is captured by the oceans (anthropogenic carbon, C_{ant}) and has been causing perturbations and changes in the carbonate system cycle. These changes in the carbonate system are now known to alter the acidification state of the oceans.

In the South Atlantic Ocean are observed the Agulhas eddies, which are among the largest mesoscale structures in the oceans. Because they are anticyclonic structures, these eddies are associated with regions where the ocean loses heat to the atmosphere, but its role in relation to the carbonate system is still poorly studied. Thus, the main objective of this doctoral research was to investigate the relationship between the Agulhas eddies and CO₂/C_{ant} uptake and transport throughout their lives and which role these structures play in the acidification state in the South Atlantic Ocean.

As a main conclusion of this thesis, we have been able to demonstrate that the Agulhas eddies are able not only to capture more CO₂ than the surrounding waters, but also to transfer into the water column and can carry more C_{ant} along their trajectories. As studies show that 30% of these structures released in the Agulhas leakage reach the west coast of the South Atlantic Ocean and even interact with the Brazilian Current, we can indicate them as one of the triggers that may be intensifying the acidification observed for the central layers of this region.

Keywords: Agulhas eddies; CO₂ fluxes; Carbonate system; Anthropogenic carbon; South Atlantic Ocean.

Resumo

Atividades humanas vêm liberando grandes quantidades de dióxido de carbono (CO_2) na atmosfera desde a Revolução Industrial. Parte desse excesso de CO_2 é capturado pelos oceanos (carbono antropogênico, C_{ant}) e vêm causando perturbações e alterações no ciclo do sistema carbonato. Essas alterações no sistema carbonato alteram o estado de acidificação dos oceanos.

No oceano Atlântico Sul observa-se os vórtices das Agulhas, que estão entre as maiores estruturas de mesoescala dos oceanos. Por serem estruturas anticiclônicas, estes vórtices estão associados às regiões em que o oceano perde calor para a atmosfera, porém seu papel em relação ao sistema carbonato ainda é pouco estudado. Dessa forma, o objetivo principal dessa pesquisa de doutorado foi investigar a relação dos vórtices das Agulhas com a captura e transporte de $\text{CO}_2/C_{\text{ant}}$ ao longo de suas vidas e qual o papel dessas estruturas no estado de acidificação no oceano Atlântico Sul.

Como conclusão principal dessa tese, pudemos demonstrar que os vórtices das Agulhas são capazes não só de capturar mais CO_2 do que as águas ao seu redor, como também de transferir para o interior da coluna d'água, podendo carregar mais C_{ant} ao longo de suas trajetórias. Como estudos mostram que 30% dessas estruturas liberadas no vazamento das Agulhas atingem a costa Oeste do Oceano Atlântico Sul e chegam a interagir com a Corrente do Brasil, podemos indicá-los como um dos gatilhos que podem estar intensificando a acidificação observada para as camadas centrais dessa região.

Palavras-chave: Vórtices das Agulhas; Fluxos de CO_2 ; Sistema carbonato; Carbono antropogênico; Oceano Atlântico Sul.

Résumé

Depuis la révolution industrielle, les activités humaines libèrent de grandes quantités de dioxyde de carbone (CO_2) dans l'atmosphère. Une partie de cet excès de CO_2 est captée par les océans (carbone anthropique, C_{ant}) et a provoqué des perturbations et des changements dans le cycle du système carbonaté. Ces perturbations du système carbonaté sont désormais connues pour altérer l'état d'acidification des océans.

Dans l'océan Atlantique Sud, les grands tourbillons des Aiguilles, sont parmi les plus grandes structures à méso-échelle des océans. Parce qu'ils sont des structures anticycloniques, ces tourbillons sont associés à des régions où l'océan perd de la chaleur vers l'atmosphère, mais leurs rôles par rapport au système carbonaté sont encore mal connus. Ainsi, l'objectif principal de cette recherche doctorale était d'étudier la relation entre les tourbillons des Aiguilles et la capture et le transport du $\text{CO}_2/C_{\text{ant}}$ tout au long de leur vie ainsi que le rôle que ces structures jouent dans l'état d'acidification de l'océan Atlantique Sud.

Lors de cette thèse, nous avons pu démontrer que les tourbillons des Aiguilles sont capables non seulement de capter plus de CO_2 que les eaux environnantes, mais aussi de transférer ce carbone en profondeur dans la colonne d'eau et peuvent transporter plus de C_{ant} le long de leur trajectoires. Etant donné que les observations indiquent que 30% de ces structures libérées dans le courant des Aiguilles atteignent la côte ouest de l'océan Atlantique Sud et interagissent même avec le courant du Brésil, nous pouvons les désigner comme l'un des déclencheurs susceptibles d'intensifier l'acidification observée pour les couches centrales de cette région.

Mots-clés : tourbillons des Aiguilles ; flux de CO_2 ; Système du carbone ; Carbone anthropique ; Océan Atlantique Sud.

Preface

Since 1896 it's being said that the human emissions of carbon dioxide (CO₂) are going to impact the earth climate ([Arrhenius, 1896](#)). Nowadays it is a confirmed fact that the earth climate system is changing, that the oceans are being impacted as well, and that these changes are bringing consequences for organisms and marine ecosystems.

I was grown totally involved to the sea, and after choosing to study the oceans, I could not close my eyes to CO₂-related and climate issues. I started to study the CO₂ system when I was still in the first year of the undergrad course in Oceanography. From then on, I just got more and more involved in this theme. Since the end of the undergrad, I had great opportunities to participate in conferences, meetings and summer schools,

which put me in contact with researchers from all over the world. Seeing all these people doing many different studies and achieving super interesting results always motivated me to keep going on this area.

When I decided to pursue the PhD, I was offered a really interesting data set and the best advisors someone could ask for. They composed a super team to study the impact of the Agulhas eddies (physical structures of the South Atlantic Ocean) on the CO₂-system. We looked at air-sea interactions and observed that those structures uptake more CO₂ than their surrounding waters. To dive inside the water column, we used different cruises and we could see that the Agulhas eddies also contain more anthropogenic carbon inside them than the same depths of the surrounding waters. Finally, we concluded that those structures could act as a trigger to the acidification of the South Atlantic Ocean.

Chapter I. Introduction

1.1 Introduction: English version

A human component is fundamental to explain the changes in the Earth climate system (e.g., ocean and atmosphere warming, glaciers melting; e.g., [IPCC 2007](#); [Campos et al., 2015](#)). This statement is reinforced by the fact that radiative forcings due to carbon dioxide (CO₂), methane (CH₄), and nitrous oxide (N₂O) are unprecedented in more than 800.000 years ([IPCC 2007, 2013](#)). These important long-lived greenhouse gases are being released in the atmosphere by human activity with a significant increase since the beginning of the Industrial Revolution (**Figure 1.1**; e.g., [Ciais et al., 2013](#); [Le Quéré et al., 2016](#)).

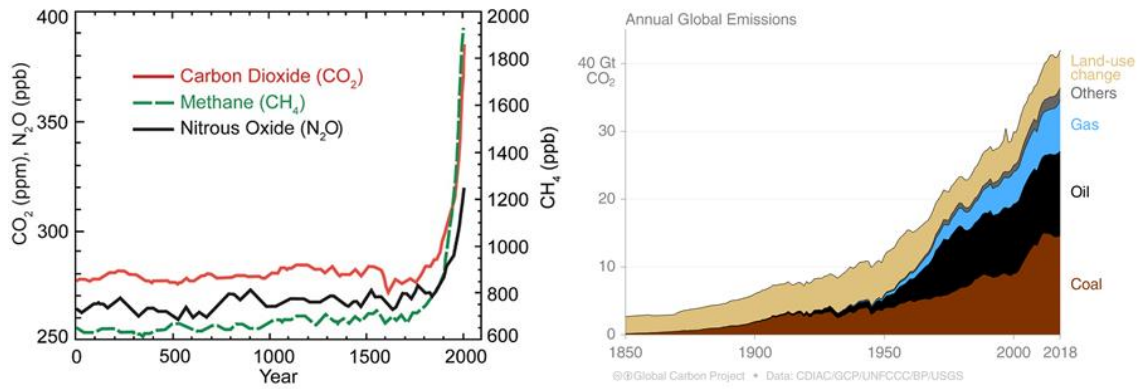


Figure 1.1. Left panel: concentrations of carbon dioxide (CO₂, red line; ppm), methane (CH₄, green line; ppb) and nitrous oxide (N₂O, black line; ppb) in the atmosphere over the last 2000 years (IPCC 2007). Right panel: annual global emissions of CO₂ since the Industrial Revolution according to the source (Global Carbon Project).

Records of continuous increasing CO₂ emission (**Figure 1.2**; Tans e Keeling, 2013) are urging the development of the marine carbon system projects. This necessity is urged mainly by virtue of oceans capacity to absorb a huge amount of the CO₂ released in the atmosphere by human activities (e.g., during fossil fuel burning, cement production; Millero, 2007; Doney et al., 2009). Some results have shown that oceans have already absorbed from about 20 to 40 % of the anthropogenic carbon¹ (C_{ant}) released in the last 200 years (e.g., Sabine et al., 2004; Ciais et al., 2013; Khatiwala et al., 2013; Gruber et al., 2019). The Intergovernmental Panel on Climate Change (IPCC) considers an averaged value of 30% of C_{ant} being uptake by the global ocean (IPCC, 2013). However, the C_{ant} storage in the ocean layers is still unclear since the ocean circulation has a huge importance in its redistribution around the global ocean, which is still a subject of discussion. Consequently, it is extremely important to better comprehend the scientific issues related to: (i) the sea-air CO₂ net fluxes (FCO₂)—to understand how the absorption occurs—; (ii) the C_{ant} distribution—to understand where this C_{ant} is storage—; (iii) its consequences to both marine organisms and ecosystems; and (iv) the whole carbon cycle,

¹ Anthropogenic carbon is the CO₂ released in the atmosphere by human activity (e.g., fossil fuel burning, cement production; Ciais et al., 2013).

in order to develop public policy and future climate projections (Le Quéré et al., 2013; Newton et al., 2015).

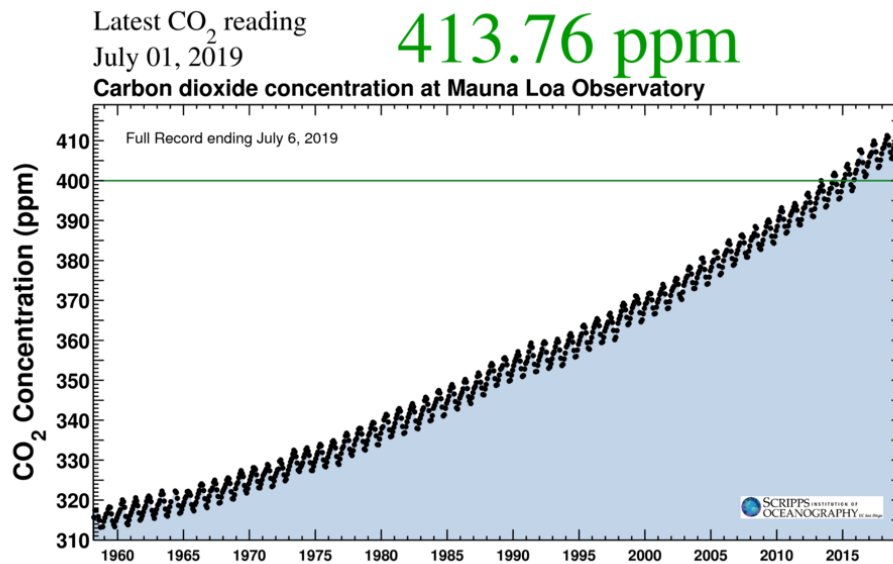


Figure 1.2. Full record of the carbon dioxide (CO₂) concentration in the atmosphere at the Mauna Loa Observatory (the Keeling curve). The green continuous line indicates the 400 ppm baseline. From: <https://scripps.ucsd.edu/programs/keelingcurve/>

In this way, two main mechanisms can describe how the CO₂ is uptaken by the oceans: the biological and the physical pumps (**Figure 1.3**). The first one can be split in organic carbon pump and carbonate counter pump (e.g., Denman et al., 2007; Ciais et al., 2013). The organic carbon pump begins when the phytoplankton organisms starts the photosynthesis process, which is the first step to convert inorganic carbon into particulate organic carbon. The carbon produced in that process is remineralized in the water column and/or transported to the ocean floor through excretion or senescent products. Furthermore, the calcium carbonate (CaCO₃) formed by CO₂ dissolution is also used by organisms to construct their calcareous shells (e.g., Cox et al., 2000). The biogenic CaCO₃ formation also releases CO₂ and reduces total alkalinity (A_T), what configures the carbonate counter pump (**Figure 1.3**; Rost & Riebesell, 2004).

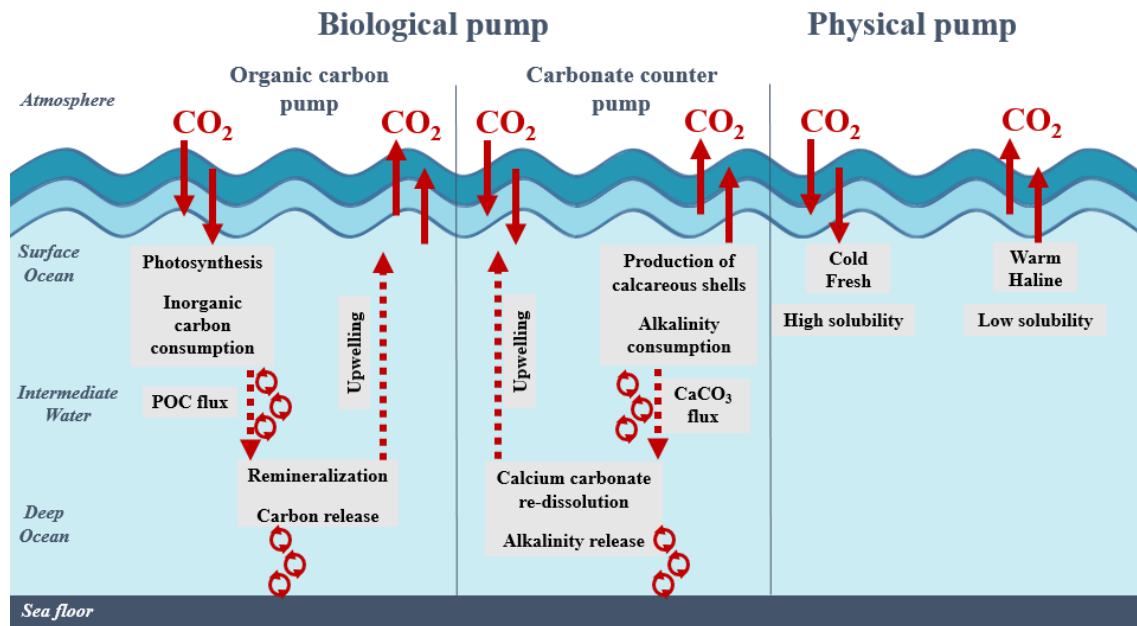


Figure 1.3. Schematic figure of the air-sea exchange of CO₂. The uptake by the oceans is split in the biological and physical pumps. The figure was created based on [Denman et al. \(2007\)](#).

The physical pump refers to the CO₂ solubility and sink (**Figure 1.3**) driven by cold and less salty waters. The water mass formation processes, essentially in high latitude areas, act sequestering the carbon and other dissolved gases to deeper regions. These processes also help the oxygenation of the entire water column, including the central, intermediate, deep and bottom waters. The conservative properties acquired by the water masses during their formation process are preserved throughout their circulation inside the oceans, and only change by water masses internal mixing processes. On the other hand, the water masses non-conservative properties are slightly modified according to biogeochemical processes that occur during their advection trajectory (e.g., [Orsi et al., 1999](#); [Rintoul, 2011](#); [Talley et al., 2011](#)). Mode and intermediate waters are formed by subduction, which is indicated as the primary mechanism for C_{ant} intrusion in the central and intermediate ocean layers (**Figure 1.4**; [Sabine et al., 2004](#); [Pardo et al., 2014](#); [Tanhua et al., 2016](#)). The same is true for deep and bottom layers, when the surface water gets

denser and mix with other water masses before sink to deep levels by the deep convection process (**Figure 1.4**), thus, carrying CO₂ and its dissociation products into the deep ocean (e.g., Cox et al., 2000; Touratier et al., 2016).

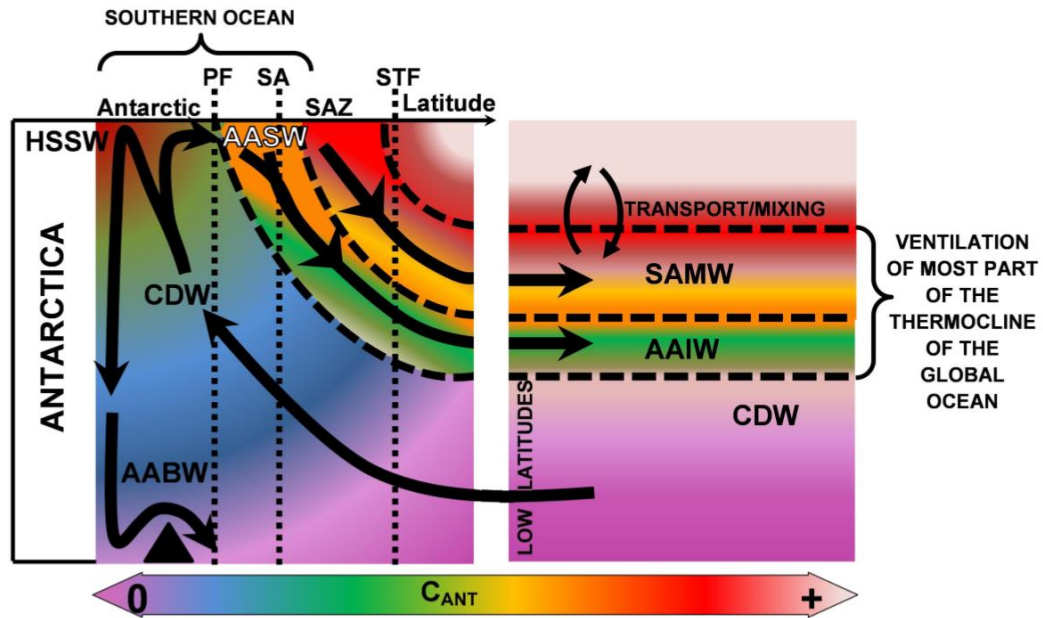


Figure 1.4. Schematic flows of water masses in the Southern Ocean in a meridional section: High Saline Shelf Water (HSSW), Antarctic Surface Water (AASW), upwelling of Circumpolar Deep Water (CDW), formation (by deep convection) of Antarctic Bottom Water (AABW), and formation (by subduction) of South Atlantic Mode Water (SAMW) and Antarctic Intermediate Water (AAIW). The last two water masses ventilate the central and intermediate layer of the oceans, as indicated. The colours indicate the C_{ant} content in the water column. From: Pardo et al. (2014).

In spite of those bombs act in a closed cycle – as the carbon and nutrients exportation in biogenic material is balanced by inorganic carbon and nutrients upwelling – the C_{ant} absorption is known to be governed mainly by physical-chemical processes (Howes et al., 2015). Accordingly, it is important to highlight that a simple CO₂ addition in the marine environment would not be a problem if this gas does not react with the water. However, the reaction of the CO₂ with water leads to changes in the marine carbonate system. One of these consequences is the ocean acidification process, which is known as ‘the other CO₂ problem’ (Doney et al., 2009). Thus, it is extremely important

to understand not only the FCO_2 and the C_{ant} absorption by the oceans, but also to quantify the seawater acidification state that is occurring and the responses and sensibility of the marine ecosystems to the CO_2 absorption. This investigation should be made using not only *in situ* data, but also through the use of ocean, climate and mathematical models (IPCC, 2013), reanalysis products and remote sensing (e.g., Balch & Utgoff, 2009).

Each ocean responds to climate changes in different ways (**Figure 1.5**), but the South Atlantic Ocean is currently facing significant alterations, such as increasing seawater temperature, salinity, and heat content (e.g., Campos et al., 2015). These local or regional climate changes lead to perturbations and alter the hydrological cycle, surface ocean currents, coastal hydrodynamics, and marine carbonate system, which drive transformation in sensitive ecosystems and marine organisms (e.g., Campos et al., 2015). The South Atlantic Ocean also plays an important role in the carbon cycle, since its polar and subpolar regions are considered as CO_2 sinking areas. They are highly dependent on temperature and phytoplankton activity (Takahashi et al. 1997). Takahashi et al. (1997) estimated an averaged FCO_2 in circa of $-0.3 \text{ Pg C yr}^{-1}$, which was also reinforced by Takahashi et al. (2002). Although Takahashi et al. (2009) improved the global carbon cycle comprehension, it is important to highlight that the scarcity of marine carbon system data has been leading to relatively few studies being conducted in the South Atlantic Ocean when compared to those on the North Atlantic Ocean. In addition, Takahashi et al. (2009) cited there is no data enough to estimate decadal flux rates in this region. Also, Gruber et al. (2019) recently demonstrated that the South Atlantic Ocean is undergoing an anomalous increasing in the C_{ant} inventory.

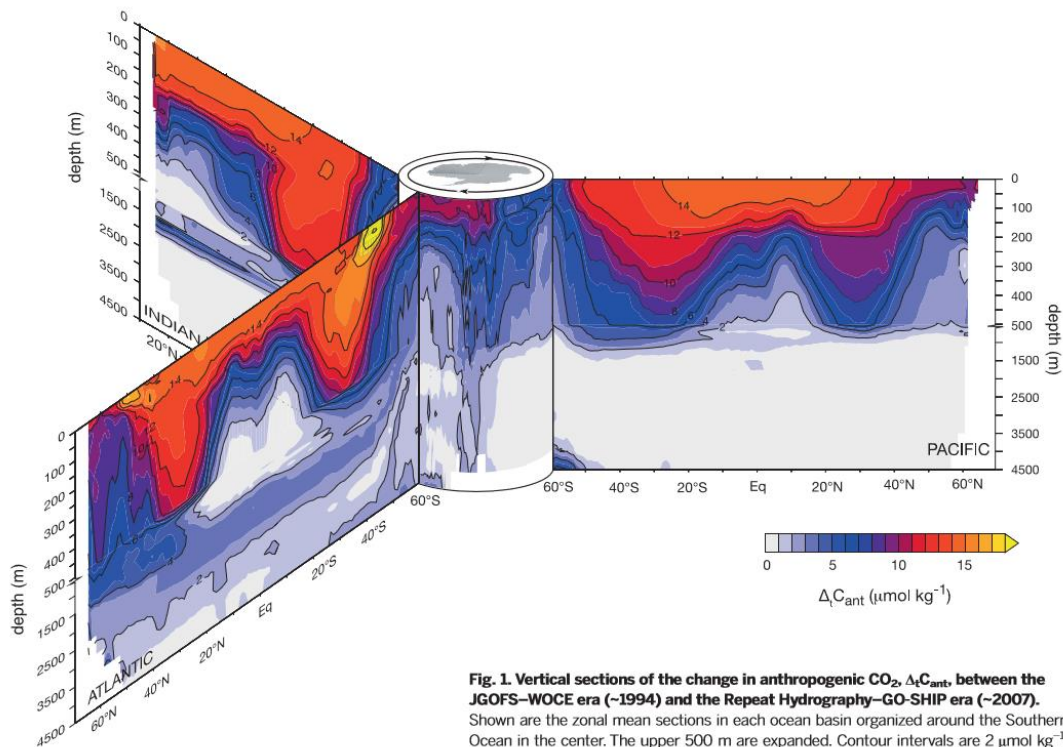


Fig. 1. Vertical sections of the change in anthropogenic CO₂, ΔC_{ant} , between the JGOFS–WOCE era (~1994) and the Repeat Hydrography–GO-SHIP era (~2007). Shown are the zonal mean sections in each ocean basin organized around the Southern Ocean in the center. The upper 500 m are expanded. Contour intervals are 2 $\mu\text{mol kg}^{-1}$.

Figure 1.5. C_{ant} content in sections of the Atlantic, Indian and Pacific oceans. From: [Gruber et al. \(2019\)](#).

Hence, to have a better overview of the South Atlantic Ocean, the surface circulation and the water masses presented in the whole water column of this basin are briefly introduced below. The Atlantic Ocean can be generally split in four vertical layers: surface to pycnocline (subducted thermocline – lower limit: $\sigma \sim 26.2 \text{ kg m}^{-3}$, ~200 m – and lower thermocline – lower limit: $\sigma \sim 26.9 \text{ kg m}^{-3}$, ~500/600 m), intermediate (lower limit: $\sigma \sim 27.4 \text{ kg m}^{-3}$, ~1200/1300 m), deep and abyssal waters ([Talley et al., 2011](#)). Surface circulation in the South Atlantic Ocean is dominated by a subtropical anticyclonic gyre closed by the following currents: Brazil Current, South Atlantic Current, Benguela Current System and the southern branch of the South Equatorial Current (**Figure 1.6**). The Brazil Current is the western boundary current flowing poleward and transporting at the surface the Tropical Water (TW). The upwelling system is observed in the eastern boundary, including the Benguela Current System flowing northward (**Figure 1.6**; e.g.,

Peterson & Stramma, 1991; Emery, 2003; Talley et al., 2011). In the same way, flowing in opposite directions in the zonal system are the South Atlantic Current (eastward) and the southern branch of the South Equatorial Current (westward). Although dominated by this gyre, the South Atlantic Ocean surface circulation is also composed by a tropical gyre and the Antarctic Circumpolar Current. South Atlantic Central Water (SACW) and Antarctic Intermediate Water (AAIW) compose the central and intermediate layers (e.g., Hanawa & Talley, 2001; van Aken, 2007; Talley et al., 2011). In the deep and bottom layers the North Atlantic Deep Water (NADW) and the Antarctic Bottom Water (AABW) are observed in both sides of the South Atlantic Ocean (e.g., Orsi et al., 1999; Talley et al., 2011), although in different proportions in the Brazil and Angola abyssal basins (Ferreira & Kerr, 2017).

Both the surface, central and intermediate waters found in the region can be influenced by the Indian Ocean waters (Souza et al., 2018), which enter the Atlantic basin through the southernmost region of the African continent, by the Agulhas Current leakage (e.g., Beal, 2009; Talley et al., 2011; Biastoch et al., 2015). This leakage is primary composed by filaments detached from the main flux of the Agulhas Current, however the major content is composed by the Agulhas eddies (Lutjeharms, 2006).

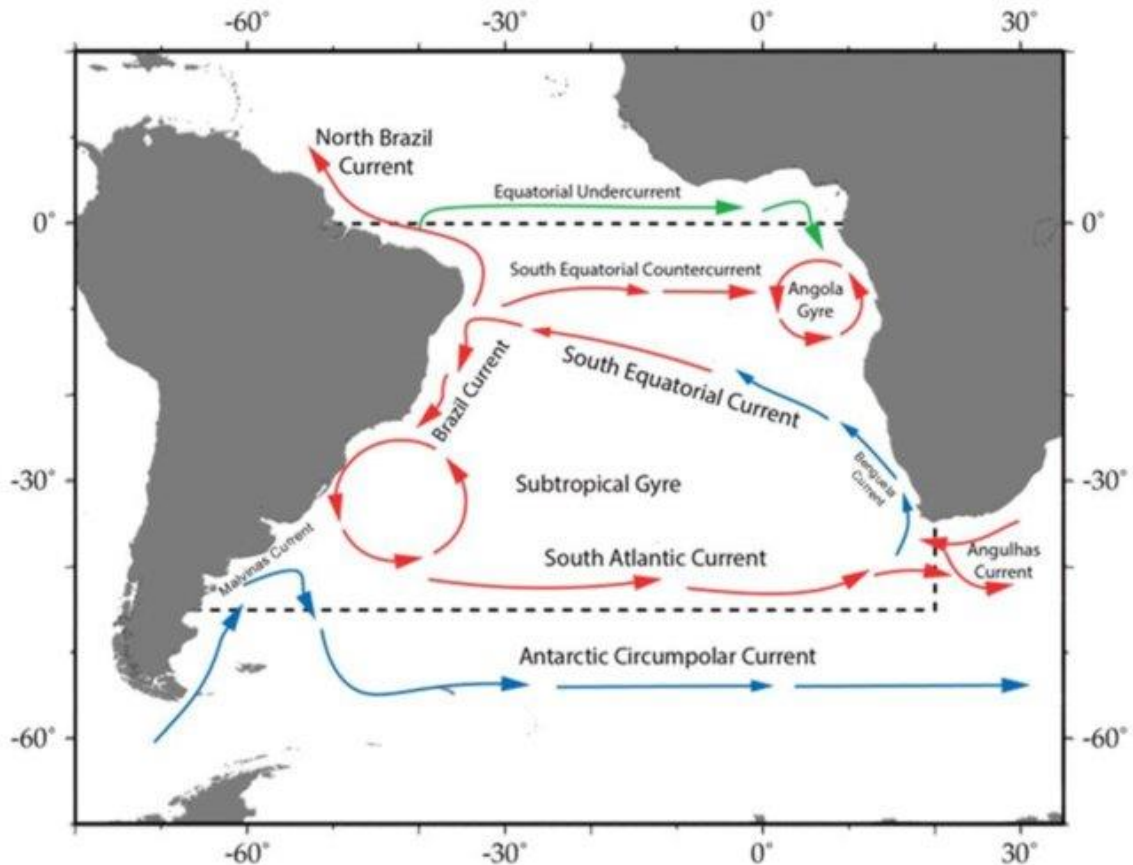


Figure 1.6. Schematic circulation of the main ocean currents at the surface South Atlantic Ocean. Red arrows indicate warm water currents and blue arrows indicate cold water currents. Please [O'Brien et al. \(2017\)](#) for further details about the ocean circulation in the area.

The role of the Agulhas Current leakage (eddies and filaments) for the Atlantic Meridional Overturning Circulation is considered meaningful in previous studies (e.g., [Lutjeharms, 2006](#); [Biaostoch et al., 2009, 2015](#)), mainly by salt advection ([Biaostoch et al., 2009](#)) since that the shedding of at least six eddies per year is expected ([Gordon, 2003](#); [Lutjeharms, 2006](#)). The integrated anomaly of salt content above the 10°C isotherm inside an Agulhas eddy varies from 1.2 to 13.1 10^6 kg, with a mean value of 4.5 10^6 kg ([Lutjeharms, 2006](#)). The intrusion of surface-to-intermediate waters from Indian Ocean carries not only salt, but also heat to the subpolar and subarctic North Atlantic, where it contributes to the deep water formation (e.g., [Beal, 2009](#); [Biaostoch et al., 2015](#)). However, the real scale of this role is still on debate (e.g., [de Ruijter et al., 1999](#); [Souza et al., 2011](#); [Casanova-Masjoan et al., 2017](#); [Souza et al., 2018](#)).

The Agulhas eddies are anticyclonic, which indicates that in the southern hemisphere their rotation is counter-clockwise and present high-pressure centres, displacing the isopycnals downward (**Figure 1.7**; e.g., [Azevedo & Mata, 2010](#)). They are released at the Agulhas leakage region as anticyclonic lens eddies and their suffer modifications that slowly induce their structures to become non-lens eddies along their trajectories through the South Atlantic Ocean (**Figure 1.7**; [Azevedo & Mata, 2010](#)).

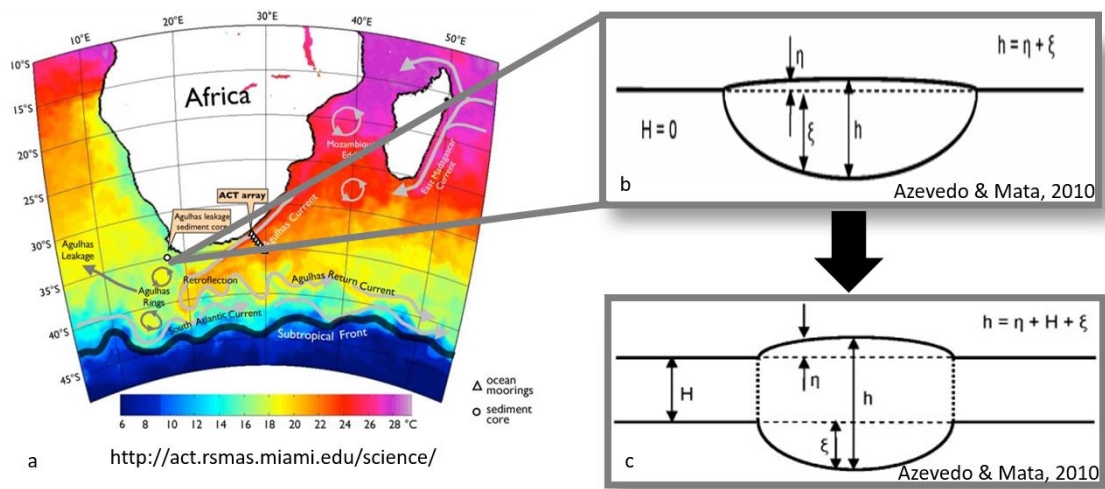


Figure 1.7. Agulhas eddies schematic representation. a) Sea surface temperature map, indicating ocean currents and Agulhas eddies at their formation region. From: <http://act.rsmas.miami.edu/science/>. b) An anticyclonic lens eddy, representing an Agulhas eddy structure as soon as it is released at the Agulhas leakage region. c) An anticyclonic non-lens eddy, representing an Agulhas eddy structure along its trajectory through the South Atlantic Ocean. For both panels b and c, each letter represents: h , depth of the eddy; η sea level anomaly caused by the eddy presence; ξ , downward displacement of the thermocline; H height of the fluid carried by the eddy movement. b and c from: [Azevedo & Mata \(2010\)](#).

The Agulhas eddies features are self-propelled westward in the South Atlantic Ocean as a result from the meridional balance of the forces acting on them. The Agulhas eddies, as anticyclonic mesoscale structures are forced to drift to the equator due to the induced vorticity, whereas the cyclonic structures are forced to drift to the poles. This induced vorticity can occur due to a planetary effect or even a topographic effect. The topographic effect can also change the direction in which the eddy is moving. Additionally, other eddies around can influence on each other. The movement of the

eddies are a result of these four mechanisms acting together. Normally, they act resulting in a north-western trajectory of the Agulhas eddies when they are crossing the South Atlantic Ocean (e.g., [Azevedo & Mata, 2010](#)). Their advection speed is in order of few centimeters per second (3-5 cm s⁻¹; [Lutjeharms, 2006](#)).

The Agulhas eddies are among the largest mesoscale structures in the global ocean ([Biaostoch et al., 2008](#)). The Agulhas eddies have a horizontal scale ranging up to 300 km, a vertical scale ranging from 1500 to 2000 m ([Biaostoch & Krauss, 1999](#)) or even more (up to 4000 m; e.g., [Beal, 2009](#)). In addition, their net volume transport varies from 0.5 to 1.5 Sv (1 Sv $\equiv 10^6$ m³ s⁻¹). Other mesoscale eddies have a temporal scale that can vary from weeks to months ([Chelton et al., 2011](#)), whereas an Agulhas eddy has a lifetime estimated to be greater than two years ([Lutjeharms, 2006](#)). Carrying also potential vorticity and biogeochemical properties from their formation areas, the eddies present distinct characteristics of the surrounding waters (e.g., [Flierl, 1979](#)) and play a major role in both physical and biological processes (e.g., [Robinson, 1983](#); [Beal, 2009](#)).

The eddies have also an impact on air-sea heat fluxes, the overlaying atmosphere circulation ([Lutjeharms, 2006](#); [Frenger et al., 2013](#)), and biogeochemistry ([McGillicuddy, 2016](#); [Moreau et al., 2017](#)). Since the Agulhas eddies are anticyclonic structures, [Villas Bôas et al. \(2015\)](#) associated them with regions with positive heat flux anomalies, that tend to warm the atmospheric boundary layer (i.e., regions where the ocean loses heat to the atmosphere because the water inside them is warmer than surrounding waters). Thus, even admitting that these mesoscale eddies play a vital role on ocean-atmosphere interactions, their impact on the changes of the marine carbonate system are not yet constrained, mainly considering the sea-air exchanges of CO₂ (e.g., [Ríos et al., 2003](#); [Woodsley et al., 2016](#); [Moreau et al., 2017](#)).

There is evidence that the leakage in the Agulhas Current retroflexion region has increased due to changes in local wind system (Biaostoch et al., 2009; Beal et al., 2011). These changes are: (i) the southward displacement of the zero line of the wind stress curl and (ii) the intensification of the Southern Hemisphere westerlies (Figure 1.8), which is known as the southward expansion of the Southern Hemisphere westerlies (e.g., Beal et al., 2011). There are also suggestions about the increasing of the leakage due to a southward displacement of the entire gyre, not only of the zero line of the wind stress curl (e.g., Oliveira, 2017). The anthropogenic forcing on the climate changes (i.e., global warming) caused these changes. This process results in an ocean warming and salinification of the South Atlantic Ocean basin (e.g., Bard et al., 2009; Biaostoch et al., 2009; Beal et al., 2011).

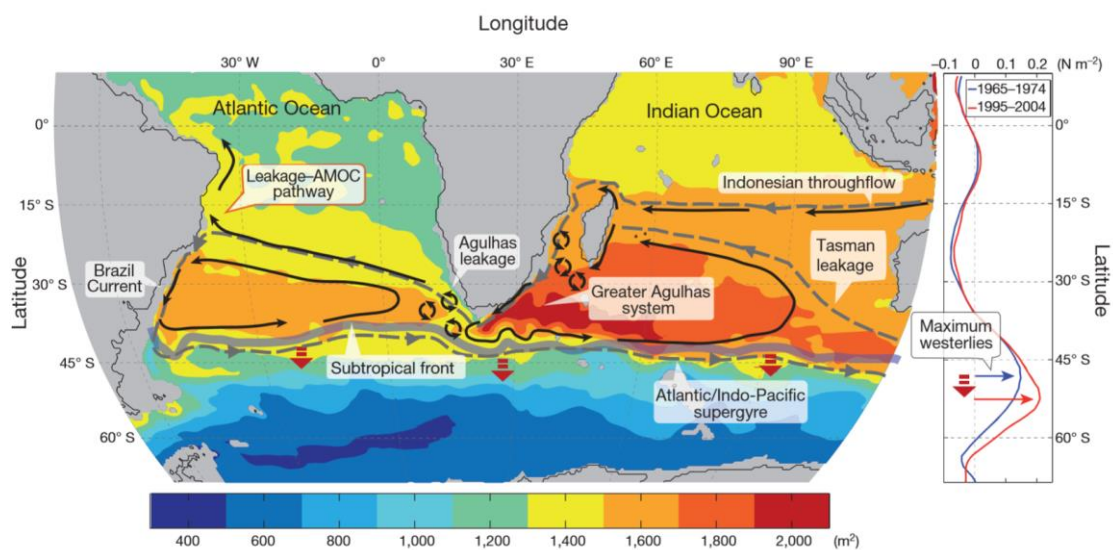


Figure 1.8. Representation of the Agulhas leakage being affected by the southward displacement of the Subtropical Front caused by the westerlies southward expansion over a 30 years period. From: Beal et al. (2011).

In addition, the recent study by Souza et al. (2018) observed that the contribution from Indian Ocean mode waters can considerably influence the properties of the SACW in the South Atlantic Ocean basin. This statement is reinforced considering the increase in the number of eddies released in the Agulhas retroflexion region (Biaostoch et al.,

2009). The Agulhas eddies transport mode waters, which are marked by the following characteristics: thermostad and halosthad layers (i.e., stable ranges of temperature and salinity, respectively) and low potential vorticity. The mode waters are primarily formed during the winter after intense mixing in the surface layers and dive between the seasonal and permanent thermoclines. These mode waters are source waters that are further advected and compose the central waters of the oceans (e.g., SACW). Thus, as the mode water formation is intensified when the heat flux increases (e.g., Hanawa & Talley, 2001), a strengthen of the formation processes of the mode waters is expected because the Agulhas eddies are able to intensify the heat flux (Villas Bôas et al., 2015). Three varieties of Subtropical Mode Water (marked by distinct ranges of temperatures depending on the source area considered) compose the central layer of the South Atlantic Ocean, i.e. the layer occupied by the SACW. The SACW layer is also influenced by contributions from the Indian Ocean Mode Water (Sato & Polito, 2014; Souza et al., 2018).

Recent studies concluded that the central waters (e.g., represented by the SACW in the South Atlantic Ocean) are among the most affected by C_{ant} penetration (Salt et al., 2015; Carvalho-Borges et al., 2018; Orselli et al., 2018). This shifted the previous idea about the main entrance to C_{ant} in the oceans from the formation of deep waters (deep convection process) to the formation of central and intermediate waters (subduction process). These studies regarding the C_{ant} uptake indicated that it is leading to an acidification rate (i.e., change in seawater pH) of -0.0016 yr^{-1} up to -0.0018 yr^{-1} in the SACW since the preindustrial period (Salt et al., 2015; Carvalho-Borges et al., 2018; Orselli et al., 2018). These trends indicate that the SACW is acidifying faster than the waters immediately above and below it, because they are higher than those already observed for these others ocean layers: e.g., -0.0013 yr^{-1} for surface waters and -0.0010

yr^{-1} at the intermediate layer, for AAIW. The pH changes observed in the South Atlantic Ocean for the deep and bottom layers are smaller than all other layers, as expected. These changes are $-0.0010/-0.0000 \text{ yr}^{-1}$ for the upper and lower varieties of CDW, $-0.0005/-0.0000 \text{ yr}^{-1}$ for upper and lower varieties of NADW, and -0.0000 yr^{-1} for AABW (e.g., [Salt et al., 2015](#); [Kitidis et al., 2017](#); [Orselli et al., 2018](#)). In addition, a recent study presented some results indicating that the Agulhas eddies are prone to carry more C_{ant} than surrounding waters ([Woosley et al., 2016](#)). In this research, the authors did not focus their investigation on quantifying C_{ant} directly on the eddies, thus they suggested that studies on this theme are necessary.

In this context, the development of this thesis was motivated by the facts that: (i) the Agulhas eddies carry surface to intermediate waters from the Indian Ocean to the South Atlantic Ocean ([Beal et al., 2009](#); [Biaostoch et al. 2009](#)), (ii) these structures are prone to strength the formation process of mode waters, and (iii) the higher acidification process is occurring in the central layers of the South Atlantic Ocean. Thus, considering the novelty about the topic, this study presents an investigation of the Agulhas eddies role in ocean biogeochemistry, which is still an additional challenge to be investigated (e.g., [Ríos et al., 2003](#); [Moreau et al., 2017](#)). Finally, the results of this study are expected to further contribute to the scientific discussion of the impacts of the Agulhas eddies on changes in the marine carbonate system.

1.2 Introdução: versão em português

Uma componente humana é fundamental para explicar as alterações no sistema climático terrestre (e.g., aquecimento dos oceanos e da atmosfera, derretimento de glaciares; e.g., [IPCC 2007](#); [Campos et al., 2015](#)). Essa afirmação é reforçada pelo fato de que as forçantes radiativas devidas ao dióxido de carbono (CO₂), metano (CH₄) e óxido nitroso (N₂O) são inéditas em mais de 800.000 anos ([IPCC 2007, 2013](#)). Esses importantes gases de efeito estufa de longa duração estão sendo liberados na atmosfera pela atividade humana, com um aumento significativo desde o início da Revolução Industrial (**Figura 1.1**; e.g., [Ciais et al., 2013](#); [Le Quéré et al., 2016](#)).

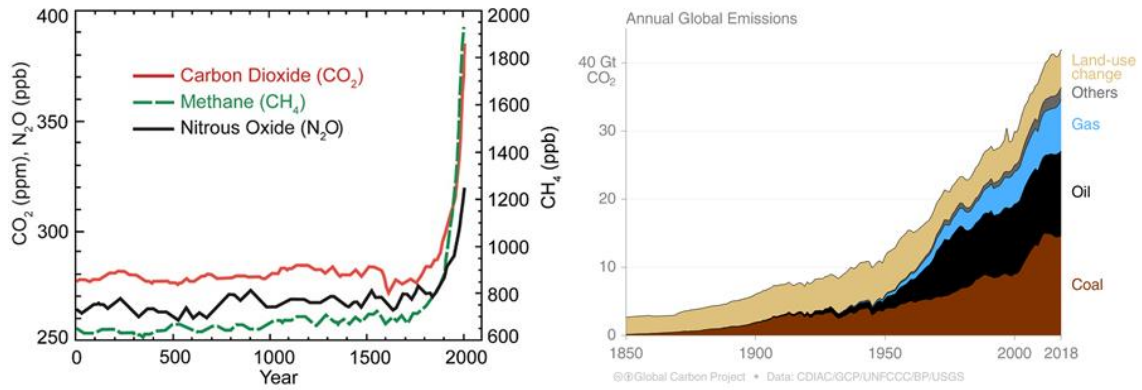


Figura 1.1. Painel esquerdo: concentrações de dióxido de carbono (CO₂, linha vermelha; ppm), metano (CH₄, linha verde; ppb) e óxido nitroso (N₂O, linha preta; ppb) na atmosfera nos últimos 2000 anos (IPCC 2007). Painel direito: emissões globais anuais de CO₂ desde a Revolução Industrial, de acordo com a fonte (Global Carbon Project).

Registros contínuos de emissão crescente de CO₂ (Figura 1.2; Tans e Keeling, 2013) estão fomentando o desenvolvimento de projetos do sistema carbonato marinho. Essa necessidade é reforçada principalmente em virtude da capacidade dos oceanos de absorver uma enorme quantidade de CO₂ liberado na atmosfera pelas atividades humanas (e.g., durante a queima de combustíveis fósseis, produção de cimento; Millero, 2007; Doney et al., 2009). Alguns resultados mostraram que os oceanos já absorveram cerca de 20 a 40% do carbono antropogênico² (C_{ant}) liberado nos últimos 200 anos (e.g., Sabine et al., 2004; Ciais et al., 2013; Khatiwala et al., 2013; Gruber et al., 2019). O Painel Intergovernamental de Mudanças Climáticas (Intergovernmental Panel on Climate Change, IPCC) considera que um valor médio de 30% de C_{ant} foi absorvido pelo oceano global (IPCC, 2013). No entanto, o armazenamento do C_{ant} nas camadas oceânicas ainda não está claro, pois a circulação oceânica tem uma enorme importância em sua redistribuição ao redor do oceano global, que ainda é objeto de discussão. Consequentemente, é extremamente importante compreender melhor as questões científicas relacionadas: (i) aos fluxos líquidos de CO₂ através da interface oceano-

² Carbono antropogênico é o CO₂ liberado na atmosfera pela atividade humana (e.g., queima de combustíveis fósseis, produção de cimento; Ciais et al., 2013).

atmosfera (FCO_2)—para entender como essa captação ocorre—; (ii) à distribuição de C_{ant} —para compreender onde esse C_{ant} é armazenado—; (iii) às consequências da absorção de CO_2 para organismos e ecossistemas marinhos; e (iv) ao ciclo do carbono como um todo, a fim de desenvolver políticas públicas e projeções climáticas futuras (Le Quéré et al., 2013; Newton et al., 2015).

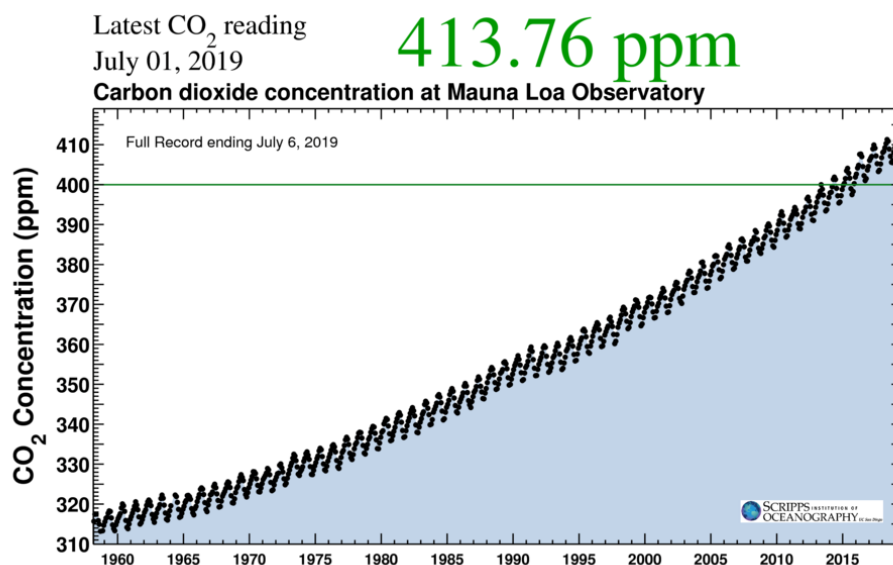


Figura 1.2. Registro completo das concentrações de dióxido de carbono (CO_2) na atmosfera no observatório de Mauna Loa (curva de Keeling). A linha verde contínua indica o patamar de 400ppm. De: <https://scripps.ucsd.edu/programs/keelingcurve/>

Dessa maneira, dois mecanismos principais podem descrever como o CO_2 é absorvido pelos oceanos: as bombas biológica e física. (**Figura 1.3**). A primeira pode ser dividida em bomba de carbono orgânico e bomba contrária de carbonato (e.g., Denman et al., 2007; Ciais et al., 2013). A bomba de carbono orgânico começa quando os organismos fitoplanctônicos iniciam o processo de fotossíntese, que é o primeiro passo para converter carbono inorgânico em carbono orgânico particulado. O carbono produzido nesse processo é remineralizado na coluna d'água e/ou transportado para o fundo do oceano através de excreção ou produtos senescentes. Além disso, o carbonato

de cálcio (CaCO_3) formado pela dissolução de CO_2 também é usado pelos organismos para construir suas carapaças calcárias (e.g., Cox et al., 2000). A formação biogênica de CaCO_3 também libera CO_2 e reduz a alcalinidade total (A_T), o que configura a bomba contrária do carbonato (**Figure 1.3**; Rost & Riebesell, 2004).

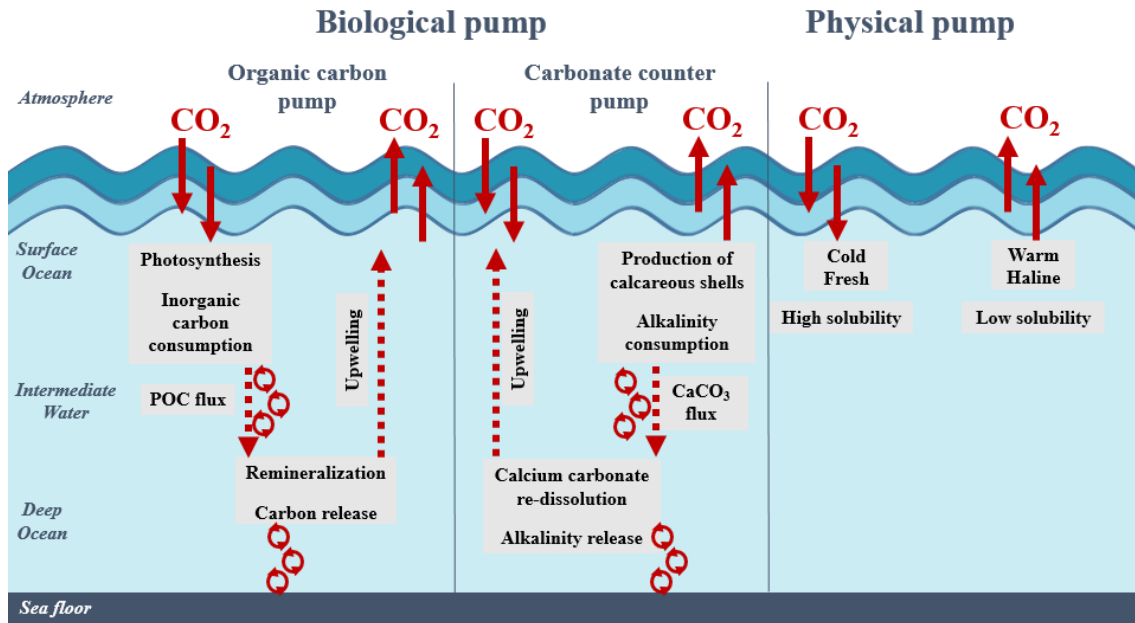


Figura 1.3. Figura esquemática da transferência de CO_2 na interface ar-mar. A captação pelos oceanos é dividida nas bombas biológica e físicas. A figura foi criada com base em Denman et al. (2007).

A bomba física refere-se à solubilidade e afundamento de CO_2 (Figura 1.3) dirigida por águas frias e menos salgadas. Os processos de formação de massa de água, essencialmente em áreas de alta latitude, agem sequestrando o carbono e outros gases dissolvidos para regiões mais profundas. Esses processos também ajudam a oxigenação de toda a coluna d'água, incluindo as águas central, intermediária, profunda e de fundo. As propriedades conservadoras adquiridas pelas massas de água durante seu processo de formação são preservadas durante toda a sua circulação nos oceanos, e somente mudam pelos processos internos de mistura das massas de água. Por outro lado, as propriedades não conservadoras das massas de água são ligeiramente modificadas de acordo com

processos biogeoquímicos que ocorrem durante sua trajetória de advecção (e.g., Orsi et al., 1999; Rintoul, 2011; Talley et al., 2011). As águas modais e intermediárias são formadas por subducção, que é indicado como o principal mecanismo de intrusão de C_{ant} nas camadas central e intermediária dos oceanos (**Figura 1.4**; Sabine et al., 2004; Pardo et al., 2014; Tanhua et al., 2016). O mesmo vale para as camadas profundas e de fundo, quando a água da superfície fica mais densa e se mistura com outras massas de água antes de afundar em níveis profundos pelo processo de convecção profunda (**Figura 1.4**), transportando assim o CO_2 e seus produtos de dissociação para o oceano profundo (e.g., Cox et al., 2000; Touratier et al., 2016).

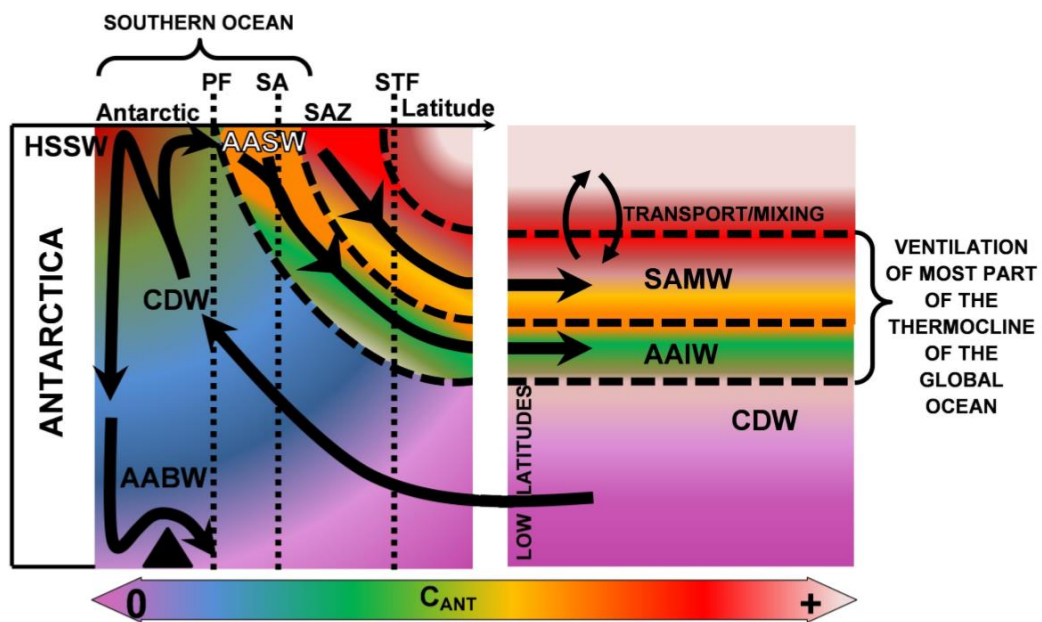


Figura 1.4. Fluxo esquemático das massas de água no Oceano Austral em uma seção meridional: High Saline Shelf Water (HSSW), Antarctic Surface Water (AASW), ressurgência da Circumpolar Deep Water (CDW), formação (por convecção profunda) de Antarctic Bottom Water (AABW), e formação (por subducção) da South Atlantic Mode Water (SAMW) e da Antarctic Intermediate Water (AAIW). As duas últimas massas de água ventilam as camadas central e intermediária dos oceanos, conforme indicado. As cores indicam o conteúdo de C_{ant} na coluna de água. De: Pardo et al. (2014).

Apesar de essas bombas agirem em ciclo fechado – já que a exportação de carbono e nutrientes na forma de material biogênico é equilibrada pela ressurgência de carbono

inorgânico e nutrientes – a absorção de C_{ant} é conhecida por ser governada principalmente por processos físico-químicos (Howes et al., 2015). Portanto, é importante destacar que uma simples adição de CO_2 no ambiente marinho não seria um problema se esse gás não reagir com a água. No entanto, a reação do CO_2 com a água leva a mudanças no sistema de carbonato marinho. Uma dessas consequências é o processo de acidificação do oceano, conhecido como "o outro problema de CO_2 " (Doney et al., 2009). Assim, é extremamente importante entender não apenas o FCO_2 e a absorção de C_{ant} pelos oceanos, mas também quantificar o estado de acidificação da água do mar que está ocorrendo e as respostas e sensibilidade dos ecossistemas marinhos à absorção de CO_2 . Essa investigação deve ser feita usando não apenas dados *in situ*, mas também através do uso de modelos oceânicos, climáticos e matemáticos (IPCC, 2013), produtos de reanálises e sensoriamento remoto (e.g., Balch & Utgoff, 2009).

Cada oceano responde às mudanças climáticas de diferentes maneiras (Figura 1.5), mas o Oceano Atlântico Sul está atualmente enfrentando alterações significativas, como aumento da temperatura da água do mar, salinidade e conteúdo de calor (e.g., Campos et al., 2015). Essas mudanças climáticas locais ou regionais levam a perturbações e alteram o ciclo hidrológico, as correntes oceânicas superficiais, a hidrodinâmica costeira e o sistema carbonato marinho, que impulsionam a transformação de ecossistemas e organismos marinhos sensíveis (e.g., Campos et al., 2015). O Oceano Atlântico Sul também desempenha um papel importante no ciclo do carbono, uma vez que suas regiões polares e subpolares são consideradas áreas de captação de CO_2 . Essas regiões são altamente dependentes da temperatura e atividade fitoplanctônica (Takahashi et al. 1997). Takahashi et al. (1997) estimou o FCO_2 em cerca de $-0.3 \text{ Pg C yr}^{-1}$, o que foi reforçado por Takahashi et al. (2002). Apesar de Takahashi et al. (2009) ter melhorado a compreensão do ciclo global de carbono, é importante destacar que a escassez de dados

do sistema carbonato marinho tem levado a relativamente poucos estudos sendo conduzidos no Oceano Atlântico Sul, quando comparados aos do Oceano Atlântico Norte. Além disso, [Takahashi et al. \(2009\)](#) menciona que não há dados suficientes para estimar taxas de fluxo decadais nessa região. Ademais, [Gruber et al. \(2019\)](#) recentemente demonstrou que o Oceano Atlântico Sul está passando por um aumento anômalo no inventário de C_{ant} .

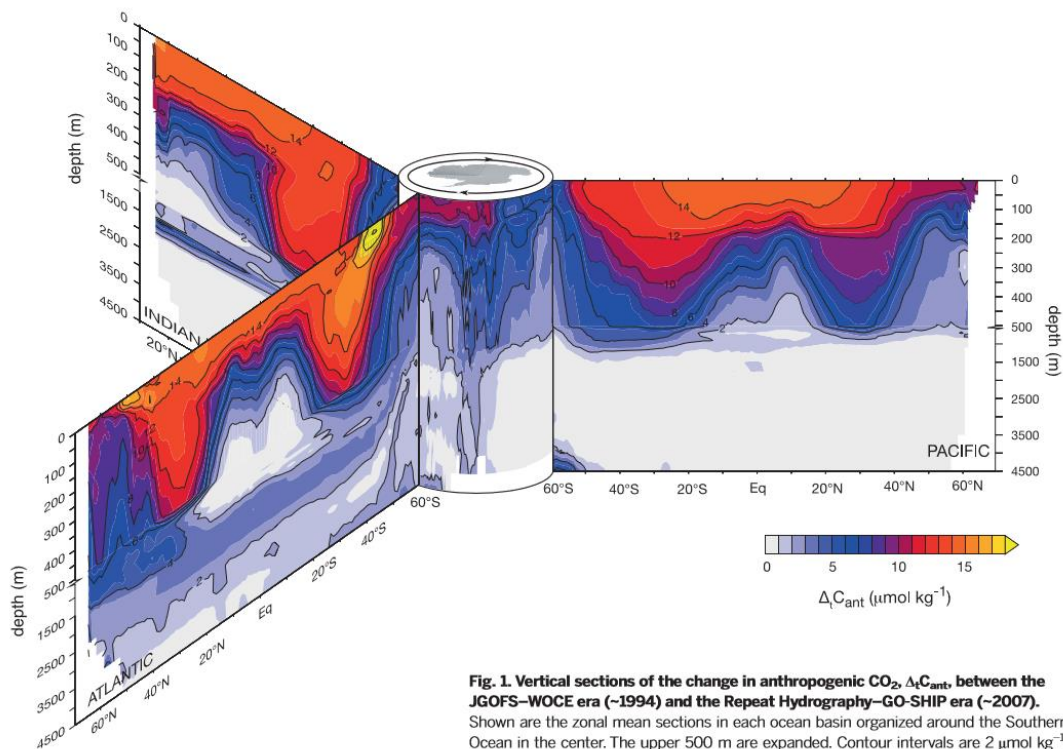


Figura 1.5. Conteúdo de C_{ant} em seções dos oceanos Atlântico, Índico e Pacífico. De: [Gruber et al. \(2019\)](#).

Portanto, para ter uma melhor visão geral do Oceano Atlântico Sul, a circulação da superfície e as massas de água apresentadas em toda a coluna de água desta bacia serão brevemente apresentadas a seguir. O Oceano Atlântico geralmente pode ser dividido em quatro camadas verticais: superfície à pycnoclina (termoclina subduzida – limite inferior: $\sigma \sim 26.2 \text{ kg m}^{-3}$, $\sim 200 \text{ m}$ – e termoclina inferior – limite inferior: $\sigma \sim 26.9 \text{ kg m}^{-3}$, $\sim 500/600 \text{ m}$), intermediária (limite inferior: $\sigma \sim 27.4 \text{ kg m}^{-3}$, $\sim 1200/1300 \text{ m}$), águas

profundas e de fundo (Talley et al., 2011). A circulação da superfície no Oceano Atlântico Sul é dominada por um giro anticiclônico subtropical fechado pelas seguintes correntes: Corrente do Brasil, Corrente do Atlântico Sul, Sistema da Corrente de Benguela e o ramo sul da Corrente Sul Equatorial (**Figura 1.6**). A Corrente do Brasil é a corrente de contorno oeste que flui em direção ao polo e transporta na superfície a “Tropical Water” (TW). O sistema de ressurgência é observado na fronteira leste, incluindo o Sistema de Correntes de Benguela que flui para o norte (**Figura 1.6**; e.g., Peterson & Stramma, 1991; Emery, 2003; Talley et al., 2011). Da mesma forma, fluindo em direções opostas no sistema zonal estão a Corrente do Atlântico Sul (leste) e o ramo sul da Corrente Sul Equatorial (oeste). Embora dominada por esse giro, a circulação da superfície do Oceano Atlântico Sul também é composta por um giro tropical e pela Corrente Circumpolar Antártica. As camadas central e intermediária são compostas pela South Atlantic Central Water (SACW) e pela Antarctic Intermediate Water (AAIW) (e.g., Hanawa & Talley, 2001; van Aken, 2007; Talley et al., 2011). Nas camadas profundas e de fundo, a North Atlantic Deep Water (NADW) e a Antarctic Bottom Water (AABW) são observados em ambos os lados do Oceano Atlântico Sul (e.g., Orsi et al., 1999; Talley et al., 2011), embora em diferentes proporções nas bacias abissais do Brasil e Angola (Ferreira & Kerr, 2017).

Tanto as águas superficiais, centrais e intermediárias encontradas na região podem ser influenciadas pelas águas do Oceano Índico (Souza et al., 2018), que entram na bacia do Atlântico através da região mais meridional do continente africano, pelo vazamento da corrente de Agulhas (e.g., Beal, 2009; Talley et al., 2011; Biastoch et al., 2015). Esse vazamento é inicialmente composto por filamentos que se desprendem do fluxo principal da Corrente das Agulhas, porém o conteúdo principal é composto pelos vórtices das Agulhas (Lutjeharms, 2006).

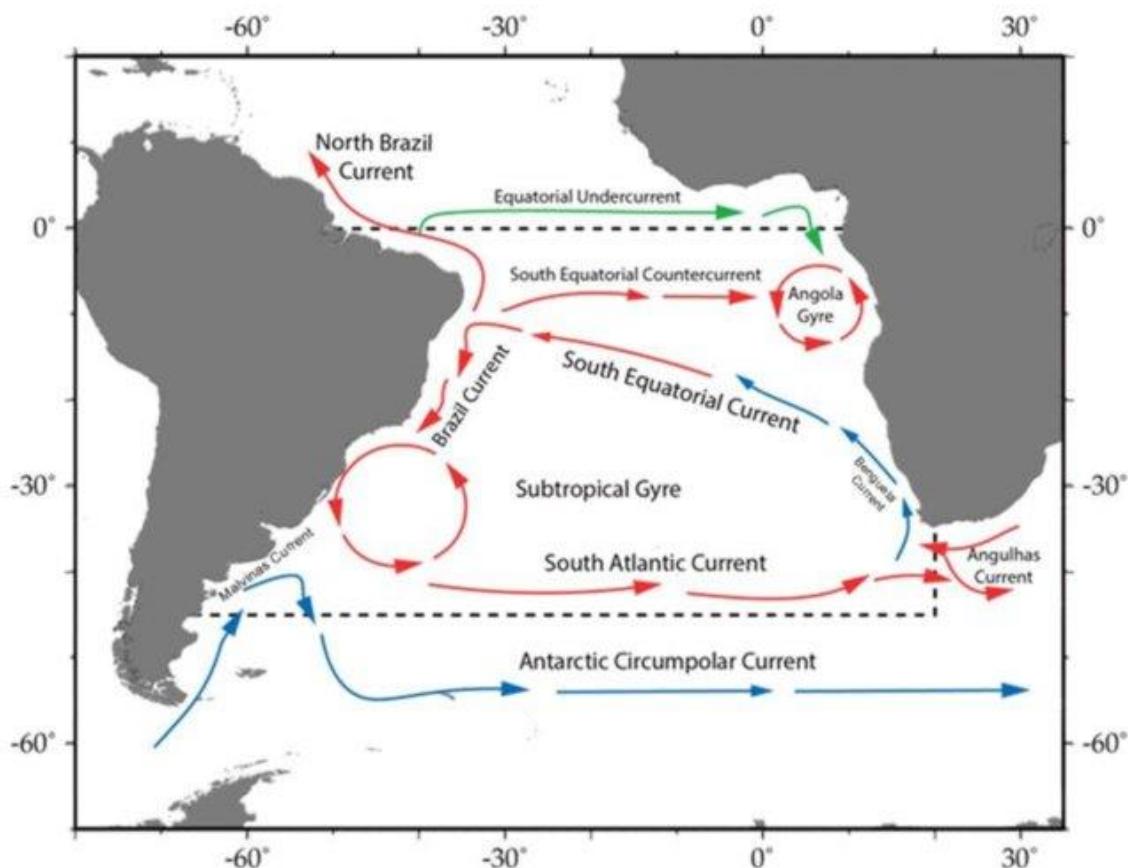


Figura 1.6. Circulação esquemática das principais correntes oceânicas na superfície do Oceano Atlântico Sul. As setas vermelhas indicam correntes de água quente e as setas azuis indicam correntes de água fria. Dirija-se a [O'Brien et al. \(2017\)](#) para mais detalhes sobre a circulação oceânica na região.

O papel do vazamento da corrente de Agulhas (vórtices e filamentos) na circulação meridional do Atlântico é considerado significativo em estudos anteriores (e.g., [Lutjeharms, 2006](#); [Biastoch et al., 2009, 2015](#)), principalmente pela advecção de sal ([Biastoch et al., 2009](#)) uma vez que é esperada a liberação de pelo menos seis vórtices por ano ([Gordon, 2003](#); [Lutjeharms, 2006](#)). A anomalia integrada da quantidade de sal acima da isoterma de 10°C dentro de um vórtice das Agulhas varia de $1,2$ a $13,1 \cdot 10^6$ kg, com um valor médio de $4,5 \cdot 10^6$ kg ([Lutjeharms, 2006](#)). A intrusão de águas superficiais a intermediárias do Oceano Índico transporta não apenas sal, mas também calor para o Atlântico Norte subpolar e subártico, onde contribui para a formação de águas profundas (e.g., [Beal, 2009](#); [Biastoch et al., 2015](#)). No entanto, a escala real desse papel ainda está

em debate (e.g., de Ruijter et al., 1999; Souza et al., 2011; Casanova-Masjoan et al., 2017; Souza et al., 2018).

Os vórtices das Agulhas são anticiclônicos, o que indica que no hemisfério sul sua rotação é no sentido anti-horário e apresenta centros de alta pressão, deslocando as isopneais para baixo (**Figura 1.7**; e.g., Azevedo & Mata, 2010). Eles são liberados na região de vazamento de Agulhas como vórtices anticiclônicos do tipo lente e sofrem modificações que induzem lentamente suas estruturas a se tornar vórtices do tipo não-lente ao longo de suas trajetórias pelo Oceano Atlântico Sul (**Figura 1.7**; Azevedo & Mata, 2010).

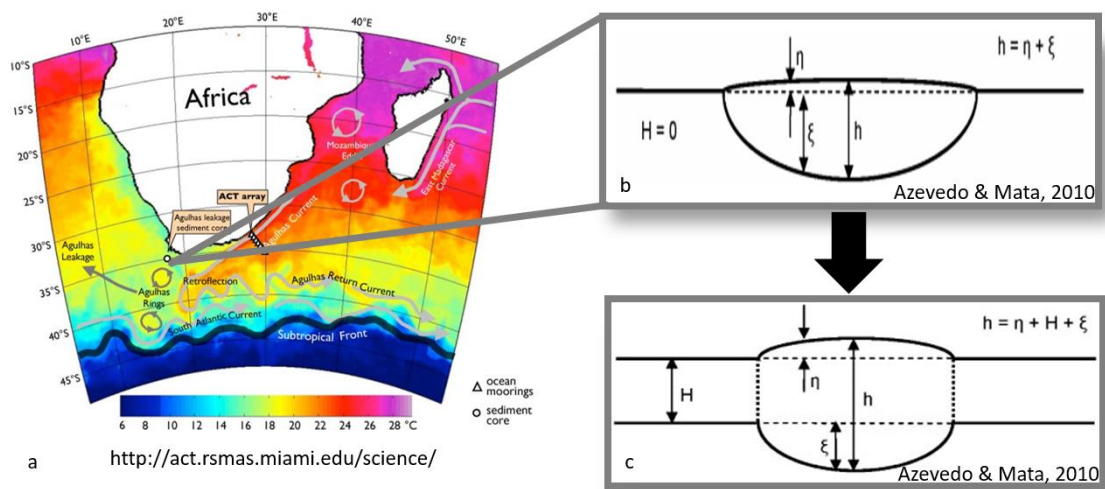


Figura 1.7. Representação esquemática dos vórtices das Agulhas. a) Mapa da temperatura da superfície do mar, indicando correntes oceânicas e vórtices das Agulhas em sua região de formação. De: <http://act.rsmas.miami.edu/science/>. b) Um vórtice anticiclônico do tipo lente, representando um vórtice das Agulhas assim que é liberado na região de vazamento das Agulhas. c) Um vórtice anticiclônico do tipo não-lente, representando uma estrutura de vórtice das Agulhas ao longo de sua trajetória pelo Oceano Atlântico Sul. Para os painéis b e c, cada letra representa: h , profundidade do vórtice; η anomalia de nível do mar causada pela presença do vórtice; ξ , deslocamento para baixo da termoclina; H altura do fluido carregado pelo movimento do vórtice. b e c de: Azevedo & Mata (2010).

Os vórtices das Agulhas são estruturas autopropulsionadas para oeste no Oceano Atlântico Sul como resultado do balanço meridional das forças que agem sobre eles. Os vórtices das Agulhas, como são estruturas de mesoscala, são forçadas a se deslocar para o equador devido à vorticidade induzida, enquanto as estruturas ciclônicas são forçadas a

se deslocar para os polos. Essa vorticidade induzida pode ocorrer devido a um efeito planetário ou mesmo a um efeito topográfico. O efeito topográfico também pode alterar a direção na qual o vórtice está se movendo. Além disso, outros vórtices ao redor podem influenciar um ao outro. O movimento dos vórtices é resultado desses quatro mecanismos atuando juntos. Normalmente, eles agem resultando em uma trajetória noroeste dos vórtices das Agulhas quando cruzam o Oceano Atlântico Sul (e.g., [Azevedo & Mata, 2010](#)). Sua velocidade de advecção é de alguns centímetros por segundo ($3-5 \text{ cm s}^{-1}$; [Lutjeharms, 2006](#)).

Os vórtices das Agulhas estão entre as maiores estruturas de mesoescala do oceano global ([Biaostoch et al., 2008](#)). Os vórtices das Agulhas têm uma escala horizontal de até 300 km, uma escala vertical de 1500 a 2000 m ([Biaostoch & Krauss, 1999](#)) ou mesmo mais (até 4000 m; e.g., [Beal, 2009](#)). Além disso, seu transporte de volume varia de 0,5 a 1,5 Sv ($1 \text{ Sv} \equiv 10^6 \text{ m}^3 \text{ s}^{-1}$). Outras estruturas de mesoescala têm uma escala temporal que pode variar de semanas a meses ([Chelton et al., 2011](#)), enquanto um vórtice das Agulhas tem uma duração estimada em mais de dois anos ([Lutjeharms, 2006](#)). Carregando também vorticidade potencial e propriedades biogeoquímicas de suas áreas de formação, os vórtices apresentam características distintas das águas ao redor (e.g., [Flierl, 1979](#)) e desempenham um papel importante nos processos físicos e biológicos (e.g., [Robinson, 1983](#); [Beal, 2009](#)).

Os vórtices também afetam os fluxos de calor entre oceano e atmosfera, a circulação da baixa atmosfera ([Lutjeharms, 2006](#); [Frenger et al., 2013](#)), e a biogeoquímica ([McGillicuddy, 2016](#); [Moreau et al., 2017](#)). Como os vórtices das Agulhas são estruturas anticiclônicas, [Villas Bôas et al. \(2015\)](#) associou-os a regiões com anomalias positivas no fluxo de calor, que tendem a aquecer a camada limite atmosférica (ou seja, regiões em que o oceano perde calor na atmosfera porque a água dentro deles é mais quente que as

águas circundantes). Dessa forma, mesmo admitindo que esses vórtices de mesoescala desempenhem um papel vital nas interações oceano-atmosfera, seu impacto nas mudanças do sistema do carbonato marinho ainda não é totalmente conhecido, principalmente considerando as trocas de CO₂ entre o oceano e atmosfera (e.g., [Ríos et al., 2003](#); [Woosley et al., 2016](#); [Moreau et al., 2017](#)).

Há evidências de que o vazamento de vórtices na região de retroflexão da Corrente de Agulhas aumentou devido a mudanças no sistema de ventos local ([Biastoch et al., 2009](#); [Beal et al., 2011](#)). Essas mudanças são: (i) o deslocamento para o sul da linha de rotacional nulo do vento e (ii) a intensificação dos ventos de oeste do hemisfério sul (**Figura 1.8**), que é conhecida como a expansão para o sul dos ventos de oeste do Hemisfério Sul (e.g., [Beal et al., 2011](#)). Há também sugestões sobre o aumento do vazamento devido a um deslocamento para o sul de todo o giro, não apenas da linha de rotacional nulo do vento (e.g., [Oliveira, 2017](#)). A forçante antropogênica das mudanças climáticas (isto é, o aquecimento global) causou essas alterações. Esse processo resulta no aquecimento do oceano e na salinificação da bacia do Oceano Atlântico Sul (e.g., [Bard et al., 2009](#); [Biastoch et al. 2009](#); [Beal et al., 2011](#)).

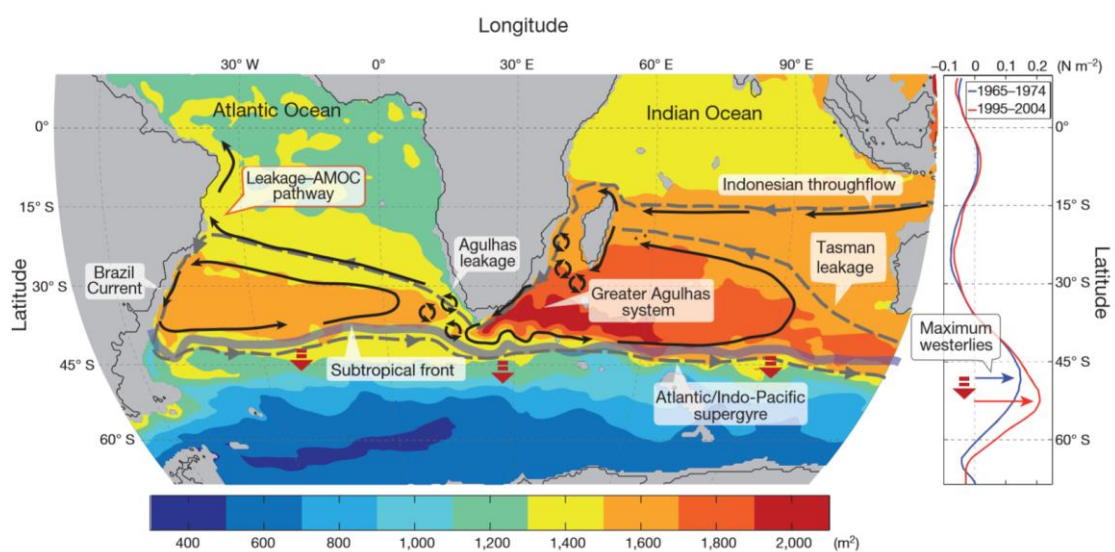


Figura 1.8. A representação do vazamento das Agulhas sendo afetado pelo deslocamento para o sul da Frente Subtropical, causado pela expansão em direção ao sul dos ventos de oeste em um período de 30 anos. De: [Beal et al. \(2011\)](#).

Além disso, o estudo recente desenvolvido por [Souza et al. \(2018\)](#) observou que a contribuição das águas modais do Oceano Índico pode influenciar consideravelmente as propriedades da SACW na bacia do Oceano Atlântico Sul. Esta afirmação é reforçada considerando o aumento no número de vórtices liberados na região de retroflexão de Agulhas ([Biaostoch et al., 2009](#)). Os vórtices das Agulhas transportam águas modais, que são marcadas pelas seguintes características: camadas de termocline e halocline (ou seja, faixas estáveis de temperatura e salinidade, respectivamente) e baixa vorticidade potencial. As águas modais são formadas principalmente durante o inverno após intensa mistura nas camadas superficiais e afundamento entre as termoclinas sazonal e permanente. Essas águas modais são águas-fonte que são posteriormente advectadas e compõem as águas centrais dos oceanos (e.g., SACW). Assim, à medida que a formação da água modal é intensificada quando o fluxo de calor aumenta (e.g., [Hanawa & Talley, 2001](#)), é esperado um fortalecimento dos processos de formação das águas modais, já que os vórtices das Agulhas são capazes de intensificar o fluxo de calor ([Villas Bôas et al., 2015](#)). Três variedades da Subtropical Mode Water (marcadas por faixas distintas de temperaturas, dependendo da área de origem considerada) compõem a camada central do Oceano Atlântico Sul, i.e. a camada ocupada pela SACW. A camada da SACW também é influenciada pelas contribuições de Indian Ocean Mode Water ([Sato & Polito, 2014](#); [Souza et al., 2018](#)).

Estudos recentes concluíram que as águas centrais (e.g., representadas pela SACW no Oceano Atlântico Sul) estão entre as mais afetadas pela captação de C_{ant} ([Salt et al., 2015](#); [Carvalho-Borges et al., 2018](#); [Orselli et al., 2018](#)). Isso mudou a ideia anterior sobre a entrada principal de C_{ant} nos oceanos da formação de águas profundas (processo de convecção profunda) para a formação de águas centrais e intermediárias (processo de

subducção). Estes estudos sobre a absorção de C_{ant} indicaram que ela está levando a uma taxa de acidificação (i.e., alteração do pH) de -0.0016 yr^{-1} até -0.0018 yr^{-1} na SACW desde o período pré-industrial (Salt et al., 2015; Carvalho-Borges et al., 2018; Orselli et al., 2018). Essas tendências indicam que a SACW está acidificando mais rapidamente do que as águas imediatamente acima e abaixo dela, porque são mais altas do que as já observadas para essas outras camadas oceânicas: e.g., -0.0013 yr^{-1} para águas superficiais e -0.0010 yr^{-1} na camada intermediária, para a AAIW. As alterações do pH observadas no Oceano Atlântico Sul para as camadas profunda e de fundo são menores que todas as outras camadas, conforme o esperado. Essas mudanças são $-0.0010/-0.0000 \text{ yr}^{-1}$ para as camadas superior e inferior da CDW, $-0.0005/-0.0000 \text{ yr}^{-1}$ para as camadas superior e inferior da NADW, e -0.0000 yr^{-1} para a AABW (e.g., Salt et al., 2015; Kitidis et al., 2017; Orselli et al., 2018). Além disso, um estudo recente apresentou alguns resultados indicando que os vórtices das Agulhas são propensos a transportar mais C_{ant} do que as águas ao redor (Woosley et al., 2016). Nesta pesquisa, os autores não concentraram suas investigações na quantificação de C_{ant} diretamente nos vórtices, sugerindo a necessidade de estudos sobre esse tema.

Nesse contexto, o desenvolvimento desta tese foi motivado pelos fatos de que: (i) os vórtices das Agulhas transportam águas desde superficiais a intermediárias do Oceano Índico ao Oceano Atlântico Sul (Beal et al., 2009; Biastoch et al. 2009), (ii) essas estruturas são propensas a fortalecer o processo de formação de águas modais e (iii) uma maior acidificação está ocorrendo nas camadas centrais do Oceano Atlântico Sul, em detrimento às outras camadas. Assim, considerando a novidade sobre o tema, este estudo apresenta uma investigação sobre o papel dos vórtices das Agulhas na biogeoquímica oceânica, o que ainda é um desafio adicional a ser investigado (e.g., Ríos et al., 2003; Moreau et al., 2017). Finalmente, espera-se que os resultados deste estudo contribuam

ainda mais para a discussão científica dos impactos dos vórtices das Agulhas nas mudanças no sistema carbonato marinho.

1.3 Introduction: version en français

Une composante humaine est fondamentale pour expliquer les changements dans le système climatique de la Terre (e.g., le réchauffement de l'océan et de l'atmosphère, la fonte des glaciers; e.g., [IPCC 2007](#); [Campos et al., 2015](#)). Cette affirmation est renforcée par le fait que les forçages radiatifs en raison du dioxyde de carbone (CO₂), du méthane (CH₄) et de l'oxyde nitreux (N₂O) sont sans précédent depuis plus de 800000 ans ([IPCC 2007, 2013](#)). Ces importants gaz à effet de serre à longue durée de vie sont libérés dans l'atmosphère par l'activité humaine avec une augmentation significative depuis le début de la révolution industrielle (**Figure 1.1**; e.g., [Ciais et al., 2013](#); [Le Quéré et al., 2016](#)).

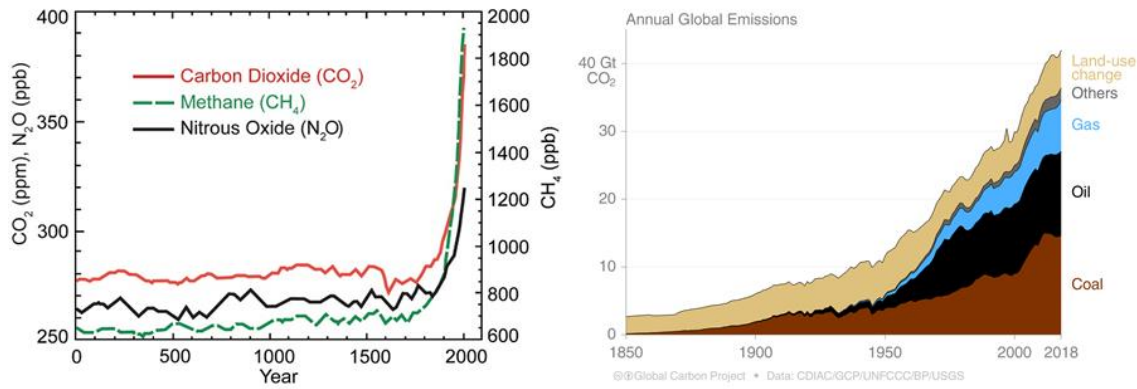


Figure 1.1. Panneau gauche: concentrations de dioxyde de carbone (CO₂, ligne rouge; ppm), méthane (CH₄, ligne verte; ppb) et de l'oxyde nitreux (N₂O, ligne noire; ppb) dans l'atmosphère au cours des 2000 dernières années (IPCC 2007). Panneau droite: émissions mondiales annuelles de CO₂ depuis la révolution industrielle selon la source (Global Carbon Project).

Les émissions de CO₂ qui sont en augmentation constante (**Figure 1.2; Tans e Keeling, 2013**) poussent au développement de projets d'études du système du carbone dans l'océan. Cette nécessité est encouragée principalement en raison de la capacité des océans à absorber une énorme quantité de CO₂ libéré dans l'atmosphère par les activités humaines (e.g., lors de la combustion de combustibles fossiles, production de ciment; **Millero, 2007; Doney et al., 2009**). Certains résultats ont montré que les océans ont déjà absorbé environ 20 à 40% du carbone anthropique³ (C_{ant}) libéré au cours des 200 dernières années (e.g., **Sabine et al., 2004; Ciais et al., 2013; Khatiwala et al., 2013; Gruber et al., 2019**). Le Groupe d'experts intergouvernemental sur l'évolution du climat (Intergovernmental Panel on Climate Change, IPCC) considère qu'une valeur moyenne de 30% de C_{ant} est absorbée par l'océan mondial (**IPCC, 2013**). Cependant, le stockage de C_{ant} dans les couches océaniques n'est pas encore clair car la circulation océanique a une énorme importance dans sa redistribution autour de l'océan mondial. Par conséquent, il est extrêmement important de mieux comprendre les questions scientifiques liées : (i) aux flux de CO₂ à travers l'interface air-mer (FCO₂)— pour comprendre comment l'absorption

³ Le carbone anthropique est le CO₂ libéré dans l'atmosphère par l'activité humaine (e.g., lors de la combustion de combustibles fossiles, production de ciment; **Ciais et al., 2013**).

s'effectue—; (ii) à la distribution du C_{ant} — pour comprendre où ce C_{ant} est stocké —; (iii) aux conséquences pour les organismes marins et les écosystèmes; et (iv) à tout le cycle du carbone, afin d'élaborer des politiques publiques et de réaliser des projections climatiques futures (Le Quéré et al., 2013; Newton et al., 2015).

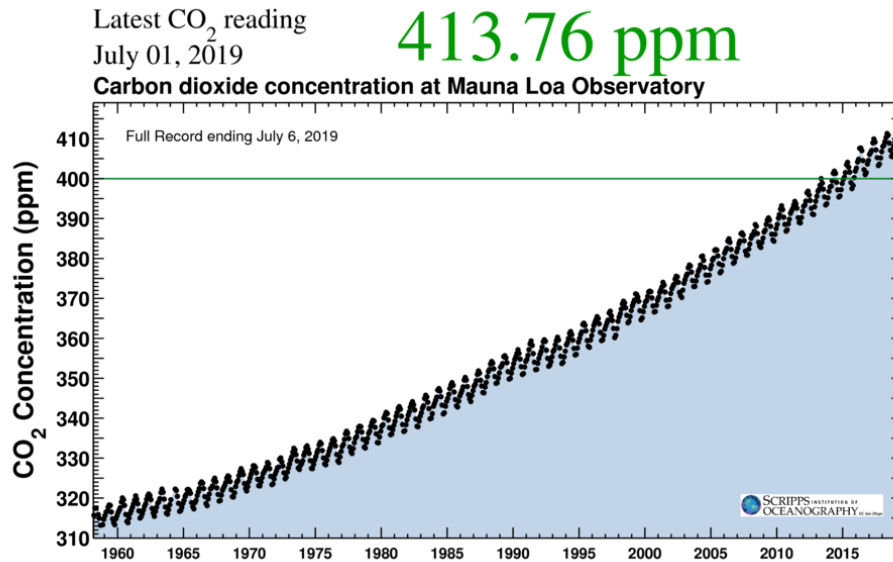


Figure 1.2. Enregistrement complet de la concentration de dioxyde de carbone (CO_2) dans l'atmosphère à l'Observatoire du Mauna Loa (courbe de Keeling). La ligne continue verte indique la ligne de base de 400 ppm. De : <https://scripps.ucsd.edu/programs/keelingcurve/>

De cette façon, deux mécanismes principaux peuvent décrire comment le CO_2 est absorbé par les océans : les pompes biologiques et physiques (**Figure 1.3**). La première peut être divisée en pompe à carbone organique et contre-pompe à carbonate (e.g., Denman et al., 2007; Ciais et al., 2013). La pompe à carbone organique démarre lorsque les organismes phytoplanctoniques commencent le processus de photosynthèse, qui est la première étape pour convertir le carbone inorganique en carbone organique particulaire. Le carbone produit lors de ce processus est reminéralisé dans la colonne d'eau et/ou transporté au fond de l'océan via des produits d'excrétion ou de dégénérescence. De plus, le carbonate de calcium (CaCO_3) formé par la dissolution du CO_2 est également utilisé par les organismes pour construire leurs coquilles calcaires (e.g., Cox et al., 2000). La

formation biogène du CaCO_3 libère également du CO_2 et réduit l'alcalinité totale (A_T), ce qui configure la contre-pompe à carbonate (**Figure 1.3**; Rost & Riebesell, 2004).

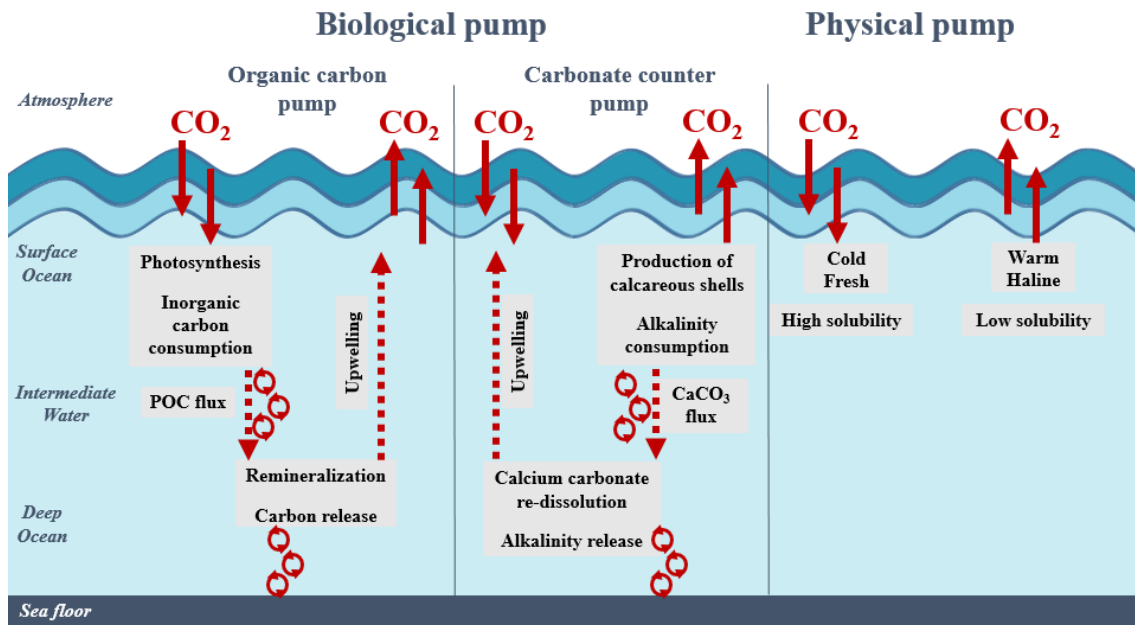


Figure 1.3 Figure schématique de l'échange air-mer de CO_2 . L'absorption par les océans est divisée en pompes biologiques et physiques. La figure a été créée sur la base de Denman et al. (2007).

La pompe physique fait référence à la solubilité et la pénétration (**Figure 1.3**) du CO_2 dans l'eau de mer. Elle est plus efficace dans les eaux froides et peu salées. Les processus de formation d'une masse d'eau, essentiellement dans les régions de haute latitude, agissent en séquestrant le carbone et d'autres gaz dissous en profondeur. Ces processus contribuent également à l'oxygénation de toute la colonne d'eau, y compris des eaux centrales, intermédiaires, profondes et de fond. Les propriétés conservatrices acquises par les masses d'eau au cours de leur processus de formation sont préservées tout au long de leur circulation à l'intérieur des océans et ne changent que par les processus de mélange interne des masses d'eau. Par contre, les propriétés non conservatrices des masses d'eau sont légèrement modifiées en fonction des processus biogéochimiques qui se produisent au cours de leur trajectoire d'advection (e.g., Orsi et al., 1999; Rintoul, 2011;

Talley et al., 2011). Les eaux ‘mode’ et ‘intermédiaires’ sont formées par subduction, ce qui est indiqué comme le principal mécanisme d'intrusion de C_{ant} dans les couches océaniques centrales et intermédiaires (**Figure 1.4**; Sabine et al., 2004; Pardo et al., 2014; Tanhua et al., 2016). Il en va de même pour les couches profondes et inférieures, lorsque l'eau de surface devient plus dense et se mélange avec d'autres masses d'eau avant de descendre à des niveaux profonds par le processus de convection profonde (**Figure 1.4**), transportant ainsi du CO_2 et ses produits de dissociation dans l'océan profond (e.g., Cox et al., 2000; Touratier et al., 2016).

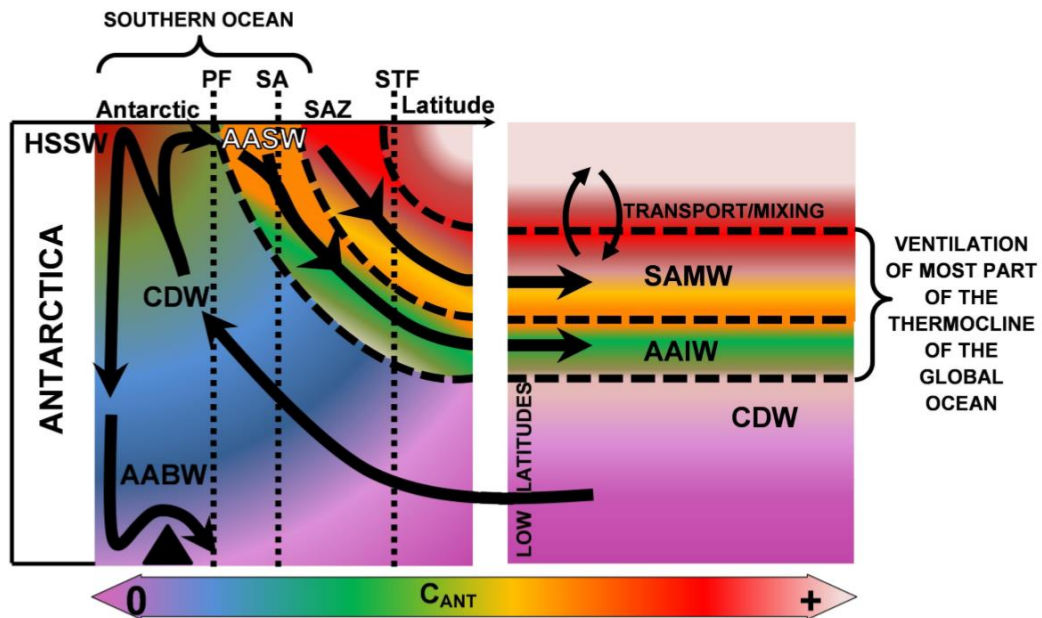


Figure 1.4. Flux schématiques des masses d'eau dans l'océan Austral dans une section méridionale : High Saline Shelf Water (HSSW), Antarctic Surface Water (AASW), remontée de Circumpolar Deep Water (CDW), formation (par convection profonde) de Antarctic Bottom Water (AABW), et formation (par subduction) de South Atlantic Mode Water (SAMW) et Antarctic Intermediate Water (AAIW). Les deux dernières masses d'eau ventilent la couche centrale et intermédiaire des océans, comme indiqué. Les couleurs indiquent le contenu C_{ant} dans la colonne d'eau. De : Pardo et al. (2014).

Bien que ces pompes agissent en circuit fermé – car l'exportation de carbone et de nutriments dans les matières biogéniques est équilibrée par le carbone inorganique et la résurgence des nutriments – l'absorption de C_{ant} est connue pour être régie principalement

par des processus physico-chimiques (Howes et al., 2015). De plus, il est important de souligner qu'un simple ajout de CO₂ dans le milieu marin ne serait pas un problème si ce gaz ne réagissait pas avec l'eau. Cependant, la réaction du CO₂ avec l'eau entraîne des changements dans le système de carbonate marin et en particulier acidifie les océans, ce qui est reconnu comme «l'autre problème du CO₂» (Doney et al., 2009). Ainsi, il est extrêmement important de comprendre non seulement le FCO₂ et l'absorption de C_{ant} par les océans, mais aussi de quantifier l'état d'acidification de l'eau de mer qui se produit ainsi que les réponses et la sensibilité des écosystèmes marins à l'absorption de CO₂. Cette recherche devrait être effectuée en utilisant non seulement des données *in situ*, mais aussi en utilisant des modèles océaniques et climatiques (IPCC, 2013), ainsi que des produits de la télédétection (e.g., Balch & Utgoff, 2009).

Chaque océan réagit aux changements climatiques de différente manière (Figure 1.5), mais l'océan Atlantique Sud est actuellement confronté à des modifications importantes, telles que l'augmentation de la température de l'eau de mer, et de la salinité (e.g., Campos et al., 2015). Ces changements climatiques locaux ou régionaux entraînent des perturbations et altèrent le cycle hydrologique, les courants océaniques de surface, l'hydrodynamique côtière et le système de carbonate marin, qui entraînent la transformation des écosystèmes et des organismes marins (e.g., Campos et al., 2015). L'océan Atlantique Sud joue également un rôle important dans le cycle du carbone, car ses régions polaires et subpolaires sont considérées comme des zones de captage de CO₂. Ils dépendent fortement de la température et de l'activité phytoplanctonique (Takahashi et al. 1997). Takahashi et al. (1997) et Takahashi et al. (2002) ont estimé que le FCO₂ moyen qui pénètre dans les océans est d'environ $-0.3 \text{ Pg C yr}^{-1}$. Bien que Takahashi et al. (2009) ont amélioré la compréhension du cycle mondial du carbone, il est important de souligner la pauvreté des données du système des carbonates dans l'océan Atlantique

Sud par rapport à l'océan Atlantique Nord. De plus, [Takahashi et al. \(2009\)](#) indiquent qu'il n'y a pas suffisamment de données pour estimer les variations décennales de ce flux dans cette région. Aussi, [Gruber et al. \(2019\)](#) a récemment démontré que l'océan Atlantique Sud subit une augmentation anormale de l'inventaire Cant.

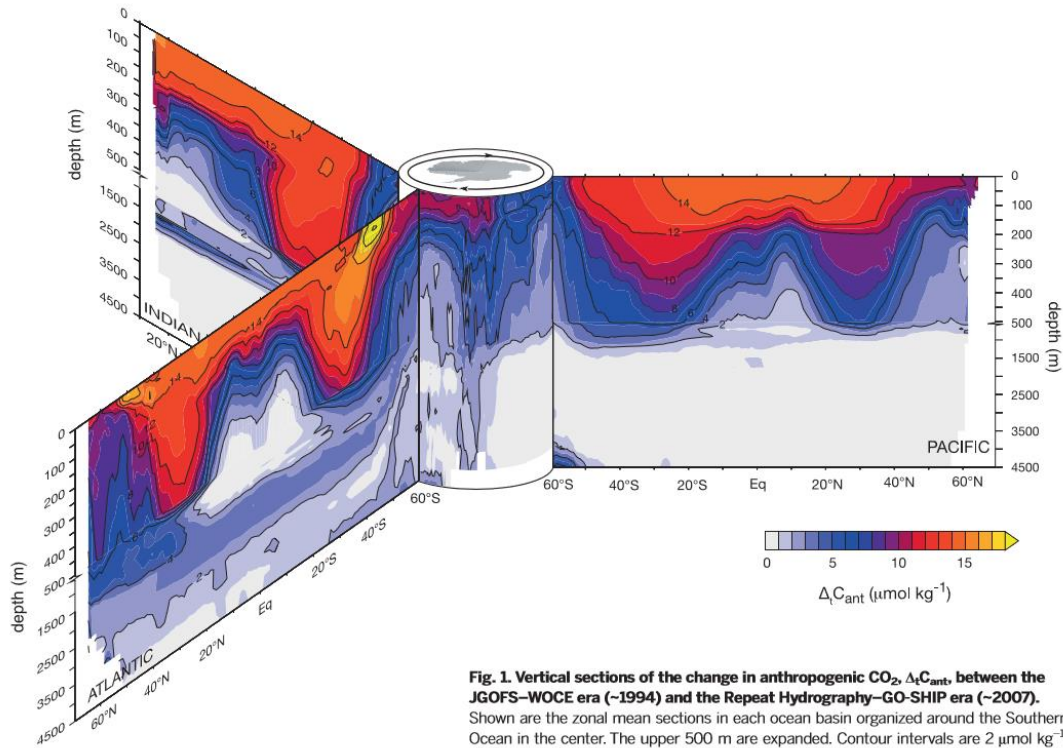


Fig. 1. Vertical sections of the change in anthropogenic CO_2 , ΔC_{ant} , between the JGOFS–WOCE era (~1994) and the Repeat Hydrography–GO-SHIP era (~2007). Shown are the zonal mean sections in each ocean basin organized around the Southern Ocean in the center. The upper 500 m are expanded. Contour intervals are $2 \mu\text{mol kg}^{-1}$.

Figure 1.5. C_{ant} contenu dans des sections des océans Atlantique, Indien et Pacifique. De : [Gruber et al. \(2019\)](#).

Ainsi, pour avoir une meilleure vue d'ensemble de l'océan Atlantique Sud, la circulation de surface et les masses d'eau présentées dans toute la colonne d'eau de ce bassin sont brièvement présentées ci-dessous. L'océan Atlantique peut généralement être divisé en quatre couches verticales: de la surface à la pycnocline (thermocline subductée – limite inférieure : $\sigma \sim 26.2 \text{ kg m}^{-3}$, $\sim 200 \text{ m}$ – et thermocline inférieure – limite inférieure : $\sigma \sim 26.9 \text{ kg m}^{-3}$, $\sim 500/600 \text{ m}$), intermédiaire (limite inférieure : $\sigma \sim 27.4 \text{ kg m}^{-3}$, $\sim 1200/1300 \text{ m}$), eaux profondes et abyssales ([Talley et al., 2011](#)). La circulation de surface dans l'océan Atlantique Sud est dominée par un gyre anticyclonique subtropical

fermé par les courants suivants : courant du Brésil, courant de l'Atlantique Sud, système du courant de Bengale et branche sud du courant équatorial (**Figure 1.6**). Le courant du Brésil est le courant de la frontière ouest circulant vers le pôle et transportant à la surface l'eau tropicale « Tropical Water (TW) ». Le système de résurgence est observé dans la limite orientale, y compris le système du courant de Bengale qui coule vers le nord (**Figure 1.6**; e.g., [Peterson & Stramma, 1991](#); [Emery, 2003](#); [Talley et al., 2011](#)). De la même manière, le courant de l'Atlantique Sud (vers l'est) et la branche sud du courant équatorial (vers l'ouest) circulent dans des directions opposées dans le système zonal. Bien que dominée par ce gyre, la circulation de surface de l'océan Atlantique Sud est également composée d'un gyre tropical et du courant circumpolaire antarctique. Les couches centrales et intermédiaires sont composées par l'eau centrale de l'atlantique sud (South Atlantic Central Water, SACW) et l'eau antarctique intermédiaire (Antarctic Intermediate Water, AAIW) (e.g., [Hanawa & Talley, 2001](#); [van Aken, 2007](#); [Talley et al., 2011](#)). Dans les couches profondes et inférieures l'eau profonde de l'atlantique nord (North Atlantic Deep Water, NADW) et l'eau de fond antarctique (Antarctic Bottom Water, AABW) sont observés des deux côtés de l'océan Atlantique Sud (e.g., [Orsi et al., 1999](#); [Talley et al., 2011](#)), bien que dans des proportions différentes dans les bassins abyssaux du Brésil et de l'Angola ([Ferreira & Kerr, 2017](#)).

Les eaux de surface, centrales et intermédiaires de la région peuvent être influencées par les eaux de l'océan Indien ([Souza et al., 2018](#)), qui pénètrent dans le bassin atlantique par la région la plus méridionale du continent africain, par le prolongement du courant des Aiguilles (e.g., [Beal, 2009](#); [Talley et al., 2011](#); [Biastoch et al., 2015](#)). Ce prolongement est principalement composé de filaments détachés du flux principal du courant des Aiguilles, mais le contenu principal est composé par les tourbillons des Aiguilles ([Lutjeharms, 2006](#)).

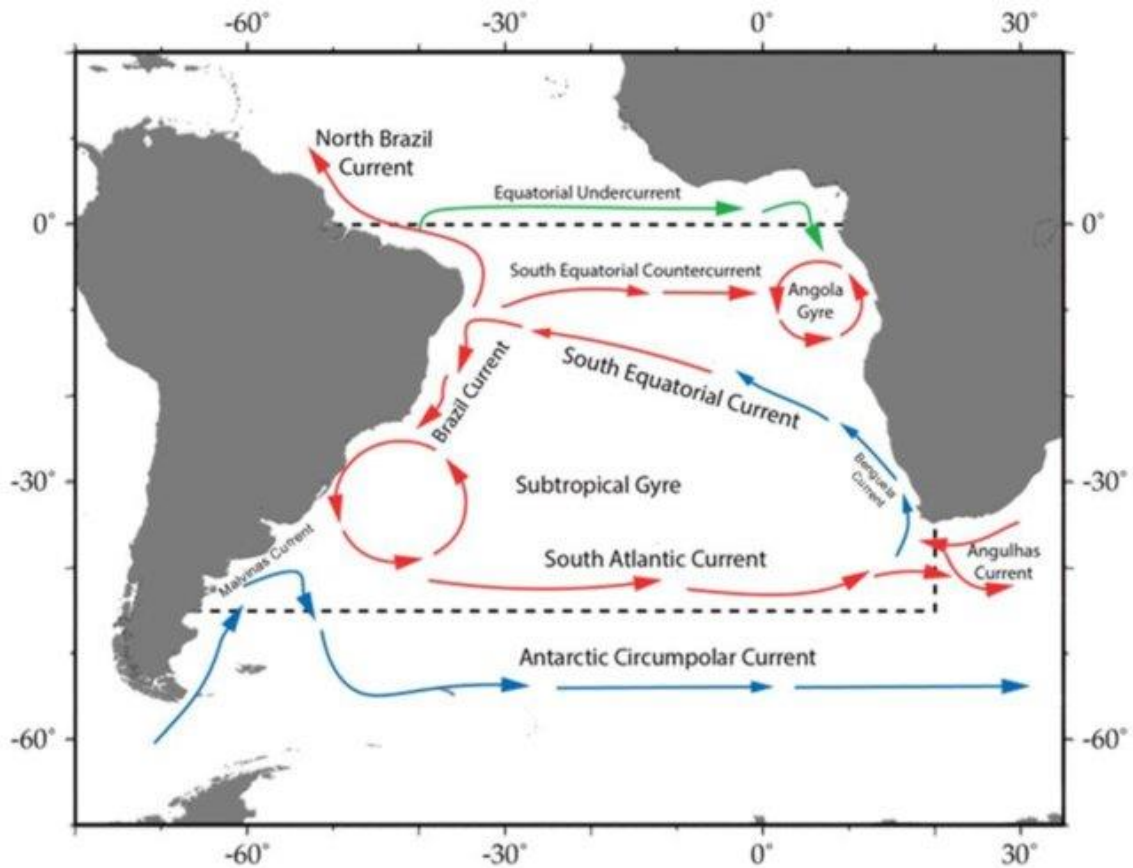


Figure 1.6. Circulation schématique des principaux courants océaniques à la surface de l'océan Atlantique Sud. Les flèches rouges indiquent les courants d'eau chaude et les flèches bleues indiquent les courants d'eau froide. Veuillez consulter [O'Brien et al \(2017\)](#) pour plus de détails sur la circulation océanique dans la région.

Le rôle des prolongements du courant des Aiguilles (tourbillons et filaments) dans la circulation de renversement méridional de l'Atlantique est considéré comme significatif dans les études précédentes (e.g., [Lutjeharms, 2006](#); [Biaostoch et al., 2009, 2015](#)), principalement par advection de sel ([Biaostoch et al., 2009](#)) étant donné que l'élimination d'au moins six tourbillons par an est attendue ([Gordon, 2003](#); [Lutjeharms, 2006](#)). L'anomalie intégrée de la teneur en sel au-dessus de l'isotherme $10\text{ }^{\circ}\text{C}$ à l'intérieur d'un tourbillon des Aiguilles varie de $1,2$ à $13,1 \cdot 10^6$ kg, avec une valeur moyenne de $4,5 \cdot 10^6$ kg ([Lutjeharms, 2006](#)). L'intrusion des eaux de surface à intermédiaires de l'océan Indien transporte non seulement du sel, mais aussi de la chaleur vers l'Atlantique Nord subpolaire

et subarctique, où il contribue à la formation des eaux profondes (e.g., [Beal, 2009](#); [Bjastoch et al., 2015](#)). Cependant, l'ampleur réelle de ce rôle fait toujours débat (e.g., [de Ruijter et al., 1999](#); [Souza et al., 2011](#); [Casanova-Masjoan et al., 2017](#); [Souza et al., 2018](#)).

Les tourbillons des Aiguilles sont anticycloniques, ce qui indique que dans l'hémisphère sud leur rotation est dans le sens antihoraire et présente des centres de haute pression, déplaçant les isopycnaux vers le bas (**Figure 1.7**; e.g., [Azevedo & Mata, 2010](#)). Ils sont libérés dans la région de prolongement des Aiguilles sous forme de tourbillons anticycloniques de type « lens » et subissent des modifications qui induisent lentement leurs structures à devenir des tourbillons anticycloniques de type « non-lens » au long de leurs trajectoires à travers l'océan Atlantique Sud (**Figure 1.7**; [Azevedo & Mata, 2010](#)).

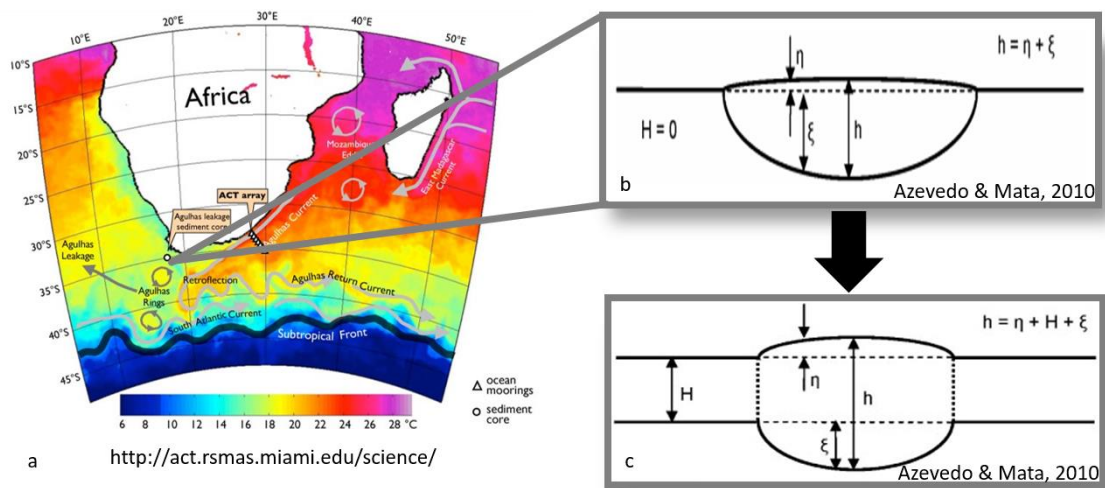


Figure 1.7. Représentation schématique des tourbillons des Aiguilles. a) Carte des températures de la surface de la mer, indiquant les courants océaniques et les tourbillons d'Aiguilles dans leur région de formation. De: <http://act.rsmas.miami.edu/science/>. b) Un tourbillons anticycloniques de type « lens », représentant une structure de tourbillon des Aiguilles dès qu'il est libéré dans la région de prolongement des Aiguilles. c) Un tourbillons anticycloniques de type « non-lens », représentant une structure de tourbillon des Aiguilles le long de sa trajectoire à travers l'océan Atlantique Sud. Pour les panneaux b et c, chaque lettre représente : h , profondeur du tourbillon; η anomalie du niveau de la mer causée par la présence du tourbillon; ξ , déplacement vers le bas de la thermocline; H hauteur du fluide porté par le mouvement des tourbillons. b et c de : [Azevedo & Mata \(2010\)](#).

Les caractéristiques des tourbillons des Aiguilles sont automotrices vers l'ouest dans l'océan Atlantique Sud en raison de l'équilibre méridien des forces qui agissent sur

ces tourbillons. Car les tourbillons des Aiguilles sont des structures anticycloniques à méso-échelle, ils sont forcés à dériver vers l'équateur en raison du tourbillon induit (induced vorticity), tandis que les structures cycloniques sont forcées à dériver vers les pôles. Ce tourbillon induit (induced vorticity) peut se produire en raison d'un effet planétaire ou même d'un effet topographique. L'effet topographique peut également changer la direction dans laquelle le tourbillon se déplace. De plus, d'autres tourbillons peuvent s'influencer les uns les autres. Le mouvement des tourbillons est le résultat de ces quatre mécanismes agissant ensemble. Normalement, ils agissent entraînant une trajectoire nord-ouest des tourbillons des Aiguilles lorsqu'ils traversent l'océan Atlantique Sud (e.g., [Azevedo & Mata, 2010](#)). Leur vitesse d'advection est de l'ordre de quelques centimètres par seconde (3-5 cm s⁻¹; [Lutjeharms, 2006](#)).

Les tourbillons des Aiguilles sont parmi les plus grandes structures à méso-échelle de l'océan mondial ([Biaostoch et al., 2008](#)). Les tourbillons des Aiguilles ont une échelle horizontale allant jusqu'à 300 km, et une échelle verticale allant de 1500 à 2000 m ([Biaostoch & Krauss, 1999](#)) ou même plus (jusqu'à 4000 m; e.g., [Beal, 2009](#)). De plus, leur transport en volume varie de 0,5 à 1,5Sv (1 Sv $\equiv 10^6$ m³ s⁻¹). D'autres tourbillons à méso-échelle ont une échelle temporelle qui peut varier de quelques semaines à plusieurs mois ([Chelton et al., 2011](#)), alors qu'un tourbillon des Aiguilles a une durée de vie estimée à plus de deux ans ([Lutjeharms, 2006](#)). Portant également des propriétés potentielles de tourbillon (potential vorticity) et biogéochimiques de leurs zones de formation, les tourbillons présentent des caractéristiques distinctes des eaux environnantes (e.g., [Flierl, 1979](#)) et jouent un rôle majeur dans les processus physiques et biologiques (e.g., [Robinson, 1983](#); [Beal, 2009](#)).

Les tourbillons ont également un impact sur les flux de chaleur à travers l'interface air-mer, la circulation de l'atmosphère superposée ([Lutjeharms, 2006](#); [Frenger et al.,](#)

2013), et biogéochimie (McGillicuddy, 2016; Moreau et al., 2017). Puisque les tourbillons des Aiguilles sont des structures anticycloniques, Villas Bôas et al. (2015) les ont associés à des régions présentant des anomalies de flux de chaleur positives, qui ont tendance à réchauffer la couche limite atmosphérique (i.e., les régions où l'océan perd de la chaleur vers l'atmosphère parce que l'eau à l'intérieur est plus chaude que les eaux environnantes). Ainsi, même en admettant que ces tourbillons à méso-échelle jouent un rôle vital sur les interactions océan-atmosphère, leur impact sur les changements du système du carbone marin n'est pas encore contraint, compte tenu notamment des échanges mer-air de (e.g., Ríos et al., 2003; Woosley et al., 2016; Moreau et al., 2017).

Il existe des preuves que les prolongements dans la région de réflexion du courant d'Aiguilles ont augmentées en raison de changements dans le système éolien local (Biaostoch et al., 2009; Beal et al., 2011). Ces changements sont: (i) le déplacement vers le sud de la ligne zéro de la boucle de contrainte du vent (wind stress curl) et (ii) l'intensification des vents d'ouest de l'hémisphère sud (**Figure 1.8**), qui est connu comme l'expansion vers le sud des vents d'ouest de l'hémisphère sud (e.g., Beal et al., 2011). Il existe également des suggestions concernant l'augmentation des fuites en raison d'un déplacement vers le sud de l'ensemble du gyre anticyclonique subtropical, non seulement de la ligne zéro de la boucle de contrainte du vent (e.g., Oliveira, 2017). Le forçage anthropique sur les changements climatiques (i.e., le réchauffement climatique) a provoqué ces changements. Ce processus se traduit par un réchauffement océanique et une salinisation du bassin de l'océan Atlantique Sud (e.g., Bard et al., 2009; Biaostoch et al. 2009; Beal et al., 2011).

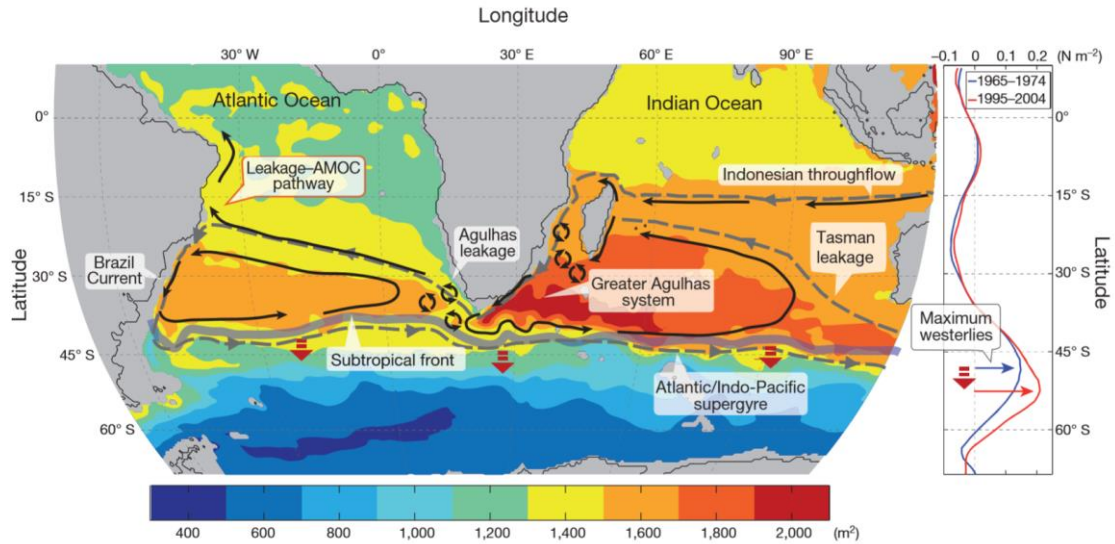


Figure 1.8. Représentation du prolongement du courant des Aiguilles affectée par le déplacement vers le sud du front subtropical causé par l'expansion vers le sud des vents d'ouest sur une période de 30 ans. De : [Beal et al. \(2011\)](#).

En outre, la récente étude de [Souza et al. \(2018\)](#) indique que la contribution des eaux du mode océan Indien peut influencer considérablement les propriétés de la SACW dans le bassin de l'océan Atlantique Sud. Cette affirmation est renforcée compte tenu de l'augmentation du nombre de tourbillons libérés dans la région de rétroflexion des Aiguilles ([Biaستoch et al., 2009](#)). Les tourbillons des Aiguilles transportent des masses d'eaux, qui sont marquées par les caractéristiques suivantes: couches thermohalines (i.e., gammes stables de température et de salinité, respectivement) et faible tourbillon potentiel (potential vorticity). Les masses d'eaux se forment principalement pendant l'hiver après un mélange intense dans les couches de surface et plongent entre les thermoclines saisonnières et permanentes. Ces masses d'eaux sont des eaux sources qui sont advectées et composent les eaux centrales des océans (e.g., SACW). Ainsi, comme la formation de masse d'eau s'intensifie lorsque le flux de chaleur augmente (e.g., [Hanawa. & Talley, 2001](#)), un renforcement des processus de formation des masses d'eaux est attendu car les tourbillons des Aiguilles sont capables d'intensifier le flux de chaleur ([Villas Bôas et al., 2015](#)). Trois variétés de masses d'eau subtropicales (marquées par des

gammas de températures distinctes en fonction de la zone source considérée), composent la couche centrale de l'océan Atlantique Sud, i.e. la couche occupée par la SACW. La couche SACW est également influencée par les contributions de la masse d'eau de l'océan indien (Sato & Polito, 2014; Souza et al., 2018).

Des études récentes ont conclu que les eaux centrales (par exemple, représentées par la SACW dans l'océan Atlantique Sud), sont parmi les plus affectées par la pénétration de C_{ant} (Salt et al., 2015; Carvalho-Borges et al., 2018; Orselli et al., 2018). Cela a renforcé l'idée précédente de l'entrée principale de C_{ant} dans les océans par la formation des eaux profondes (processus de convection profonde) et par la formation des eaux centrales et intermédiaires (processus de subduction). Ces études concernant l'absorption de C_{ant} indiquent qu'il conduit à un taux d'acidification (i.e., changement du pH de l'eau de mer) de -0.0016 yr^{-1} à -0.0018 yr^{-1} dans la SACW depuis la période préindustrielle (Salt et al., 2015; Carvalho-Borges et al., 2018; Orselli et al., 2018). Ces tendances indiquent que la SACW s'acidifie plus rapidement que les eaux immédiatement au-dessus et en dessous, car elles sont plus élevées que celles déjà observées pour ces autres couches océaniques : e.g., $-0,0013 \text{ yr}^{-1}$ pour les eaux de surface et $-0,0010 \text{ yr}^{-1}$ à la couche intermédiaire, pour AAIW. Comme prévu, les changements de pH observés dans l'océan Atlantique Sud pour les couches profondes et inférieures sont plus petits que toutes les autres couches. Ces changements sont $-0.0010/-0.0000 \text{ yr}^{-1}$ pour les couches supérieures et inférieures de CDW, $-0.0005/-0.0000 \text{ yr}^{-1}$ pour les couches supérieures et inférieures de NADW, et 0.0000 yr^{-1} pour l'AABW (e.g., Salt et al., 2015; Kitidis et al., 2017; Orselli et al., 2018). De plus, une étude récente a présenté certains résultats indiquant que les tourbillons des Aiguilles sont susceptibles de transporter plus C_{ant} que les eaux environnantes (Woosley et al., 2016). Dans cette recherche, les auteurs n'ont pas

concentré leur recherche sur la quantification directe de C_{ant} dans les tourbillons, mais ils ont suggéré que des études sur ce thème seraient les bienvenues.

Dans ce contexte, le développement de cette thèse a été motivé par les faits suivants : (i) les tourbillons des Aiguilles transportent le C_{ant} de la surface vers les eaux intermédiaires de l'océan Indien à l'océan Atlantique Sud ([Beal et al., 2009](#); [Biaستoch et al. 2009](#)), (ii) ces structures sont susceptibles de renforcer le processus de formation des masses d'eaux, et (iii) le processus d'acidification plus élevé se produit dans les couches centrales de l'océan Atlantique Sud. Ainsi, compte tenu de la nouveauté sur le sujet, cette étude présente une recherche sur le rôle des tourbillons des Aiguilles sur la biogéochimie des océans, qui reste un défi supplémentaire à étudier (e.g., [Ríos et al., 2003](#); [Moreau et al., 2017](#)). Enfin, les résultats de cette étude devraient contribuer davantage à la discussion scientifique des impacts des tourbillons des Aiguilles sur les changements climatiques dûs au cycle du carbone océanique et ses échanges avec l'atmosphère.

Chapter II. Hypothesis

Hypothesis

As presented before, in the introduction, the anthropogenic forcing on the climate changes are increasing the leakage in the Agulhas Current retroflection region due to changes in local wind system (i.e., the Southern Hemisphere westerlies; [Biastoch et al., 2009](#); [Beal et al., 2011](#)). In addition to this, a higher acidification process is occurring in the central layers of the South Atlantic Ocean.

Thus, the hypothesis investigated in this thesis was: the Agulhas leakage intensification process increases the CO₂ absorption by the ocean, and consequently changes the ocean acidification state in South Atlantic Ocean central waters.

Chapter III. Objectives

Objectives

3.1 Main objective:

The main goal of this research was to evaluate the Agulhas eddies role in changing the ocean acidification state in the South Atlantic Ocean using data collected by the Brazilian High Latitude Oceanography Group – GOAL group (acronym from Portuguese *Grupo de Oceanografia de Altas Latitudes*; [Mata et al., 2018](#)) in two projects (FORSA and Trans-Atlantic II, described in the methods section, **Chapter 4.1**) and online data bases (e.g., CDIAC, SOCAT). To achieve this, other specific objectives are proposed:

3.2 Specific objectives:

- a) To investigate the f_{CO_2} in the Agulhas eddies, using CO_2 molar fraction (x_{CO_2}) data from the cruises;
- b) To develop algorithms (biogeochemical models) to recalculate the carbonate system parameters (total alkalinity $-A_T-$, total dissolved inorganic carbon $-C_T-$ and/or pCO_2) from physical and biogeochemical data to apply to results of the cruises in which they were not directly measured;
- c) To quantify the C_{ant} absorption inside the eddies and in the surrounding waters by two independent methods;

Chapter IV. Methods

The dataset (i.e., oceanographic cruises surveys, satellite data) and the methods applied in each article developed during this PhD research is presented in this section. The description of the methodology shown here is more detailed than those presented on the published papers.

4.1. Oceanographic cruises

The cruises surveys used in this study were the *Following Ocean Rings in the South Atlantic* (FORSA), the *Trans-Atlantic II* (TAII) and the *CLIVAR/WOCE Repeat Hydrography Section A10* (A10; **Figure 4.1**; **Table 4.1**). FORSA and TAIL cruises were conducted by the GOAL group ([Mata et al., 2018](#)) in close cooperation with scientists from different research institutions in Brazil. In 2003, the cruise A10_2003 was

conducted under the responsibility of JAMSTEC through the project Blue Earth Global Expedition 2003 (Uchida et al., 2005). In 2011, the cruise A10_2011 was funded by NOAA-OGP and NSF-OCE through the U.S. CLIVAR/CO₂/hydrography/tracer program (Wanninkhof et al., 2013). More details about the cruises and sampling are given in Table 4.1.

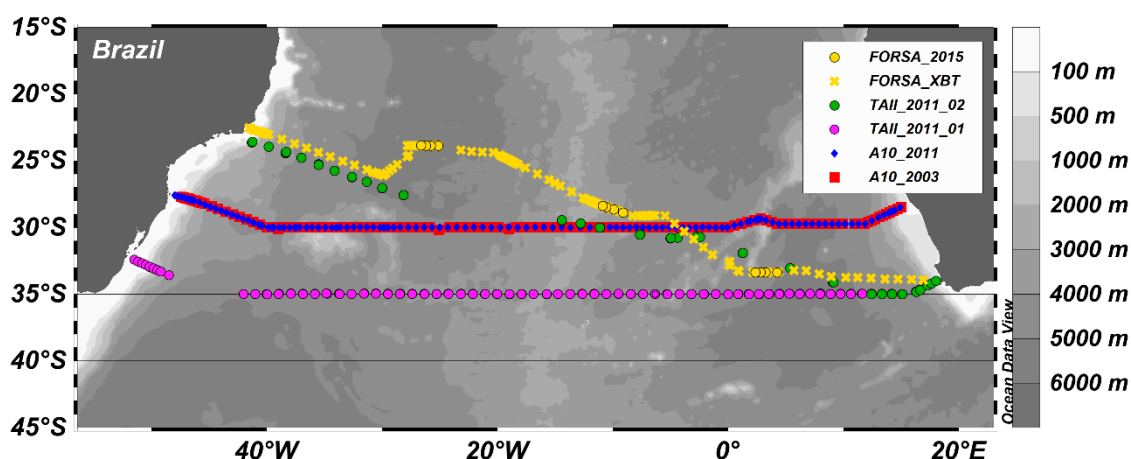


Figure 4. 1. Map of the sampled region in the South Atlantic Ocean. The yellow crosses correspond to the XBT profiles performed during the FORSA cruise (FORSA_XBT). The CTD stations are indicated by yellow dots (FORSA_2015), green dots (TAII_2011_02), purple dots (TAII_2011_01), blue diamonds (A10_2011), and red squares (A10_2003). The bottom bathymetry is represented by colour shadings.

Table 4. 1. Table of cruise details presenting each study considered to develop this thesis.

Cruises	Sampling period	Year	Season	Region	Research vessel	Published results
FORSA	June 27 th to July 15 th	2015	Early Winter	20°S – 35°S	RV NPqHo Vital de Oliveira	Carvalho et al., 2019; Orselli et al., 2019a, b
	October 24 th to November 25 th	2011	Spring	Along 35°S	RV NHo	Lencina-Avila et al., 2016
TAII	December 2 nd to December 22 nd	2011	Late Spring	20°S – 35°S	Cruzeiro do Sul	Orselli et al., 2019b
A10	November 6 th to December 5 th	2003	Late Spring	Along 30°S	RV Mirai	Uchida et al., 2005
	September 26 th to October 31 th	2011	Early Spring	Along 30°S	RV Ronald H. Brown	Wanninkhof et al., 2013

4.1.1. Following Ocean Rings in the South Atlantic (FORSA)

The FORSA cruise occurred in 2015 on board the first research cruise of the Brazilian Navy RV NPqHo Vital de Oliveira. The cruise survey was conducted between June 27th and July 15th in a Southwestern-Northeastern section (from Cape Town – South Africa to Arraial do Cabo – Brazil; **Figure 4.1**; **Table 4.1**; [Carvalho et al., 2019](#); [Orselli et al., 2019a, b](#)). Along this cruise track, 12 hydrographic conductivity-temperature-depth (CTD) stations were sampled and 118 expendable bathythermographs (XBTs) were deployed. In addition to these physical data, discrete seawater samples were collected for chemical and biological analyses, which included dissolved oxygen, phytoplankton pigments, dissolved inorganic nutrients, total, particulate and dissolved organic carbon, A_T and pH. These samples were taken using a combined Sea-Bird CTD/Carrousel 911+system® equipped with 24 twelve-litre Niskin bottles. Continuous measurements of temperature, salinity and seawater and atmospheric CO₂ molar fraction (xCO_2^{sw} and xCO_2^{atm} , respectively) were conducted. The underway temperature and salinity were sampled using a Sea-Bird® Thermosalinograph SBE21. The underway xCO_2 sampling was taken using an autonomous system GO-8050, General Oceanic®, equipped with a non-dispersive infrared gas analyser (LI-7000, LI-COR®). Seawater intake to measure those parameters by the continuous systems was set at ~5 m below the sea surface.

The FORSA cruise was conducted focusing on crossing six Agulhas eddies ([Orselli et al., 2019a](#)), but CTD stations throughout the water column were performed just in three of them ([Orselli et al., 2019b](#)). Hydrographic stations were conducted to have profiles outside and inside of the eddies, using CTD and/or XBT probes.

4.1.2. Trans-Atlantic II (TAII)

The TAI cruise occurred in 2011 on board the Brazilian Navy RV NHo Cruzeiro do Sul. This survey is a component of the project “*Measurements and modeling of CO₂ fluxes in the South Atlantic and Southern Oceans*”. The first leg (TAII_01) was conducted from October 24th to November 25th along 35°S (from Rio Grande – Brazil to Cape Town – South Africa; [Lencina-Avila et al., 2016](#)), and the second leg (TAII_02) was conducted from December 2nd to December 22nd in a Southwestern-Northeastern section (from Cape Town – South Africa to Rio de Janeiro – Brazil; **Figure 4.1**; **Table 4.1**). Along the TAI cruises, 93 hydrographic stations were sampled. In addition to physical data, discrete seawater samples were collected for chemical and biological analyses, which included dissolved oxygen, phytoplankton pigments, and dissolved inorganic nutrients, using a combined Sea-Bird CTD/Carrousel 911+system® equipped with 12 five-litre Niskin bottles. Sea-air $x\text{CO}_2$ measurements were also taken, however they were not used in this study.

4.1.3. CLIVAR/WOCE Repeat Hydrography Section A10 (A10)

The CLIVAR/WOCE Repeat Hydrography Section A10 occurred along 30°S (**Figure 4.1**; **Table 4.1**). The A10_2003 was conducted on board the RV Mirai from November 6th to December 5th (from Santos – Brazil to Cape Town – South Africa; [Uchida et al., 2005](#)). The A10_2011 cruise was conducted on board the RV Ronald H. Brown from September 26th to October 31th (from Cape Town – South Africa to Rio de Janeiro – Brazil; [Wanninkhof et al., 2013](#)). Along the A10 cruises, 110 hydrographic stations were sampled in 2003 and 120 in 2011. Physical data and discrete seawater samples were collected for chemical analysis. Using a combined Sea-Bird CTD/Carrousel 911+system® equipped with 35 twelve-litre and 24 ten/eleven-litre Niskin bottles, in the

A10_2003 and A10_2011 cruises, the following properties were determined: salinity, dissolved oxygen, dissolved inorganic nutrients, and carbonate system (total dissolved inorganic carbon – C_T ; A_T ; pH). Sea-air xCO_2 measurements were taken in the cruise conducted in 2011, however they were not used here. The A10 datasets analysed during the current study are available from the NODC/NOAA data centre (https://www.nodc.noaa.gov/ocads/oceans/RepeatSections/clivar_a10.html).

4.2. First article - PhD 01: The Sea-Air CO₂ Net Fluxes in the South Atlantic Ocean and the Role Played by Agulhas Eddies

4.2.1. CO₂ partial pressure data analysis

The GO-8050 (General Oceanic®) is a state-of-the-art complete system to measure the xCO_2 (Pierrot et al., 2009; **Figure 4.2**). The principle of the system is conditioned to the permanently seawater supply, which meets the recirculating air inside the equilibrator (headspace air; **Figure 4.3**). The design of this reservoir (i.e., the shower equilibrator) stimulate rapid air-liquid exchange, which is recognized as the equilibrator-based surface CO₂ measurements. The air-water in the equilibrator is never in equilibrium, although it is considered to be. When the equilibrated air moves out of the equilibrator, it goes to the sensor, a device that detects at least one gas species (i.e., just a CO₂ analyser or CO₂ and H₂O analyser; **Figure 4.2**). The system used in the FORSA cruise was equipped with a differential, non-dispersive infrared gas analyser LI-7000 (LI-COR®), which is a CO₂/H₂O analyser, recommended for oceanic measurements (*LI-7000 CO₂/H₂O analyser Instruction Manual*). The CO₂/H₂O measurements are based on the difference in absorption of infrared radiation between two cells, the reference and the

sample cells, because the LI-7000 is a differential analyser. The reference cell receives a standard gas of known CO_2 and H_2O concentrations in an open or closed path. The open path requirement is to pump continuously the standard gas. We used the closed path, in which a scrubber tube is attached to the reference cell (**Figure 4.4a**). This scrubber tube contains chemicals that absorb the CO_2 (Ascarite II) and H_2O (Magnesium Perchlorate), and are separated by fiberglass wool, as recommended in the manual “*Using CO_2 and H_2O scrubbers with LI-COR gas analysers*” (**Figure 4.4b**).

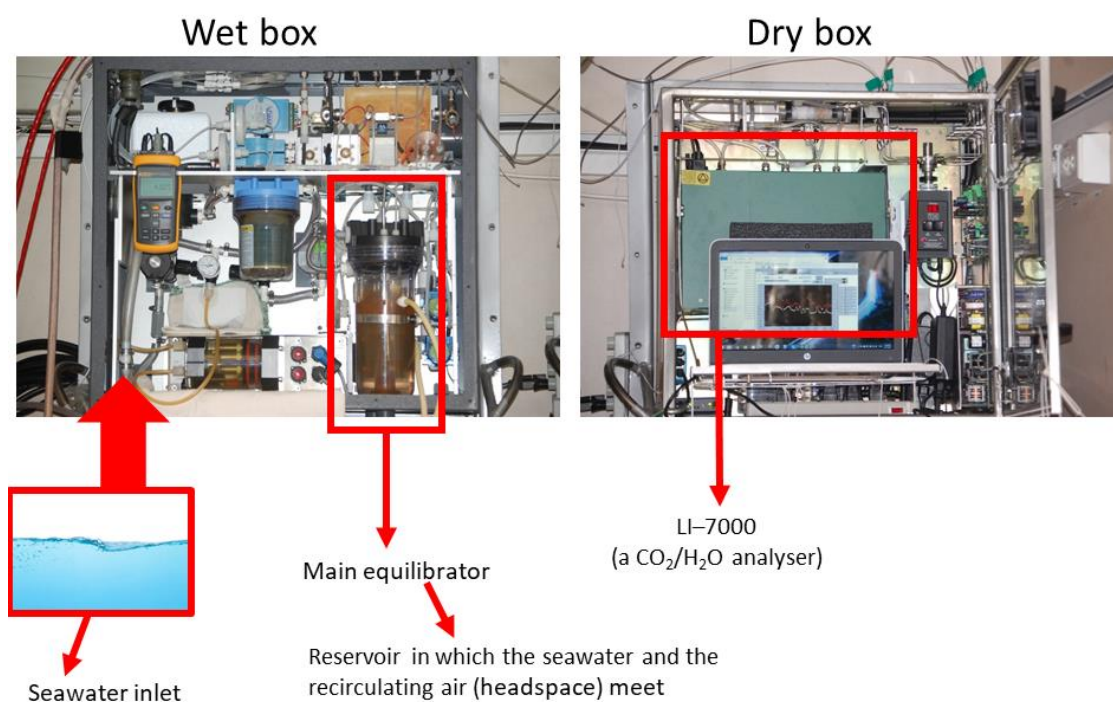


Figure 4. 2. Scheme presenting the GO-8050 CO_2 analyser. The upper panels present the ‘wet box’ and the ‘dry box’ of the system. The red rectangles highlight the main parts of the system: the seawater inlet region, the main equilibrator and the infrared gas analyser (LI-7000).

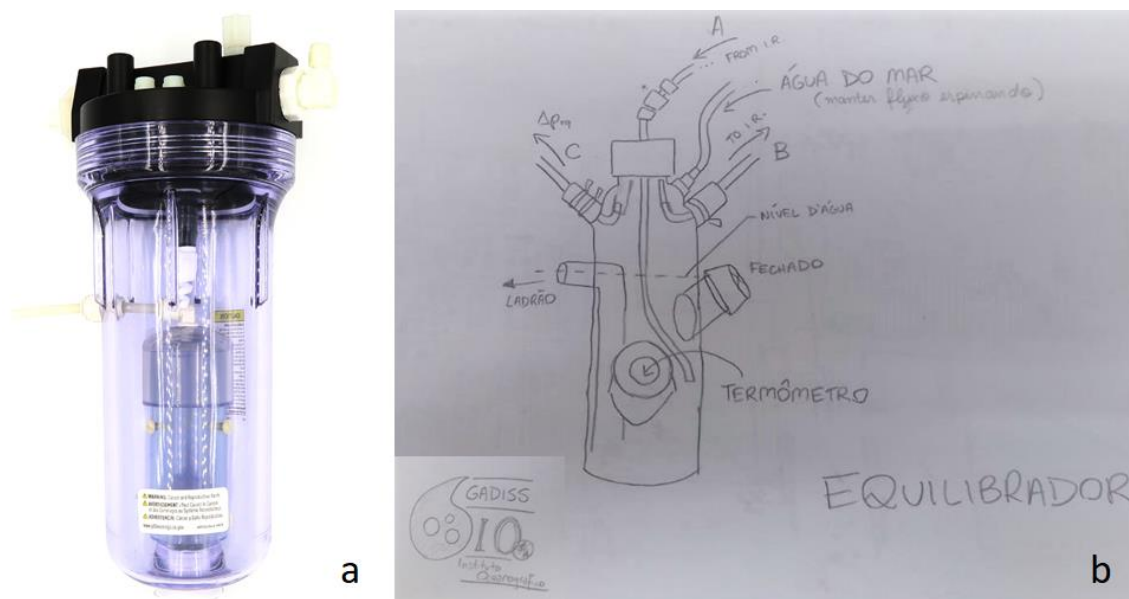


Figure 4.3. The main equilibrator. a) An image of the shower equilibrator supplied by General Oceanic®. b) A scheme of a shower-type equilibrator, indicating the seawater inlet (“água do mar”), the connections from (“A”) and to (“B”) the infrared system, the pressure and thermometer sockets and seawater escape.

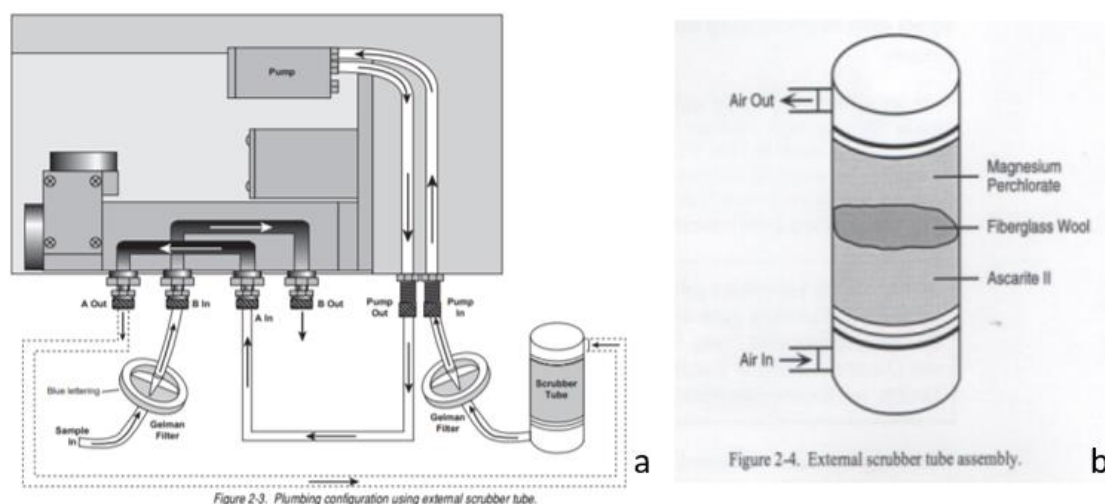


Figure 4.4. a) Scheme of the LI-7000 operational system, considered the application of the closed system set up for the reference, including the scrubber tube on the reference path. b) The scrubber tube contain chemicals that absorb the CO_2 (Ascarite II) and H_2O (Magnesium Perchlorate).

Apart from the choice to use an open or closed path for the reference cell, it is necessary to calibrate the sample cell. Thus, to accurately measure the $x\text{CO}_2$, the GO-8050 system was calibrated with four standard gases (CO_2 concentrations of 0, 202.10, 403.20, and 595.50 μatm) within a 12 h interval along the entire cruise. Every 3 h the system underwent a standard reading, to check the derivation and allow the $x\text{CO}_2$

corrections. The $x\text{CO}_2$ measurements were taken within 90 seconds interval. After a hundred of $x\text{CO}_2^{\text{sw}}$ readings, the system was changed to atmosphere and five $x\text{CO}_2^{\text{atm}}$ readings were taken (Pierrot et al., 2009).

As it is necessary to have accurate temperature and salinity measurements to calculate the CO_2 partial pressure ($p\text{CO}_2$), the thermosalinograph data were corrected using the CTD surface data. Then, together with the pressure data (Setra Pressure transducer⁴, coupled in the main equilibrator of the GO-8050), these data were used to calculate the $p\text{CO}_2$ of the equilibrator and atmosphere ($p\text{CO}_2^{\text{eq}}$ and $p\text{CO}_2^{\text{atm}}$, respectively), following Eqs. 4.1 to 4.4 (Weiss & Price, 1980):

$$p\text{CO}_2^{\text{eq}} = x\text{CO}_2^{\text{sw}} * (P_{\text{atm}} - P_{\text{H}_2\text{O}^{\text{eq}}}) \quad (4.1)$$

$$P_{\text{H}_2\text{O}^{\text{eq}}} = \exp \left[24.4543 - \left(\frac{6745.09}{T_{\text{eq}} + 273.15} \right) - 4.8489 * \ln \left(\frac{T_{\text{eq}} + 273.15}{100} \right) - 0.000544 * S \right] \quad (4.2)$$

$$p\text{CO}_2^{\text{atm}} = x\text{CO}_2^{\text{atm}} * \left[\left(P_{\text{atm}} - \frac{1.5}{101.325} \right) - P_{\text{H}_2\text{O}} \right] \quad (4.3)$$

$$P_{\text{H}_2\text{O}} = \exp \left[24.4543 - \left(\frac{6745.09}{T_{\text{is}} + 273.15} \right) - 4.8489 * \ln \left(\frac{T_{\text{is}} + 273.15}{100} \right) - 0.000544 * S \right] \quad (4.4)$$

where $x\text{CO}_2$ ($\mu\text{mol mol}^{-1}$) inputs were corrected by the CO_2 standards (Pierrot et al., 2009); P_{atm} is the atmospheric pressure (atm); $P_{\text{H}_2\text{O}^{\text{eq}}}$ is the water vapor pressure (atm) inside the equilibrator; $P_{\text{H}_2\text{O}}$ is the water vapor pressure (atm); T_{eq} is the equilibrator temperature ($^{\circ}\text{C}$); T_{is} is the *in situ* temperature ($^{\circ}\text{C}$); and S is the salinity; T_{eq} was obtained by a Hart® digital thermometer probe installed in the CO_2 -system main equilibrator,

⁴ The Setra Pressure transducer is a differential sensor which means that it measures the pressure difference between the equilibrator air and the surrounding air. In order to calculate the pressure inside the equilibrator, one needs to add the output of the Setra to the pressure value given by the LICOR at the time of measurement since the LICOR measurement is made at ambient pressure by opening the 3-way solenoid to the vent (GO-8050 Instruction Manual, General Oceanic®)

(Figure 4.3; Pierrot et al., 2009). The T_{is} and S were obtained from the thermosalinograph.

Using the pCO_2^{eq} , which is calculated at the equilibrator temperature, it is possible to calculate the pCO_2 at the *in situ* temperature (pCO_2^{sw}), according to Eq. 4.5 (Takahashi et al., 2009):

$$pCO_2^{sw} = pCO_2^{eq} * \exp[0.0433 * (T_{is} - T_{eq}) - (4.35 * 10^{-5}) * (T_{is}^2 - T_{eq}^2)] \quad (4.5)$$

The pressure and temperature inside the equilibrator are measured within ± 0.2 mbar and ± 0.01 °C to guarantee the desired accuracy of the GO-8050 system in 0.2 μ atm for atmospheric measurements and 2 μ atm for seawater measurements (Pierrot et al., 2009).

Another common calculation regarding pCO_2^{sw} data, is the temperature-normalized pCO_2^{sw} ($NpCO_2^{sw}$). This means that the temperature effect is removed when one calculates the $NpCO_2^{sw}$ for the mean cruise temperature. The procedure followed the Eq. 4.6 (Takahashi et al., 2009) and considered the mean cruise temperature of 20.39°C (T_{mean}).

$$NpCO_2^{sw} = pCO_2^{sw} * \exp[0.0433 * (T_{mean} - T_{is}) - (4.35 * 10^{-5}) * (T_{mean}^2 - T_{is}^2)] \quad (4.6)$$

The results obtained from these calculations (pCO_2^{sw} , pCO_2^{atm} ; Eqs. 4.1 to 4.5) allow one to investigate the exchanges of CO_2 at the ocean-atmosphere interface by calculating the pCO_2 difference between these two reservoirs (ΔpCO_2 , Eq. 4.7). Negative (positive) ΔpCO_2 results indicate that the ocean acts as a CO_2 sink (source) for the atmosphere.

$$\Delta p\text{CO}_2 = p\text{CO}_2^{sw} - p\text{CO}_2^{atm} \quad (4.7)$$

4.2.2. Sea-air CO₂ net fluxes

To determine the FCO₂, the monthly mean wind speed data of July 2015 (at 10 m height) were extracted from the ERA-Interim atmospheric reanalysis product of the European Centre for Medium Range Weather Forecast (<http://apps.ecmwf.int/datasets/data/interim-full-moda/levtype=sfc/>) because the use of long-term mean is usual (e.g., Takahashi et al., 2009). The average wind speed for the period and whole area was $6.8 \pm 0.6 \text{ m s}^{-1}$, ranging from 5.6 to 8.3 m s^{-1} (Figure S1). The CO₂ transfer coefficients (K_T) proposed by Takahashi et al. (2009) and Wanninkhof (2014) were chosen for evaluation (Eqs. 4.8 and 4.9):

$$K_T \text{ Takahashi et al. (2009)} = 0.26 * u^2 * \frac{Sc^{-1/2}}{660} \quad (4.8)$$

$$K_T \text{ Wanninkhof (2014)} = 0.251 * u^2 * \frac{Sc^{-1/2}}{660}$$

(4.9)

where K_T is the CO₂ transfer coefficients according to the references indicated; u is the wind speed (m s^{-1}) at 10 m height; Sc is the Schmidt number, defined for seawater and FCO₂ studies. For the calculation using Eq. 4.8, Schmidt number is: $Sc = A - B * t + C * t^2 - D * t^3$, where t is the *in situ* temperature ($^{\circ}\text{C}$); $A = 2073.1$; $B = 125.62 \text{ }^{\circ}\text{C}^{-1}$; $C = 3.6276 \text{ }^{\circ}\text{C}^{-2}$; and $D = 0.043219 \text{ }^{\circ}\text{C}^{-3}$ (Jähne & Dietrich, 1987). For the calculation of using Eq. 4.9, Schmidt number is: $Sc = A - Bt + Ct^2 - Dt^3 + Et^4$, where t is temperature; $A = 2116.8$; $B = 136.25 \text{ }^{\circ}\text{C}^{-1}$; $C = 4.7353 \text{ }^{\circ}\text{C}^{-2}$; $D = 0.092307 \text{ }^{\circ}\text{C}^{-3}$; and $E = 0.000755 \text{ }^{\circ}\text{C}^{-4}$ (Wanninkhof, 2014).

Because the difference between the FCO_2 determined with [Takahashi et al. \(2009\)](#) and [Wanninkhof \(2014\)](#) coefficients ($\text{FCO}_2^{\text{T09}}$ and $\text{FCO}_2^{\text{W14}}$, respectively) was relatively small ($\text{FCO}_2^{\text{T09}} - \text{FCO}_2^{\text{W14}} = -0.14 \pm 0.06 \text{ mmol m}^{-2} \text{ d}^{-1}$), the FCO_2 is hereafter represented as the $\text{FCO}_2^{\text{T09}}$ in all figures in this paper. This choice was made because the monthly mean wind speed data were used to calculate the FCO_2 , which is recommended for the K_T model determined by [Takahashi et al. \(2009\)](#).

With all these data together, the FCO_2 was determined according to **Eq. 4.10** ([Broecker & Peng, 1982](#)):

$$\text{FCO}_2 = K_T * K_S * \Delta p\text{CO}_2 \quad (4.10)$$

where FCO_2 is the sea-air CO_2 net flux, which is multiplied by 0.24, to give the FCO_2 in $\text{mmol m}^{-2} \text{ d}^{-1}$; K_T is the gas transfer coefficient according to the authors cited in **Eqs. 4.8** and **4.9**; K_S is the CO_2 solubility coefficient, as a function of temperature and salinity ([Weiss, 1974](#)), as described below (**Eqs. 4.11** to **4.13**):

$$K_S = \exp(LA + LB) \quad (4.11)$$

$$LA = -58.0931 + \left[90.5069 * \left(\frac{100}{T_{is} (\text{°K})} \right) \right] + \left[22.294 * \text{LN} \left(\frac{T_{is} (\text{°K})}{100} \right) \right] \quad (4.12)$$

$$LB = S * \left\{ 0.027766 + \left[-0.023656 * \left(\frac{T_{is} (\text{°K})}{100} \right) \right] + \left[0.0050578 * \left(\frac{T_{is} (\text{°K})}{100} \right)^2 \right] \right\} \quad (4.13)$$

where T_{is} is the *in situ* temperature measured in $^{\circ}\text{C}$ transformed to $^{\circ}\text{K}$, and S is the salinity.

4.2.3. FORSA cruise eddies' identification

We used the mesoscale eddy trajectory AVISO product (downloaded from <https://www.aviso.altimetry.fr/en/data/products/value-added-products/global-mesoscale-eddy-trajectory-product.html>, last data from January 6th 2017; Chelton, et al., 2011; Schlax & Chelton, 2016), to identify the six sampled eddies and their back and forward trajectories. This procedure allowed the determination of the radius (km) and lifetime (days – d). More information about the AVISO product, radius and lifetime determinations, are included in the Supporting Information of the published manuscript, included in the articles chapter of this thesis (**5.1 Text S1**; Orselli et al., 2019a). With the eddies description parameters and the FCO₂ estimates (i.e., daily CO₂ sink estimated for the FORSA cruise track, **Eq. 4.10**), the CO₂ uptake for the entire area of each eddy was calculated, extrapolated for one year and also for the lifetime of the eddy.

We used geometric means to establish an ‘Agulhas typical’ eddy, which can be considered a representative eddy among the sampled ones. Geometric means are frequently used when comparing different elements that have multiple properties (with different numerical scales), thus allowing a representative figure to be constructed for all the elements (e.g., Fleming & Wallace, 1986; Pal, 1998). In addition, we determined some eddy parameters to represent an ‘Agulhas true’ eddy and an ‘Agulhas evolved’ eddy, thus better characterizing these mesoscale structures in each of the South Atlantic Ocean basins (**Table 4.2**). This procedure was adopted because the first three sampled eddies (hereafter referred to as V1, V2 and V3) were surveyed on the eastern side of the Mid-Atlantic Ridge (13°W), whereas the last three (hereafter referred to as V4, V5 and V6) were in the western basin. The ‘Agulhas true’ eddy represents the recent and young mesoscale structures shed by the Agulhas retroflexion. The ‘Agulhas evolved’ can be considered a modified Agulhas eddy because the last three eddies suffered splitting and/or

merging processes during their trajectories. Observing the sea level anomaly data along their trajectories (**Figure 4.5**; **Video S1**, <https://doi.org/10.1016/j.pocean.2018.10.006>), these three eddies were found to interact with each other (**Figures 4.6, 4.7 and 4.8**) even when they were in the eastern basin (V4 and V5, **Figures 4.7a, 4.7b**; V5 and V6, **Figure 4.6**) or when they were close to the Mid-Atlantic Ridge (V4 and V5 **Figure 4.7c**). A short period of interaction was also observed for V2 and V3 (**Figure 4.8**). In addition, the V1 signal was strong throughout its entire life, not only in the eastern basin, where it was sampled in the FORSA cruise. Apart from the interactions between these six eddies, there are interactions between these eddies and other features. In these cases, the merging (splitting) process causes their radii to increase (reduce) during their lives. Thus, this approach allowed us to distinguish a more detailed picture of the Agulhas eddies evolution throughout the South Atlantic Ocean, because the determination of the ‘Agulhas typical’ eddy probably masks the evolution of its spatial and temporal dynamics.

Table 4. 2. Radius (km), lifetime (d) and sea-air CO₂ net flux calculated using [Takahashi et al. \(2009\)](#) and [Wanninkhof \(2014\)](#) coefficients – FCO₂^{T09} and FCO₂^{W14} (first and second lines for each FCO₂ result presented in the table). Results are presented for each eddy (Vn, n=1 to 6), for the ‘Agulhas true’ eddy, the ‘Agulhas evolved’ eddy and the ‘Agulhas typical’. The FCO₂ reported in this table are in different units, as indicated in the respective line. *indicates that the eddy lifetime accounting was finished with the data availability until the analysis.

Eddy	V1	V2	V3	V4	V5	V6	Agulhas true	Agulhas evolved	Agulhas typical
Radius [km]	94.23	84.19	96.43	95.08	97.14	91.05	91.46	91.73	92.91
Lifetime [d]	798*	931*	949	825	1090	1117	890.03	939.96	969.93
FCO ₂ [mmol m ⁻² d ⁻¹]	-5.0	-3.8	-4.1	-2.3	-2.9	-3.2	-4.3	-3.3	-3.5
	-4.8	-3.7	-3.9	-2.3	-2.9	-3.1	-4.1	-3.2	-3.3
FCO ₂ [g CO ₂ d ⁻¹]	-3156.7	-1937.7	-2701.8	-1510.0	-1966.7	-1870.0	-2574.1	-1992.1	-2123.8
	-3042.6	-1866.8	-2602.2	-1451.9	-1919.5	-1804.9	-2454.1	-1917.7	-2050.6
FCO ₂ [t CO ₂ yr ⁻¹]	-1.2	-0.7	-1.0	-0.6	-0.7	-0.7	-0.9	-0.7	-0.8
	-1.1	-0.7	-1.0	-0.5	-0.7	-0.7	-0.9	-0.7	-0.8
FCO ₂ [t CO ₂ life ⁻¹]	-2.5	-1.8	-2.6	-1.3	-2.1	-2.1	-2.3	-1.8	-2.0
	-2.4	-1.7	-2.5	-1.2	-2.1	-2.0	-2.2	-1.7	-1.9

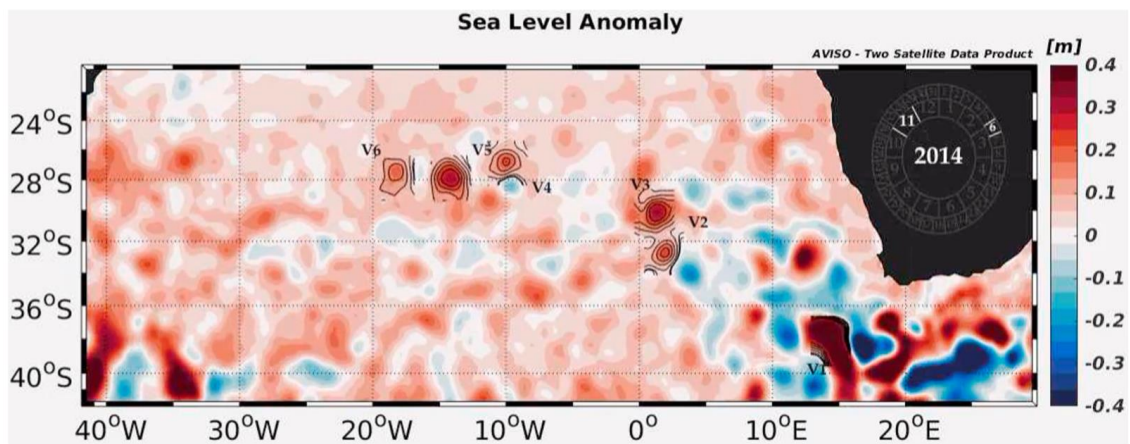


Figure 4. 5. Snapshot of the **Video S1**. Animation map of the South Atlantic Ocean composed from the sea level anomaly (SLA – m) data. The black continuous line corresponds to the SLA contours of 0.01, 0.02, 0.05, 0.1, 0.15, 0.2 and 0.25 m. The V_n ($n = 1$ to 6) correspond to each eddy sampled in the FORSA cruise trajectory. Supplementary data to this article and this video can be found online at <https://doi.org/10.1016/j.pocean.2018.10.006>

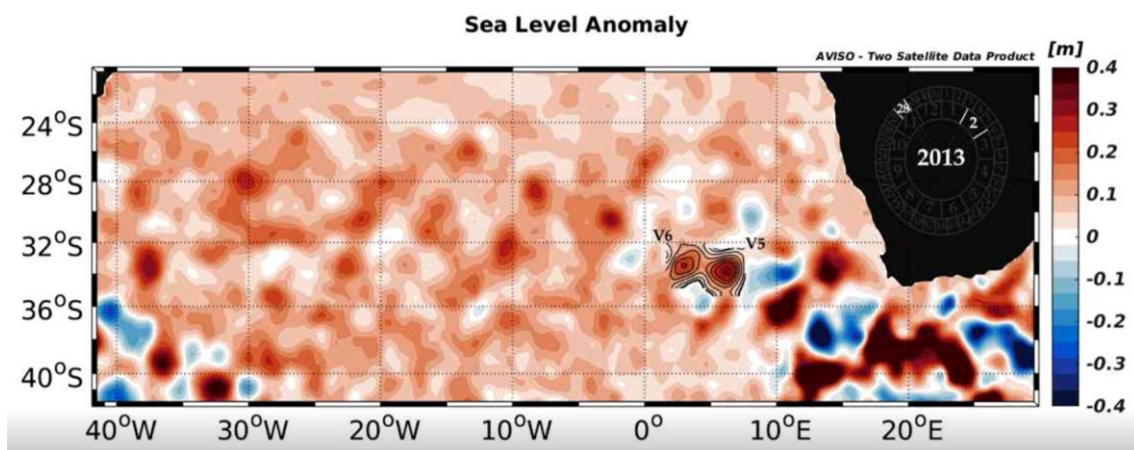


Figure 4. 6. Snapshot of the **Video S1** at the moment when V5 and V6 interact with each other. Animation map of the South Atlantic Ocean composed from the sea level anomaly (SLA – m) data. The black continuous line corresponds to the SLA contours of 0.01, 0.02, 0.05, 0.1, 0.15, 0.2 and 0.25 m. The V_n ($n = 1$ to 6) correspond to each eddy sampled in the FORSA cruise trajectory. Supplementary data to this article and this video can be found online at <https://doi.org/10.1016/j.pocean.2018.10.006>

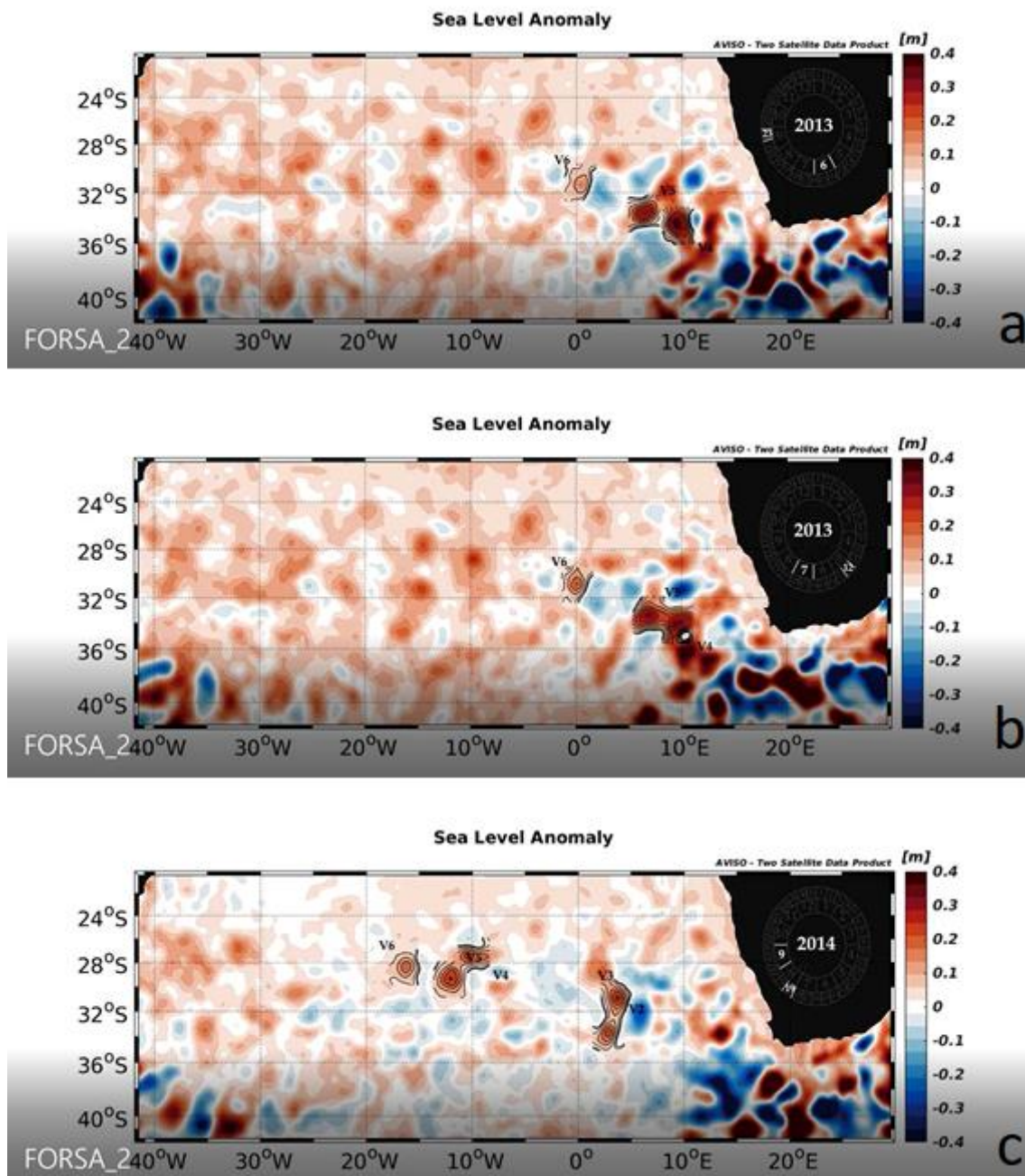


Figure 4. 7. Snapshots of the **Video S1** at the moment when V4 and V5 interact with each other. Animation map of the South Atlantic Ocean composed from the sea level anomaly (SLA – m) data. The black continuous line corresponds to the SLA contours of 0.01, 0.02, 0.05, 0.1, 0.15, 0.2 and 0.25 m. The Vn (n = 1 to 6) correspond to each eddy sampled in the FORSA cruise trajectory. Supplementary data to this article and this video can be found online at [https:// doi.org/10.1016/j.pocean.2018.10.006](https://doi.org/10.1016/j.pocean.2018.10.006)

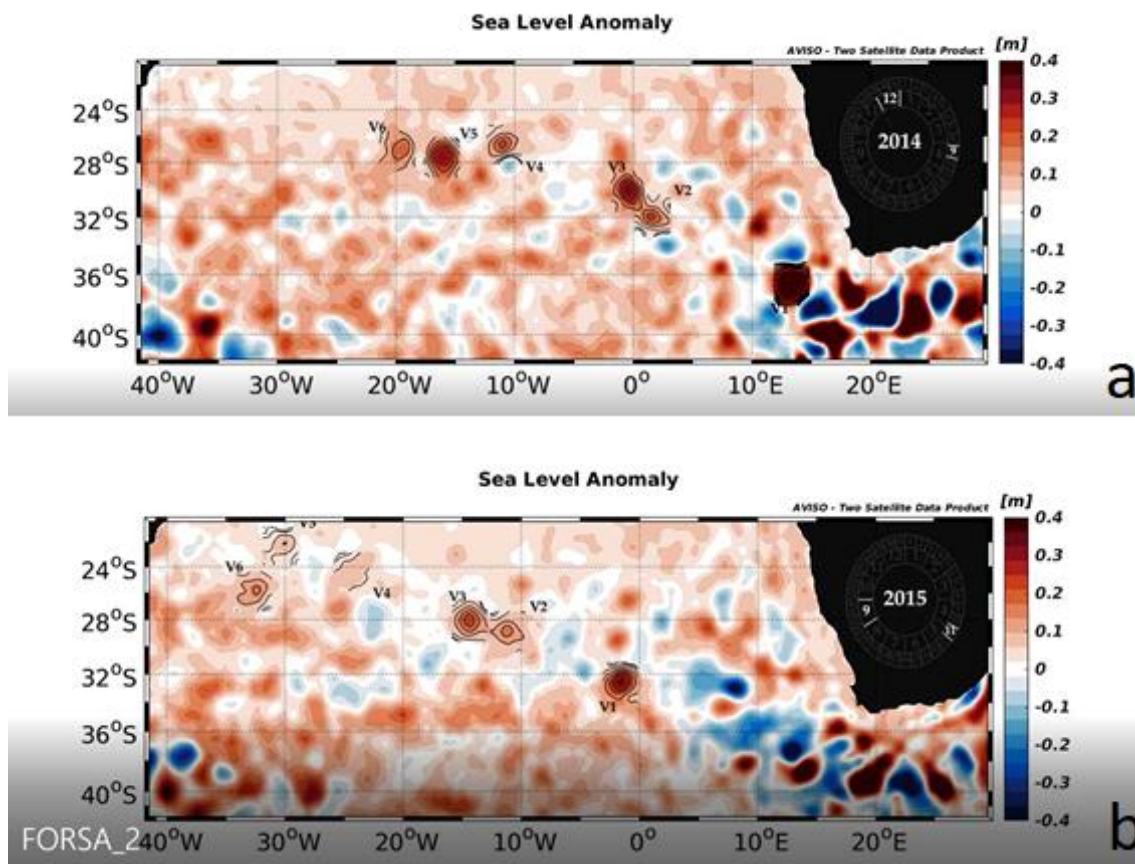


Figure 4. 8. Snapshot of the **Video S1** at the moment when V2 and V3 interact with each other. Animation map of the South Atlantic Ocean composed from the sea level anomaly (SLA – m) data. The black continuous line corresponds to the SLA contours of 0.01, 0.02, 0.05, 0.1, 0.15, 0.2 and 0.25 m. The V_n ($n = 1$ to 6) correspond to each eddy sampled in the FORSA cruise trajectory. Supplementary data to this article and this video can be found online at [https:// doi.org/10.1016/j.pocean.2018.10.006](https://doi.org/10.1016/j.pocean.2018.10.006)

4.2.4. Satellite-derived data and CO_2 modelling

The data from MODIS-AQUA (<http://oceancolor.gsfc.nasa.gov/>), daily 4 km resolution, level 3, were used to calculate the satellite-derived sea surface chlorophyll-*a* (chl-*a*, $mg\ m^{-3}$). This process was conducted using the OC3M algorithm, which returns the near-surface chl-*a*, calculated using an empirical relationship derived from *in situ* measurements of chl-*a* and remote sensing reflectance in the blue-to-green region of the

visible spectrum (e.g., [Lencina-Avila et al., 2016](#)). On cloudy days, the chl-*a* average for that day ± 1 was used.

We used chl-*a*, temperature and salinity to model the CO₂^{sw}-related parameters ($p\text{CO}_2^{\text{sw}}$, CO₂ fugacity – $f\text{CO}_2^{\text{sw}}$, $Np\text{CO}_2^{\text{sw}}$, temperature-normalized CO₂ fugacity – $Nf\text{CO}_2^{\text{sw}}$). Underway temperature and salinity were obtained from the thermosalinograph and adjusted to match the chl-*a* resolution. These data were used to feed a multiple linear regression (MLR) model (e.g., [Hales et al., 2012](#); [Signorini et al., 2013](#)). The MLR equation used to estimate the modeled CO₂^{sw} ($m\text{CO}_2^{\text{sw}}$) in the South Atlantic Ocean is described by **Eq. 4.14** (e.g., [Ito et al., 2016](#); [Lencina-Avila et al., 2016](#)):

$$m\text{CO}_2^{\text{sw}} = \alpha + \beta_1 * (T - \bar{T}) + \beta_2 * (S - \bar{S}) + \beta_3 * (\text{chl}a - \overline{\text{chl}a}) \quad (4.14)$$

where α is the intercept of the linear regression, and β_i ($i = 1, 2, 3$) are the unknown coefficients to be determined for each parameter and are presented below (**Table 4.3**). The temperature, salinity and chl-*a* were previously standardized by subtracting the mean of that same variable before developing the model coefficients.

Table 4. 3. Considering Eq. 4.14, this table presents the coefficients determined for each parameter in the multiple linear regression model. CO₂-related parameters are: seawater CO₂ partial pressure/fugacity ($p\text{CO}_2^{\text{sw}}/f\text{CO}_2^{\text{sw}}$, μatm), temperature-normalized $p\text{CO}_2^{\text{sw}}/f\text{CO}_2^{\text{sw}}$ ($Np\text{CO}_2^{\text{sw}}/Nf\text{CO}_2^{\text{sw}}$ μatm , @ 20.39°C). The measured vs. modeled parameter coefficients of determination are referred to as R². The units of each determined parameter are: α (μatm), β_1 ($\mu\text{atm}^\circ\text{C}^{-1}$), β_2 (μatm), β_3 ($\mu\text{atm mg}^{-1} \text{m}^3$), standard error (μatm). The number of data points used is 8650.

	α	β_1	β_2	β_3	R ²	Standard error
$p\text{CO}_2^{\text{sw}}$	352.05	4.91	-9.60	-26.86	0.81	6.74
$Np\text{CO}_2^{\text{sw}}$	350.40	-9.61	-10.62	-24.22	0.91	7.37
$f\text{CO}_2^{\text{sw}}$	336.10	5.41	-8.82	-29.17	0.86	6.21
$Nf\text{CO}_2^{\text{sw}}$	334.33	-8.51	-9.60	-29.59	0.90	6.72

Along with the FORSA cruise data, we used some other database. Apart from the TAI and A10, these other cruises were not previously described in this section because we got already published CO₂-related data. The $p\text{CO}_2^{\text{sw}}$ and $f\text{CO}_2^{\text{sw}}$ were calculated from C_T and A_T data from the A10_2003 database, because it was not directly measured. These data were considered to compare results of CO₂-related parameters ($p\text{CO}_2^{\text{sw}}$, $f\text{CO}_2^{\text{sw}}$, $\Delta p\text{CO}_2$, $\Delta f\text{CO}_2$, FCO_2) to the FORSA results, presented in **Table 5** (chapter 5.1), of the main text of [Orselli et al. \(2019a\)](#), and a map of each study is also reported in the supplementary material of this paper (**Figure S7**, chapter 5.1). These data are the following: a) the AMT cruises transects studied by [Lefèvre and Moore \(2000\)](#), obtained from SOCAT v5 database ([Bakker et al., 2016](#)). b) All FICARAM cruises sections studied by [Padin et al. \(2010\)](#), obtained from SOCAT v5 database ([Bakker et al., 2016](#)). c) The TAI_2011_01 cruise conducted in 2011 studied by [Lencina-Avila et al. \(2016\)](#) and included in the first section of this chapter (**chapter 4.1.2**). d) The data from the [Sutherland et al. \(2015\)](#) report of the R/V Nathaniel B. Palmer cruise 15/8, conducted in 2015, available at www.ldeo.columbia.edu/res/pi/CO2/carbondioxide/Palmer_data/1508SFC.PRT. e) The data used from the [Uchida et al. \(2005\)](#) report of the A10 CLIVAR/ WOCE cruise, conducted in 2003, available at www.nodc.noaa.gov/ocads/oceans/RepeatSections/clivar_a10.html. f) The data used from the [Wanninkhof and Castle \(2013\)](#) report of the A10 CLIVAR/ WOCE cruise, conducted in 2011 (A10_2011), available at www.cdiac.ornl.gov/ftp/oceans/CLIVAR/A10_2011/ and included in the first section of this chapter (**chapter 4.1.3**). g) The data used from the [Takahashi et al. \(2009\)](#) database, available at www.ldeo.columbia.edu/res/pi/CO2/carbondioxide/air_sea_flux/month_flux_2006c.txt. h) The data used from the [Bakker et al. \(2016\)](#) report of the SOCAT v5 database, available at www.socat.info/index.php/data-access/.

4.3. Second article - PhD 02: The Effect of Agulhas Eddies on Absorption and Transport of Anthropogenic Carbon in the South Atlantic Ocean

4.3.1. Identification of the Agulhas eddies

During the FORSA cruise, eddy identification was conducted by analysing the daily sea level anomaly data in conjunction with the temperature profiles obtained by high-resolution spatially distributed XBT deployments. Once the eddies were found, water sampling was performed inside and outside of them (see [Carvalho et al., 2019](#)). The FORSA cruise was the only one previously planned to sample the Agulhas eddies, and therefore, we needed to identify the eddies sampled in all of the other cruises, as well as their positions. Therefore, we used the mesoscale eddy AVISO product (downloaded from <https://www.aviso.altimetry.fr/en/data/products/value-added-products/global-mesoscale-eddy-trajectory-product.html>, last data from January 6th, 2017; [Chelton, et al., 2011](#); [Schlax & Chelton, 2016](#)). Eddy identification in the TAI and A10 cruises was performed by looking for the CTD station positions in the SLA field of the day in which the station was performed (**Figure 4.9**). In cases of an anticyclonic eddy (positive sea level anomaly) matching the station position (**Figure 4.10**), the back trajectory was investigated to determine whether it could be considered an Agulhas eddy or not (**Figure 4.11**). In positive cases, the life history of the eddy was used to determine its mean radius (km) and lifetime (days, d) as well as the sampled day's radius and age (**Table 4.4**), according to the AVISO product, as performed by [Orselli et al. \(2019a\)](#). In the end of this, we ended up with 13 Agulhas eddies to perform this study. The track of each cruise and the sampling position of these identified eddies in the South Atlantic Ocean are presented in **Figure 4.12**.

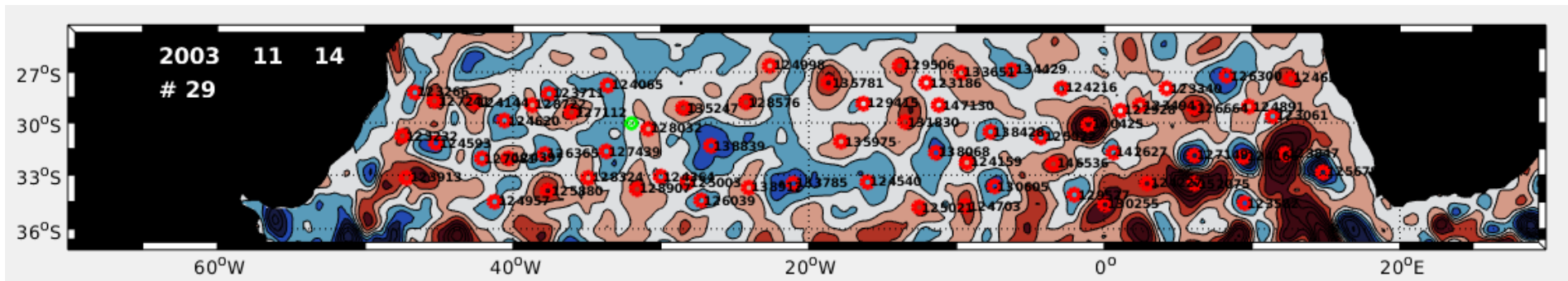


Figure 4. 9. Plot of the CTD station position (green circle) in the sea level anomaly field of the day in which the station was performed. The numbers indicate the eddies' IDs in the database.

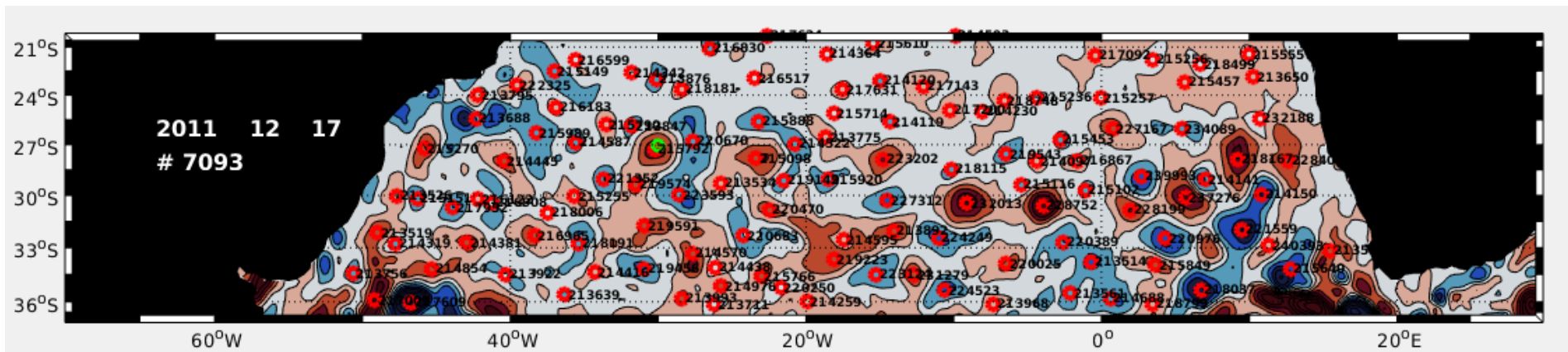


Figure 4. 10. Plot of the CTD station position (green circle) in the sea level anomaly field of the day in which the station was performed. This is an example of one time that an anticyclonic eddy (positive sea level anomaly) was observed matching the station position. The numbers indicate the eddies' IDs in the database.

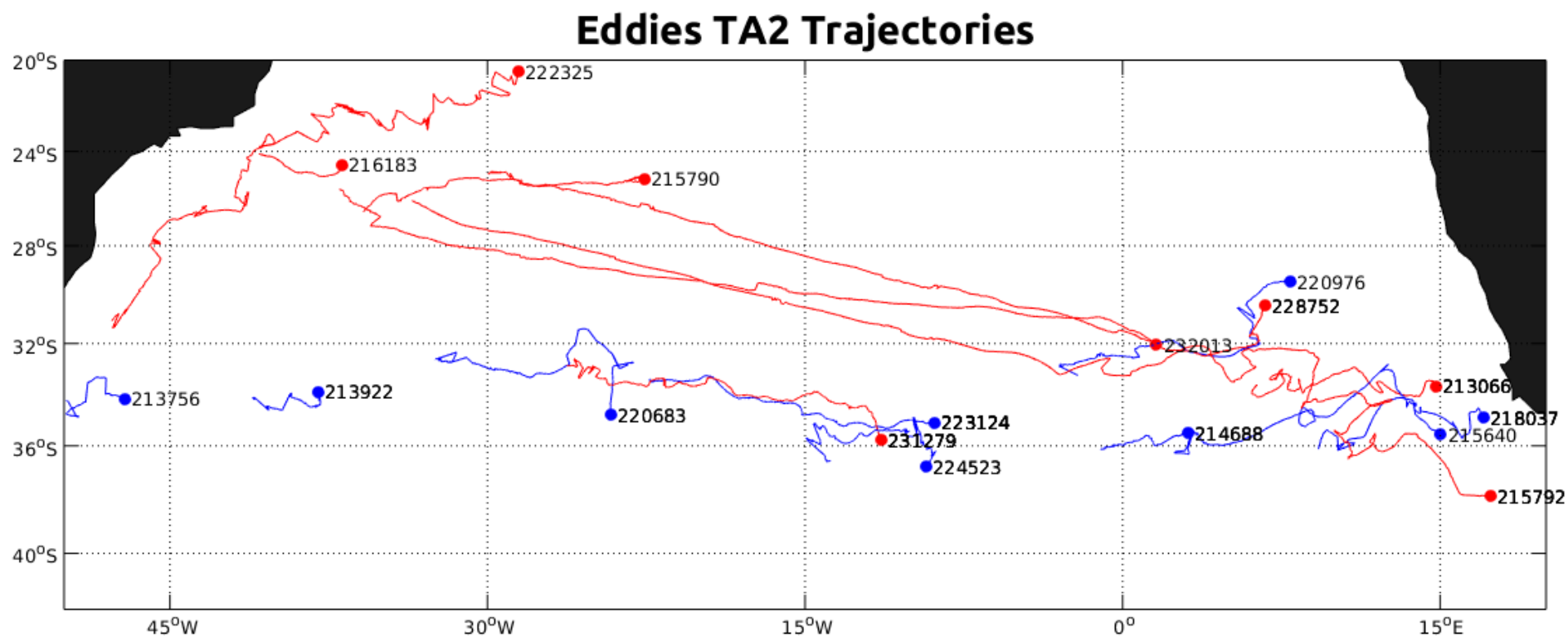


Figure 4. 12. Plot the back and forward trajectories of the eddies that match the CTD stations positions. The red (blue) dots and lines correspond to anticyclonic (cyclonic) eddies. This was used to determine whether it could be considered an Agulhas eddy or not. The numbers indicate the eddies' IDs in the database.

Table 4. 4. Radius (km) and lifetime (d) of each eddy investigated on this study in the in situ sampling day and life history. Superscript T or E indicates whether the eddy can be considered a true or evolved eddy according to the classification of Orselli et al. (2019a). * indicates that the eddy lifetime accounting was completed together with the data availability in the AVISO product until analysis. # indicates that the eddy was formed during the splitting of a 925-day old Agulhas eddy.

Cruise Year (season)	Eddy	Sampled day		Life history mean	
		Radius [km]	Age [d]	Radius [km]	Lifetime [d]
FORSA 2015 (winter)	V1 ^T	82.44	244	94.23	798*
	V3 ^T	94.30	440	96.43	949
	V5 ^E	101.86	1052	98.86	1222
TAII 2011 (early spring)	VT62 ^T	123.82	354	106.00	367
	VT85 ^T	92.09	263	87.40	767
	VT87 ^T	95.58	245	97.47	854
	VT93 ^E	122.06	1177	101.39	1251
A10 2011 (early spring)	VA42 ^T	83.72	181	97.47	854
	VA63 ^E	114.92	600	111.35	714
	VA91 ^E	136.64	125 [#]	105.34	211 [#]
A10 2003 (late spring)	VA04 ^E	130.55	1177	111.11	1223
	VA55 ^T	85.43	494	93.70	782
	VA71 ^T	92.44	308	96.65	874

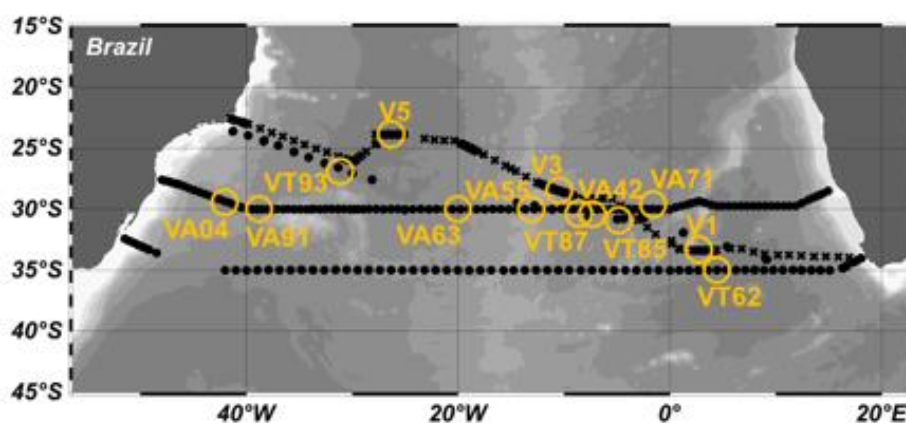


Figure 4. 13. Map indicating the approximate CTD-sampling position of the 13 Agulhas eddies used in this study: V1, V3, and V5 (FORSA_2015); VT62 (TAII_2011_01); VT85, VT87, and VT93 (TAII_2011_02); VA42, VA63, and VA91 (A10_2011); and VA04, VA55, and VA71 (A10_2003).

4.3.2. Carbonate system sampling and analysis

4.3.2.1. A10_2003 cruise

The seawater samples for C_T were collected into 300 mL borosilicate glass bottles, which were fixed with 100 μL of a saturated mercuric chloride solution (DOE, 1994). Analysis were performed with two C_T measurement systems (systems A and B; Nippon ANS, Inc.) composed of a CO_2 extraction system and a coulometer (Model 5012, UIC Inc.), following Johnson et al. (1998). The systems were calibrated using sodium carbonate (Na_2CO_3) solutions (nominally 500, 1000 1500, 2000, and 2500 $\mu\text{mol L}^{-1}$; Goyet & Hacker, 1992) and analysis of certified reference material (CRM, batch 60, provided by Prof. A. G. Dickson of Scripps Institution of Oceanography, Dickson et al., 2003). The standard deviations of CRM- C_T for systems A and B were 1.1 and 0.9 $\mu\text{mol kg}^{-1}$ ($n = 35$; $n = 28$), respectively. For A_T , the samples were collected into 130 ml borosilicate glass bottles. Analyses were conducted with a Metrohm autoburette and a Thermo Orion pH meter, which were automatically controlled. The system was calibrated using 5 solutions of Na_2CO_3 in 0.7 M sodium chloride (NaCl) solutions (nominally 0, 100, 1000, 2000 and 2500 $\mu\text{mol kg}^{-1}$) as well as analysis of CRM (batch 60; Dickson et al., 2003). The standard deviation of CRM- A_T for the system was 1.7 $\mu\text{mol kg}^{-1}$ ($n = 162$). The cruise report supplies detailed information on these systems and analysis processes (Uchida et al., 2005).

4.3.2.2. A10_2011 cruise

The seawater samples for C_T were collected into precombusted 300 mL Pyrex bottles, which were fixed with 0.122 mL of a 50% saturated mercuric chloride solution. Analysis were conducted with two C_T measurement systems (PMEL-1 and PMEL-2) composed of a coulometer (UIC Inc.) and a SOMMA (Single Operator Multiparameter

Metabolic Analyser) inlet system, following [Johnson et al. \(1985; 1998\)](#) and [Johnson \(1992\)](#). The systems were calibrated using pure CO₂ (99.995%) and secondary standards, as well as the analysis of CRM (batch 98; [Dickson et al., 2003](#)). The C_T error was not included in the cruise report. For A_T, the samples were collected into 500 mL borosilicate glass bottles. Analysis were performed with a Metrohm 665 Dosimat titrator and an Orion 720A pH meter. The system was calibrated using CRM (batches 96 and 112; [Dickson et al., 2003](#)). The reported error for A_T was 0.3 μmol kg⁻¹. The cruise report supplies detailed information on the systems and analysis processes ([Wanninkhof et al., 2013](#)).

4.3.3. Models development for carbonate system parameters

To gather the carbonate system data along all of the cruise sections investigated in this study, different types of models for C_T and A_T parameters were tested using the two A10 sections (A10_2003 and A10_2011) in which accurate biogeochemical data were available with good precision ([Uchida et al., 2005](#); [Wanninkhof et al., 2013](#)). We tested different types of models in order to find the one that best represented the biogeochemical data and produced the smallest associated errors.

These tests were firstly performed including the MLR models, because they are commonly applied to carbonate system data reconstruction. When using nutrients (or other carbonate system data) the results of these MLR tests were relatively good compared to other results from the literature. A comparison of the standard errors of each MLR and their input parameters are included in the **Tables 4.5** and **4.6**, for C_T and A_T results, respectively.

Table 4. 5. Results from the C_T multiple linear regression (MLR) tests (at cruise sampling year). Each test was conducted using a different set of input parameters. T is temperature ($^{\circ}\text{C}$), S is salinity, A_T , DO is dissolved oxygen ($\mu\text{mol kg}^{-1}$), AOU is apparent oxygen utilization ($\mu\text{mol kg}^{-1}$), NO_3 is nitrate ($\mu\text{mol kg}^{-1}$), Pres is pressure (dbar), Lon is longitude, Lat is latitude. N indicates the number of measurements used in each test. R^2 is coefficient of determination. The standard error is in $\mu\text{mol kg}^{-1}$.

Modelled parameter	Input parameters for each multilinear model test						N	R^2	Standard error
C_T _2003	T	S	A_T	-	-	-	1096	0.96	10.65
C_T _2011	T	S	A_T	-	-	-	1455	0.95	11.34
C_T _2003	T	S	DO	-	-	-	1271	0.98	8.02
C_T _2011	T	S	DO	-	-	-	1693	0.98	6.53
C_T _2003	T	S	AOU	-	-	-	1271	0.99	6.86
C_T _2011	T	S	AOU	-	-	-	1693	0.99	5.73
C_T _2003	T	S	AOU	A_T	-	-	1081	0.99	3.56
C_T _2011	T	S	AOU	A_T	-	-	1455	0.99	3.25
C_T _2003	T	S	AOU	NO_3	-	-	1079	0.99	5.89
C_T _2011	T	S	AOU	NO_3	-	-	1098	0.99	4.78
C_T _2003	T	S	AOU	A_T	Pres	-	1079	0.99	3.35
C_T _2011	T	S	AOU	A_T	Pres	-	1455	0.99	3.18
C_T _2003	T	S	AOU	NO_3	Pres	-	1079	0.99	3.67
C_T _2011	T	S	AOU	NO_3	Pres	-	1098	0.99	3.85
C_T _2003	T	S	AOU	A_T	NO_3	-	1079	0.99	3.47
C_T _2011	T	S	AOU	A_T	NO_3	-	1098	0.99	3.08
C_T _2003	T	S	AOU	PO_4	NO_3	-	1258	0.99	5.17
C_T _2011	T	S	AOU	PO_4	NO_3	-	624	0.99	4.10
C_T _2003	T	S	AOU	A_T	NO_3	Pres	1079	0.99	3.03
C_T _2011	T	S	AOU	A_T	NO_3	Pres	1098	0.99	2.90
C_T _2003	T	S	AOU	Lon	Lat	Pres	1271	0.99	4.93
C_T _2011	T	S	AOU	Lon	Lat	Pres	1693	0.99	4.92

Table 4. 6. Results from the A_T multiple linear regression (MLR) tests (at cruise sampling year). Each test was conducted using a different set of input parameters. T is temperature ($^{\circ}\text{C}$), S is salinity, A_T , DO is dissolved oxygen ($\mu\text{mol kg}^{-1}$), AOU is apparent oxygen utilization ($\mu\text{mol kg}^{-1}$), NO_3 is nitrate ($\mu\text{mol kg}^{-1}$), Pres is pressure (dbar), Lon is longitude, Lat is latitude. N indicates the number of measurements used in each test. R^2 is the coefficient of determination. The standard error is in $\mu\text{mol kg}^{-1}$.

Modelled parameter	Input parameters for each multilinear model test						N	R^2	Standard error
A_T _2003	T	S	Pres				1079	0.83	8.63
A_T _2003	T	S	AOU	Pres			1079	0.90	6.88
A_T _2011	T	S	AOU	Pres			1098	0.93	6.38
A_T _2003	T	S	Pres	Lon	Lat		1079	0.84	8.55
A_T _2003	T	S	AOU	Pres	Lon	Lat	1079	0.90	6.76

However, we aimed here to try to match the quality required by the GOA-ON community (*GOA-ON Requirements and Governance Plan*; [Newton et al., 2015](#)): climate and weather errors. These errors correspond to the precision in the calculation of carbonate ion concentration to be used to each type of study. The climate quality corresponds to an uncertainty of 1% in the estimation of the dissolved carbonate ion, and are defined as measurements of quality sufficient to assess long term trends. The weather quality corresponds to an uncertainty of 10% in the estimation of the dissolved carbonate ion, and are defined as measurements of quality sufficient to identify spatial patterns and short-term variations. Regarding ocean acidification, the climate data can be used to identify anthropogenically-driven changes in hydrographic conditions and carbonate chemistry over multidecadal timescales, whereas the weather data can be used to identify impacts/ecosystem responses on local and immediate carbonate system dynamics. Because this calculation can be performed using a pair of the carbonate system parameters (i.e. A_T , C_T , pH, $p\text{CO}_2$), the climate and weather definitions establish a limit on the precision of their measurements. The uncertainties for each parameter in both quality standards are presented on **Table 4.7**.

Table 4. 7. Limits of the uncertainties required for each carbonate system parameter in the climate and weather conditions, defined by the GOA-ON Requirements and Governance Plan (Newton et al., 2015).

Carbonate system parameter	Climate	Weather
Relative uncertainty of the dissolved carbonate ion	1%	10%
A_T	0.1% (2 μmol kg ⁻¹)	0.1% (10 μmol kg ⁻¹)
C_T	0.1% (2 μmol kg ⁻¹)	0.1% (10 μmol kg ⁻¹)
pH	~0.02% (0.003 pH units)	~0.14% (0.02 pH units)
pCO₂	0.5% (2 μatm)	2.5% (10 μatm)

As we can observe in **Tables 4.5** and **4.6**, none of those MLR models would be precise enough to fit in the GOA-ON climate requirements (**Table 4.7**), mainly without using nutrients and carbonate system, which would reduce the applicability of the models. Additionally, another goal of this modelling was to be able to apply the models in the greatest number of data as possible. Thus, we decided to test other types of models. We also chose to keep using just the standard CTD parameters as inputs. Thus, we use only potential temperature (θ), salinity and apparent oxygen utilization (AOU) to develop the models, allowing us to apply the models with the greatest number of data as possible, because this approach facilitated the reconstruction of C_T and A_T in all stations and depths where thermohaline properties were available. The C_T and A_T polynomial model tests are included on **Table 4.8** and **4.9**. As we can see, the errors reduced enough to match the climate criteria. It is interesting to reinforce that just a limited number of laboratories/facilities are able to match the climate requirements. However, the weather requirement is normally achieved. Regarding the sensors, even the best autonomous

sensors are not able to fit in the climate requirements, just in the weather (Newton et al., 2015).

Table 4. 8. Results from the C_T polynomial model tests (at cruise sampling year). Each test was conducted using a different set of input parameters. θ is potential temperature ($^{\circ}\text{C}$), S is salinity, AOU is apparent oxygen utilization ($\mu\text{mol kg}^{-1}$). N indicates the number of measurements used in each test. R^2 is the coefficient of determination. The RMSE – root mean square error is in $\mu\text{mol kg}^{-1}$.

Modelled parameter	Input parameters for each polynomial model test		N	R^2	RMSE
C_T_{2003}	θ	S	1271	0.99	3.05
C_T_{2011}	θ	S	1693	0.99	3.00
C_T_{2003}	θ	AOU	1081	0.99	1.66
C_T_{2011}	θ	AOU	1445	0.99	1.39

Table 4. 9. Results from the A_T polynomial model tests (at cruise sampling year). Each test was conducted using a different set of input parameters. θ is potential temperature ($^{\circ}\text{C}$), S is salinity, Pres is pressure (dbar). N indicates the number of measurements used in each test. R^2 is the coefficient of determination. The RMSE – root mean square error is in $\mu\text{mol kg}^{-1}$.

Modelled parameter	Input parameters for each polynomial model test		N	R^2	RMSE
A_T_{2003}	θ	-	1081	0.93	5.90
A_T_{2003}	θ	Pres	1081	0.99	2.60
A_T_{2003}	θ	S	1081	0.99	2.19
A_T_{2011}	θ	S	1445	0.99	1.45

Thus, we ended up choosing nonlinear regression, because the best fit to the A10 data was obtained with the polynomial models introduced in this work (Eq. 4.15; Tables 4.8 and 4.9). These models were developed using the ‘curve fitting tool’ toolbox of MATLAB®, with the Least Absolute Residual mode. This option considered all data as important, minimized the residuals, and can be used when the data series have few nonconfinable values (Patil, & Rao, 1994). The models were developed through polynomial equations introduced in this work and have the following form (Eq. 4.15):

$$f(x, y) = \sum_{i=0, j=0}^{5, 5-i} p_{ij} x^i y^j \quad (4.15)$$

where f represents the C_T or A_T functions ($\mu\text{mol kg}^{-1}$), x is the potential temperature (θ °C) for both C_T and A_T equations, y is the apparent oxygen utilization (AOU $\mu\text{mol kg}^{-1}$) for the C_T equation and the salinity for the A_T equation, x and y are standardized by the mean and standard deviations, and P_{ij} are the coefficients determined in this modelling, and are presented in **Table 4.10**. Specifically, i and j are the indices that indicate the exponent of the parameters corresponding to x and y in **Eq. 4.15**.

These polynomial models were subsequently applied to the dataset of the hydrographic sections of the TAI and FORSA cruises, allowing the subsequent analysis to be performed.

Table 4. 10. The p_{ij} coefficients (with 95% confidence bounds) of the polynomial models developed for C_T and A_T , according to Equation 1.

p_{ij}	C_T 2003	C_T 2011	A_T 2003	A_T 2011
p_{50}	5.58 (3.15, 8.00)	-0.75 (-2.90, 1.41)	23 (14.29, 31.72)	36.68 (29.17, 44.20)
p_{41}	20.60 (13.05, 28.15)	6.95 (0.15, 13.74)	-29.40 (-57.37, -1.43)	-96.18 (-120.20, -72.13)
p_{40}	0.45 (-2.98, 3.88)	6.93 (4.43, 9.43)	-7.85 (-20.30, 4.59)	30.47 (25.75, 35.19)
p_{32}	24.07 (15.41, 32.73)	11.43 (3.72, 19.14)	6.55 (-37.11, 50.21)	125.40 (89.63, 161.20)
p_{31}	-20.33 (-28.73, -11.93)	-6.88 (-14.14, 0.39)	-18.53 (-46.38, 9.33)	-73.75 (-86.35, -61.15)
p_{30}	-13.24 (-16.48, -9.99)	-3.11 (-5.78, -0.44)	-79 (-91.45, -66.56)	-62.81 (-73.50, -52.12)
p_{23}	15.78 (11.40, 20.15)	5.72 (1.32, 10.12)	4.30 (-32.74, 41.33)	-94.36 (-126.30, -62.47)
p_{22}	-24.29 (-32.38, -16.21)	-9.21 (-18.36, -0.063)	34.17 (9.75, 58.59)	44.70 (28.38, 61.01)
p_{21}	1.77 (-5.61, 9.16)	9.98 (3.77, 16.19)	93.98 (70.24, 117.70)	51.81 (28.92, 74.70)
p_{20}	12.64 (9.98, 15.30)	0.72 (-1.50, 2.95)	24.31 (13.12, 35.50)	-17.50 (-23.39, -11.62)
p_{14}	5.95 (4.07, 7.83)	1.48 (-0.75, 3.71)	-1.88 (-17.55, 13.81)	37.95 (22.51, 53.39)
p_{13}	-16.16 (-22.09, -10.24)	-2.89 (-9.13, 3.35)	-17.88 (-29.89, -5.87)	-5.77 (-17.95, 6.41)
p_{12}	6.77 (0.13, 13.41)	0.86 (-4.41, 6.13)	-27.04 (-45.30, -8.77)	5.61 (-13.96, 25.18)
p_{11}	1.35 (-2.96, 5.66)	-1.45 (-5.82, 2.93)	48.87 (36.32, 61.43)	88.42 (80.30, 96.55)
p_{10}	-25.28 (-26.49, -24.06)	-18.90 (-19.92, -17.88)	15.52 (11.26, 19.77)	15.70 (12.27, 19.14)
p_{05}	0.77 (0.09, 1.44)	-0.01 (-0.58, 0.55)	0.10 (-2.50, 2.71)	-6.18 (-9.16, -3.19)
p_{04}	-4.93 (-7.30, -2.57)	-0.83 (-2.67, 1.00)	3.53 (0.72, 6.34)	-1.66 (-5.20, 1.89)
p_{03}	5.13 (2.26, 8.00)	0.31 (-1.56, 2.18)	1.77 (-4.01, 7.54)	-5.85 (-12.48, 0.78)
p_{02}	1.38 (-1.43, 4.18)	4.13 (1.50, 6.78)	-35.18 (-41.12, -29.24)	-42.50 (-47.48, -37.52)
p_{01}	27.71 (26.21, 29.22)	25.69 (24.39, 26.99)	-18.71 (-23.04, -14.38)	-4.31 (-8.04, -0.58)
p_{00}	2158 (2158, 2158)	2156 (2156, 2156)	2303 (2300, 2306)	2309 (2308, 2311)

4.3.4. Anthropogenic carbon estimate

Considering that CO₂ can be continuously exchanged across the ocean-atmosphere interface and absorbed/produced by biological activity in the ocean photic layer (i.e., the carbon reservoirs are not in equilibrium), it is considered that the carbon permanently taken up by the ocean is below the surface mixed layer, where it can be split into natural and anthropogenic origin. Thus, the lower limit of the surface mixed layer is the upper ocean boundary, which is used to define the region in which the C_{ant} content can be estimated (Goyet et al., 2000). Therefore, in this work, we considered quantifying the C_{ant} below 200 m depth, excluding the surface mixed layer data (e.g., Touratier et al., 2007). This 200 m data for the surface mixed layer was defined by considering the deeper estimative from previous works found for the winter season (e.g., Talley et al., 2011).

We applied the *Tracer combining Oxygen, inorganic Carbon, and total Alkalinity* (TrOCA) method to estimate the C_{ant} (C_{ant-TrOCA}; Eq. 4.16; Touratier & Goyet, 2004a, 2004b; Touratier et al., 2007).

$$C_{ant-TrOCA} = \frac{DO + 1.279 * (C_T - 0.5 * A_T) - e^{\left[7.511 - (1.087 * 10^{-2}) * \theta - \left(\frac{7.81 * 10^5}{A_T^2}\right)\right]}}{1.279} \quad (4.16)$$

where DO, C_T and A_T are in μmol kg⁻¹, and θ is in °C.

In our calculations, we used the C_T and A_T obtained either from *in situ* measurements (for the A10_2003 and A10_2011 cruises) or the model results (for the FORSA and TAI cruises). Thus, we were able to estimate the C_{ant} content for all South Atlantic Ocean sections we wanted to. In addition, we decided to fix the C_{ant} content estimated in the 2003 cruise as a reference to calculate the C_{ant} content difference between

the cruise years ($\Delta C_{\text{ant-TrOCA}} 2011 - 2003$). Additionally, using the C_T model developed for the A10 cruises and applied in all of the cruise sections, the C_T content difference between years was determined ($\Delta C_T 2011 - 2003$). Considering the year of the cruise, we used the 2011 coefficients to apply for the TAII – 2011 cruise data to evaluate the snapshot period of this sampling moment. For the FORSA – 2015 cruise, we assumed a linear change between 2003 and 2011 and we added half of this C_T difference to derive the C_T increase between 2011 and 2015. Therefore, we evaluated the C_{ant} content for the entire industrial period ($C_{\text{ant-TrOCA}}$) and compared the C_{ant} and C_T differences between 2011 and 2003 (2015 and 2003, for the FORSA cruise section).

Chapter V. Articles

In order to obtain a Doctorate Degree from the graduation program in Physical, Chemical and Geological Oceanography, it is required to submit two manuscripts as a first author in a qualified scientific journal. Due to this, the results obtained during the thesis research period are presented here, in this section, as articles. They are included in their published version. Some details about them are included below.

The first manuscript “*The Sea-Air CO₂ Net Fluxes in the South Atlantic Ocean and the Role Played by Agulhas Eddies*”, by **Iole B. M. Orselli**, Rodrigo Kerr, José L. de Azevedo, Felipe Galdino, Moacyr Araujo and Carlos A. E. Garcia, was published in “*Progress in Oceanography*”.

The second manuscript “*The Effect of Agulhas Eddies on Absorption and Transport of Anthropogenic Carbon in the South Atlantic Ocean*”, by Iole B. M. Orselli, Catherine Goyet, Rodrigo Kerr, José L. L. de Azevedo, Moacyr Araujo, Felipe Galdino, Franck Touratier and Carlos A. E. Garcia, was published in the special issue “*Ocean Warming, Acidification and Deoxygenation*” of the journal “*Climate*”.

The focus of the study in the first manuscript was on investigate the role played by the Agulhas eddies in the fCO_2 along their trajectories through the South Atlantic Ocean and model the seawater CO_2 -related properties (pCO_2 , fCO_2 , $NpCO_2$, $NfCO_2$) as function of environmental parameters (temperature, salinity and chlorophyll-*a*). We used hydrographic and CO_2 -system properties continuously measured in a southeast-northwest transect in the South Atlantic Ocean in which six Agulhas eddies were sampled. The *Following Ocean Rings in the South Atlantic* (FORSA) cruise occurred in 2015 on board the first research cruise of the Brazilian Navy RV *Vital de Oliveira*, as part of an effort of the Brazilian High Latitude Oceanography Group (GOAL). We demonstrate that Agulhas eddies increase the CO_2 uptake at the sea surface when compared to surrounding waters.

In the second manuscript, the focus was on quantifying the C_{ant} content inside and outside the Agulhas eddies and on modelling the carbonate system parameters (C_T and A_T) in the South Atlantic Ocean. We used hydrographic and CO_2 -system data from the A10 CLIVAR/WOCE cruises from 2003 and 2011, the Trans-Atlantic II from 2011, and the FORSA cruise, all of them conducted along the South Atlantic Ocean. These 5 transects were used to investigate the anthropogenic carbon content inside 13 Agulhas eddies. In this study, we show that they contain up to 29% more anthropogenic carbon than surrounding waters, which could be influenced by the modal water formation process. Since the modal waters compose the SACW, and the Brazilian coastal region is being acidified, we conclude that the Agulhas eddies play a significant role in the

acidification state of the central waters of the South Atlantic Ocean, accelerating this process.

**5.1 First article – PhD 01: The sea-air CO₂ net
fluxes in the South Atlantic Ocean and the role
played by Agulhas eddies**



The sea-air CO₂ net fluxes in the South Atlantic Ocean and the role played by Agulhas eddies

Iole B.M. Orselli^{a,b,c,d,*}, Rodrigo Kerr^{a,b}, José L.L. de Azevedo^a, Felipe Galdino^a, Moacyr Araujo^{e,f}, Carlos A.E. Garcia^{a,g}

^a Laboratório de Estudos dos Oceanos e Clima, Instituto de Oceanografia, Universidade Federal do Rio Grande (FURG), Av. Itália km 8, s/n, Rio Grande, 96203-900 RS, Brazil

^b Brazilian Ocean Acidification Network (BrOA), Av. Itália km 8, Rio Grande, 96203-900 RS, Brazil

^c IMAGES ESPACE-DEV, Université de Perpignan Via Domitia (UPVD), 52 ave. Paul Alduy, 66860 Perpignan, France

^d ESPACE-DEV UMR UG UA UM IRD, Maison de la télédétection, 500 rue Jean-François Breton, 34093 Montpellier Cedex 5, France

^e Laboratório de Oceanografia Física, Estuarina e Costeira (LOFEC), Departamento de Oceanografia, Centro de Tecnologia, Universidade Federal de Pernambuco (UFPE), Av. Arquitetura, s/n, Recife, 50740550 PE, Brazil

^f Brazilian Research Network on Global Climate Change (Rede CLIMA), São José dos Campos, 12227-010 SP, Brazil

^g Programa de Pós-graduação em Oceanografia, Universidade Federal de Santa Catarina (UFSC), Campus Reitor João David Ferreira Lima, s/n, Florianópolis, 88040-900 SC, Brazil

ARTICLE INFO

Keywords:

Agulhas eddies
Agulhas corridor
CO₂ fluxes
South Atlantic Ocean

ABSTRACT

The South Atlantic Ocean is vitally important to the global overturning circulation, which is influenced by heat, salt and other properties carried by Agulhas eddies. However, this influence is not yet fully understood, mainly in the context of the biogeochemistry changes on the CO₂ system. This study uses *in situ* data obtained during the *Following Ocean Rings in the South Atlantic* cruise, which occurred between Cape Town, South Africa and Arraial do Cabo, Brazil in July 2015 when six eddies and the surrounding waters were sampled. The seawater and atmospheric CO₂ molar fraction, surface temperature and salinity were continuously measured to calculate the oceanic and atmospheric CO₂ partial pressures ($p\text{CO}_2^{\text{sw}}$ and $p\text{CO}_2^{\text{atm}}$, respectively). This study investigated the role played by the Agulhas eddies in the sea-air CO₂ net flux (FCO₂) and modeled the seawater CO₂ as a function of environmental parameters. The mean $p\text{CO}_2^{\text{sw}}$ and $p\text{CO}_2^{\text{atm}}$ for the entire region were 351.5 and 390.6 μatm , respectively. The mean difference ($\Delta p\text{CO}_2$) was $-39.1 \mu\text{atm}$. The CO₂ uptake was dominated by temperature ($r = 0.88$) during the period analyzed. The mean FCO₂ was -3.76 and $-3.62 \text{ mmol m}^{-2} \text{ d}^{-1}$ using two different K_T -models. We show that an Agulhas eddy can contribute to an ocean uptake of $-3.16 \text{ kg CO}_2 \text{ d}^{-1}$, leading to the capture of approximately $2.52 \text{ t CO}_2 \text{ lifetime}^{-1}$. Thus, providing evidence that the Agulhas eddies propagation can likely play a key role on the rapid seawater acidification of the South Atlantic Central Water. A multiple linear regression model was developed that could reliably reconstruct the cruise survey with better results than previously published.

1. Introduction

Carbon dioxide (CO₂) has been released into the atmosphere by human activities at significantly increasing levels since the beginning of the Industrial Revolution (e.g., Ciais et al., 2013; Le Quéré et al., 2016). These emissions cause important changes in the Earth's climate system and the marine carbon cycle (e.g., Ciais et al., 2013; Le Quéré et al., 2015). Previous studies considered the South Atlantic Ocean (SAO) as an atmospheric CO₂ sink, with an average sea-air CO₂ net flux (FCO₂) of $-0.3 \text{ Pg C yr}^{-1}$ (e.g., Takahashi et al., 1997, 2002). Although

Takahashi et al. (2009) improved the global carbon cycle comprehension, the scarcity of marine carbon system data has led to few studies being conducted in the SAO compared to the North Atlantic Ocean. Zeng et al. (2014), using a model study conducted at the global scale, found a good agreement with the climatology results reported by Takahashi et al. (2009), even using a finer spatial data resolution to derive a basin scale product. In addition, Wang et al. (2015) conducted a comparative study between equatorial Pacific and Atlantic oceans and concluded that the latter behaved as a CO₂ source to the atmosphere with a strong seasonality, but with slight interannual variability. Other

* Corresponding author at: LEOC, Instituto de Oceanografia – FURG, Avenida Itália km 8 s/n°, Campus Carreiros, Rio Grande 96203–900, Brazil.
E-mail address: iole.orselli@furg.br (I.B.M. Orselli).

<https://doi.org/10.1016/j.pocean.2018.10.006>

Received 20 March 2018; Received in revised form 2 October 2018; Accepted 6 October 2018

Available online 06 October 2018

0079-6611/ © 2018 Published by Elsevier Ltd.

studies concluded that subtropical waters from both hemispheres acted as a sink of CO₂ during the spring and a source during the autumn (e.g., Padin et al., 2010), which was recently corroborated by Lencina-Avila et al. (2016). Those authors reported a CO₂ sink behavior in the SAO along 35°S during the spring of 2011.

Two main mechanisms drive the ocean CO₂ uptake: the biological and the physical pumps, and the former can be divided into the organic carbon and the carbonate counter pumps (e.g., Sarmiento and Gruber, 2006; Denman et al., 2007; Ciaia et al., 2013). The organic carbon pump is related to CO₂ uptake by phytoplankton organisms during the photosynthesis process. On the other hand, the calcium carbonate (CaCO₃) used by organisms to construct their calcareous shells (e.g., Cox et al., 2000) also releases CO₂ and reduces the total alkalinity in the seawater, configuring the carbonate counter pump (e.g., Rost and Riebesell, 2004). The physical pump refers to the CO₂ solubility and sinking regulated by colder and less salty waters. The water mass formation processes act to sequester the CO₂ to deeper regions (e.g., Orsi et al., 1999; Sabine et al., 2004; Rintoul, 2011; Talley et al., 2011; Pardo et al., 2014).

Because this study focuses on the sea-air CO₂ interactions in a cruise section of the SAO, we only describe here the ocean surface circulation of the subtropical anticyclonic gyre that dominates this basin, which encompasses the region of this study. This gyre is formed by the Brazil Current, South Atlantic Current, Benguela Current System and South Equatorial Current (Fig. 1). The Brazil Current is the western boundary current of the SAO gyre that flows southward, whereas the east-upwelling system includes the Benguela Current System that flows northward. In the same way, flowing in opposite directions in the zonal system, the South Atlantic Current (eastward) and the South Equatorial Current (westward) close the gyre. The subtropical gyre is also affected by the intrusion of Indian Ocean central and intermediate waters that enter the SAO carried by eddies shed from the Agulhas Current retroflexion zone (e.g., Peterson and Stramma, 1991; Gordon et al., 1992; Talley et al., 2011; de Souza et al., 2018).

The Agulhas Current leakage is primary composed of filaments detached from the main flux, but the major escape of the Agulhas Current retroflexion region is constituted by the Agulhas eddies (Lutjeharms, 2006). The role of the Agulhas Current leakage (eddies and filaments) in the Atlantic Meridional Overturning Circulation is considered meaningful in previous studies (e.g., Lutjeharms, 2006; Biastoch et al., 2009, 2015), but the real scale of this role is still debated (e.g., de Ruijter et al., 1999; Souza et al., 2011; Casanova-Masjoan et al., 2017; de Souza et al., 2018). The Agulhas eddies are among the largest mesoscale structures in the global ocean (Biastoch et al., 2008), thus they can transport important amounts of heat and salt (e.g., Lutjeharms, 2006). They also carry potential vorticity and biogeochemical properties from their formation regions, so they present distinct characteristics

from the surrounding waters (e.g., Flierl, 1979) and play a major role in physical and biological processes (e.g., Robinson, 1983; Beal, 2009), molding the biological production (Lehahn et al., 2011). Those features are self-propelled westward in the SAO as a result of the meridional balance of the forces acting on them. They are also forced to drift to the equator due to the induced vorticity, resulting in a northwestern trajectory when crossing the SAO (e.g., Azevedo and Mata, 2010). A common mesoscale eddy has a temporal scale that can vary from weeks to months (Chelton et al., 2011), whereas an Agulhas eddy has an estimated lifetime of more than two years (Lutjeharms, 2006). They have a horizontal scale ranging up to 300 km, a vertical scale ranging from 1500 to 2000 m (Biastoch and Krauss, 1999) or even farther (e.g., Beal, 2009). Their net volume transport varies from 0.5 to 1.5 Sv (1 Sv = 10⁶ m³ s⁻¹), which can affect the Atlantic Meridional Overturning Circulation in decadal or even larger scales primarily by salt advection (e.g., Beal, 2009; Biastoch et al., 2009). The transport of heat and salt from the Agulhas eddies reinforces their role in the SAO (e.g., Lutjeharms, 2006), because a release of approximately six eddies per year is expected (Gordon, 2003; Lutjeharms, 2006). These structures also have an effect on air-sea heat fluxes, the overlaying atmosphere circulation (Lutjeharms, 2006; Frenger et al., 2013), and biogeochemistry (McGillicuddy, 2016; Moreau et al., 2017). Villas Bôas et al. (2015) associated the presence of anticyclonic eddies with the positive heat flux anomalies that tend to warm the atmospheric boundary layer. In addition, Woosley et al. (2016) indicated that eddies in the SAO can contain approximately 20% more anthropogenic carbon than the surrounding waters.

Thus, even admitting that these mesoscale eddies play a vital role in ocean-atmosphere interactions, their effect on the changes in the marine carbonate system are not yet constrained, primarily considering the sea-air exchanges of CO₂ (e.g., Ríos et al., 2003; Woosley et al., 2016; Moreau et al., 2017). To shed new light on this complex issue, in this work we investigate the role played by the Agulhas eddies in the CO₂ exchanges within the ocean-atmosphere interface while they are crossing the region of the subtropical gyre of the SAO. We also model the CO₂-related parameters (e.g., partial pressure – pCO₂) aiming to reduce the lack of knowledge on the marine CO₂ system in this region.

2. Data and methods

2.1. Sampling strategy

This study was conducted as part of the efforts of the *Following Ocean Rings in the South Atlantic* (FORSA) cruise, from Cape Town – South Africa to Arraial do Cabo – Brazil (Fig. 1), on board the first research cruise of the Brazilian Navy RV *Vital de Oliveira* between 27th June and 15th July 2015, conducted under the umbrella of the

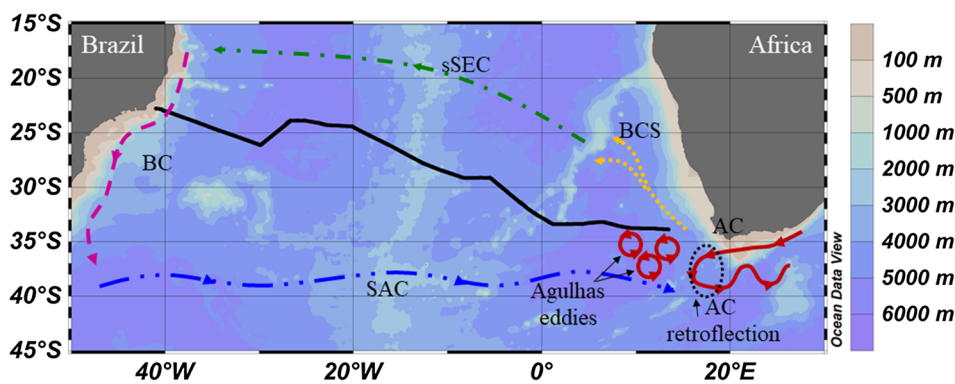


Fig. 1. Map of the study region in the South Atlantic Ocean. The black continuous line corresponds to the FORSA cruise section. The schematic flows of the main ocean currents of the subtropical anticyclonic gyre are indicated as: The Benguela Current System (BCS, yellow dotted line), southern branch of the South Equatorial Current (sSEC, green dot-dashed line), Brazil Current (BC, magenta dashed line) and South Atlantic Current (SAC, blue dot-dot-dashed line). The Agulhas Current (AC, red continuous line), Agulhas eddies (red continuous circles) and Agulhas Current retroflexion zone (black dotted ellipse) are also indicated in this representative map. Please see Peterson and Stramma (1991) for further details about the

ocean circulation in the region. The bottom bathymetry is represented by color shadings. (For interpretation of the references to color in this figure legend, the reader is referred to the web version of this article.)

Brazilian High Latitudes Oceanographic Group (GOAL). During this cruise six mesoscale eddies were sampled crossing the subtropical gyre of the SAO.

The seawater and atmospheric CO₂ molar fraction ($x\text{CO}_2^{\text{sw}}$ and $x\text{CO}_2^{\text{atm}}$, respectively) were continuously measured during the cruise track, as well as the sea surface temperature (T) and salinity (S). The underway $x\text{CO}_2$ sampling was taken using an autonomous system GO-8050, General Oceanic®, equipped with a non-dispersive infrared gas analyzer (LI-7000, LI-COR®). The underway T and S were sampled using a Sea-Bird® Thermosalinograph SBE21. Seawater intake to measure those parameters by the continuous systems was set at ~5 m below the sea surface.

Hydrographic stations were conducted to have profiles outside and inside of each eddy, using CTD and XBT probes. Apart from physical data, discrete seawater samples were collected for chemical and biological analysis, including: dissolved oxygen (DO), phytoplankton pigments, dissolved inorganic nutrients, total, particulate and dissolved organic carbon, total alkalinity and pH, using a combined Sea-Bird CTD/Carrousel 911 + system® equipped with 24 twelve-liter Niskin bottles. Here, we only focus on describing the parameters that are related to this study.

2.2. CO₂ partial pressure data analysis

To accurately measure the $x\text{CO}_2$, the system was calibrated with four standard gases (CO₂ concentrations of 0, 202.10, 403.20, and 595.50 μatm) within a 12 h interval throughout the entire cruise. Every 3 h the system underwent a standard reading, to check the derivation and allow the $x\text{CO}_2$ corrections. The $x\text{CO}_2$ measurements were taken within 90 s intervals. After a hundred $x\text{CO}_2^{\text{sw}}$ readings, the system was changed to monitor the atmosphere and five $x\text{CO}_2^{\text{atm}}$ readings were taken (Pierrot et al., 2009).

As it is necessary to have accurate T and S measurements to calculate the $p\text{CO}_2$, the thermosalinograph data were corrected using the CTD surface data. Then, together with the pressure data, these data were used to calculate the $p\text{CO}_2$ of the equilibrator and atmosphere ($p\text{CO}_2^{\text{eq}}$ and $p\text{CO}_2^{\text{atm}}$, respectively), following Weiss and Price (1980). The parameters used to develop this calculation were: $x\text{CO}_2$ ($\mu\text{mol mol}^{-1}$) inputs, corrected by the CO₂ standards (Pierrot et al., 2009); the atmospheric pressure (atm); the water vapor pressure (atm) inside the equilibrator; the water vapor pressure (atm); the equilibrator temperature (°C); the *in situ* temperature (°C); and the salinity. The equilibrator temperature was obtained using a Hart® digital thermometer probe installed in the CO₂-system main equilibrator (Pierrot et al., 2009). The *in situ* temperature and the salinity were obtained from the thermosalinograph.

Using the $p\text{CO}_2^{\text{eq}}$, which is calculated at the equilibrator temperature, it is possible to calculate the $p\text{CO}_2$ at the *in situ* temperature ($p\text{CO}_2^{\text{sw}}$), according to Takahashi et al. (2009).

Another common calculation involving $p\text{CO}_2^{\text{sw}}$ data is the temperature-normalized $p\text{CO}_2^{\text{sw}}$ ($Np\text{CO}_2^{\text{sw}}$). This means that the temperature effect is removed when one calculates the $Np\text{CO}_2^{\text{sw}}$ for the mean cruise temperature. This procedure followed Takahashi et al. (2009) and considered the mean cruise temperature of 20.39 °C.

The results obtained from these calculations ($p\text{CO}_2^{\text{sw}}$, $p\text{CO}_2^{\text{atm}}$) allow one to investigate the exchanges of CO₂ at the ocean-atmosphere interface by calculating the $p\text{CO}_2$ difference between these two reservoirs ($\Delta p\text{CO}_2$). Negative (positive) $\Delta p\text{CO}_2$ results indicate that the ocean acts as a CO₂ sink (source) for the atmosphere.

2.3. Sea-air CO₂ net fluxes

To determine the FCO₂, the monthly mean wind speed data of July 2015 (at 10 m height) were extracted from the ERA-Interim atmospheric reanalysis product of the European Centre for Medium Range Weather Forecast (<http://apps.ecmwf.int/datasets/data/interim-full->

[moda/levtype=sfc/](http://apps.ecmwf.int/datasets/data/interim-full-)) because the use of a long-term mean is usual (e.g., Takahashi et al., 2009). The average wind speed for the period and entire region was $6.8 \pm 0.6 \text{ m s}^{-1}$, ranging from 5.6 to 8.3 m s^{-1} (Fig. S1). The CO₂ transfer coefficients (K_T) proposed by Takahashi et al. (2009) and Wanninkhof (2014) were chosen for evaluation. Because the difference between the FCO₂ determined with Takahashi et al. (2009) and Wanninkhof (2014) coefficients (FCO₂^{T09} and FCO₂^{W14}, respectively) was relatively small (FCO₂^{T09} – FCO₂^{W14} = $-0.14 \pm 0.06 \text{ mmol m}^{-2} \text{ d}^{-1}$), the FCO₂ is hereafter represented as the FCO₂^{T09} in all figures in this paper. This choice was made because the monthly mean wind speed data were used to calculate the FCO₂, which is recommended for the K_T model determined by Takahashi et al. (2009). The equation describing this coefficient is presented below (Eq. (1)):

$$K_T = 0.26 * u^2 * \left(\frac{Sc}{660} \right)^{-1/2} \quad (1)$$

where K_T is the CO₂ transfer coefficient according to the reference indicated; u is the wind speed (m s^{-1}) at a height of 10 m; Sc is the Schmidt number, defined for seawater and FCO₂ studies as: $Sc = A - B * t + C * t^2 - D * t^3$, where t is the *in situ* temperature (°C); $A = 2073.1$; $B = 125.62 \text{ °C}^{-1}$; $C = 3.6276 \text{ °C}^{-2}$; and $D = 0.043219 \text{ °C}^{-3}$ (Jahne and Dietrich, 1987). The FCO₂ was determined according to Eq. (2) (Broecker and Peng, 1982):

$$\text{FCO}_2 = K_T * K_S * \Delta p\text{CO}_2 \quad (2)$$

where FCO₂ is the sea-air CO₂ net flux ($\text{mmol m}^{-2} \text{ d}^{-1}$); K_T is the gas transfer coefficient; K_S is the CO₂ solubility coefficient, which is a function of the temperature and salinity (Weiss, 1974).

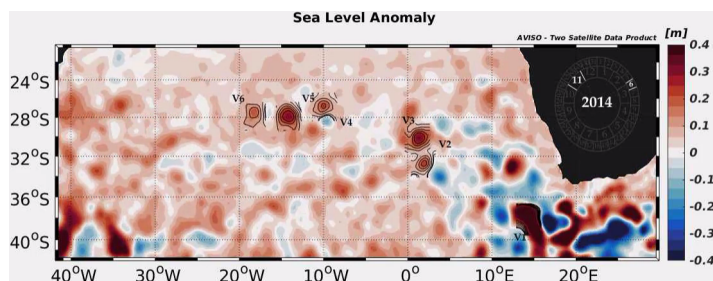
2.4. FORSA cruise eddy identification

We used the mesoscale eddy trajectory AVISO product (downloaded from <https://www.aviso.altimetry.fr/en/data/products/value-added-products/global-mesoscale-eddy-trajectory-product.html>, last data from January 6th 2017; Chelton, et al., 2011; Chelton and Schlax, 2016; Schlax and Chelton, 2016), to identify the six sampled eddies and their back and forward trajectories. This procedure allowed the determination of the radius (km) and lifetime (days – d). More information about the AVISO product, radius and lifetime determinations are included in the Supporting Information (Text S1). With the eddies description parameters and the FCO₂ estimates (i.e., daily CO₂ sink estimated for the FORSA cruise track, Eq. (2)), the CO₂ uptake for the entire region of each eddy was calculated, extrapolated for one year and for the lifetime of the eddy.

We used geometric means to establish an ‘Agulhas typical’ eddy, which can be considered a representative eddy among the sampled ones. Geometric means are frequently used when comparing different elements that have multiple properties (with different numerical scales), thus allowing a representative figure to be constructed for all the elements (e.g., Fleming and Wallace, 1986; Pal, 1998). In addition, we determined some eddy parameters to represent an ‘Agulhas true’ eddy and an ‘Agulhas evolved’ eddy, thus better characterizing these mesoscale structures in each of the SAO basins. This procedure was adopted because the first three sampled eddies (hereafter referred to as V1, V2 and V3) were surveyed on the eastern side of the Mid-Atlantic Ridge (13°W), whereas the last three (hereafter referred to as V4, V5 and V6) were in the western basin. The ‘Agulhas true’ eddy represents the recent and young mesoscale structures shed by the Agulhas retro-reflection. The ‘Agulhas evolved’ can be considered a modified Agulhas eddy because the last three eddies suffered splitting and/or merging processes during their trajectories. Observing the sea level anomaly data along their trajectories, these three eddies were found to interact with each other (Video S1) even when they were in the eastern basin (V4 and V5, V5 and V6) or when they were close to the Mid-Atlantic Ridge (V4 and V5). A short period of interaction was also observed for

V2 and V3. In addition, the V1 signal was strong throughout its entire life, not only in the eastern basin, where it was sampled in the FORSA cruise. Apart from the interactions between these six eddies, there are interactions between these eddies and other features. In these cases, the merging (splitting) process causes their radii to increase (reduce) during their lives. Thus, this approach allowed us to distinguish a more detailed picture of the Agulhas eddies evolution throughout the SAO, because the determination of the ‘Agulhas typical’ eddy probably masks the evolution of its spatial and temporal dynamics.

upper layer of the western sampled region (this reference point coincided with the Longitude 0°); South Atlantic Central Water ($\theta < 18.5^\circ\text{C}$, $34.3 < S$); Antarctic Intermediate Water ($2^\circ\text{C} < \theta < 6^\circ\text{C}$, $33.8 < S < 34.8$); and North Atlantic Deep Water ($1.5^\circ\text{C} < \theta < 4^\circ\text{C}$, $34.8 < S < 35$). Some authors consider the Upper Circumpolar Deep Water as the deepest water mass that can be observed in the upper ocean, being present above the North Atlantic Deep Water at an approximately 1000 m depth in the tropics (e.g., Stramma and England, 1999). However, a better characterization of this water mass



Video S1.

2.5. Satellite-derived data and CO₂ modeling

The data from MODIS-AQUA (<http://oceancolor.gsfc.nasa.gov/>), daily 4 km resolution, level 3, were used to calculate the satellite-derived sea surface chlorophyll-*a* (chl-*a*, mg m⁻³). This process was conducted using the OC3M algorithm, which returns the near-surface chl-*a*, calculated using an empirical relationship derived from *in situ* measurements of chl-*a* and remote sensing reflectance in the blue-to-green region of the visible spectrum (e.g., Lencina-Avila et al., 2016). On cloudy days, the chl-*a* average for that day ± 1 was used.

To model the CO₂^{sw}-related parameters ($p\text{CO}_2^{\text{sw}}$, CO₂ fugacity – $f\text{CO}_2^{\text{sw}}$, $Np\text{CO}_2^{\text{sw}}$, temperature-normalized CO₂ fugacity – $Nf\text{CO}_2^{\text{sw}}$), we used chl-*a*, T and S. Underway T and S were obtained from the thermosalinograph and adjusted to match the chl-*a* resolution. These data were used to feed a multiple linear regression (MLR) model (e.g., Hales et al., 2012; Signorini et al., 2013). The MLR equation used to estimate the modeled CO₂^{sw} ($m\text{CO}_2^{\text{sw}}$) in the SAO is described by Eq. (3) (e.g., Ito et al., 2016; Lencina-Avila et al., 2016):

$$m\text{CO}_2^{\text{sw}} = \alpha + \beta_1 \cdot (T - \bar{T}) + \beta_2 \cdot (S - \bar{S}) + \beta_3 \cdot (\text{chl}a - \bar{\text{chl}a}) \quad (3)$$

where α is the intercept of the linear regression, and β_i ($i = 1, 2, 3$) are the unknown coefficients to be determined for each parameter (e.g., Ito et al., 2016; Lencina-Avila et al., 2016). The anomalies of T, S and chl-*a* were previously calculated by subtracting the mean of that same variable before developing the model coefficients, as shown in.

3. Results

3.1. Hydrographic structure

The thermal structure obtained from the XBT data along the FORSA transect allowed the visualization of the vertical structure of the six Agulhas eddies sampled during the cruise (Fig. 2). The eddy temperature signals, i.e., isothermal downward displacement, are identifiable until depths higher than 1000 m (Fig. 2b). Apart from the expected temperature difference between eastern and western basins, it is important to note that this difference was even larger because the cruise track was conducted in a southeast-northwest direction. According to the thermohaline ranges described by Emery (2003) and Möller et al. (2008), the main water masses identified in the FORSA section are (Fig. 2b): Tropical Water (potential temperature, $\theta \geq 18.5^\circ\text{C}$), in the

would be possible if we had other tracers (Stramma and England, 1999), which is not the focus of this study. The physico-chemical diagrams constructed with the CTD profiles are shown in Fig. S2.

3.2. CO₂ partial pressure and sea-air CO₂ net fluxes in the South Atlantic basins

In this section we present the results from the entire region and the eastern and western basins (Tables 1 and S1, Figs. 3 and 4) as we

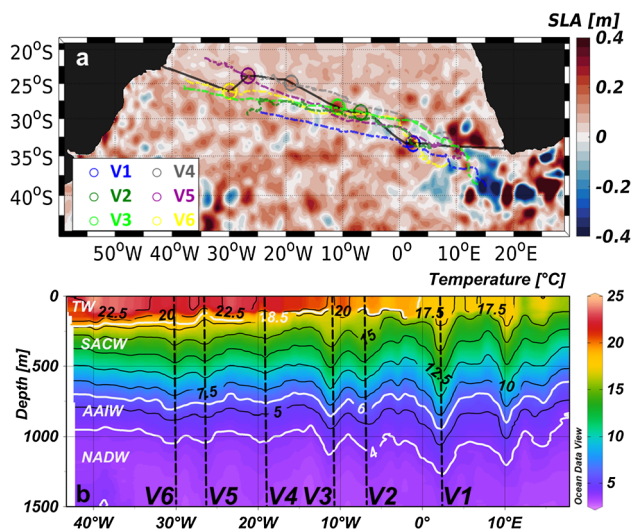


Fig. 2. (a) Map of the South Atlantic Ocean composed from a snapshot of the sea level anomaly (SLA – m) data of 4th July 2015. The black continuous line corresponds to the FORSA trajectory. The colored-dashed lines correspond to each eddy trajectory. The colored circles indicate the position of each eddy when sampled during the FORSA cruise. The colors used to represent each eddy are indicated in the plot. (b) The XBT temperature section for the cruise transect. The vertical black-dashed lines indicate the center of the eddies. The white continuous lines show the isotherms splitting each indicated water mass, as follows: TW – Tropical Water, SACW – South Atlantic Central Water, AAIW – Antarctic Intermediate Water, NADW – North Atlantic Deep Water. In both subplots, V_n ($n = 1$ to 6) indicates the number of each sampled eddy. (For interpretation of the references to color in this figure legend, the reader is referred to the web version of this article.)

Table 1

Average \pm standard deviation (std) and range (min; max) of the results from: temperature (T, °C); salinity (S); and CO₂-related parameters: seawater CO₂ partial pressure ($p\text{CO}_2^{\text{sw}}$, μatm), temperature-normalized $p\text{CO}_2^{\text{sw}}$ ($Np\text{CO}_2^{\text{sw}}$, μatm , @ 20.39 °C), sea-air CO₂ difference ($\Delta p\text{CO}_2$, μatm) and sea-air CO₂ net flux calculated using Takahashi et al. (2009) coefficient ($\text{FCO}_2^{\text{T09}}$, $\text{mmol m}^{-2} \text{d}^{-1}$). n is the number of measurements.

Parameter	Western basin (n = 5010)	Eastern basin (n = 5400)	Entire area (n = 10410)
T	22.60 \pm 1.44 20.07; 26.13	18.34 \pm 1.25 14.78; 20.85	20.39 \pm 2.51 14.78; 26.13
S	35.70 \pm 0.37 34.73; 36.24	35.53 \pm 0.16 34.58; 35.80	35.61 \pm 0.30 34.58; 36.24
$p\text{CO}_2^{\text{sw}}$	362.0 \pm 10.5 348.5; 394.4	341.5 \pm 11.0 306.3; 358.9	351.5 \pm 14.9 306.2; 394.4
$p\text{CO}_2^{\text{atm}}$	388.2 \pm 2.8 383.5; 400.8	392.9 \pm 1.9 388.0; 397.8	390.6 \pm 3.3 383.5; 400.8
$Np\text{CO}_2^{\text{sw}}$	330.5 \pm 11.4 308.0; 357.6	372.0 \pm 15.6 343.9; 425.3	351.4 \pm 24.4 308.0; 425.3
$\Delta p\text{CO}_2$	-26.5 \pm 11.7 -45.7; 10.3	-51.4 \pm 11.5 -86.8; -30.8	-39.1 \pm 17.1 -86.8; 10.3
$\text{FCO}_2^{\text{T09}}$	-2.5 \pm 1.1 -4.3; 1.0	-4.9 \pm 1.2 -8.3; -2.9	-3.8 \pm 1.7 -8.3; 1.0

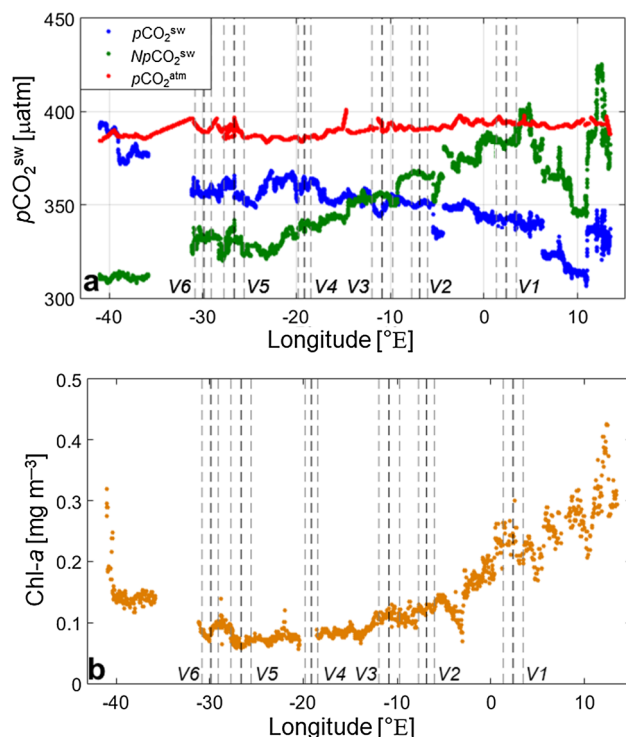


Fig. 3. Longitudinal distribution of: (a) $p\text{CO}_2^{\text{atm}}$ (red, μatm), $p\text{CO}_2^{\text{sw}}$ (blue, μatm) and temperature-normalized $p\text{CO}_2^{\text{sw}}$ ($Np\text{CO}_2^{\text{sw}}$, green, μatm). The $Np\text{CO}_2^{\text{sw}}$ calculation considered a mean temperature of 20.39 °C. (b) Chl-*a* (mg m^{-3}). The black-dashed lines indicate the center of the eddies whereas the gray-dashed lines indicate their eastern and western limits. (For interpretation of the references to color in this figure legend, the reader is referred to the web version of this article.)

established the Mid-Atlantic Ridge (13°W) as a boundary between the two basins.

The surface T and S, as well as the $p\text{CO}_2^{\text{sw}}$, were lower in the eastern basin than in the western basin (Table 1, Figs. 3 and 4). The western basin $p\text{CO}_2^{\text{atm}}$ was lower than that of the eastern basin. Apart from the

behavior of both basins as a sink, the eastern basin $\Delta p\text{CO}_2$ and FCO_2 values were lower, indicating a stronger CO₂ uptake in this basin, almost two-fold higher than the western basin uptake (Table 1, Fig. 4b and 4c). In addition, the most intense CO₂ sink was observed in the easternmost part of the eastern basin, achieving a $\Delta p\text{CO}_2$ of $-86.81 \mu\text{atm}$ near the Agulhas leakage region (Figs. 3 and 4b). The T, S and chl-*a* vs. $p\text{CO}_2^{\text{sw}}/Np\text{CO}_2^{\text{sw}}$ linear correlation coefficients indicate that the temperature dominates this behavior as sink (Table S1), with a linear correlation coefficient of 0.88 ($p < 0.01$) for the entire cruise section. However, the role played by chl-*a* cannot be neglected, because the linear correlation coefficient between $p\text{CO}_2^{\text{sw}}$ and chl-*a* was -0.55 ($p < 0.01$; Table S1). Analyzing the eastern basin, primarily focusing on the region east of 7°E, we see that the chl-*a* concentration is high in the same region that the $Np\text{CO}_2^{\text{sw}}$ does not change the pattern, and the opposition of the $Np\text{CO}_2^{\text{sw}}$ becomes noticeable when the chl-*a* decreases (Fig. 3). In addition, in this basin the linear correlation coefficient supports this interpretation, because between $p\text{CO}_2^{\text{sw}}$ and the temperature it was 0.61 ($p < 0.01$), whereas between $p\text{CO}_2^{\text{sw}}$ and chl-*a* it was -0.69 ($p < 0.01$; Table S1, Fig. 4). In the western basin, the temperature was the strongest driver with a linear correlation coefficient of 0.92 ($p < 0.01$), but the salinity also had an important contribution, as the correlation coefficient was -0.65 ($p < 0.01$; Table S1, Fig. 4). Regarding the biological contribution, there was a positive correlation between $p\text{CO}_2^{\text{sw}}$ and chl-*a* of 0.81 ($p < 0.01$), which indicates the possibility of an indirect contribution from the biological production to the $p\text{CO}_2^{\text{sw}}$. In addition, the correlation coefficient between the $Np\text{CO}_2$ and chl-*a* was -0.66 ($p < 0.01$), corroborating the interpretation of an indirect contribution (Table S1).

Although the mean CO₂-related parameters indicate CO₂ uptake by the ocean in the entire western basin (Table 1), a release of CO₂ to the atmosphere is observed near the Brazilian coast. We explore this region in more detail in the Supporting Information (Fig. S3, Table S2) and a brief discussion regarding these results is presented in Section 4.1.2.

3.3. Eddy CO₂ partial pressure and sea-air CO₂ net fluxes

All six eddies sampled during the FORSA cruise behaved as CO₂ sinks, with mean $\Delta p\text{CO}_2$ values ranging from -51.87 to $-24.74 \mu\text{atm}$ and mean $\text{FCO}_2^{\text{T09}}$ values ranging from -4.98 to $-2.34 \text{mmol m}^{-2} \text{d}^{-1}$ (V1 and V4, respectively; Table 2). The longitudinal distributions of $p\text{CO}_2^{\text{sw}}$, $\Delta p\text{CO}_2$, $\text{FCO}_2^{\text{T09}}$ and T in each eddy are presented in Fig. S4. The linear correlation coefficients for environmental parameters vs. $p\text{CO}_2^{\text{sw}}$ and vs. $Np\text{CO}_2^{\text{sw}}$ for each eddy indicate that the physical parameters dominate the CO₂ uptake, but the biological activity also contribute to this (Table S3). Analyzing the $\text{FCO}_2^{\text{T09}}$ distribution, it can be verified that the sinking capacity is reduced along the northwestern trajectory. This reduction coincides with the fact that the downward displacement of the isopycnals is shallower in the eddies present at the western basin than in those in the eastern basin (Fig. 2b and S5), in which the surface temperature is lower and the temperature anomaly is more prominent (Figs. 2, S4, S5).

Despite being slightly larger and having a longer lifetime, the ‘Agulhas evolved’ eddy is less efficient in the uptake of CO₂ from the atmosphere than the ‘Agulhas true’ eddy, suggesting that the capacity of the Agulhas eddies to act as a CO₂ sink mesoscale structure is reduced along their northwestward trajectory. Nevertheless, the ‘Agulhas typical’ eddy can be considered a representative eddy of the FORSA sampled eddies and can uptake 2.08 t of CO₂ over its lifetime (Table 3).

3.4. South Atlantic ocean CO₂^{sw}-related parameters modeling

Modeled vs. measured coefficients of determination ranged from 0.81 to 0.91 ($p\text{CO}_2^{\text{sw}}$ and $Np\text{CO}_2^{\text{sw}}$, respectively). The temperature-normalized properties (i.e., $Np\text{CO}_2^{\text{sw}}$ and $Nf\text{CO}_2^{\text{sw}}$) showed no significant difference between each other, and a small variation was identified when compared to the non-normalized (i.e., $p\text{CO}_2^{\text{sw}}$ and

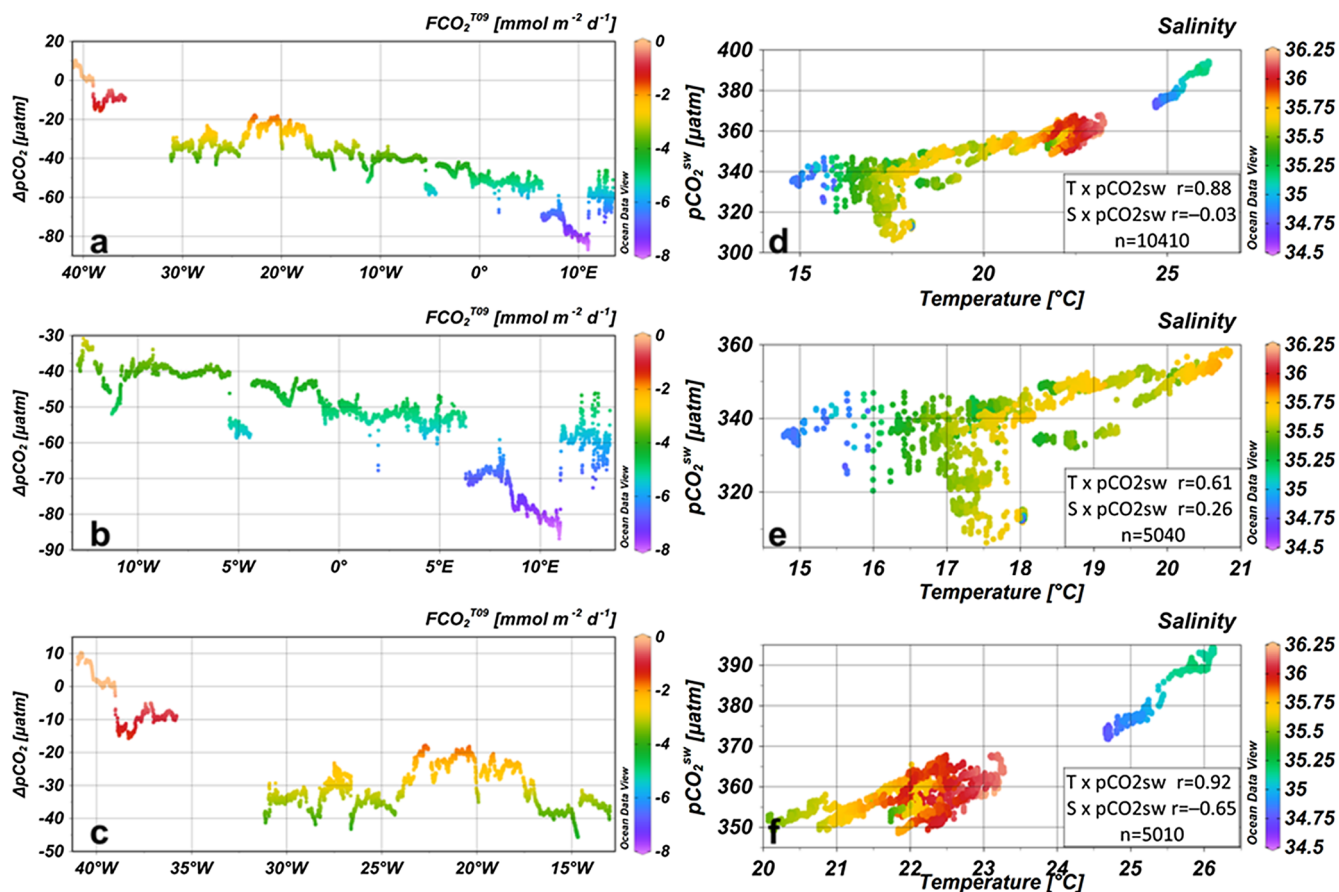


Fig. 4. Left column: Longitudinal distribution of $\Delta p\text{CO}_2$ (μatm) with sea-air CO_2 net flux ($\text{FCO}_2^{\text{T09}}$, $\text{mmol m}^{-2} \text{d}^{-1}$) calculated using the K_T determined by Takahashi et al. (2009) in colors. Right column: temperature ($^{\circ}\text{C}$) vs. $p\text{CO}_2^{\text{sw}}$ (μatm) diagrams, with salinity in colors. Inside each right panel are inserted the linear correlation coefficients (r) between temperature and salinity vs. $p\text{CO}_2^{\text{sw}}$ and the number of data points used (n). Significance at 95% confidence level ($p < 0.01$). Panels (a and d) encompass all cruise data. Panels (b and e) show the eastern basin data. Panels (c and f) show the western basin data. Note that the color scales used for $\text{FCO}_2^{\text{T09}}$ and salinity are in the same range for all panels. (For interpretation of the references to color in this figure legend, the reader is referred to the web version of this article.)

$f\text{CO}_2^{\text{sw}}$ data (Table 4, Fig. 5). The MLR model standard errors varied from 6.21 to 7.37 μatm (for $f\text{CO}_2^{\text{sw}}$ and $Np\text{CO}_2^{\text{sw}}$, respectively). Most outliers of all models correspond to positions in the easternmost portion of the FORSA cruise section (east of $\sim 8^{\circ}\text{E}$; Fig. S6). The intervals where

the modeled properties were less realistic encompass a region where the lowest $p\text{CO}_2^{\text{sw}}$ values were observed (Figs. 5 and 4b). In addition, in this region the CO_2^{sw} could be under the influence of the Agulhas Current retroflection (Figs. 1 and 2a).

Table 2

Average \pm standard deviation, range (min; max) of the results from: temperature (T , $^{\circ}\text{C}$); salinity (S); and CO_2 -related parameters: seawater CO_2 partial pressure ($p\text{CO}_2^{\text{sw}}$, μatm), temperature-normalized $p\text{CO}_2^{\text{sw}}$ ($Np\text{CO}_2^{\text{sw}}$, μatm , @ 20.39 $^{\circ}\text{C}$), the sea-air CO_2 difference ($\Delta p\text{CO}_2$, μatm) and the sea-air CO_2 net flux calculated using the Takahashi et al. (2009) coefficient ($\text{FCO}_2^{\text{T09}}$, $\text{mmol m}^{-2} \text{d}^{-1}$) for each sampled eddy.

Parameter	V1	V2	V3	V4	V5	V6
T	17.66 \pm 0.06 17.31; 17.71	19.3 \pm 0.12 19.14; 19.53	20.01 \pm 0.34 19.56; 20.70	21.92 \pm 0.25 21.49; 22.35	22.27 \pm 0.32 21.91; 23.19	22.1 \pm 0.24 21.65; 22.71
S	35.45 \pm 0.04 35.24; 35.47	35.57 \pm 0.02 35.55; 35.61	35.61 \pm 0.09 35.52; 35.80	0.25 \pm 0.11 35.53; 35.96	35.80 \pm 0.13 35.61; 36.17	35.97 \pm 0.06 35.87; 36.13
$p\text{CO}_2^{\text{sw}}$	342.5 \pm 1.1 336.7; 345.7	350.4 \pm 1.0 348.7; 352.4	349.1 \pm 3.6 343.7; 356.0	360.8 \pm 2.3 355.5; 365.2	358.9 \pm 3.1 352.1; 365.5	356.8 \pm 1.7 354.0; 362.7
$Np\text{CO}_2^{\text{sw}}$	383.7 \pm 2.0 365.3; 392.5	366.6 \pm 1.0 364.1	354.7 \pm 1.5 349.8; 356.9	338.6 \pm 1.8 335.3; 341.8	332.0 \pm 4.1 320.9; 341.7	332.4 \pm 2.7 362.4; 338.0
$\Delta p\text{CO}_2$	-51.9 \pm 1.3 -67.7; -47.6	-40.2 \pm 0.9 -41.8; -38.0	-42.8 \pm 4.2 -52.0; -36.5	-24.7 \pm 2.2 -28.4; -20.3	-30.9 \pm 4.3 -43.1; -22.6	-33.6 \pm 1.2 -36.4; -29.3
$\text{FCO}_2^{\text{T09}}$	-5.0 \pm 0.1 -6.1; -4.6	-3.8 \pm 0.1 -4.0; -3.6	-4.1 \pm 0.4 -5.0; -3.5	-2.3 \pm 0.2 -2.7; -1.9	-2.9 \pm 0.4 -4.1; -2.2	-3.2 \pm 0.1 -3.4; -2.8

Table 3

Radius (km), lifetime (d) and sea-air CO₂ net flux calculated using the Takahashi et al. (2009) coefficient (FCO₂^{T09}). The results are presented for each eddy (Vn, n = 1 to 6), for the ‘Agulhas true’ eddy, the ‘Agulhas evolved’ eddy and the ‘Agulhas typical’. The FCO₂ reported in this table are in different units, as indicated in the respective line. * indicates that the eddy lifetime accounting was completed with the data available during the analysis.

Eddy	V1	V2	V3	V4	V5	V6	Agulhas true	Agulhas evolved	Agulhas typical
Radius [km]	94.23	84.19	96.43	95.08	98.86	89.76	91.46	94.49	92.96
Lifetime [d]	798*	931	949	825	1222	1249	890.03	1235.43	1014.78
FCO ₂ [g CO ₂ d ⁻¹]	-3156.7	-1937.7	-2701.8	-1510.0	-2037.1	-1817.4	-2547.1	-1774.8	-2126.2
FCO ₂ [t CO ₂ yr ⁻¹]	-1.2	-0.7	-1.0	-0.6	-0.7	-0.7	-0.9	-0.7	-0.8
FCO ₂ [t CO ₂ life ⁻¹]	-2.5	-1.8	-2.6	-1.3	-2.5	-2.2	-2.3	-1.9	-2.1

Table 4

Considering Eq. (3), this table presents the coefficients determined for each parameter in the multiple linear regression model. CO₂-related parameters are: seawater CO₂ partial pressure/fugacity (pCO₂^{sw}/fCO₂^{sw}, μatm), temperature-normalized pCO₂^{sw}/fCO₂^{sw} (NpCO₂^{sw}/NfCO₂^{sw} μatm, @ 20.39 °C). The measured vs. modeled parameter coefficients of determination are referred to as r². The units of each determined parameter are: α (μatm), β₁ (μatm °C⁻¹), β₂ (μatm), β₃ (μatm mg⁻¹ m³), standard error (μatm). The number of data points used is 8650.

	α	β ₁	β ₂	β ₃	r ²	Standard error
pCO ₂ ^{sw}	352.05	4.91	-9.60	-26.86	0.81	6.74
NpCO ₂ ^{sw}	350.40	-9.61	-10.62	-24.22	0.91	7.37
fCO ₂ ^{sw}	336.10	5.41	-8.82	-29.17	0.86	6.21
NfCO ₂ ^{sw}	334.33	-8.51	-9.60	-29.59	0.90	6.72

4. Discussion

4.1. How much CO₂ is taken up by the South Atlantic Ocean?

4.1.1. The off-shore region

The general pattern of the ΔpCO₂^{sw} indicates that the studied region of the SAO behaved as a CO₂ sink during the winter FORSA cruise, primarily due to the temperature effect, which is in good agreement with previous results for this region (Table 5). First, considering the north-south cruise sections crossing the SAO, Lefèvre and Moore (2000) reported the AMT results of 1995 and 1996, conducted from 50°N to 50°S (Fig. S7a). When considering only the SAO, the sampling was in the western basin and the reported pCO₂^{sw} had a range smaller than that found in the FORSA cruise (Table 5). Similarities regarding the range of the pCO₂^{sw} results are found by considering the western basin of the FORSA cruise (Table 1) and can be related to the physical parameters, because temperature and salinity are higher in the western

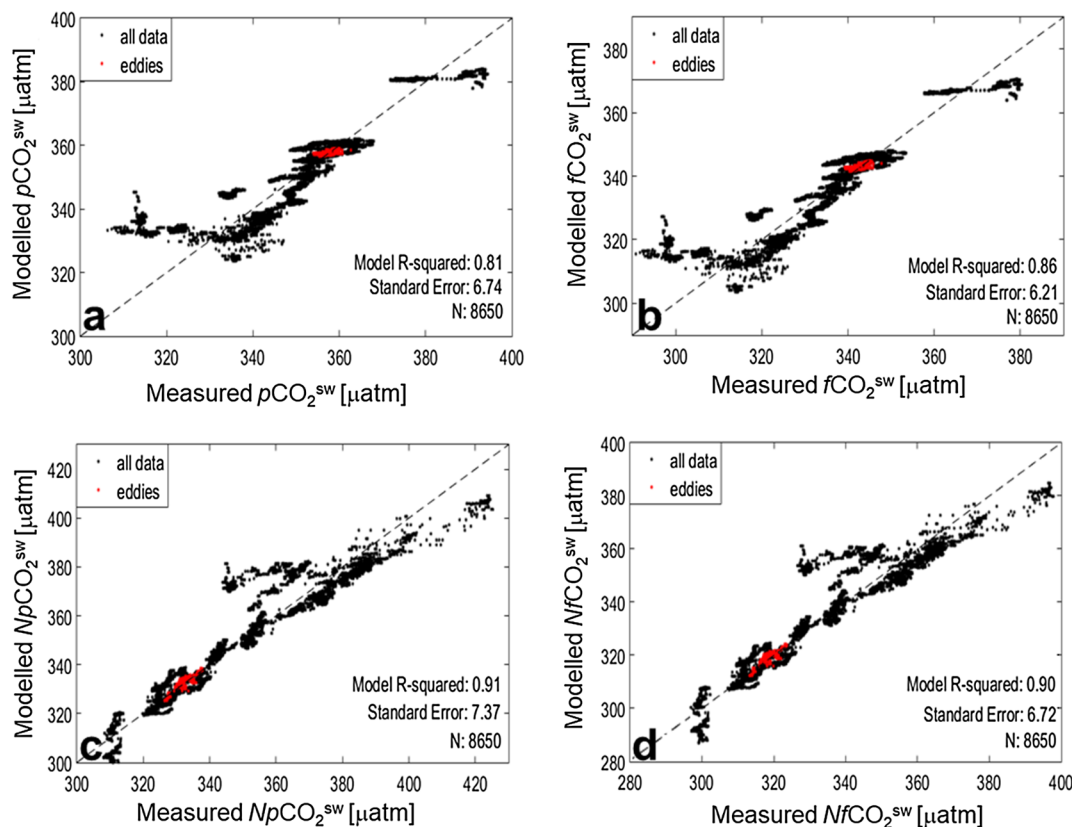


Fig. 5. Measured vs. modeled results, where: (a) pCO₂^{sw} (μatm), (b) fCO₂^{sw} (μatm), (c) NpCO₂^{sw} (μatm) and (d) NfCO₂^{sw} (μatm). Note that the black dots consider all cruise data and the red dots represent only the data inside the eddies. In each diagram the coefficients of determination, the standard error (μatm) and the number of data points (N) are presented. (For interpretation of the references to color in this figure legend, the reader is referred to the web version of this article.)

Table 5

Comparative results of CO₂-related parameters: seawater CO₂ partial pressure ($p\text{CO}_2^{\text{sw}}$, μatm), seawater CO₂ fugacity ($f\text{CO}_2^{\text{sw}}$, μatm), sea-air $p\text{CO}_2$ difference ($\Delta p\text{CO}_2$, μatm), sea-air $f\text{CO}_2$ difference ($\Delta f\text{CO}_2$, μatm), and sea-air CO₂ net flux (FCO_2 , $\text{mmol m}^{-2} \text{d}^{-1}$) obtained for the South Atlantic Ocean and used in the FORSA results discussion. The sampling season is included. Each transference coefficient used in the FCO_2 estimate, as well as other specificities for each study are indicated. A map of each considered study region was inserted in Fig. S7.

	Author	Area, sampling year, Season	$p\text{CO}_2^{\text{sw}}$ (μatm)	$f\text{CO}_2^{\text{sw}}$ (μatm)	$\Delta p\text{CO}_2$ (μatm)	$\Delta f\text{CO}_2$ (μatm)	FCO_2 ($\text{mmol m}^{-2} \text{d}^{-1}$)
	This study	20°S - 35°S 2015 Winter	351.5 ± 14.9 306.3; 394.4	335.5 ± 15.9 290.8; 380.4	-39.1 ± 17.1 -86.8; 10.3	-36.3 ± 15.7 -80.2; 9.9	-3.8 ± 1.7 -8.3; 1.0 ^a
Meridional sections	Lefèvre and Moore (2000)	AMT 10°S - 30°S 1995, 1996 Spring/Autumn	330; 380	-	“Close to equilibrium”	-	-0.5; -0.3 ^b
	Padin et al. (2010)	15°S - 31°S 2001–2008 Spring/Autumn	-	-	-	21 ± 14 (aut.); -5 ± 17 (spr.)	$0.6 \pm 0.6 - 0.2 \pm 0.7$ ^c
	Sutherland et al. (2015)	20°S - 30°S 2015 Winter	385.9 ± 8.8 353.5; 410.5	-	-	-	-
	Kitidis et al. (2017)	AMT 20°S - 40°S 1995–2013 Spring/Autumn	-	250; 400	-	-100; 25	-
Zonal sections	Uchida et al. (2005)	A10 30°S 2003 [†] Spring	352.6 ± 12.7 317.3; 377.0	351.4 ± 12.7 316.2; 375.7	-	-	-
	Wanninkhof and Castle (2013)	A10 30°S 2011 Spring	351.3 ± 10.4 308.5; 391.6	350.1 ± 10.3 307.4; 390.3	-	-31.4 ± 11.9 -75.8; 15.9	-
	Lencina-Avila et al. (2016)	35°S 2011 Spring	-	335.9 ± 9.6	-	-49.0 ± 9.7	-2.0 ± 1.5 ^a
Databases	Takahashi et al. (2009)	20°S - 35°S 2000 Annual	365.2 ± 19.4 294.9; 425.1	-	5.1 ± 20.6 -66.8; 67.7	-	$0.0 \pm 0.1 - 0.3$; 0.1 ^{a,d} -0.0 \pm 0.5 -3.5; 1.2 ^{a,e}
	Bakker et al. (2016)	SOCAT v.5 20°S - 35°S 2017 Annual	-	370.3 ± 24.2 144.3; 656.0	-	-	-

^a FCO_2 was calculated using the K_T from Takahashi et al. (2009).

^b FCO_2 was calculated using the K_T from Tans et al. (1990).

^c FCO_2 was calculated using the K_T from Wanninkhof (1992).

^d FCO_2 was reported in $\text{mol m}^{-2} \text{month}^{-1}$.

^e FCO_2 was converted to $\text{mmol m}^{-2} \text{d}^{-1}$ because it was originally reported in $\text{mol m}^{-2} \text{month}^{-1}$.

* $p\text{CO}_2^{\text{sw}}$ and $f\text{CO}_2^{\text{sw}}$ were calculated from total dissolved inorganic carbon and total alkalinity data from this database, using the *Best Practices Handbook* (Dickson et al. 2007) constants and the *Ocean Data View* software (Schlitzer, 2016, <http://odv.awi.de>). Please see the software user's guide for further details about the constants (Derived variables/Parameters) of the carbon dioxide system in sea water.

basin. Lefèvre and Moore (2000) also reported that the seawater was near equilibrium with the atmosphere in both sampled seasons (autumn and spring) for the results obtained in the SAO gyre (from approximately 17°S to 30°S), and justified this by the low chl-*a*. Considering the region from 10°S to 30°S, the FCO_2 ranged from -0.30 to $-0.54 \text{ mol m}^{-2} \text{yr}^{-1}$, calculated using the K_T determined by Tans et al. (1990). Apart from the different K_T used, the magnitude of the FCO_2 difference can be due to the wind speed, because Lefèvre and Moore (2000) did not report the value used in this region but referred to a mean value of 8.6 m s^{-1} as a strong wind speed, and our results were of this order of magnitude (mean of 6.8 m s^{-1}). In addition, as the AMT samplings were performed during autumn and spring and the FORSA survey during winter, the sea surface temperature could be leading to a weak (strong) physical solubility pump during the AMT (FORSA) sampling, and it was the main driver of the CO₂ sink in the FORSA cruise. In the latest AMT-CO₂^{sw} published results, Kitidis et al. (2017) focused on ocean acidification. Even so, they reported some new $f\text{CO}_2^{\text{sw}}$ observations, but the ranges for this parameter and the $\Delta f\text{CO}_2$ that could be extracted from their study were larger than those from the

FORSA cruise. These cruises were conducted in the same time of year as that of Lefèvre and Moore (2000): samplings occurred during autumn and spring, probably leading to a difference in the sea surface temperature when compared to the FORSA winter sampling, which primarily governed the $p\text{CO}_2^{\text{sw}}$ behavior. Padin et al. (2010) reported that the sea surface acted as a source of CO₂ to the atmosphere during the austral autumn and as a weak sink during the austral spring (Fig. S7b; Table 5). The differences found between these previous investigations and the FORSA cruise can be related to the fact that the sea surface is warmer and saltier during spring/summer seasons, indicating that the physical solubility pump was weaker in those periods. In addition, Iida et al. (2015) reinforced the idea that strong CO₂ uptake occurs in the winter (e.g., Takahashi et al., 2002; Ishii et al., 2011), because the $p\text{CO}_2^{\text{sw}}$ decreases together with temperature due to the vigorous vertical mixing in winter, enhancing the gradient in the sea-air interface. Evaluating the $p\text{CO}_2^{\text{sw}}$ data from the report of Sutherland et al. (2015), which refers to a cruise conducted along the western basin (Fig. S7c) in the same year and season as the FORSA cruise, the values were as high as what we found in that region (Table 1).

Considering the results of cruises crossing the SAO zonally, Wanninkhof and Castle (2013) determined the $p\text{CO}_2^{\text{sw}}$ through the analyses of the CLIVAR/WOCE A10 section (SAO crossing along 30°S, Fig. S7d) sampled in the spring of 2011 (Table 5). Apart from very similar mean values, the temperature seems to present a smaller influence on the $p\text{CO}_2^{\text{sw}}$ in these results ($r = 0.55$, $p < 0.01$) than on those of the FORSA cruise ($r = 0.88$, $p < 0.01$). When evaluating the A10 section sampled in the spring of 2003 (Uchida et al., 2005; Fig. S7e), the mean values were also very similar (Table 5), but the temperature played an even smaller role in $p\text{CO}_2^{\text{sw}}$ observations ($r = 0.17$, $p < 0.01$). In the latest CLIVAR/WOCE A10 section sample, their $\Delta p\text{CO}_2$ values were very close to the results reported here (Table 5). The behavior as CO_2 sink identified during the FORSA cruise was also observed in a previous study in the SAO, but conducted farther south along the latitude of 35°S, during the spring of 2011 (Lencina-Avila et al., 2016; Fig. S7f). Those authors reported that the mean $f\text{CO}_2^{\text{sw}}$ for the entire cruise is $335.9 \pm 9.6 \mu\text{atm}$, which agrees with the FORSA cruise results ($335.5 \pm 15.9 \mu\text{atm}$) considering the close mean values (Table 5). The slightly larger standard deviations observed for the FORSA cruise compared to those of Lencina-Avila et al. (2016) can be attributed to the fact that the FORSA cruise was conducted not only in a meridional crossing line, but also in a southeast-northwest direction. This difference between the range of latitudes crossed by each cruise shows that the FORSA section encompasses a larger (and warmer) temperature range: $20.39 \pm 2.51 \text{ }^\circ\text{C}$ compared to $16.4 \pm 1.4 \text{ }^\circ\text{C}$, from Lencina-Avila et al. (2016), leading to a weaker absorption in the FORSA section: $\Delta f\text{CO}_2$ of $-36.3 \pm 15.7 \mu\text{atm}$ compared to $-49.0 \pm 9.7 \mu\text{atm}$ in the study of Lencina-Avila et al. (2016). The results (Table 5) indicate that the $f\text{CO}_2$ was stronger in the FORSA than in the study conducted by Lencina-Avila et al. (2016). The differences are relatively small and of the same magnitude order, but could be caused by the wind speed difference: $3.7 \pm 1.4 \text{ m s}^{-1}$ reported by Lencina-Avila et al. (2016) and $6.8 \pm 0.6 \text{ m s}^{-1}$ observed in this study. A major difference between the results from these cruises and the FORSA results is related to the season of the sampling. During the spring a phytoplankton bloom is expected, which can drive a seasonal absorption of the same magnitude despite a warmer temperature than that in the winter, as observed in Wanninkhof and Castle (2013) and Uchida et al. (2005). In these A10 cruises, sampled in springtime, the $p\text{CO}_2^{\text{sw}}$ values were close to those of the FORSA results, but the temperature effect on the $p\text{CO}_2^{\text{sw}}$ was small. These blooms could persist during the beginning of the summer, but as the temperature increases, the solubility decreases even more. Although the cruise reported in Lencina-Avila et al. (2016) was also in springtime, it was conducted in a colder region. When the sampling occurs in autumn, as reported by Padin et al. (2010), a release of CO_2 to the atmosphere can be related to the period in which the biological pump was playing a minor role, due to the period of post-phytoplankton blooms, together with a slow restart of the temperature decrease. In the winter, the strong mixing caused by the winds, in addition to the lower temperature, favors the physical drawdown of CO_2 (e.g., Iida et al., 2015).

The longitudinal gradient of $p\text{CO}_2^{\text{sw}}$ was also observed in Wanninkhof and Castle (2013), Uchida et al. (2005), and Lencina-Avila et al. (2016), but in these studies the difference was smaller. These three surveys were developed on continuous latitude lines (30°S and 35°S), whereas the FORSA section had a latitudinal variation (ranging from 20°S to 35°S). Thus, this gradient is also due to the stronger difference in temperature between the eastern and western basins in this latitudinal range. Regarding the strong absorption in the easternmost part, the biological effect is also important to the CO_2 sink, which was also observed in Lencina-Avila et al. (2016).

Evaluating the database used by Takahashi et al. (2009) and considering only data for the same latitude range as the FORSA cruise (Fig. S7g), their average $p\text{CO}_2^{\text{sw}}$ was higher and their range was wider than that of the FORSA cruise (Table 5). In addition, their average $\Delta p\text{CO}_2$ and $f\text{CO}_2$ values were positive, indicating that CO_2 was being released

to the atmosphere from the selected region. This finding reinforces the statement made by these authors that there are not enough data from the SAO to define this basin as a sink or source of CO_2 for the atmosphere. On the other hand, analyzing the Bakker et al. (2016) database (Fig. S7h), neither the mean $f\text{CO}_2^{\text{sw}}$ values nor the ranges were close or similar to the FORSA results or even the other cruises results (Table 5). This could be caused by the large period considered in the SOCAT database. These observed discrepancies (sink/source behavior, magnitude) appear when comparing single cruises to existing databases, which emphasizes the importance of increasing the large-scale observations in the SAO to define with certainty this basin as a CO_2 sink region, which was observed in most of the individual cruises, including the FORSA survey.

4.1.2. The Brazilian southeast continental shelf-break

When considering the region closer to the Brazilian coast, which included the outer continental shelf and slope regions (west of 39.25°W and shallower than 3000 m), the sea surface changed from a sink to a small source of CO_2 to the atmosphere (Fig. S3, Table S2). The high positive correlation of T vs. $p\text{CO}_2^{\text{sw}}$ ($r = 0.70$, $p < 0.01$, Table S1) indicated that the temperature was the main factor driving the $p\text{CO}_2^{\text{sw}}$ distribution pattern. However, the biological activity probably played a role in $p\text{CO}_2^{\text{sw}}$ changes ($r = 0.52$, $p < 0.01$, Table S1). Ito et al. (2005) studied a region located south of the FORSA cruise section (24°S – 28°S) in different seasons (summer and spring) and reported that the continental shelf and slope regions (north of 25°S) acted as CO_2 sources for the atmosphere, regardless of the season or water mass found. The results indicated that the CO_2 release is lowest in winter and strongest during the summer. This difference is justified by the upwelling of central waters (i.e., SACW), which is less intense in winter than summer. These authors also observed a sink of CO_2 for the offshore waters during winter. Ito et al. (2016) studied the South and the Southeast Brazilian coast, encompassing a region in which the part of the FORSA cruise section closer to the Brazilian coast can be zonally included. The authors concluded that the coastal ocean waters between São Tomé Cape (22°S, 41°W) and Frio Cape (23°S, 42°W) release CO_2 to the atmosphere due to upwelling events, because this process brings CO_2 -rich waters towards the surface (e.g., Carvalho-Borges et al., 2018). Findings in this study are in consonance with early results reported by Padin et al. (2010), who concluded that the distal shelf of the Brazilian coast acted as a weak source of CO_2 to the atmosphere, even in the spring and autumn. Considering the study conducted by Chen and Borges (2009), who evaluated different continental shelf margins along the global ocean, the results obtained from the FORSA cruise enriches what was previously observed, because those coastal regions are reported to behave as a source of CO_2 to the atmosphere (e.g., Cai, 2003). In addition, the behavior observed here for the FORSA sector close to the Brazilian continental shelf-break (i.e., a gradient from the continental shelf acting as a source and an outer-slope region acting as a sink) is expected according to previous studies (e.g., Laruelle et al., 2013, 2014, 2015). On the other hand, Jiang et al. (2008) suggested that continental shelf regions can behave as CO_2 sinks or sources to the atmosphere, depending on the season (winter and summer, respectively) and on cross-shelf processes. Frankignoulle and Borges (2001) reported that the CO_2 dynamics in coastal regions depend on the local biogeochemical pathways/cycles observed (i.e., inorganic and organic carbon riverine inputs), confirming that defining them as sinks or sources of atmospheric CO_2 remains a challenge (Kerr et al., 2016). Additionally, Guerra et al. (2018) found that, over 23 years, one third of the identified Agulhas eddies released in the retroflexion zone reached the western boundary of the SAO.

4.2. What is the role of Agulhas eddies in net sea-air CO_2 net fluxes?

Agulhas eddies are anticyclonic structures, which indicate that in the southern hemisphere their rotation is counter-clockwise and present

high-pressure centers, displacing isopycnals downward, thus presenting a typical signature of sea surface warming (e.g., Tilburg et al., 2002; Azevedo and Mata, 2010; Talley et al., 2011). Therefore, they are associated with positive heat flux anomalies, which means that in the regions where they can be identified, the ocean loses heat to the atmosphere, and thus, tends to warm the atmospheric boundary layer (Villas Bôas et al., 2015). In addition, the CO₂ solubility in seawater is higher when the water is cold and less salty (e.g., Denman et al., 2007). Consequently, the theoretically expected effect of the recently released anticyclonic structures is to decrease the CO₂ solubility not only by physical sinking processes but also by biological activity, because they hypothetically do not favor the phytoplankton productivity/biomass increase (e.g., Kahru et al., 2007; Eden and Dietze, 2009). Angel-Benavides et al. (2016) compared the different mechanisms that act inside the cyclonic and anticyclonic eddies at the Brazil-Malvinas Confluence, one of the most energetic regions of the global ocean. Regarding eddy-pumping, the anticyclonic eddies were related to lower chl-*a* concentrations, due to the isopycnals downward displacement. With respect to the eddy Ekman pumping, the authors agreed with Martin and Richards (2001) that seasonal pycnoclines were displaced upward, resulting in a biological response similar to that of the cyclonic eddies. Lehahn et al. (2011), studying an Agulhas eddy, observed that they could induce the biological production in the SAO due to the nutrient transport along its advection, primarily caused by vertical mixing. The authors do not believe that the eddy-pumping mechanism played a role in this high chl-*a* concentration, because it is an anticyclonic structure.

Despite their intrinsic characteristics, we observed that the sampled Agulhas eddies act as an intensified CO₂ sinking zone when compared to the surrounding waters. Song et al. (2016) also highlighted this contradictory behavior, stating that anticyclonic eddies in the Drake Passage can absorb more CO₂ than the surrounding regions in the summer. They based their results on the theory proposed by Dufois et al. (2016), which explains this apparent contradiction in terms of the strong vertical mixing within the anticyclonic eddies. In addition, Wang et al. (2013) observed that the total dissolved inorganic carbon in an anticyclonic eddy was lower than that in the surrounding waters, in a western boundary margin of the Gulf of Mexico, sampled in 2007. Moreover, Jones et al. (2017) reported that cyclonic and anticyclonic eddies sampled in the Southern Ocean can act as CO₂ absorbers. Chen et al. (2007) described a cyclonic eddy studied in 2005 in the subtropical North Pacific gyre as a source of CO₂ to the atmosphere, due to the upwelling in the center of the eddy of waters rich in CO₂ to the surface. These authors reported that the $p\text{CO}_2^{\text{sw}}$ was lower and controlled by temperature in the eddy periphery, as also observed by Moreau et al. (2017) through an eddy released from the Subantarctic Front.

In this way, it is ambitious to establish an expected behavior for cyclonic (anticyclonic) eddies as CO₂ uptake (release) regions of the oceans, as it was previously defined or even expected. The challenges are due to the intrinsic processes that can act in each eddy-region. Some regions presenting cyclonic structures can be related to upwelling of old-ventilated and CO₂-rich waters, behaving as sources of CO₂ to the atmosphere. On the other hand, anticyclonic eddies can be associated with strong vertical mixing or to concentrations of total dissolved inorganic carbon lower than that of the surrounding waters, probably acting as CO₂ sinking zones. The latter situation was found in this study, which highlighted that the Agulhas eddies are probably intensifying the CO₂ uptake in the SAO. This is particularly intriguing because the behavior of the Agulhas eddies could also contribute to strength the acidification of central and modal waters in the SAO, since they are being acidified in faster rates than the surface and intermediate waters (Salt et al., 2015; Kitidis et al., 2017; Carvalho-Borges et al., 2018). However, a more detailed investigation should be performed to verify this conclusion.

4.3. How much CO₂ is forced down by the sampled Agulhas eddies?

Using data published before 1997, Lutjeharms (2006) evaluated the number of eddies shed per year in different studies using different identification methods (i.e., infrared, altimeter and echo sounder) and stated that this number is not persistent. The author estimated that an average of ~6.19 eddies are released per year, which agrees with the number of eddies, six, provided by Gordon (2003). Considering the characteristics of the 'Agulhas typical' eddy, the CO₂ uptake can reach up to $-2.12 \text{ kg CO}_2 \text{ d}^{-1}$, leading to $-0.78 \text{ t CO}_2 \text{ yr}^{-1}$ or $-2.00 \text{ t CO}_2 \text{ lifetime}^{-1}$ (Table 3). Assuming a total of six 'Agulhas typical' eddies released per year, the total CO₂ uptake can be estimated as $-4.65 \text{ t CO}_2 \text{ yr}^{-1}$. This value is relatively small ($\sim 1.55 \cdot 10^{-6}\%$) on a basin-scale as the CO₂ net sink in the SAO is estimated to be around of $-0.3 \text{ Pg C yr}^{-1}$ (e.g., Takahashi et al., 2002). However, it is interesting to highlight that some studies are reporting an increase in the number of Agulhas eddies being released per year (Biaostoch et al., 2009) to the SAO and that their lifetimes are expected to be longer than two years (e.g., Lutjeharms, 2006).

In addition, studies concerning the role of Agulhas eddies on biogeochemical cycles are recent. Some previous studies focusing on mesoscale eddies behavior have indicated that they can act: (i) as mechanisms to induce interaction of physics, biology and biogeochemistry (McGillicuddy, 2016), and (ii) to enhance nutrients availability and thus, biological production (Martin and Richards, 2001; Kahru et al., 2007; Dufois et al., 2016). Apart from that, studies concerning the behavior of the mesoscale eddies on the FCO₂ pattern have just begun to be developed (Chen et al., 2007). It is also known that the mesoscales eddies can (i) affect the total dissolved inorganic carbon distribution (Wang et al., 2013) and (ii) change the FCO₂ (Song et al., 2016; Jones et al., 2017) and the inherent biogeochemistry where they are advected (Moreau et al., 2017). Woosley et al. (2016) recently indicated that the Agulhas eddies can be prone to contain an extra anthropogenic carbon concentration than that found in the surrounding waters at the same depth-levels. Here, we provided evidences that the Agulhas eddies can be hotspots of CO₂ uptake in the SAO, which could be leading to further strength the acidification of the central waters of the SAO (e.g. Carvalho-Borges et al., 2018; Orselli et al., 2018). Thus, shedding new light on the scientific discussion about the role of the Agulhas eddies on the biogeochemical processes in the SAO.

4.4. What is driving the CO₂ sink in the sampled eddies?

The FCO₂ variability is known to be controlled primarily by $p\text{CO}_2^{\text{sw}}$, and thus understanding the drivers of the $p\text{CO}_2^{\text{sw}}$ is crucial for determining the ocean carbon sink (e.g., Feely et al., 2001; Takahashi et al., 2002; McKinley et al., 2004, 2011, 2017; Lovenduski et al., 2008; Schuster et al., 2009, 2013; Fay and McKinley, 2013; Landschützer et al., 2015). Thus, we compared the FORSA results to the suggested scheme of Fay and McKinley (2017) for a subtropical permanently stratified biome, in which the SAO can be encompassed, to constrain these drivers in each sampled eddy.

Evaluating the role played by the physical parameters and the chl-*a* for each sampled eddy, we can see that neither the physical nor the biological parameters are correlated to the $p\text{CO}_2^{\text{sw}}$ for the V1 (Table S3). For the $\text{NpCO}_2^{\text{sw}}$, a weak correlation is achieved with S (Table S3). According to Fay and McKinley (2017), this situation occurs only in the subtropical regions, when anomalies in temperature and mixing favor the drawdown of CO₂ by the ocean. We can also separate the V2 and V3 from the other eddies, because their uptake seems to be physically driven. The V4 uptake was primarily driven via temperature and salinity conditions, but the primary production role in the carbon sink cannot be discarded, because a negative correlation between $p\text{CO}_2^{\text{sw}}$ and chl-*a* ($r = -0.66$, $p < 0.01$) indicates that biological activity is also acting on the CO₂ uptake (Table S3). The V5 seems to be influenced by physical and biological processes, as observed for V4, whereas in the

V6 the biological process apparently also plays a minor role, but cannot be neglected (Table S3). In V5, a negative linear correlation between $NpCO_2^{sw}$ and chl-*a* ($r = -0.75$, $p < 0.01$; Table S3) suggests an indirect contribution, which could also have been acting in the last sampled eddy, in which a positive linear correlation between pCO_2^{sw} and chl-*a* was observed. This is supported by Lehahn et al. (2011), which stated that an Agulhas eddy can act to mold the biological production; thus an older eddy can have a longer time to induce the CO_2 absorption. In addition, some species of phytoplankton with small cells do not present a high chl-*a* response apart from being responsible for an important CO_2 uptake (Craig et al., 2014). Moreover, in these eddies, the salinity can also have an indirect effect on the primary production.

According to what has been stated, we split the eddies into eastern and western basins due to their CO_2 sink strengths. This means that they are primarily driven by physical mechanisms when closer to their releasing region and, as they age, the biological activity starts to contribute to their uptake behavior. This can be related to the fact that when they start to age, the sea level anomaly is maintained due to the downward displacement of the isopycnals, allowing them to still be identified, but the thermal signature in the surface becomes less visible (Fig. S5). Thus, these surface physical properties could also be less effective in the CO_2 sinking process. Hence, the ‘Agulhas true’ eddy FCO_2 sink could be driven by physical forcings, because they are more prominent in the sea surface in the eastern basin, whereas the ‘Agulhas evolved’ eddy could be driven by physical and biological processes. However, it is interesting to note that V1 had an intense sea level anomaly signal for a longer period than the other eddies, suggesting that this structure could have behaved as the most intense sink not only for being sampled close to its releasing region but also for presenting a stronger sea level anomaly during its lifetime (Video S1).

4.5. Can this model reproduce the observed CO_2 parameters during the FORSA cruise?

Because CO_2^{sw} -related samples are scarce in the SAO, some authors are developing models to estimate the CO_2 -related parameters from physical data. Lencina-Avila et al. (2016) developed a MLR model to predict the fCO_2^{sw} and $NfCO_2^{sw}$ for a specific cruise in the SAO (Fig. S7). Their results showed that the coefficients of determination between the cruise data and the model results were higher for the $NfCO_2^{sw}$ than the fCO_2^{sw} for the open ocean region ($r^2 = 0.87$ and 0.11 , respectively). Zeng et al. (2014) modeled the fCO_2^{sw} for the global oceans using the T, S, chl-*a*, month, latitude and longitude. The modeled vs. observed fCO_2 fitting for the training samples yielded a linear correlation coefficient of 0.89. The coefficients of determination for measured vs. modeled fCO_2^{sw} and $NfCO_2^{sw}$ for the FORSA cruise MLR model are very similar to this reported model’s results, being 0.86 and 0.90, respectively. Iida et al. (2015) also used the T, S, chl-*a* and year to model the xCO_2^{sw} , aiming to model the FCO_2 in the global ocean. They used the RMSE between the measured and the modeled pCO_2^{sw} to determine an uncertainty of $\pm 16.3 \mu\text{atm}$ in their estimate. The standard error of the modeled pCO_2^{sw} for the FORSA cruise (Table 4) was $\pm 6.74 \mu\text{atm}$, thus this MLR could represent not only the $fCO_2^{sw}/NfCO_2^{sw}$ but also the $pCO_2^{sw}/NpCO_2^{sw}$. Accordingly, the MLR standard error results presented for the FORSA cruise (Fig. 5, Table 4) are smaller than those of previously published investigations that were conducted to model the fCO_2^{sw}/pCO_2^{sw} on the basin scale. Because we could better reconstruct the CO_2^{sw} parameters not only with a smaller error but also with better correlation coefficients than the previous published studies, we believe that the MLR model can reconstruct the SAO pCO_2^{sw} distribution for the FORSA cruise region and the sampling period.

5. Conclusions

In this study, we investigated the pCO_2^{sw} and the FCO_2 distribution in a southeast-northwest section of the SAO and the role played by the

Agulhas eddies in this pattern. We used data from a southeast-northwest transect conducted in the winter of 2015, in which six Agulhas eddies were sampled. The overall pCO_2^{sw} and ΔpCO_2 were 351.51 and $-39.08 \mu\text{atm}$, respectively. The mean FCO_2 was $-3.76 \text{ mmol m}^{-2} \text{ d}^{-1}$ as calculated using Takahashi et al. (2009) transfer coefficients. The temperature dominated this CO_2 sink behavior, but the biological activity also contributed to the observed sea-air CO_2 exchanges. Concerning the Agulhas eddies, they act as CO_2 sinking intensifying structures. The physical processes seem to be the driving forces of the CO_2 uptake by the Agulhas eddies in the eastern basin, and continue acting throughout their lifetimes, although biological activity cannot be neglected when they are in the western basin. Considering an ‘Agulhas typical’ eddy, the calculated uptake can achieve $-2.12 \text{ kg } CO_2 \text{ d}^{-1}$, leading to $-2.08 \text{ t } CO_2 \text{ lifetime}^{-1}$ for an average lifetime of ~ 1014 days. With coefficients of determination between measured vs. modeled results ranging from 0.81 to 0.91 (for pCO_2^{sw} and $NpCO_2^{sw}$, respectively) and standard errors varying from 6.21 to $7.37 \mu\text{atm}$ (for fCO_2^{sw} and $NpCO_2^{sw}$, respectively), we could model the CO_2^{sw} -parameters during the FORSA cruise. A potential outcome of this work is the possibility of orienting future processes via high-resolution numerical modeling experiments, in which physical-biogeochemical mechanisms can be examined together as drivers of the sea-air interactions along the Agulhas eddy corridor. In addition, as we found that the presence of the Agulhas eddies acts to intensify the CO_2 uptake in the SAO, they are probably responsible for transporting anthropogenic carbon through the entire basin (Woosley et al., 2016) and, thus, act as a trigger structure for the increase of ocean acidification in the central and modal waters (e.g., Salt et al., 2015; Carvalho-Borges et al., 2018).

Acknowledgments

This study provides a contribution to the activities of the Brazilian High Latitude Oceanography Group (GOAL) and the Brazilian Ocean Acidification Network (BrOA; www.broa.furg.br). The project was sponsored by the Brazilian Coastal Monitoring System (SIMCosta), the Brazilian National Council for Scientific and Technological Development (CNPq), the Brazilian Improving Coordination of Higher Education Personnel (CAPES), with logistic supported by the Ministry of Science, Technology, Innovation, and Communication (MCTIC), the Brazilian Ministerial Secretary for the Resources of the Sea (SECIRM), and the Brazilian Navy. This study also contributes to the project ‘Estudos Avançados de Médias e Altas Latitudes’ (CAPES grant n° 23038.001421/2014–30). I. B. M. Orselli acknowledges CAPES/CMAR2 for the Ph.D. funding (CAPES process n°. 23038.001421/2014–30 and BEX 0077/17–8). R. Kerr acknowledges CNPq researcher grant n° 302604/2015–4. M.A. thanks the support of the Brazilian Research Network on Global Climate Change-Rede CLIMA (FINEP grants 01.13.0353-00). We thank all researchers and students from LEOC/FURG and LOFEC/UFPE for their contribution with cruise planning, sampling, and analysis. We also wish to acknowledge the invaluable support of Cdr. Aluizio Oliveira and the crew of the Brazilian RV *Vital de Oliveira* for their logistic assistance. Because we used the Mesoscale Eddy Trajectory Atlas product, we would like to thank its producers, supporters, collaborators and distributors: SSALTO/DUACS, CNES, Oregon State University, NASA and AVISO. Additionally, we would like to thank the SOCAT scientists and funding agencies. We are grateful for the constructive comments provided by Sébastien Moreau and the anonymous reviewer, who substantially helped to improve the manuscript.

Appendix A. Supplementary material

Supplementary data to this article can be found online at <https://doi.org/10.1016/j.pcean.2018.10.006>.

References

- Angel-Benavides, I.M., Pilo, G.S., Dias, F.B., Garcia, C.A.E., 2016. Influência dos Vórtices de Mesoescala na Concentração de Clorofila da Confluência Brasil-Malvinas: Mecanismos Inferidos por Sensoriamento Remoto. *Braz. J. Aquatic Sci. Technol.* 20 (1), 10–20.
- Azevedo, J.L.L., Mata, M.M., 2010. O mecanismo de autopropulsão de vórtices oceânicos: uma revisão. *Revista Brasileira de Geofísica* 28 (3), 153–172.
- Bakker, D.C.E., Pfeil, B., Landa, C.S., Metz, N., O'Brien, K.M., Olsen, A., et al., 2016. A multi-decade record of high-quality fCO₂ data in version 3 of the Surface Ocean CO₂ Atlas (SOCAT). *Earth Syst. Sci. Data* 8, 383–413. <https://doi.org/10.5194/essd-8383-2016>.
- Beal, L.M., 2009. A time series of Agulhas undercurrent transport. *J. Phys. Oceanogr.* 39, 2436–2450.
- Biastoch, A., Krauss, W., 1999. The role of mesoscale eddies in the source regions of the Agulhas current. *J. Phys. Oceanogr.* 29, 2303–2317.
- Biastoch, A., Böning, C.W., Lutjeharms, J.R.E., 2008. Agulhas leakage dynamics affects decadal variability in Atlantic overturning circulation. *Nature* 456, 489–492. <https://doi.org/10.1038/nature07426>.
- Biastoch, A., Böning, C.W., Swartzkopf, F.U., Lutjeharms, J.R.E., 2009. Increase in Agulhas leakage due to poleward shift of southern hemisphere westerlies. *Nature* 462, 495–498. <https://doi.org/10.1038/nature08519>.
- Biastoch, A., Durgadoo, J.V., Morrison, A.K., van Sebille, E., Weijer, W., Griffies, S.M., 2015. Atlantic multi-decadal oscillation covaries with Agulhas leakage. *Nat. Commun.* 6, 10082. <https://doi.org/10.1038/ncomms10082>.
- Broecker, W.S., Peng, T.-H., 1982. Tracers in the Sea. *Lamont-Doherty Geological Observatory, Palisades, NY*, pp. 690p.
- Cai, W.-J., 2003. Riverine inorganic carbon flux and rate of biological uptake in the Mississippi River plume. *Geophys. Res. Lett.* 30 (2), 1032. <https://doi.org/10.1029/2002GL016312>.
- Carvalho-Borges, M., Orselli, I.B.M., de Ferreira, M.L., Carvalho, Kerr, R., 2018. Seawater acidification and anthropogenic carbon distribution on continental shelf and slope of the western South Atlantic Ocean. *J. Mar. Syst.* <https://doi.org/10.1016/j.jmarsys.2018.06.008>.
- Casanova-Masjoan, M., Pelegrí, J.L., Sangrà, P., Martínez, A., Grisolia-Santos, D., Pérez-Hernández, M.D., Hernández-Guerra, A., 2017. Characteristics and evolution of an Agulhas ring. *J. Geophys. Res. Oceans* 122. <https://doi.org/10.1002/2017JC012969>.
- Chelton, D.B., Schlax, M.G., Samelson, R.G., 2011. Global observations of nonlinear mesoscale eddies. *Prog. Oceanogr.* 91 (2), 167–216. <https://doi.org/10.1016/j.pcean.2011.01.002>.
- Chelton & Schlax, 2016. Mesoscale Eddies in Altimeter Observations of SSH. Database. <http://wombat.coas.oregonstate.edu/eddies>.
- Chen, C.-T.A., Borges, A.V., 2009. Reconciling opposing views on carbon cycling in the coastal ocean: continental shelves as sinks and near-shore ecosystems as sources of atmospheric CO₂. *Deep-Sea Res.* II 56, 578–590.
- Chen, F., Cai, W.-J., Benitez-Nelson, C., Wang, Y., 2007. Sea surface pCO₂-SST relationships across a cold-core cyclonic eddy: implications for understanding regional variability and air-sea gas exchange. *Geophys. Res. Lett.* 34, L10603. <https://doi.org/10.1029/2006GL028058>.
- Ciais, P., Sabine, C., Bala, G., Bopp, L., Brovkin, V., Canadell, J., 2013. Carbon and Other Biogeochemical Cycles. In: Stocker, T.F., Qin, D., Plattner, G.-K., Tignor, M., Allen, S.K., Boschung, J. (Eds.), *Climate Change 2013: The Physical Science Basis. Contribution of Working Group I to the Fifth Assessment Report of the Intergovernmental Panel on Climate Change*. Cambridge University Press, Cambridge, United Kingdom and New York, NY, USA.
- Cox, P.M., Betts, R.A., Jones, C.D., Spall, S.A., Totterdell, I.J., 2000. Acceleration of global warming due to carbon-cycle feedbacks in a coupled climate model. *Nature* 408, 184–187.
- Craig, S.E., Thomas, H., Jones, C.T., Li, W.K.W., Greenan, B.J.W., Shadwick, E.H., Burt, W.J., 2014. The effect of seasonality in phytoplankton community composition on CO₂ uptake on the Scotian Shelf. *J. Mar. Syst.* <https://doi.org/10.1016/j.jmarsys.2014.07.006>.
- Denman, K.L., Brasseur, G., Chidthaisong, A., Ciais, P., Cox, P.M., Dickinson, R.E., 2007. Couplings Between Changes in the Climate System and Biogeochemistry. In: Solomon, S., Qin, D., Manning, M., Chen, Z., Marquis, M., Averyt, K.B. (Eds.), *Climate Change 2007: The Physical Science Basis. Contribution of Working Group I to the Fourth Assessment Report of the Intergovernmental Panel on Climate Change*. Cambridge University Press, Cambridge, United Kingdom and New York, NY, USA, pp. 499–587.
- de Ruijter, W.P.M., Biastoch, A., Drijfhout, S.S., Lutjeharms, J.R.E., Matano, R.P., Pichevin, T., et al., 1999. Dynamics, estimation and impact of South Atlantic inter-ocean exchange. *J. Geophys. Res.* 104, 20885–20910. <https://doi.org/10.1029/1998JC900099>.
- de Souza, A.G.Q., Kerr, R., Azevedo, J.L.L., 2018. On the influence of Subtropical Mode Water on the South Atlantic Ocean. *J. Mar. Syst.* 185, 13–24. <https://doi.org/10.1016/j.jmarsys.2018.04.006>.
- Dickson, A.G., Sabine, C.L., Christian, J.R., 2007. Guide to best practices for ocean CO₂ measurements. *PICES Special Publication* 3, 1–191.
- Dufois, F., Hardman-Mountford, N.J., Greenwoog, J., Richardson, A.J., Feng, M., Matear, R.J., 2016. Anticyclonic eddies are more productive than cyclonic eddies in subtropical gyres because of winter mixing. *Sci. Adv.* 2 (5), e1600282. <https://doi.org/10.1126/sciadv.1600282>.
- Eden, C., Dietze, H., 2009. Effects of mesoscale eddy/ wind interactions on biological new production and eddy kinetic energy. *J. Geophys. Res.* 114 (C5). <https://doi.org/10.1029/2008JC005129>. C05023–C05023.
- Emery, W.J., 2003. Water types and water masses. In: *Ocean Circulation*. Elsevier, pp. 1556–1567 ISBN: 978-0-12-391851-2.
- Fay, A.R., McKinley, G.A., 2013. Global trends in surface ocean pCO₂ from in situ data. *Global Biogeochem. Cycles* 27, 541–557. <https://doi.org/10.1002/gbc.20051>.
- Fay, A.R., McKinley, G.A., 2017. Correlations of surface ocean pCO₂ to satellite chlorophyll on monthly to interannual timescales. *Global Biogeochem. Cycles* 31, 436–455. <https://doi.org/10.1002/2016GB005563>.
- Feely, R.A., Sabine, C.L., Takahashi, T., Wanninkhof, R., 2001. Uptake and storage of carbon dioxide in the ocean: the global CO₂ survey. *Oceanography* 14 (4), 18–32.
- Fleming, P.J., Wallace, J.J., 1986. How not to lie with statistics: the correct way to summarize benchmark results. *Commun. ACM* 29 (3), 218–221. <https://doi.org/10.1145/5666.5673>.
- Flierl, G.R., 1979. A simple model for a structure of warm and cold core rings. *J. Geophys. Res.* 84 (C2), 781–785.
- Frankignoulle, M., Borges, A.V., 2001. European continental shelf as a significant sink for atmospheric carbon dioxide. *Global Biogeochem. Cycles* 15 (3), 569–576. <https://doi.org/10.1029/2000GB001307>.
- Frenger, I., Gruber, N., Knutti, R., Münnich, M., 2013. Imprint of Southern Ocean eddies on winds, clouds and rainfall. *Nat. Geosci.* 6 (8), 608–612.
- Gordon, A.L., Weiss, R.F., Smethie Jr., W.M., Warner, M.J., 1992. Thermocline and intermediate water communication between the South Atlantic and Indian Oceans. *J. Geophys. Res.* 97, 7223–7240. <https://doi.org/10.1029/92JC00485>.
- Gordon, A.L., 2003. Oceanography: The browniest retroflection. *Nature* 421 <https://doi.org/10.1038/421904a>. 904 805.
- Guerra, L.A.A., Paiva, A.M., Chassignet, E.P., 2018. On the translation of Agulhas rings to the western South Atlantic Ocean. *Deep-sea Res.* 139, 104–113. <https://doi.org/10.1016/j.dsr.2018.08.005>.
- Hales, B., Stratton, P.G., Saraceno, M., Letelier, R., Takahashi, T., Feely, R.A., et al., 2012. Satellite-based prediction of pCO₂ in coastal waters of the eastern North Pacific. *Prog. Oceanogr.* 103, 1–15. <https://doi.org/10.1016/j.pcean.2012.03.001>.
- Iida, Y., Kojima, A., Takatani, Y., Nakano, T., Sugimoto, H., Midorikawa, T., Ishii, M., 2015. Trends in pCO₂ and sea-air CO₂ flux over the global open oceans for the last two decades. *J. Oceanogr.* 71 (6), 637–661. <https://doi.org/10.1007/s10872-015-0306-4>.
- Ishii, M., Kosugi, N., Sasano, D., Saito, S., Midorikawa, T., Inoue, H.Y., 2011. Ocean acidification off the south coast of Japan: a result from time series observations of CO₂ parameters from 1994 to 2008. *J. Geophys. Res.* 116 (C06022). <https://doi.org/10.1029/2010JC006831>.
- Ito, R.G., Schneider, B., Thomas, H., 2005. Distribution of surface fCO₂ and air-sea fluxes in the Southwestern subtropical Atlantic and adjacent continental shelf. *J. Mar. Syst.* 56, 227–242.
- Ito, R.G., Garcia, C.A.E., Tavano, V.M., 2016. Net sea-air CO₂ fluxes and modelled pCO₂ in the southwestern subtropical Atlantic continental shelf during spring 2010 and summer 2011. *Cont. Shelf Res.* 119, 68–84.
- Jahne, B.H.G., Dietrich, W., 1987. Measurement of the diffusion coefficients of sparingly soluble gases in water. *J. Geophys. Res.* 92, 10767–10776. <https://doi.org/10.1029/JC092iC10p10767>.
- Jiang, L.-Q., Cai, W.-J., Wanninkhof, R., Wang, Y., Lüger, H., 2008. Air-sea CO₂ fluxes on the U.S. South Atlantic Bight: Spatial and seasonal variability. *J. Geophys. Res.* 113 (C07019). <https://doi.org/10.1029/2007JC004366>.
- Jones, E.M., Hoppema, M., Strass, V., Hauck, J., Salt, L., Ossebaar, S., et al., 2017. Mesoscale features create hotspots of carbon uptake in the Antarctic Circumpolar Current. *Deep-Sea Res.* II 138, 39–51. <https://doi.org/10.1016/j.dsr2.2015.10.006>.
- Kahru, M., Mitchell, B.G., Gille, S.T., Hewes, C.D., Holm-Hansen, O., 2007. Eddies enhance biological production in the Weddell-Scotia Confluence of the Southern Ocean. *Geophys. Res. Lett.* 34, L14603. <https://doi.org/10.1029/2007GL030430>.
- Kerr, R., Cunha, L.C., Kikuchi, R.K.P., Horta, P., Ito, R.G., Muller, M.N., et al., 2016. The western South Atlantic Ocean in a high-CO₂ world: current measurement capabilities and perspectives. *Environ. Manage.* 57, 740–752.
- Kitidis, V., Brown, I., Hardman-Mountford, N., Lefèvre, N., 2017. Surface ocean carbon dioxide during the Atlantic Meridional Transect (1995–2013): evidence of ocean acidification. *Prog. Oceanogr.* 158, 65–75. <https://doi.org/10.1016/j.pcean.2016.08.005>.
- Landschützer, P., Gruber, N., Haumann, F.A., Rödenbeck, C., Bakker, D.C., Van Heuven, S., et al., 2015. The reinvigoration of the Southern Ocean carbon sink. *Science* 349 (6253), 1221–1224.
- Laruelle, G.G., Dürr, H.H., Lauerwald, R., Hartmann, J., Slomp, C.P., Goossens, N., Regnier, P.A.G., 2013. Global multi-scale segmentation of continental and coastal waters from the watersheds to the continental margins. *Hydro. Earth Syst. Sci.* 17, 2029–2051.
- Laruelle, G.G., Lauerwald, R., Pfeil, B., Regnier, P., 2014. Regionalized global budget of the CO₂ exchange at the air-water interface in continental shelf seas. *Global Biogeochem. Cycles* 28 (11), 1199–1214. <https://doi.org/10.1002/2014GB004832>.
- Laruelle, G.G., Lauerwald, R., Rotschi, J., Raymond, A., Hartmann, J., Regnier, P., 2015. Seasonal response of air-water CO₂ exchange along the land-ocean aquatic continuum of the northeast North American coast. *Biogeosciences* 12, 1447–1458. <https://doi.org/10.5194/bg12-1447-2015>.
- Lefèvre, N., Moore, G.F., 2000. Distribution of the CO₂ partial pressure along an Atlantic meridional transect. *Prog. Oceanogr.* 45, 401–413.
- Le Quéré, C., Moriarty, R., Andrew, R.M., Peters, G.P., Ciais, P., Friedlingstein, P., et al., 2015. Global carbon budget 2014. *Earth Syst. Sci. Data* 7, 47–85.
- Le Quéré, C., Moriarty, R., Andrew, R.M., Canadell, J.G., Sitch, S., Korsbakken, P., et al., 2016. Global Carbon Budget 2016. *Earth Syst. Sci. Data* 8, 605–649.
- Lehahn, Y., d'Ovidio, F., Lévy, M., Amitai, Y., Heifetz, E., 2011. Long range transport of a quasi isolated chlorophyll patch by an Agulhas ring. *Geophys. Res. Lett.* 38, L16610. <https://doi.org/10.1029/2011GL048588>.
- Lencina-Avila, J.M., Ito, R.G., Garcia, C.A.E., Tavano, V.M., 2016. Sea-air carbon dioxide

- fluxes along 35°s in the Atlantic Ocean and adjacent continental shelves. *Deep-Sea Research I* 115, 175–187. <https://doi.org/10.1016/j.dsr.2016.06.004>.
- Lovenduski, N.S., Gruber, N., Doney, S.C., 2008. Toward a mechanistic understanding of the decadal trends in the Southern Ocean carbon sink. *Global Biogeochem. Cycles* 22 (3), GB3016. <https://doi.org/10.1029/2007GB003139>.
- Lutjeharms, J.R.E., 2006. *The Agulhas Current*. Springer, Berlin, Heidelberg. <http://doi.org/10.1007/3-540-37212-1>.
- Martin, A.P., Richards, K.J., 2001. Mechanisms for vertical nutrient transport within a North Atlantic mesoscale eddy. *Deep-Sea Res. II* 48, 757–773.
- McGillicuddy, D.J., 2016. Mechanisms of physical-biological-biochemical interaction at the Oceanic Mesoscale. *Annu. Rev. Marine Sci.* 8, 125–159. <https://doi.org/10.1146/annurev-marine-010814-015606>.
- McKinley, G.A., Fay, A.R., Takahashi, T., Metzl, N., 2011. Convergence of atmospheric and North Atlantic carbon dioxide trends on multidecadal timescales. *Nat. Geosci.* 4 (9), 606–610.
- McKinley, G.A., Fay, A.R., Lovenduski, N., Pilcher, D.J., 2017. Natural variability and anthropogenic trends in the ocean carbon sink. *Annu. Rev. Marine Sci.* 9, 125–150. <https://doi.org/10.1146/annurev-marine-010816-060529>.
- McKinley, G.A., Follows, M.J., Marshall, J., 2004. Mechanisms of air-sea CO₂ flux variability in the equatorial Pacific and the North Atlantic. *Global Biogeochem. Cycles* 18 (2), GB2011. <https://doi.org/10.1029/2003GB002179>.
- Möller Jr., O.O., Piola, A.R., Freitas, A.C., Campos, E.J.D., 2008. The effects of river discharge and seasonal winds on the shelf off Southeastern South America. *Cont. Shelf Res.* 28, 1607–1624.
- Moreau, S., Penna, A.D., Llorc, J., Patel, R., Langlais, C., Boyd, P.W., et al., 2017. Eddy-induced carbon transport across the Antarctic Circumpolar Current. *Global Biogeochem. Cycles* 31 (9), 1368–1386. <https://doi.org/10.1002/2017GB005669>.
- Orselli, I.B.M., Kerr, R., Ito, R.G., Tavano, V.M., Mendes, C.R.B., Garcia, C.A.E., 2018. How fast is the Patagonian shelf-break acidifying? *J. Mar. Syst.* 178, 1–14. <https://doi.org/10.1016/j.jmarsys.2017.10.007>.
- Orsi, A.H., Johnson, G.C., Bullister, J.L., 1999. Circulation, mixing and production of Antarctic bottom water. *Prog. Oceanogr.* 43, 55–109. [https://doi.org/10.1016/S0079-6611\(99\)00004-X](https://doi.org/10.1016/S0079-6611(99)00004-X).
- Padin, X.A., Vázquez-Rodríguez, M., Castañol, M., Velo, A., Alonso-Pérez, F., Gago, J., et al., 2010. Air-sea CO₂ fluxes in the Atlantic as measured during boreal spring and autumn. *Biogeosciences* 7, 1587–1606.
- Pal, S.K., 1998. *Statistics for Geoscientists: Techniques and Applications*. ISBN 81-7022-712-1. New Delhi, India.
- Pardo, P.C., Pérez, F.F., Khaliwala, S., Ríos, A.F., 2014. Anthropogenic CO₂ estimates in the Southern Ocean: storage partitioning in the different water masses. *Prog. Oceanogr.* 120, 230–242. <https://doi.org/10.1016/j.pocean.2013.09.005>.
- Peterson, R.G., Stramma, L., 1991. Upper-level circulation in the South Atlantic ocean. *Prog. Oceanogr.* 2 (6), 1–73.
- Pierrot, D., Neil, C., Sullivan, K., Castle, R., Wanninkhof, R., Lüger, H., et al., 2009. Recommendations for autonomous underway pCO₂ measuring systems and data-reduction routines. *Deep-Sea Res. II* 56, 512–522.
- Rintoul, S., 2011. *The Southern Ocean in the Earth System*. Smithsonian Institution Scholarly Press, Washington.
- Ríos, A.F., Álvarez-Salgado, X.A., Pérez, F.F., Bingler, L.S., Aristegui, J., Mémary, L., 2003. Carbon dioxide along WOCE line A14: water masses characterization and anthropogenic entry. *J. Geophys. Res.* 108 (C4), 3123. <https://doi.org/10.1029/2000JC000366>.
- Robinson, A., 1983. *Eddies in Marine Science*. Springer-Verlag.
- Rost, B., Riebesell, U., 2004. Coccolithophores and the biological pump: responses to environmental changes. In: Thierstein, H.R., Young, J.R. (Eds.), *Coccolithophores: from Molecular Processes to Global Impact*. Springer, Berlin, pp. 99–125.
- Sabine, C.L., Feely, R.A., Gruber, N., Key, R.M., Lee, K., Bullister, J.L., et al., 2004. The Ocean Sink for Anthropogenic CO₂. *Science* 305 (5682), 367–371.
- Sarmiento, J.L., Gruber, N., 2006. *Ocean Biogeochemical Dynamics*. Princeton University Press, Princeton, Woodstock.
- Salt, L.A., van Heuven, S.M.A.C., Claus, M.E., et al., 2015. Rapid acidification of mode and intermediate waters in the southwestern Atlantic Ocean. *Biogeosciences* 12, 1387–1401.
- Schlitzer, R., 2016. Ocean Data View, <<http://odv.awi.de>>.
- Schlax, M.G., Chelton, D.B., 2016. *The “Growing Method” of Eddy Identification and Tracking in Two and Three Dimensions*. College of Earth, Ocean and Atmospheric Sciences. Oregon State University, Corvallis, Oregon July 8, 2016.
- Schuster, U., Watson, A.J., Bates, N.R., Corbiere, A., Gonzalez-Davila, M., Metzl, N., et al., 2009. Trends in North Atlantic sea-surface fCO₂ from 1990 to 2006. *Deep-Sea Res. II* 56 (8), 620–629. <https://doi.org/10.1016/j.dsr2.2008.12.011>.
- Schuster, U., McKinley, G.A., Bates, N., Chevallier, F., Doney, S.C., Fay, A.R., et al., 2013. Na assessment of the Atlantic and Arctic sea-air CO₂ fluxes, 1990–2009. *Biogeosciences* 10, 607–627. <https://doi.org/10.5194/bg-10-607-2013>.
- Signorini, S.R., Mannino, A., Najjar Jr., R.G., Friedrichs, M.A.M., Cai, W.-J., Salisbury, J., et al., 2013. Surface ocean pCO₂ seasonality and sea-air CO₂ flux estimates for the North American east coast. *J. Geophys. Res. Oceans* 118, 5439–5460. <https://doi.org/10.1002/jgrc.20369>.
- Song, H.J.M., Munro, D.R., Dutkiewicz, S., Sweeney, C., McGillicuddy, D.J., Hausmann, U., 2016. Mesoscale modulation of air-sea CO₂ flux in Drake Passage. *J. Geophys. Res. Oceans* 121, 6635–6649. <https://doi.org/10.1002/2016JC011714>.
- Souza, J.M.A.C., de Boyer Montegut, C., Cabanes, C., Klein, P., 2011. Estimation of the Agulhas ring impacts on meridional heat fluxes and transport using ARGO floats and satellite data. *Geophys. Res. Lett.* 38, L21602. <https://doi.org/10.1029/2011GL049359>.
- Stramma, L., England, M., 1999. On the Water masses and mean circulation of the South Atlantic Ocean. *J. Geophys. Res.* 104 (C9), 20863–20883.
- Sutherland, S.C., Newberger, T., Takahashi, T., Sweeney, C., 2015. Report of underway pCO₂ measurements in surface waters and the atmosphere during August 2015 R/V Nathaniel B. Palmer Cruise 15/8. Lamont-Doherty Earth Observatory of Columbia University. Palisades, NY 10964. 1 December 2015.
- Takahashi, T., Feely, R.A., Weiss, R., Wanninkhof, R.H., Chipman, D.W., Sutherland, S.C., Takahashi, T.T., 1997. Global air-sea flux of CO₂: an estimate based on measurements of sea-air pCO₂ difference. *Proc. Natl. Acad. Sci.* 94, 8292–8299.
- Takahashi, T., Sutherland, S.C., Sweeney, C., Poisson, A., Metzl, N., Tilbrook, B., et al., 2002. Global sea-air CO₂ flux based on climatological surface ocean pCO₂, and seasonal biological and temperature effects. *Deep-Sea Res. II* 49, 1601–1622. [https://doi.org/10.1016/S0967-0645\(02\)00003-6](https://doi.org/10.1016/S0967-0645(02)00003-6).
- Takahashi, T., Sutherland, S.C., Wanninkhof, R., Sweeney, C., Feely, R.A., Chipman, D.W., et al., 2009. Climatological mean and decadal change in surface ocean pCO₂, and net sea-air CO₂ flux over the global oceans. *Deep-Sea Res. II* 56, 554–557.
- Talley, L., Pickard, G., Emery, W., Swift, J., 2011. *Descriptive Physical Oceanography: an Introduction*. Elsevier, Boston.
- Tans, P.P., Fung, I.Y., Takahashi, T., 1990. Observational constraints on the global atmospheric CO₂ budget. *Science* 247, 1431–1438.
- Tilburg, C.E., Subrahmanyam, B., O'Brien, J.J., 2002. Ocean color variability in the Tasman Sea. *Geophys. Res. Lett.* 29 (10), 1487. <https://doi.org/10.1029/2001GL014071>.
- Uchida, H., Fukasawa, M., Murata, A., 2005. WHP P6, A10, I3/14 Revisit Data Book Blue Earth Global Expedition 2003 (BEAGLE2003). JAMSTEC Publication, pp. 2.
- Villas Bôas, A.B., Sato, O.T., Chaigneau, A., Castelão, G.P., 2015. The signature of mesoscale eddies on the air-sea turbulent heat fluxes in the South Atlantic Ocean. *Geophys. Res. Lett.* 42 (6), 1856–1862. <https://doi.org/10.1002/2015GL063105>.
- Zeng, J., Nojiri, Y., Landschützer, P., Telszewski, M., Nakaoka, S., 2014. A global surface ocean fCO₂ climatology based on a feed-forward neural network. *J. Atmos. Oceanic Technol.* 31, 1838–1849.
- Wang, Z.A., Wanninkhof, R., Cai, W.-J., Byrne, R.H., Hu, X., Peng, T.-H., Huang, W.-J., 2013. The marine inorganic carbon system along the Gulf of Mexico and Atlantic coasts of the United States: Insights from a transregional coastal carbon study. *Limnol. Oceanogr.* 58 (1), 325–342.
- Wang, X., Murtugudde, R., Hackert, E., Wang, J., Beauchamp, J., 2015. Seasonal to decadal variations of sea surface pCO₂ and sea-air CO₂ flux in the equatorial oceans over 1984–2013: a basin-scale comparison of the Pacific and Atlantic Oceans. *Global Biogeochem. Cycles* 29, 597–609. <https://doi.org/10.1002/2014GB005031>.
- Wanninkhof, R., 1992. Relationship between wind speed and gas exchange over the ocean. *J. Geophys. Res.* 97 (C5), 7373–7382. <https://doi.org/10.1029/92JC00188>.
- Wanninkhof, R., 2014. Relationship between wind speed and gas exchange over the ocean revisited. *Limnol. Oceanogr. Methods* 12 (6), 351–362. <https://doi.org/10.4319/lom.2014.12.351>.
- Wanninkhof, R., Castle, R., 2013. Underway measurements of surface partial pressure of CO₂ during the R/V Ronald H. Brown in the Atlantic Ocean on CLIVAR Repeat Hydrography Section A10 (September 26 - October 31, 2011). Carbon Dioxide Information Analysis Center, Oak Ridge National Laboratory, US Department of Energy, Oak Ridge, Tennessee. <http://doi.org/10.3334/CDIAC/OTG.CLIVAR_A10_2011_UW>.
- Weiss, R.F., 1974. Carbon dioxide in water and seawater: the solubility of a non-ideal gas. *Mar. Chem.* 2, 203–215.
- Weiss, R.F., Price, B.A., 1980. Nitrous oxide solubility in water and seawater. *Mar. Chem.* 8, 347–359.
- Woosley, R.J., Millero, F., Wanninkhof, R., 2016. Rapid Anthropogenic Changes in CO₂ and pH in the Atlantic Ocean: 2003–2014. *Global Biogeochem. Cycles* 30, 70–90. <https://doi.org/10.1002/2015GB005248>.

Article – PhD 01: supporting information

Progress in Oceanography

Supporting Information for

The Sea-Air CO₂ Net Fluxes in the South Atlantic Ocean and the Role Played by Agulhas Eddies

Iole B. M. Orselli^{1,2,3,4*}, Rodrigo Kerr^{1,2}, José L. L. de Azevedo¹, Felipe Galdino¹, Moacyr Araujo^{5,6}, Carlos A. E. Garcia^{1,7}

¹Laboratório de Estudos dos Oceanos e Clima, Instituto de Oceanografia, Universidade Federal do Rio Grande (FURG), Av. Itália km 8, s/n, Rio Grande, 96203-900, RS, Brazil.

²Brazilian Ocean Acidification Network (BrOA), Av. Itália km 8, Rio Grande, 96203-900, RS, Brazil.

³IMAGES_ESPACE-DEV, Université de Perpignan Via Domitia (UPVD), 52 ave. Paul Alduy, 66860, Perpignan, France.

⁴ESPACE-DEV UMR UG UA UM IRD, Maison de la télédétection, 500 rue Jean-François Breton, 34093, Montpellier Cedex 5, France.

⁵Laboratório de Oceanografia Física, Estuarina e Costeira (LOFEC), Departamento de Oceanografia, Centro de Tecnologia, Universidade Federal de Pernambuco (UFPE), Av. Arquitetura, s/n, Recife, 50740550, PE, Brazil.

⁶Brazilian Research Network on Global Climate Change (Rede CLIMA), São José dos Campos, 12227-010, SP, Brazil.

⁷Programa de Pós-graduação em Oceanografia, Universidade Federal de Santa Catarina (UFSC), Campus Reitor João David Ferreira Lima, s/n, Florianópolis, 88040-900, SC, Brazil.

*Corresponding author: Iole B. M. Orselli (iole.orselli@furg.br / iole.orselli@gmail.com)

Address: LEOC, Instituto de Oceanografia – FURG, Avenida Itália km 8 s/n°, Campus Carreiros, Rio Grande, Brazil, 96203–900.

Contents of this file:

Text S1
Figures S1 to S7
Tables S1 to S3
Caption for Video S1

Introduction

This Supporting Information file includes some extra information on the databases used to perform specific analysis that is not relevant for the main text comprehension but can be interesting to some readers. [Text S1](#) provides a brief explanation of the AVISO product used to determine the radius and lifetime of each eddy. [Fig. S1](#) presents the monthly mean wind speed data applied to the sea-air CO₂ net fluxes calculations.

We also present some results obtained from the *Following Ocean Rings in the South Atlantic* (FORSA) cruise that would be newsworthy, such as the physico-chemical diagrams constructed with the CTD profiles ([Fig. S2](#)) and some general results ([Table S1](#)). Because there is a historical lack of CO₂-system measurements in the region near the Brazilian coast, we considered doing a zoom in this region and presenting some specific results ([Fig. S3](#), [Table S2](#)), although a brief discussion regarding this is presented in the main text (section 4.1.2). The eddy-focused ([Figs. S4, S5](#), [Table S3](#)) specific results are also inserted here.

Regarding the multiple linear regression model developed to reproduce the CO₂^{sw}-parameters of the FORSA cruise, we included [Fig. S6](#) to clarify the region in which the model was less representative.

To help the readers to easily comprehend where each study used for the comparison with FORSA results ([Table 5](#)) was conducted, we included a composite figure with all the maps from those studies in [Fig. S7](#).

Text S1.

The AVISO product uses the algorithm of [Schlax & Chleton \(2016\)](#) to identify an eddy in the sea level anomaly (SLA) field. This algorithm uses a low pass filter in the SLA field to find points with extrema SLAs, which can possibly be eddies. In these cases, the eddy detection process starts by searching for other specific characteristics around these points (e.g., the surrounding points must be equal or smaller in amplitude than the area defined, the two most remote points must be localized not farther than a maximum eddy-likely diameter, etc.). If these specifications are achieved in the SLA, it is considered an eddy field. Therefore, this detection is applied for several consecutive days to reconstruct the back and forward eddy trajectory. In this way, the lifetime is the period in which the eddy matches the criteria of the algorithm from its first to its last detection time in the SLA dataset. The determination of the eddy radius is made by taking the radius of a circle that delineates the enclosed contour of maximum circum-average geostrophic speed. For detailed information about the algorithm and criteria, the reader is referred to [Schlax & Chleton \(2016\)](#). Because we used the Mesoscale Eddy Trajectory Atlas product, we would like to thank its producers, supporters, collaborators and distributors: SSALTO/DUACS, CNES, Oregon State University, NASA and AVISO.

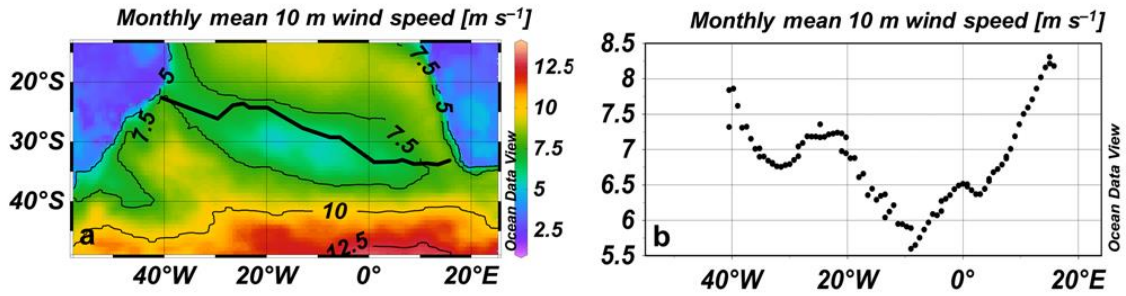


Figure S1. a) Map of the monthly mean wind speed (m s^{-1}) data of July 2015 (at a 10 m height) for the South Atlantic Ocean. The black line corresponds to the FORSA section. b) The longitudinal distribution of monthly mean wind speed (m s^{-1}) data of July 2015 (at a 10 m height) in the FORSA section. These data were extracted from the ERA-Interim atmospheric reanalysis product of the European Centre for Medium Range Weather Forecast (<http://apps.ecmwf.int/datasets/data/interim-full-moda/levtype=sfc/>).

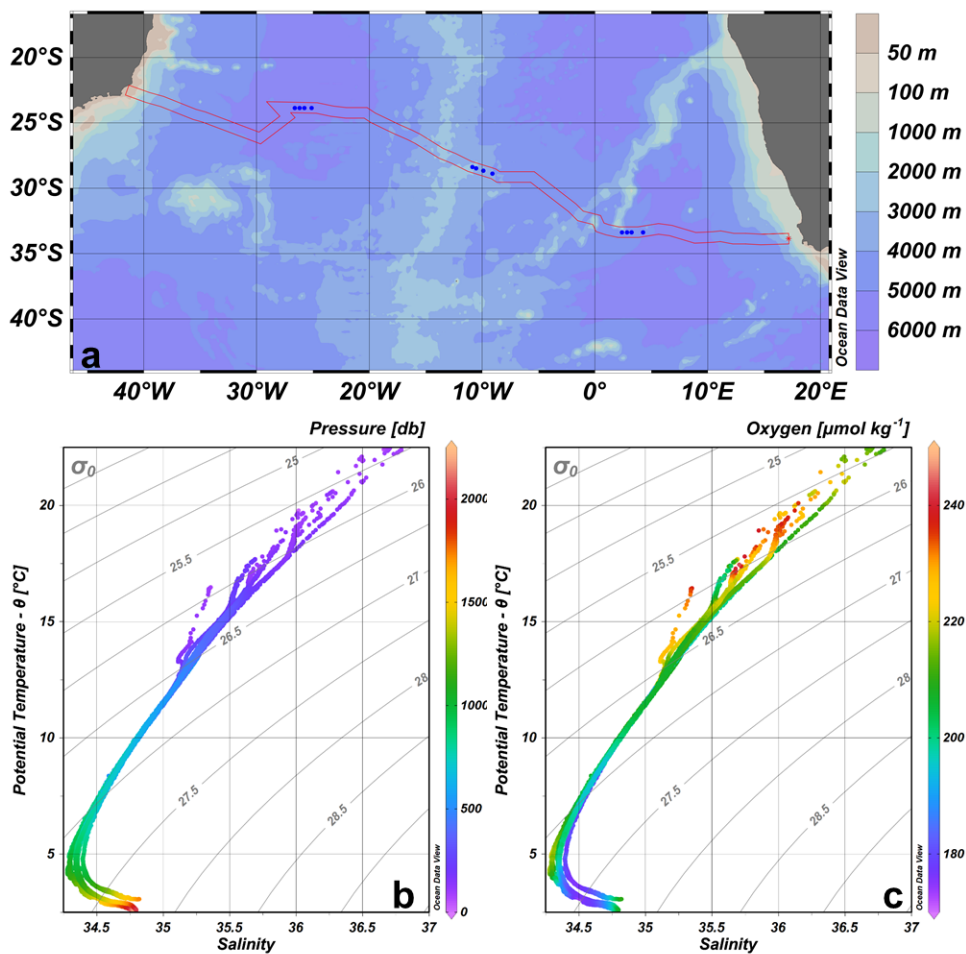


Figure S2. a) Map of the study region in the South Atlantic Ocean. The red continuous line corresponds to the FORSA cruise section. The blue dots indicate the position of the CTD profiles executed during the cruise. The bottom bathymetry is represented by color shadings. b) θ/S pressure diagram. c) θ/S -DO diagram. Isopycnals are indicated by gray lines. Potential temperature (θ) is in $^{\circ}\text{C}$, pressure is in db and OD is in $\mu\text{mol kg}^{-1}$.

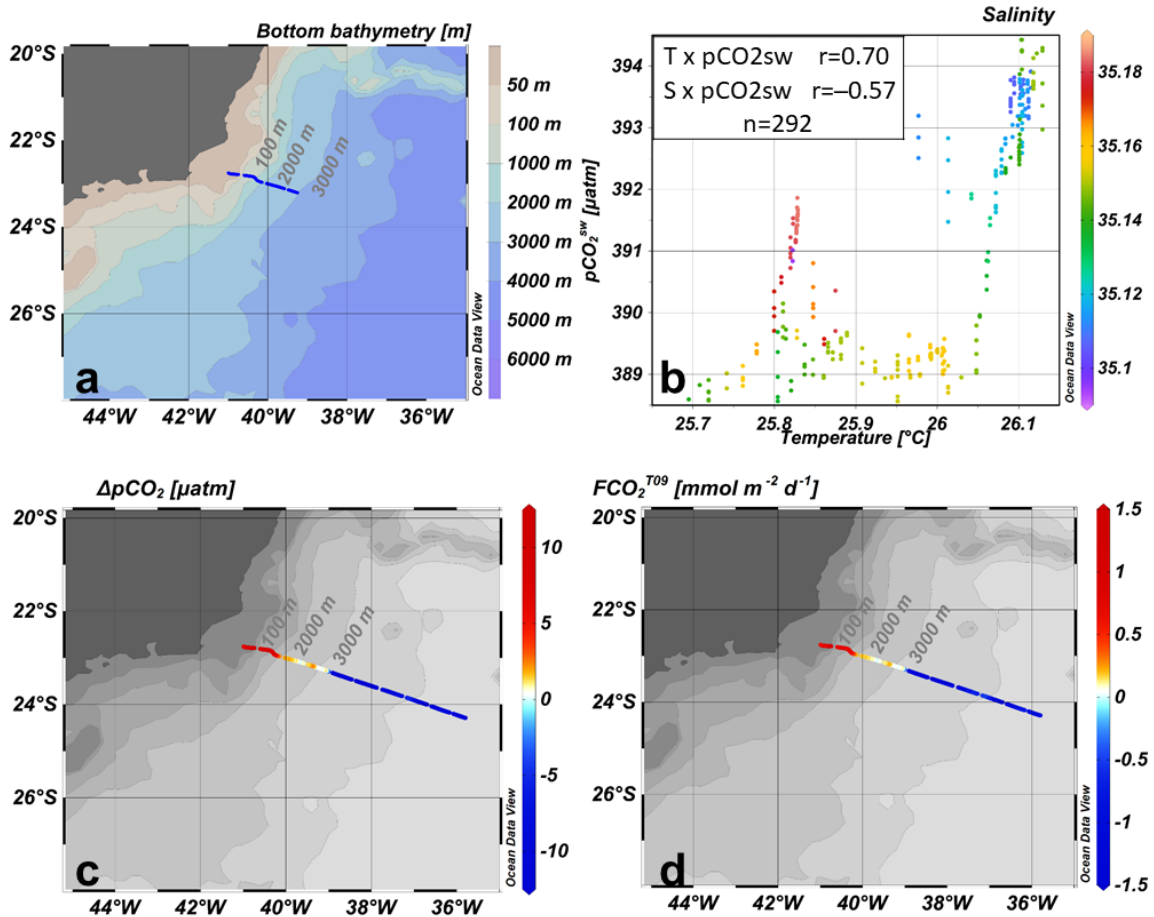


Figure S3. a) Map of the region near the Brazilian coast (west of 39.25°W, shallower than 3000 m), at the westernmost part of the occidental basin of the South Atlantic Ocean. The blue continuous line corresponds to the FORSA cruise data considered in this brief zoom of the region (subplot b and Table S2). The bottom bathymetry is represented by color shadings. b) Temperature (°C) vs. $p\text{CO}_2^{\text{sw}}$ (µatm) diagram, with salinity in colors, considering only the region included in the subplot a). Inside this diagram are inserted the linear correlation coefficients (r) between temperature and salinity vs. $p\text{CO}_2^{\text{sw}}$ and the number of data points used (n). Significance at 95% confidence level ($p < 0.05$). c) Map of the spatial distribution of $\Delta p\text{CO}_2$ (µatm) at the westernmost part of the occidental basin. d) Map of the sea-air CO_2 net flux ($\text{FCO}_2^{\text{T09}}$, $\text{mmol m}^{-2} \text{d}^{-1}$) calculated using the K_T determined by Takahashi et al. (2009) at the westernmost part of the occidental basin. c and d) Encompasses more data than considered for the subplots a and b and Table S2, to highlight the difference between the region near the Brazilian coast and the deeper regions. The bottom bathymetry is also represented in subplots c and d by gray color shadings.

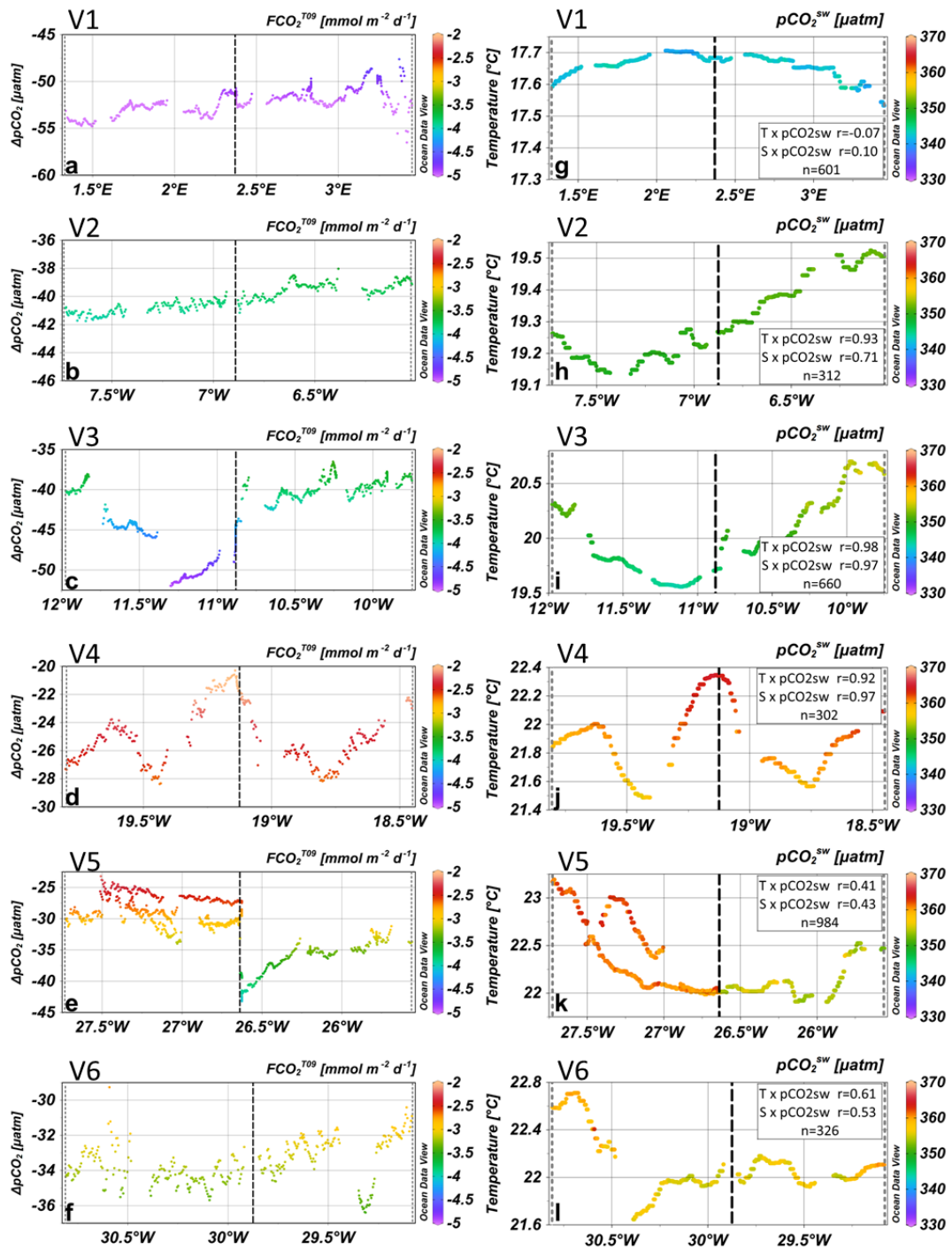


Figure S4. a to f) Longitudinal distribution of $\Delta p\text{CO}_2$ (μatm) with sea-air CO_2 net flux ($\text{FCO}_2^{\text{T09}}$, $\text{mmol m}^{-2} \text{d}^{-1}$) calculated using the K_T determined by Takahashi et al. (2009) in colors. g to l) Longitudinal distribution of temperature ($^{\circ}\text{C}$) with $p\text{CO}_2^{\text{sw}}$ (μatm) in colors. Inside each diagram are inserted the linear correlation coefficients (r) between temperature and salinity vs. $p\text{CO}_2^{\text{sw}}$ and the number of data points used (n) for each eddy. Significance at 95% confidence level ($p < 0.05$). The number of the eddy is indicated in the top-north-western side of each subplot. Note that the color scales used for $\text{FCO}_2^{\text{T09}}$ and $p\text{CO}_2^{\text{sw}}$ are in the same range for all subplots.

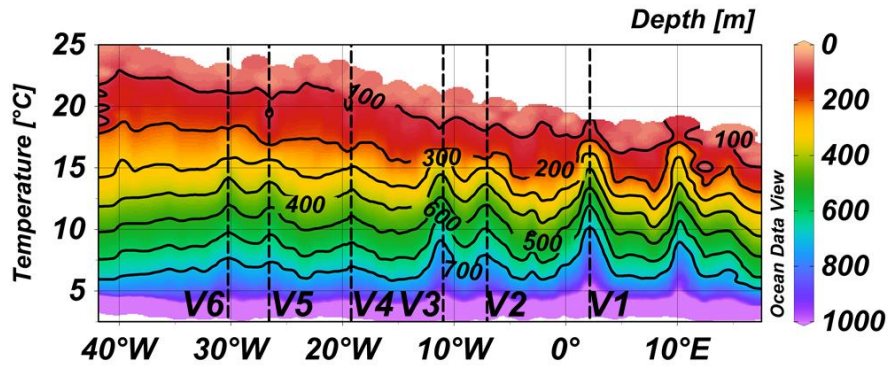


Figure S5. Longitudinal distribution of temperature ($^{\circ}\text{C}$) with depth (m) in colors. The black-dashed lines indicate the center of the eddies.

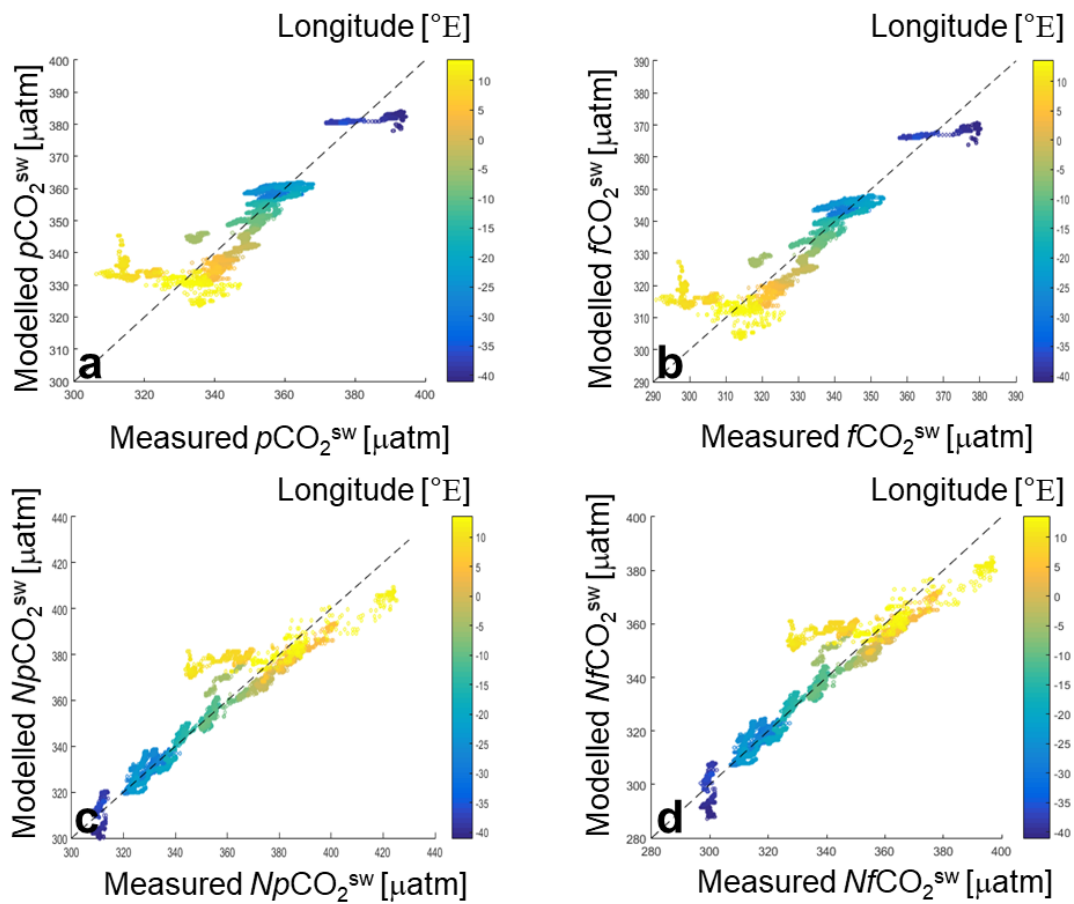


Figure S6. Measured vs. modeled results including the longitude ($^{\circ}\text{E}$) in colors. a) $p\text{CO}_2^{\text{sw}}$ (μatm). b) $f\text{CO}_2^{\text{sw}}$ (μatm). c) $Np\text{CO}_2^{\text{sw}}$ (μatm). d) $Nf\text{CO}_2^{\text{sw}}$ (μatm).

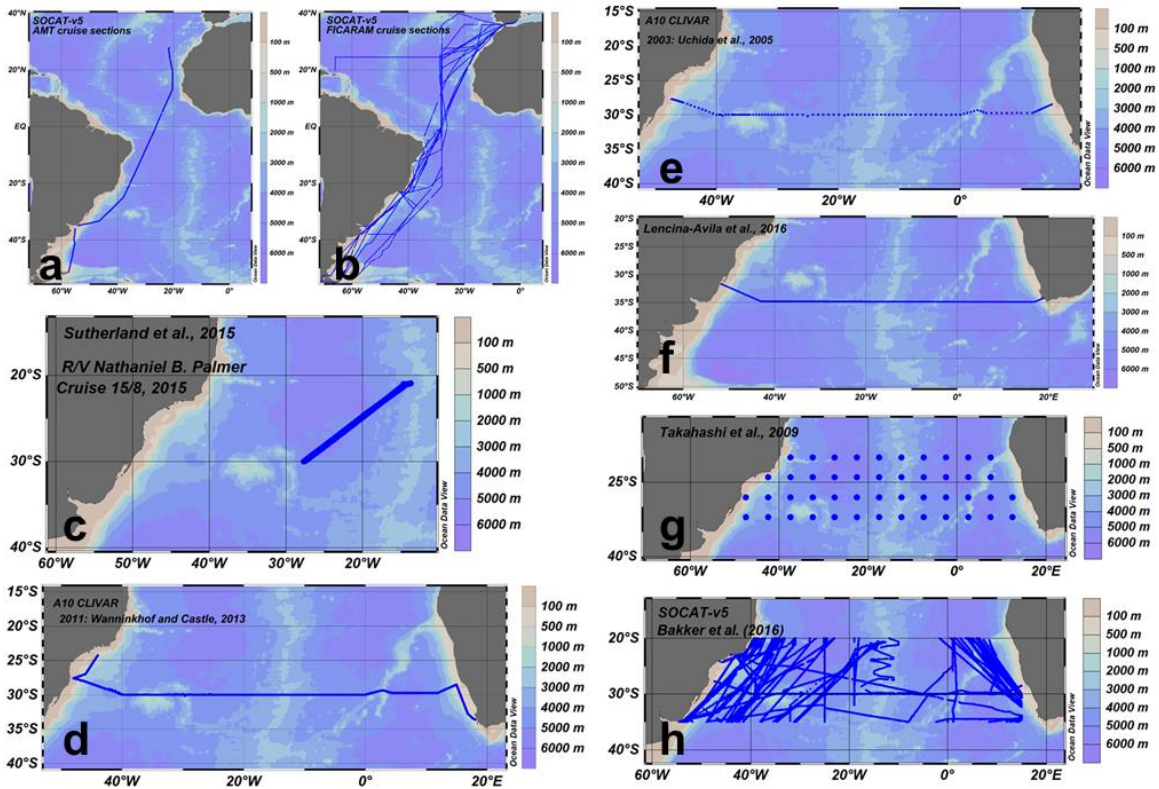


Figure S7. Maps of each study considered to compare results of CO_2 -related parameters ($p\text{CO}_2^{\text{sw}}$, $f\text{CO}_2^{\text{sw}}$, $\Delta p\text{CO}_2$, $\Delta f\text{CO}_2$, FCO_2) to the FORSA results, used in Table 5, main text. a) Map of AMT cruises transects studied by Lefèvre & Moore (2000), obtained from the SOCAT v5 database (Bakker et al., 2016). b) Map of all FICARAM cruises sections studied by Padin et al. (2010), obtained from the SOCAT v5 database (Bakker et al., 2016). c) Map representing the data used from the Sutherland et al. (2015) report of the R/V Nathaniel B. Palmer cruise 15/8, conducted in 2015, available at www.ldeo.columbia.edu/res/pi/CO2/carbondioxide/Palmer_data/1508SFC.PRT. d) Map representing the data used from the Wanninkhof & Castle (2013) report of the A10 CLIVAR/ WOCE cruise, conducted in 2011, available at cdiac.ornl.gov/ftp/oceans/CLIVAR/A10_2011/. e) Map representing the data used from the Uchida et al. (2005) report of the A10 CLIVAR/ WOCE cruise, conducted in 2003, available at www.nodc.noaa.gov/ocads/oceans/RepeatSections/clivar_a10.html. f) Map representing the cruise conducted in 2011 studied by Lencina-Avila et al. (2016). g) Map representing the data used from the Takahashi et al. (2009) database, available at www.ldeo.columbia.edu/res/pi/CO2/carbondioxide/air_sea_flux/month_flux_2006c.txt. h) Map representing the data used from the Bakker et al. (2016) report of the SOCAT v5 database, available at www.socat.info/index.php/data-access/. The bottom bathymetry is represented by color shadings, as indicated in the color bars.

Table S1. The linear correlation coefficients for temperature – T (°C), salinity – S and chlorophyll-*a* – chl-*a* (mg m⁻³) vs. seawater CO₂ partial pressure – $p\text{CO}_2^{\text{sw}}$ (µatm) and/or temperature-normalized $p\text{CO}_2^{\text{sw}}$ – $Np\text{CO}_2^{\text{sw}}$ (µatm) @ 20.39°C for each region. The number of data points used is referred to as n. The significance level for each correlation is also included.

	South Atlantic Ocean		Western basin		Eastern basin		Near the Brazilian coast	
	$p\text{CO}_2^{\text{sw}}$	$Np\text{CO}_2^{\text{sw}}$	$p\text{CO}_2^{\text{sw}}$	$Np\text{CO}_2^{\text{sw}}$	$p\text{CO}_2^{\text{sw}}$	$Np\text{CO}_2^{\text{sw}}$	$p\text{CO}_2^{\text{sw}}$	$Np\text{CO}_2^{\text{sw}}$
T	0.88 $p<0.01$ (n=10410)		0.92 $p<0.01$ (n=5010)		0.61 $p<0.01$ (n=5400)		0.70 $p<0.01$ (n=292)	
S	-0.03 $p<0.01$ (n=10410)	-0.20 $p<0.01$ (n=10410)	-0.65 $p<0.01$ (n=5010)	0.48 $p<0.01$ (n=5010)	0.26 $p<0.01$ (n=5400)	-0.57 $p<0.01$ (n=5400)	0.57 $p<0.01$ (n=292)	0.11 $p<0.01$ (n=292)
chl-<i>a</i>	-0.55 $p<0.01$ (n=8690)	0.61 $p<0.01$ (n=8690)	0.81 $p<0.01$ (n=4264)	-0.66 $p<0.01$ (n=4264)	-0.69 $p<0.01$ (n=4426)	0.53 $p<0.01$ (n=4426)	0.52 $p<0.01$ (n=292)	0.18 $p<0.01$ (n=292)

Table S2. Average, standard deviation (std), range (min, max) and number of measurements (n) of the results from hydrographic (temperature – T in °C, salinity – S) and CO₂-related parameters (seawater CO₂ partial pressure – $p\text{CO}_2^{\text{sw}}$ µatm, temperature-normalized $p\text{CO}_2^{\text{sw}}$ – $Np\text{CO}_2^{\text{sw}}$ µatm @ 20.39°C; sea-air CO₂ difference – $\Delta p\text{CO}_2$ µatm; sea-air CO₂ net flux calculated using the Takahashi et al. (2009) coefficient ($\text{FCO}_2^{\text{T09}}$, mmol m⁻² d⁻¹). These results encompass only the region near the Brazilian coast (west of 39.25°W, shallower than 3000 m), at the westernmost part of the occidental basin of the South Atlantic Ocean (Figure S4a).

	Near the Brazilian coast (n = 202)			
	mean	std	min	max
T	25.98	0.12	25.70	26.13
S	35.14	0.02	35.09	35.18
$p\text{CO}_2^{\text{sw}}$	391.18	1.89	388.56	394.43
$p\text{CO}_2^{\text{atm}}$	386.99	1.79	384.10	389.86
$Np\text{CO}_2^{\text{sw}}$	310.6	1.19	307.98	313.04
$\Delta p\text{CO}_2$	4.19	3.40	-0.46	10.33
$\text{FCO}_2^{\text{T09}}$	0.39	0.32	-0.40	0.97

Table S3. The linear correlation coefficients for temperature – T (°C), salinity – S and chlorophyll-*a* – Chl-*a* (mg m⁻³) vs. seawater CO₂ partial pressure – $p\text{CO}_2^{\text{sw}}$ (μatm) and/or temperature-normalized $p\text{CO}_2^{\text{sw}}$ – $Np\text{CO}_2^{\text{sw}}$ (μatm) @ 20.39°C for sampled eddies. The results are presented for each eddy (Vn, n=1 to 6). The number of data points used is referred to as n. The significance level for each correlation is also included.



Eddy	V1	V2	V3	V4	V5	V6
T vs $p\text{CO}_2^{\text{sw}}$	-0.07 <i>p</i> <0.01 (n=601)	0.93 <i>p</i> <0.01 (n=312)	0.98 <i>p</i> <0.01 (n=660)	0.92 <i>p</i> <0.01 (n=302)	0.41 <i>p</i> <0.01 (n=984)	0.61 <i>p</i> <0.01 (n=326)
S vs $p\text{CO}_2^{\text{sw}}$	0.10 <i>p</i> <0.01 (n=601)	0.71 <i>p</i> <0.01 (n=312)	0.97 <i>p</i> <0.01 (n=660)	0.97 <i>p</i> <0.01 (n=302)	0.43 <i>p</i> <0.01 (n=984)	0.53 <i>p</i> <0.01 (n=326)
S vs $Np\text{CO}_2^{\text{sw}}$	-0.35 <i>p</i> <0.01 (n=605)	-0.85 <i>p</i> <0.01 (n=312)	-0.87 <i>p</i> <0.01 (n=660)	-0.75 <i>p</i> <0.01 (n=302)	-0.74 <i>p</i> <0.01 (n=984)	-0.91 <i>p</i> <0.01 (n=326)
Chl-<i>a</i> vs $p\text{CO}_2^{\text{sw}}$	0.05 <i>p</i> <0.01 (n=207)	0.41 <i>p</i> <0.01 (n=312)	0.05 <i>p</i> <0.01 (n=527)	-0.66 <i>p</i> <0.01 (n=12)	0.10 <i>p</i> <0.01 (n=733)	0.30 <i>p</i> <0.01 (n=321)
Chl-<i>a</i> vs $Np\text{CO}_2^{\text{sw}}$	-0.14 <i>p</i> <0.01 (n=207)	-0.17 <i>p</i> <0.01 (n=312)	0.19 <i>p</i> <0.01 (n=527)	0.06 <i>p</i> <0.01 (n=12)	-0.75 <i>p</i> <0.01 (n=733)	0.01 <i>p</i> <0.01 (n=321)

Video S1. Animation map of the South Atlantic Ocean composed from the sea level anomaly (SLA – m) data. The black continuous line corresponds to the SLA contours of 0.01, 0.02, 0.05, 0.1, 0.15, 0.2 and 0.25 m. The Vn (n = 1 to 6) correspond to each eddy sampled in the FORSA cruise trajectory.

**5.2 Second article – PhD 02: The Effect of
Agulhas eddies on absorption and transport of
anthropogenic carbon in the South Atlantic
Ocean**

Article

The Effect of Agulhas Eddies on Absorption and Transport of Anthropogenic Carbon in the South Atlantic Ocean

Iole B. M. Orselli ^{1,2,3,4,*} , Catherine Goyet ^{3,4}, Rodrigo Kerr ^{1,2} , José L. L. de Azevedo ¹ , Moacyr Araujo ^{5,6}, Felipe Galdino ¹, Franck Touratier ^{3,4} and Carlos A. E. Garcia ^{1,7}

- ¹ Laboratório de Estudos dos Oceanos e Clima, Instituto de Oceanografia, Universidade Federal do Rio Grande (FURG), Av. Itália km 8, s/n, Rio Grande, RS 96203-900, Brazil; rodrigokerr@furg.br (R.K.); joseazevedo@furg.br (J.L.L.d.A.); felippe.gs.fg@gmail.com (F.G.); dfsgar@furg.br (C.A.E.G.)
 - ² Brazilian Ocean Acidification Network (BrOA), Av. Itália km 8, Rio Grande, RS 96203-900, Brazil
 - ³ IMAGES_SPACE-DEV, Université de Perpignan Via Domitia (UPVD), 52 ave. Paul Alduy, 66860 Perpignan, France; cgoyet@univ-perp.fr (C.G.); touratier@univ-perp.fr (F.T.)
 - ⁴ ESPACE-DEV UMR UG UA UM IRD, Maison de la télédétection, 500 rue Jean-François Breton, CEDEX 5, 34093 Montpellier, France
 - ⁵ Laboratório de Oceanografia Física, Estuarina e Costeira (LOFEC), Departamento de Oceanografia, Centro de Tecnologia, Universidade Federal de Pernambuco (UFPE), Av. Arquitetura, s/n, Recife, PE 50740550, Brazil; moa.ufpe@gmail.com
 - ⁶ Brazilian Research Network on Global Climate Change (Rede CLIMA), São José dos Campos, SP 2227-010, Brazil
 - ⁷ Programa de Pós-graduação em Oceanografia, Universidade Federal de Santa Catarina (UFSC), Campus Reitor João David Ferreira Lima, s/n, Florianópolis, SC 8040-900, Brazil
- * Correspondence: iole.orselli@furg.br or iole.orselli@gmail.com

Received: 17 May 2019; Accepted: 11 June 2019; Published: 18 June 2019



Abstract: The South Atlantic Ocean is currently undergoing significant alterations due to climate change. This region is important to the global carbon cycle, but marine carbon data are scarce in this basin. Additionally, this region is influenced by Agulhas eddies. However, their effects on ocean biogeochemistry are not yet fully understood. Thus, we aimed to model the carbonate parameters in this region and investigate the anthropogenic carbon (C_{ant}) content in 13 eddies shed by the Agulhas retroflection. We used in situ data from the CLIVAR/WOCE/A10 section to elaborate total dissolved inorganic carbon (C_T) and total alkalinity (A_T) models and reconstruct those parameters using in situ data from two other Brazilian initiatives. Furthermore, we applied the Tracer combining Oxygen, inorganic Carbon, and total Alkalinity (TrOCA) method to calculate the C_{ant} , focusing on the 13 identified Agulhas eddies. The C_T and A_T models presented root mean square errors less than 1.66 and 2.19 $\mu\text{mol kg}^{-1}$, indicating Global Ocean Acidification Observing Network climate precision. The C_{ant} content in the Agulhas eddies was 23% higher than that at the same depths of the surrounding waters. We observed that Agulhas eddies can play a role in the faster acidification of the South Atlantic Central Water.

Keywords: carbonate system; anthropogenic carbon; Agulhas eddies; South Atlantic Ocean

1. Introduction

Different oceans respond to climate changes in varying ways, but the South Atlantic Ocean is currently facing significant alterations, such as increasing seawater temperature, salinity, and heat content [1]. These local or regional climate changes lead to perturbations and alter the hydrological cycle, surface ocean currents, coastal hydrodynamics, and marine carbonate system, which drive

transformations in sensitive ecosystems and marine organisms [1]. Apart from playing an important role in the global carbon cycle, marine carbon data on the South Atlantic Ocean are notably scarce compared with those on the North Atlantic Ocean e.g., [2]. The South Atlantic Ocean is responsible for the permanent uptake of a great amount of carbon dioxide (CO₂) released into the atmosphere by human activity e.g., [3–6], which is further transferred along other ocean basins through thermohaline circulation. Additionally, Gruber et al. [7] recently demonstrated that the South Atlantic Ocean is undergoing an anomalous increase in anthropogenic carbon (C_{ant}) inventory.

Uptake of C_{ant} by the oceans is primarily governed by physical processes [8], although physical, chemical, and biological pumps could act to remove CO₂ from the atmosphere. In addition, the formation of water masses and the consequent ocean ventilation have important roles in convection of the C_{ant} stored in the upper waters towards the inner ocean. Thus, the CO₂ absorbed at the surface layers is transferred throughout the water column e.g., [9]. Mode and intermediate waters are formed by subduction, which is the primary mechanism for CO₂ intrusion in the central and intermediate ocean layers e.g., [9–11], and the same is true for the deep and bottom layers. When the deep convection process occurs, the water masses sink, carrying CO₂ and its dissociation products to the deeper layers [12,13]. The water mass formation processes favor oxygenation and consequent ventilation of the water column, including the central, intermediate, deep, and bottom layers. The conservative properties acquired by water masses during its formation time are preserved and only changed by internal mixing processes, whereas the nonconservative properties are slightly modified by biogeochemical processes e.g., [14–16].

The water column of the South Atlantic Ocean is composed of four vertical layers: surface to pycnocline, intermediate, deep, and abyssal waters [16]. The water masses present in the entire water column of the South Atlantic Ocean are briefly introduced below. The surface layer is different on each side of the South Atlantic Ocean and is composed of relatively cold water in the Eastern boundary side, which flows from the pole to the equator and is sourced by the upwelling system in the East, whereas the warm and salty Tropical Water (TW) flows poleward in the West through the Western boundary current e.g., [16,17]. The central and intermediate layers are composed of the South Atlantic Central Water (SACW) and Antarctic Intermediate Water (AAIW) e.g., [16,18,19]. The surface, central, and intermediate waters of the South Atlantic Ocean can be influenced by waters sourced in the Indian Ocean [20], which enter the Atlantic basin through the southernmost region of the African continent and are carried by the Agulhas eddies and filaments e.g., [16,21,22]. The Upper Circumpolar Deep Water (uCDW) is the deepest water mass that can be described in the upper ocean, placed below the Antarctic Intermediate Water [23]. The North Atlantic Deep Water (NADW) and the Antarctic Bottom Water (AABW) are observed in the deep and bottom layers of both sides of the South Atlantic Ocean e.g., [14,16], although in different proportions in the Brazil and Angola abyssal basins [24].

The Agulhas eddies are anticyclonic structures, meaning that their rotation in the Southern Hemisphere is counterclockwise, have high pressure centers, and displace isopycnals downward [25]. Considered the largest mesoscale structures of the world's oceans, the Agulhas eddies are approximately 300 km in size and 2 km deep (up to 4 km deep) and have lifetimes of 2–3 years e.g., [26]. Certain studies suggested that these structures influence Atlantic Meridional Overturning Circulation due to their size and the large amounts of heat and salt that they transport (0.5–1.5 Sv; 1 Sv \equiv 10⁶ m³ s⁻¹). This transport of surface to intermediate waters from the Indian Ocean to the South Atlantic Ocean could be crucial to the Atlantic Meridional Overturning Circulation by maintaining the deep convection process that produces the NADW e.g., [21,27–30]. Biastoch et al. [29] reported an abrupt intensification of the Atlantic thermohaline circulation, which was caused in part by the expansion of mass transport in the Agulhas leakage due to eddies and filaments [26,28]. The leakage in the Agulhas Current retroflexion region has increased due to the southward displacement of the zero line of the wind stress curl and the intensification of the Southern Hemisphere westerlies, which is caused by anthropogenic forcing on the global warming. This process results in oceanic warming and the salinification of the South Atlantic Ocean basin e.g., [29,31].

In addition, a recent study by Souza et al. [20] observed that contribution from Indian Ocean mode waters can considerably influence the properties of the SACW in the South Atlantic Ocean basin, which is reinforced by the increase in the number of eddies released in the Agulhas retroflection region [29]. The Agulhas eddies transport mode waters, which are marked by the following characteristics: thermohaline and halohaline layers (i.e., stable ranges of temperature and salinity, respectively) and low potential vorticity. The mode waters are primarily formed during the winter after intense mixing in the surface layers and dive between the seasonal and permanent thermoclines. These are source waters that are further advected and compose the central waters of the oceans (e.g., the SACW is composed of different varieties of Subtropical Mode Water, formed in both the Atlantic and Indian oceans) [20,32]. It is well known that mode water formation is intensified when the heat flux increases e.g., [18]. Therefore, because the Agulhas eddies are able to intensify the heat flux [33], these mesoscale structures can also strengthen the formation processes of the mode waters. Three varieties of South Atlantic Mode Water (marked by distinct ranges of temperatures, depending on the source area considered) compose the layer of the SACW. The SACW layer is also influenced by contributions from the Indian Ocean Mode Water [20].

Recent studies noted that the central waters represented by the SACW in the South Atlantic Ocean are among the most affected by C_{ant} penetration, leading to an acidification rate (i.e., change in seawater pH) of -0.0016 yr^{-1} and up to -0.0018 yr^{-1} for SACW since the preindustrial period [3–5]. These trends are higher than those already observed for the ocean layers immediately above and below the SACW, e.g., -0.0013 yr^{-1} for surface waters and -0.0010 yr^{-1} at the intermediate layer, for AAIW. As expected, the pH changes observed in the South Atlantic Ocean for the deep and bottom layers are smaller than all other layers, namely, $-0.0010/-0.0000 \text{ yr}^{-1}$ for the upper and lower varieties of CDW, $-0.0005/-0.0000 \text{ yr}^{-1}$ for upper and lower varieties of NADW, and -0.0000 yr^{-1} for AABW e.g., [3,5,6]. Additionally, Orselli et al. [34] observed that the Agulhas eddies are capable of removing more CO_2 from the atmosphere than their surrounding waters. This intensification of CO_2 absorption at the sea surface is governed mainly by physical processes when the eddy is located in the Eastern basin of the South Atlantic Ocean. However, biological processes also influence the CO_2 uptake when these structures move to the Western basin [34].

Motivated by the facts that the Agulhas eddies carry surface to intermediate waters from the Indian Ocean to the South Atlantic Ocean [21,22], and because these structures are prone to absorb more CO_2 than the surrounding waters [34], we investigate their role in ocean biogeochemistry, which is still a matter of interest e.g., [35,36]. Thus, we propose: (i) to model the marine carbonate parameters in the South Atlantic Ocean, (ii) to quantify the C_{ant} content in the 13 identified Agulhas eddies, and (iii) to investigate the impact of the Agulhas eddies on the ocean acidification state. The results of this study are expected to further contribute to the scientific discussion of the impact of the Agulhas eddies on changes in the marine carbonate system.

2. Data and Methods

2.1. Cruises Surveys

The Trans-Atlantic II and Following Ocean Rings in the South Atlantic (FORSA) cruises were conducted by the Brazilian High Latitude Oceanography Group (GOAL) [37] in close cooperation with scientists from different research institutions in Brazil (Figure 1). The Trans-Atlantic II (TAII) cruise that occurred in 2011 on board the Brazilian Navy RV NHO Cruzeiro do Sul is a component of the project, “Measurements and modeling of CO_2 fluxes in the South Atlantic and Southern Oceans”. The first leg (TAII_01) was conducted from October 24th to November 25th along 35°S (from Rio Grande, Brazil, to Cape Town, South Africa) [38], and the second leg (TAII_02) was conducted from December 2nd to December 22nd in a Southwestern–Northeastern section (from Cape Town, South Africa, to Rio de Janeiro, Brazil). The FORSA cruise occurred in 2015 on board the Brazilian Navy RV, NPqHo Vital de Oliveira from June 27th to July 15th in a Southwestern–Northeastern section (from Cape

Town, to South Africa to Arraijal do Cabo, to Brazil) [34,39]. Along these cruise tracks, hydrographic conductivity-temperature-depth (CTD) stations were sampled: 93 in 2011 during the TAII and 12 in 2015 during the FORSA cruise. In addition to physical data, discrete seawater samples were collected for chemical and biological analyses, which included dissolved oxygen (DO), phytoplankton pigments, and dissolved inorganic nutrients, using a combined Sea-Bird CTD/Carrousel 911+system[®] equipped with 12 five liter and 24 twelve liter Niskin bottles for the TAII and FORSA cruises, respectively. We conducted continuous measurements when crossing six Agulhas eddies during the FORSA cruise [34], but in this work, we present the results from three of them, i.e., those in which CTD stations were performed throughout the water column. The TAII and FORSA datasets are available by request.

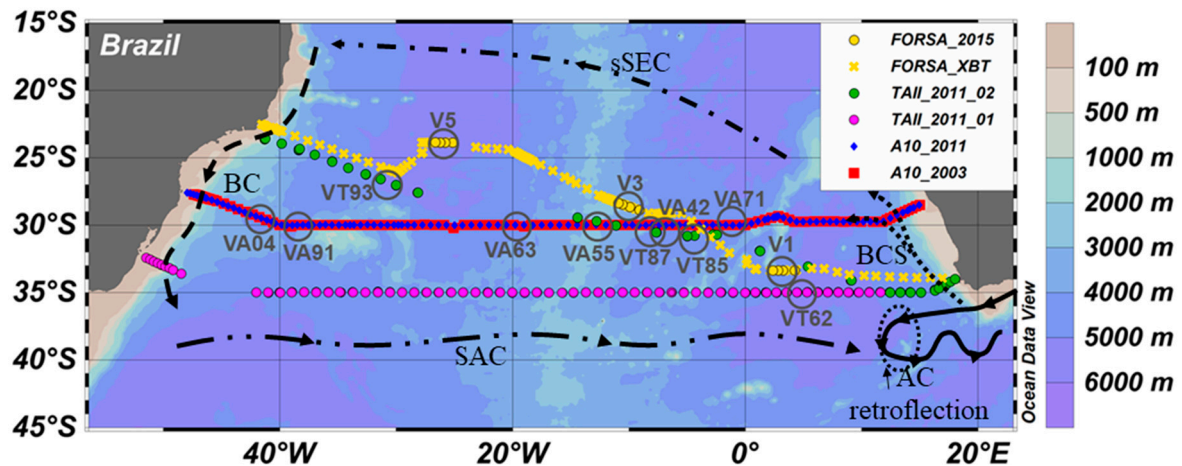


Figure 1. Map of the sampled region in the South Atlantic Ocean. The yellow crosses correspond to the expendable bathythermograph (XBT) profiles performed during the Following Ocean Rings in the South Atlantic (FORSA) cruise (FORSA_XBT). The conductivity-temperature-depth (CTD) stations are indicated by yellow dots (FORSA_2015), green dots (Trans-Atlantic II (TAII)_2011_02), purple dots (TAII_2011_01), blue diamonds (A10_2011), and red squares (A10_2003). The gray circles indicate the approximate positions at which the eddies were sampled: V1, V3, and V5 (FORSA_2015); VT62 (TAII_2011_01); VT85, VT87, and VT93 (TAII_2011_02); VA42, VA63, and VA91 (A10_2011); and VA04, VA55, and VA71 (A10_2003). The black lines represent the main currents of the surface circulation, which are the Benguela Current System (BCS, dotted line), southern branch of the South Equatorial Current (sSEC, dot-dashed line), Brazil Current (BC, dashed line) and South Atlantic Current (SAC, dot-dot dashed line). The Agulhas Current (AC, continuous line) and Agulhas Current retroflection zone (black dotted ellipse) are also indicated. The bottom bathymetry is represented by color shadings.

The CLIVAR/WOCE Repeat Hydrography Section A10 occurred along 30°S (Figure 1). In 2003 (A10_2003), the cruise was conducted under the responsibility of JAMSTEC through the project Blue Earth Global Expedition 2003. The A10_2003 was conducted on board the RV Mirai from November 6th to December 5th (from Santos, Brazil to Cape Town, South Africa) [40]. In 2011 (A10_2011), the cruise was funded by NOAA-OGP and NSF-OCE through the U.S. CLIVAR/CO₂/hydrography/tracer program. The A10_2011 cruise was conducted on board the RV Ronald H. Brown from September 26th to October 31st (from Cape Town, South Africa to Rio de Janeiro, Brazil) [41]. Along the A10 cruises, 110 stations were sampled in 2003 and 120 in 2011. Physical data and discrete seawater samples were collected for chemical analysis. Using a combined Sea-Bird CTD/Carrousel 911+system[®] equipped with 35 twelve liter and 24 ten/eleven liter Niskin bottles, in the A10_2003 and A10_2011 cruises, the following properties were determined: salinity, DO, dissolved inorganic nutrients, and carbonate system (total dissolved inorganic carbon—C_T; total alkalinity—A_T; pH). The A10 datasets analyzed during the current study are available from the NODC/NOAA data center (https://www.nodc.noaa.gov/ocads/oceans/RepeatSections/clivar_a10.html).

2.2. Identification of the Agulhas Eddies

During the FORSA cruise, eddy identification was conducted by analyzing the daily Sea Level Anomaly (SLA) data in conjunction with the temperature profiles obtained by high-resolution spatially distributed XBT deployments. Once the eddies were found, water sampling was performed inside and outside of them (see Carvalho et al. [39] for details). The FORSA cruise was the only one previously planned to sample the Agulhas eddies, and, therefore, we needed to identify the eddies sampled in all of the other cruises, as well as their positions. Therefore, we used the mesoscale eddy AVISO product (downloaded from <https://www.aviso.altimetry.fr/en/data/products/value-added-products/global-mesoscale-eddy-trajectory-product.html>, last data from January 6th, 2017) [42,43]. Eddy identification in the TAI and A10 cruises was performed by looking for the CTD station positions in the SLA field of the day, in which the station was performed. In cases of an anticyclonic eddy (positive SLA) matching the station position, the back trajectory was investigated to determine whether it could be considered an Agulhas eddy or not. In positive cases, the life history of the eddy was used to determine its mean radius (km) and lifetime (days, d), as well as the sampled day's radius and age (Table 1), according to the AVISO product, as performed by Orselli et al. [34]. The track of each cruise and the position of the identified eddies in the South Atlantic Ocean are presented in Figure 1.

Table 1. Radius (km) and lifetime (d) of each eddy investigated on this study in the in situ sampling day and life history. Superscript T or E indicates whether the eddy can be considered a true or evolved eddy according to the classification of Orselli et al. [34]. * indicates that the eddy lifetime accounting was completed together with the data availability in the AVISO product until analysis. # indicates that the eddy was formed during the splitting of a 925 day old Agulhas eddy.

Cruise Year (Season)	Eddy	Sampled Day		Life History Mean	
		Radius [km]	Age [d]	Radius [km]	Lifetime [d]
FORSA 2015 (winter)	V1 ^T	82.44	244	94.23	798*
	V3 ^T	94.30	440	96.43	949
	V5 ^E	101.86	1052	98.86	1222
TAII 2011 (early spring)	VT62 ^T	123.82	354	106.00	367
	VT85 ^T	92.09	263	87.40	767
	VT87 ^T	95.58	245	97.47	854
	VT93 ^E	122.06	1177	101.39	1251
A10 2011 (early spring)	VA42 ^T	83.72	181	97.47	854
	VA63 ^E	114.92	600	111.35	714
	VA91 ^E	136.64	125 #	105.34	211 #
A10 2003 (late spring)	VA04 ^E	130.55	1177	111.11	1223
	VA55 ^T	85.43	494	93.70	782
	VA71 ^T	92.44	308	96.65	874

2.3. Carbonate System Sampling and Analysis

2.3.1. A10_2003 Cruise

The seawater samples for C_T were collected into 300 mL borosilicate glass bottles, which were fixed with 100 μ L of a saturated mercuric chloride solution [44]. Analysis was performed with two C_T measurement systems (systems A and B; Nippon ANS, Inc.) composed of a CO_2 extraction system and a coulometer (Model 5012, UIC Inc.), following Johnson et al. [45]. The systems were calibrated using Na_2CO_3 solutions (nominally 500, 1000 1500, 2000, and 2500 μ mol L^{-1}) [46] and analysis of certified reference material (CRM, batch 60, provided by Prof. A. G. Dickson of Scripps Institution of

Oceanography). The standard deviations of CRM- C_T for systems A and B were 1.1 and 0.9 $\mu\text{mol kg}^{-1}$ ($n = 35$; $n = 28$), respectively. For A_T , the samples were collected into 130 mL borosilicate glass bottles. Analyses were conducted with a Metrohm autoburette and a Thermo Orion pH meter, which were automatically controlled. The system was calibrated using 5 solutions of Na_2CO_3 in 0.7 M NaCl solutions (nominally 0, 100, 1000, 2000, and 2500 $\mu\text{mol kg}^{-1}$), as well as analysis of CRM (batch 60). The standard deviation of CRM- A_T for the system was 1.7 $\mu\text{mol kg}^{-1}$ ($n = 162$). The cruise report supplies detailed information on these systems and analysis processes [40].

2.3.2. A10_2011 Cruise

The seawater samples for C_T were collected into precombusted 300 mL Pyrex bottles, which were fixed with 0.122 mL of a 50% saturated mercuric chloride solution. Analysis was conducted with two C_T measurement systems (PMEL-1 and PMEL-2) composed of a coulometer (UIC Inc.) and a SOMMA (Single Operator Multiparameter Metabolic Analyser) inlet system, following Johnson et al. [47,48] and Johnson [49]. The systems were calibrated using pure CO_2 (99.995%) and secondary standards, as well as the analysis of CRM (batch 98). The C_T error was not included in the cruise report. For A_T , the samples were collected into 500 mL borosilicate glass bottles. Analysis were performed with a Metrohm 665 Dosimat titrator and an Orion 720A pH meter. The system was calibrated using CRM (batches 96 and 112). The reported error for A_T was 0.3 $\mu\text{mol kg}^{-1}$. The cruise report supplies detailed information on the systems and analysis processes [41].

2.4. Polynomial Model Development for Carbonate System Parameters

To gather the carbonate system data along all of the cruise sections investigated in this work, polynomial models for C_T and A_T parameters were developed using the two A10 sections in which accurate biogeochemical data were available with good precision [40,41]. We chose to use only potential temperature (θ), salinity, and apparent oxygen utilization (AOU) to develop the models, allowing us to apply the models with the greatest number of data as possible, because this approach facilitated the reconstruction of C_T and A_T in all stations and depths where thermohaline properties were available.

The models were developed through polynomial equations introduced in this work and have the following form (Equation (1)):

$$f(x, y) = \sum_{i=0}^{5,5-i} \sum_{j=0} p_{ij} x^i y^j \quad (1)$$

where f represents the C_T or A_T functions ($\mu\text{mol kg}^{-1}$), x is the potential temperature ($\theta^\circ\text{C}$) for both C_T and A_T equations, y is the apparent oxygen utilization (AOU $\mu\text{mol kg}^{-1}$) for the C_T equation, and the salinity for the A_T equation, x and y are standardized by the mean and standard deviations, and P_{ij} are the coefficients determined in this model (presented in Table 2). Specifically, i and j are the indices that indicate the exponent of the parameters corresponding to x and y in Equation (1). These polynomial models were subsequently applied to the dataset of the hydrographic sections of the TAIL and FORSA cruises.

We tested different types of models to find the one that best represented the biogeochemical data and produced the smallest associated errors. These tests were also performed with the multilinear regression models, because they are commonly applied to carbonate system data reconstruction. In our study, we ultimately chose nonlinear regression, because the best fit to the A10 data was obtained with the polynomial models introduced in this work (Equation (1), Table 2). These models were developed using the curve fitting tool toolbox of MATLAB[®], with the least absolute residual mode. This option considered all data as important, minimized the residuals, and can be used when the data series have few nonconfinable values [50].

Table 2. The p_{ij} coefficients (with 95% confidence bounds) of the polynomial models developed for C_T and A_T , according to Equation (1).

P_{ij}	C_T 2003	C_T 2011	A_T 2003	A_T 2011
p_{50}	5.58 (3.15, 8.00)	−0.75 (−2.90, 1.41)	23 (14.29, 31.72)	36.68 (29.17, 44.20)
p_{41}	20.60 (13.05, 28.15)	6.95 (0.15, 13.74)	−29.40 (−57.37, −1.43)	−96.18 (−120.20, −72.13)
p_{40}	0.45 (−2.98, 3.88)	6.93 (4.43, 9.43)	−7.85 (−20.30, 4.59)	30.47 (25.75, 35.19)
p_{32}	24.07 (15.41, 32.73)	11.43 (3.72, 19.14)	6.55 (−37.11, 50.21)	125.40 (89.63, 161.20)
p_{31}	−20.33 (−28.73, −11.93)	−6.88 (−14.14, 0.39)	−18.53 (−46.38, 9.33)	−73.75 (−86.35, −61.15)
p_{30}	−13.24 (−16.48, −9.99)	−3.11 (−5.78, −0.44)	−79 (−91.45, −66.56)	−62.81 (−73.50, −52.12)
p_{23}	15.78 (11.40, 20.15)	5.72 (1.32, 10.12)	4.30 (−32.74, 41.33)	−94.36 (−126.30, −62.47)
p_{22}	−24.29 (−32.38, −16.21)	−9.21 (−18.36, −0.063)	34.17 (9.75, 58.59)	44.70 (28.38, 61.01)
p_{21}	1.77 (−5.61, 9.16)	9.98 (3.77, 16.19)	93.98 (70.24, 117.70)	51.81 (28.92, 74.70)
p_{20}	12.64 (9.98, 15.30)	0.72 (−1.50, 2.95)	24.31 (13.12, 35.50)	−17.50 (−23.39, −11.62)
p_{14}	5.95 (4.07, 7.83)	1.48 (−0.75, 3.71)	−1.88 (−17.55, 13.81)	37.95 (22.51, 53.39)
p_{13}	−16.16 (−22.09, −10.24)	−2.89 (−9.13, 3.35)	−17.88 (−29.89, −5.87)	−5.77 (−17.95, 6.41)
p_{12}	6.77 (0.13, 13.41)	0.86 (−4.41, 6.13)	−27.04 (−45.30, −8.77)	5.61 (−13.96, 25.18)
p_{11}	1.35 (−2.96, 5.66)	−1.45 (−5.82, 2.93)	48.87 (36.32, 61.43)	88.42 (80.30, 96.55)
p_{10}	−25.28 (−26.49, −24.06)	−18.90 (−19.92, −17.88)	15.52 (11.26, 19.77)	15.70 (12.27, 19.14)
p_{05}	0.77 (0.09, 1.44)	−0.01 (−0.58, 0.55)	0.10 (−2.50, 2.71)	−6.18 (−9.16, −3.19)
p_{04}	−4.93 (−7.30, −2.57)	−0.83 (−2.67, 1.00)	3.53 (0.72, 6.34)	−1.66 (−5.20, 1.89)
p_{03}	5.13 (2.26, 8.00)	0.31 (−1.56, 2.18)	1.77 (−4.01, 7.54)	−5.85 (−12.48, 0.78)
p_{02}	1.38 (−1.43, 4.18)	4.13 (1.50, 6.78)	−35.18 (−41.12, −29.24)	−42.50 (−47.48, −37.52)
p_{01}	27.71 (26.21, 29.22)	25.69 (24.39, 26.99)	−18.71 (−23.04, −14.38)	−4.31 (−8.04, −0.58)
p_{00}	2158 (2158, 2158)	2156 (2156, 2156)	2303 (2300, 2306)	2309 (2308, 2311)

2.5. Anthropogenic Carbon Estimate

Considering that CO₂ can be continuously exchanged across the ocean–atmosphere interface and absorbed/produced by biological activity in the ocean photic layer (i.e., the carbon reservoirs are not in equilibrium), it is believed that the carbon permanently taken up by the ocean is below the surface mixed layer, where it can be split into natural and anthropogenic origin. Thus, the lower limit of the surface mixed layer is the upper ocean boundary, which is used to define the region in which the C_{ant} content can be estimated [51]. Therefore, in this work, we considered quantifying the C_{ant} below 200 m depth, excluding the surface mixed layer data e.g., [52].

We applied the Tracer combining Oxygen, inorganic Carbon, and total Alkalinity (TrOCA) method to estimate the C_{ant} (C_{ant-TrOCA}) [52–54]. In our calculations, we used the C_T and A_T obtained either from in situ measurements or the model results for all South Atlantic Ocean sections. In addition, we decided to fix the C_{ant} content estimated in the 2003 cruise as a reference to calculate the C_{ant} content difference between the cruise years ($\Delta C_{\text{ant-TrOCA } 2011-2003}$). Additionally, using the C_T model developed for the A10 cruises and applied in all the cruise sections, the C_T content difference between years was determined ($\Delta C_{\text{T } 2011-2003}$). Considering the year of the cruise, we used the 2011 coefficients to apply for the TAII–2011 cruise data to evaluate the snapshot period of this sampling moment. For the FORSA–2015 cruise, we assumed a linear change between 2003 and 2011 and we added half of this C_T difference to derive the C_T increase between 2011 and 2015. In this way, we evaluated the C_{ant} content for the entire industrial period (C_{ant-TrOCA}) and compared the C_{ant} and C_T differences between 2011 and 2003 (2015 and 2003, for the FORSA cruise section).

3. Results

3.1. Physical Structure and Hydrographic Properties along the Cruise Tracks

The differences of the salinity and temperature distribution among the sections are presented in the vertical profiles and θ/S -longitude diagrams (Figures 2 and 3), and the thermohaline properties of the water masses are included in Table 3. Close to the Brazilian coast, the Subtropical Shelf Water (STSW) is observed in the surface of the TAII_01, TAII_02, and A10_2011 cruise sections. TW is observed in the surface in the Western side of all sections. The South Atlantic Subtropical Surface Water (SASTSW) [38,55], which is fresher and colder than the TW, was observed along the TAII_01 section and in the Eastern side of the other sections. The difference in temperature between the Eastern and Western basins for both the FORSA and TAII_02 cruises was stronger than the others because of the Southeast–Northwest direction of the sections (Figures 2 and 3). The SACW and AAIW were identified in the central and intermediate layers, respectively, in all sections. The former is marked by a wide range of temperature and salinity, and the latter has a narrow variation of these parameters, because it is also fresher and colder. We were not able to observe the uCDW in the cruise sections, although previous studies have found it [23]. The NADW, which presented saltier and colder characteristics compared to AAIW, was identified immediately below the AAIW e.g., [24].

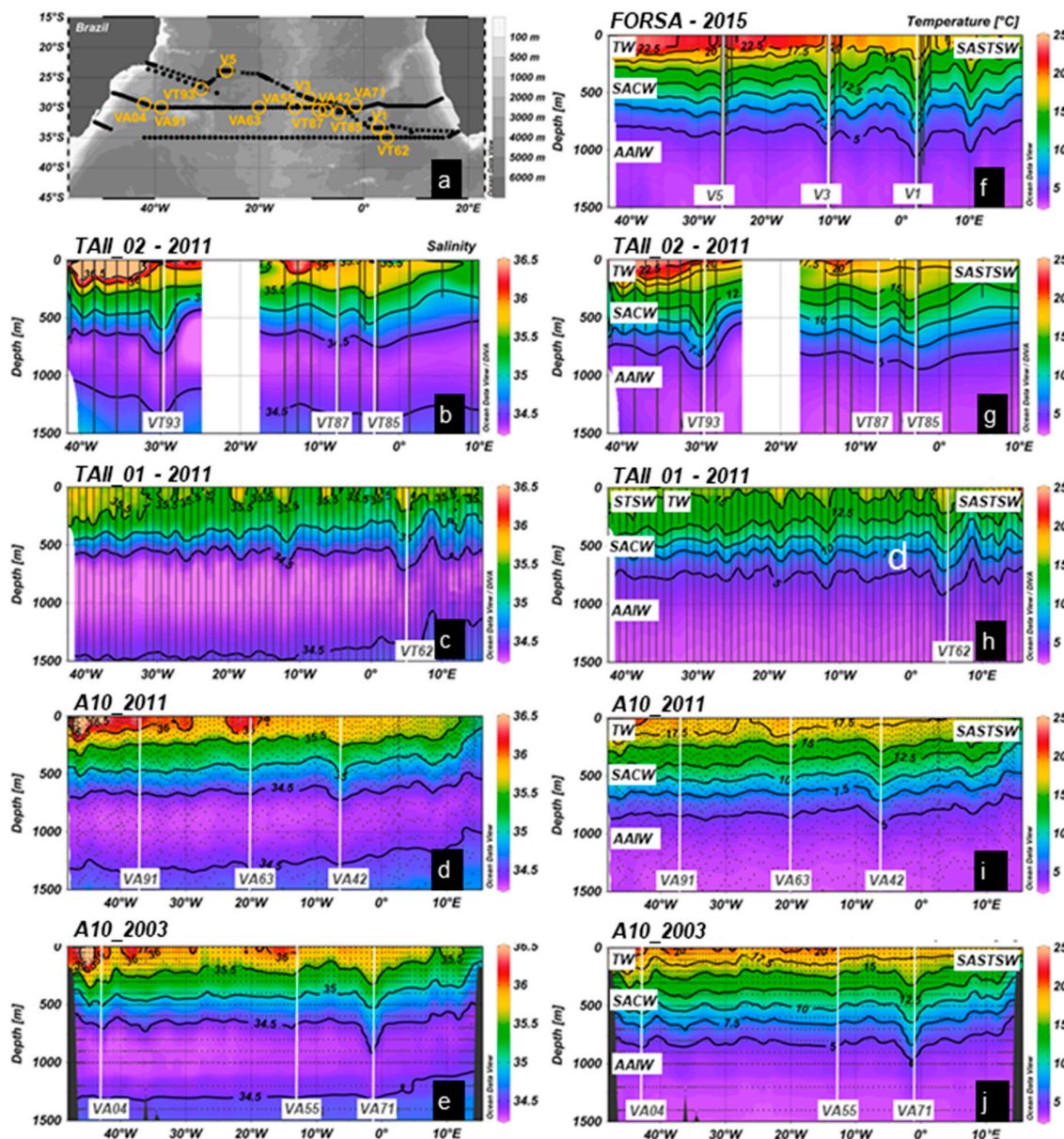


Figure 2. Map of the cruise sections and sampled eddies (a). For a complete description of this map, please see Figure 1. Left panels show the salinity profiles (b–e), while right panels show potential temperature (°C; f–j) profiles. The hydrographic sections are TAIL_02–2011 (b,g), TAIL_01–2011 (c,h), A10_2011 (d,i) and A10_2003 (e,j). The continuous gray lines or gray dots indicate the position of the CTD stations (at each 1 m for the TAIL and FORSA cruises). Temperatures from the XBT of the FORSA–2015 cruise section and CTD stations are indicated by continuous gray lines (f). The sampled eddies are indicated in the hydrographic sections of all cruises by vertical white lines. The water mass positions in the water column are indicated by their acronyms in panels f to j, referring to: Subtropical Shelf Water (STSW), Tropical Water (TW), South Atlantic Subtropical Surface Water (SASTSW), South Atlantic Central Water (SACW), and Antarctic Intermediate Water (AAIW). For details, please see the θ/S diagrams (Figure 3) and the water masses properties (Table 3).

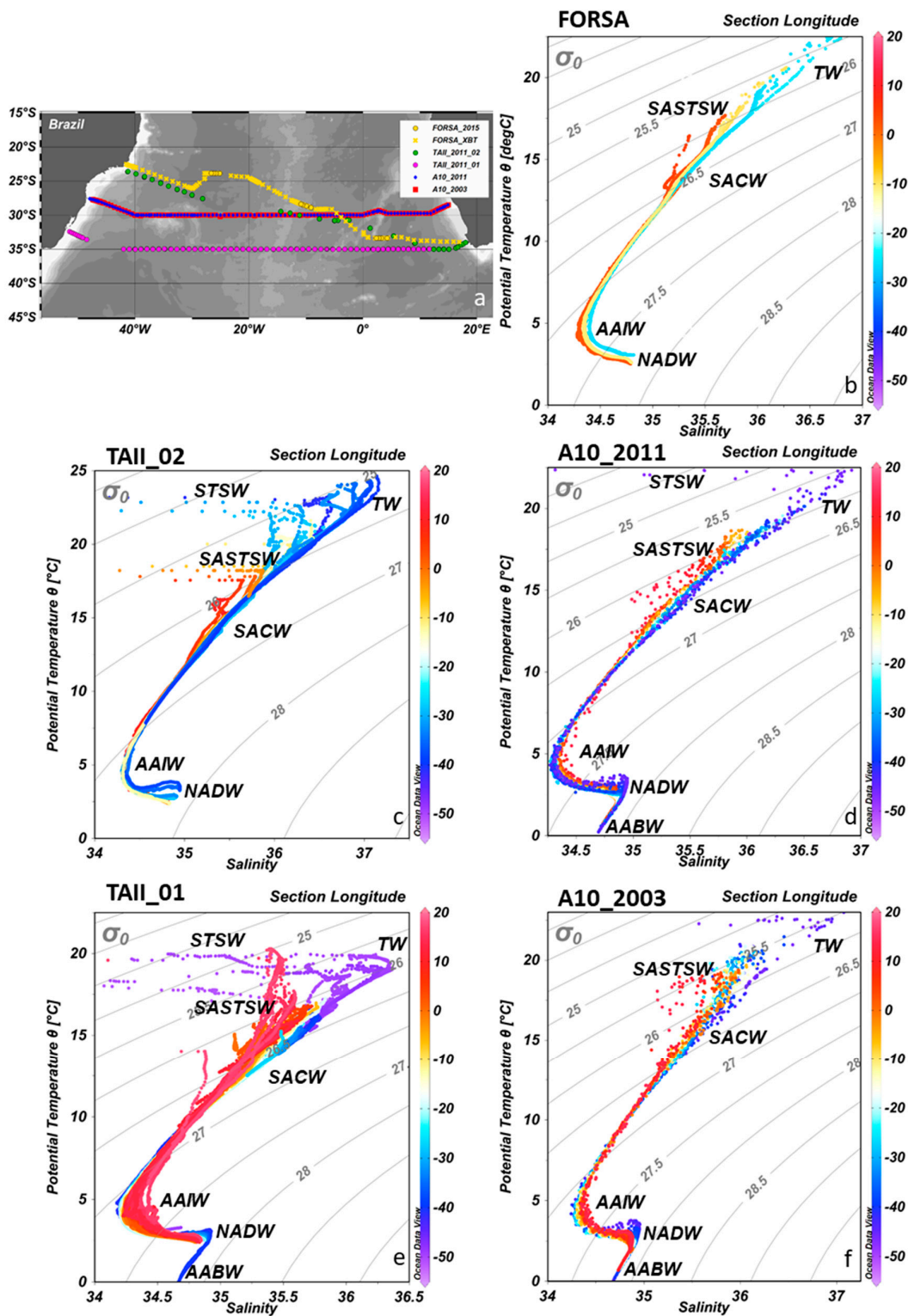


Figure 3. Map of the cruise sections (a). For a complete description of this map, please see Figure 1. θ /S-longitude diagrams for each section (b–f). θ /S-longitude of the FORSA–2015 cruise section (b), TAI_02–2011 section (c), A10_2011 section (d), TAI_01–2011 section (e), and A10_2003 section (f). The continuous gray lines represent the isopycnals. The water masses are indicated by their acronyms, referring to: Subtropical Shelf Water (STSW), Tropical Water (TW), South Atlantic Subtropical Surface Water (SASTSW), South Atlantic Central Water (SACW), Antarctic Intermediate Water (AAIW), North Atlantic Deep Water (NADW), and Antarctic Bottom Water (AABW). For details please see the water masses properties (Table 3).

Table 3. Thermohaline ranges used to characterize the water masses observed in this study, including their positions in the water column layer and references.

Water Column Layer	Water Mass	θ ($^{\circ}\text{C}$)	Salinity	Reference
Surface	Subtropical Shelf Water (STSW)	$\theta > 14$	$33.5 < S < 35.3$	[56]
		$\theta > 18.5$	$35.3 \leq S < 36$	
	Tropical Water (TW)	$\theta \geq 18.5$	$S \geq 36$	[56]
	South Atlantic Subtropical Surface Water (SASTSW)	$\theta > 16$	$35.3 \leq S < 35.7$	[38,55]
Central	South Atlantic Central Water (SACW)	$\theta < 18.5$	$34.3 < S$	[17]
Intermediate	Antarctic Intermediate Water (AAIW)	$2 < \theta < 6$	$33.8 < S < 34.8$	[17]
Deep	North Atlantic Deep Water (NADW)	$1.5 < \theta < 4$	$34.8 < S < 35$	[17]
Bottom	Antarctic Bottom Water (AABW)	$-0.9 < \theta < 1.7$	$34.64 < S < 34.72$	[17]

3.2. Polynomial Models for Carbonate System Parameters

The polynomial models introduced in this work (Equation (1), Table 2), have the smallest standard deviations from the in situ data and the best precision for both C_T and A_T data (Figures 4 and 5). The C_T models presented root mean square error (RMSE) values of $1.66 \mu\text{mol kg}^{-1}$ ($r^2 = 0.997$, $n = 1081$, $p < 0.05$) and $1.39 \mu\text{mol kg}^{-1}$ ($r^2 = 0.997$, $n = 1445$, $p < 0.05$), whereas A_T presented RMSE values of $2.19 \mu\text{mol kg}^{-1}$ ($r^2 = 0.983$, $n = 1081$, $p < 0.05$) and $1.45 \mu\text{mol kg}^{-1}$ ($r^2 = 0.984$, $n = 1445$, $p < 0.05$), for 2003 and 2011, respectively (Figures 4 and 5). The low RMSE values demonstrated that the developed models were able to correctly represent the C_T and A_T parameters throughout the entire water column. The errors reported are within the values determined by the Global Ocean Acidification Observing Network (GOA-ON) as climate precision (i.e., estimated within an uncertainty of approximately $2 \mu\text{mol kg}^{-1}$ in measurements of C_T and A_T) [57]. Some differences between the measured and modeled data were found at the sea surface due to the influence of abiotic processes and gas transfer at the sea-air interface (uptake/release), as well as water masses mixing with different CO_2 sources e.g., [52,58]. However, the data above the surface mixed layer were not used. These models were developed in the region of the South Atlantic gyre. Thus, they can be used for C_T and A_T reconstruction in the South Atlantic Ocean when considering the follow ranges of input data: $0 < T$ ($^{\circ}\text{C}$) < 25 ; $33.5 < S < 37.5$; $92 < \text{DO}$ ($\mu\text{mol kg}^{-1}$) < 265 .

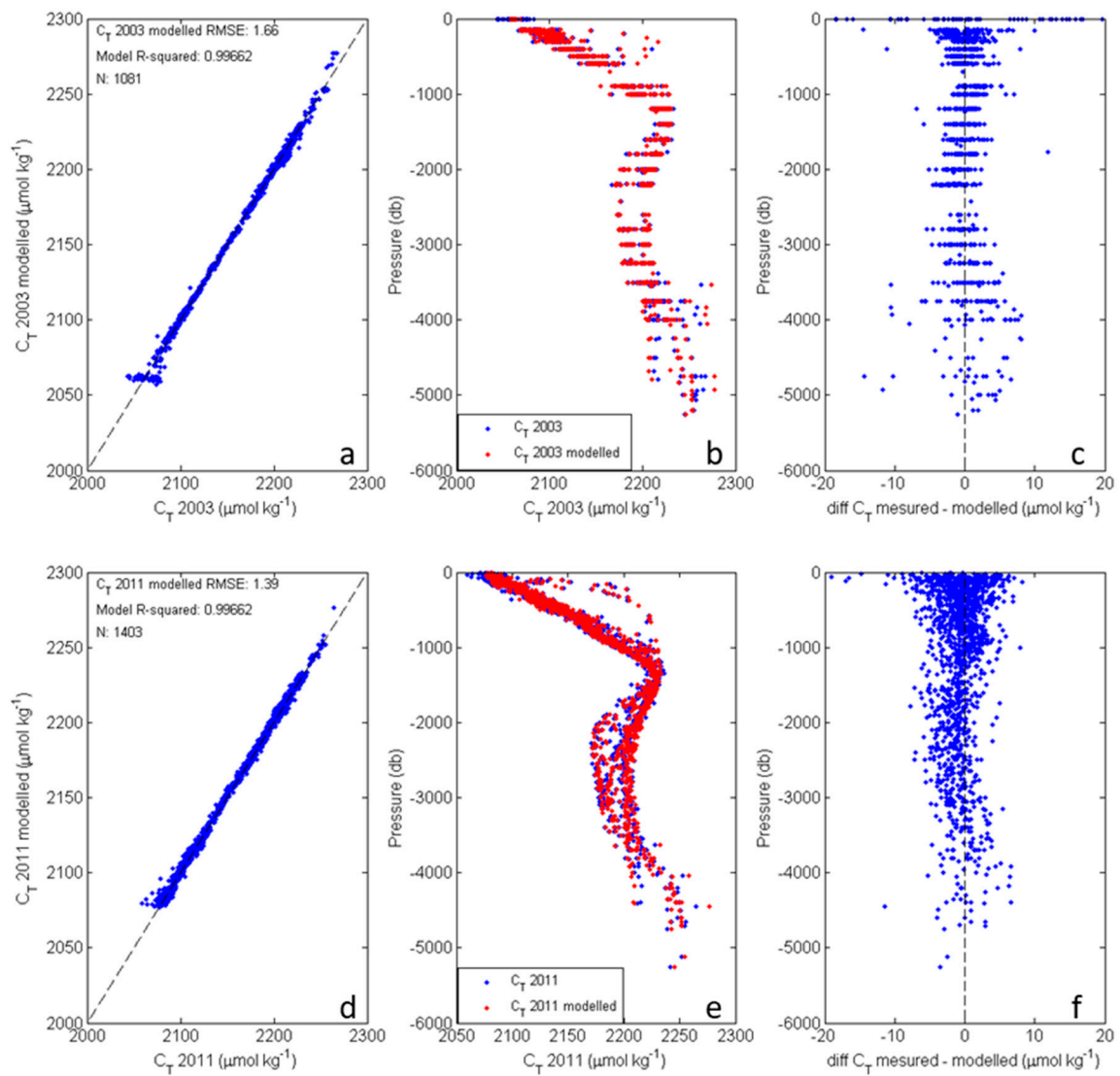


Figure 4. C_T model results considering the A10 section of 2003 (a–c) and 2011 (d–f); measured vs. modeled C_T (a,d), including the RMSE of the model equation, measured vs. modeled r^2 , and number of measurements (N); measured (blue dots) and modeled (red dots) vertical profiles (b,e); vertical profiles of the difference between the measured and modeled C_T (c,f). The C_T and C_T -differences units are $\mu\text{mol kg}^{-1}$.

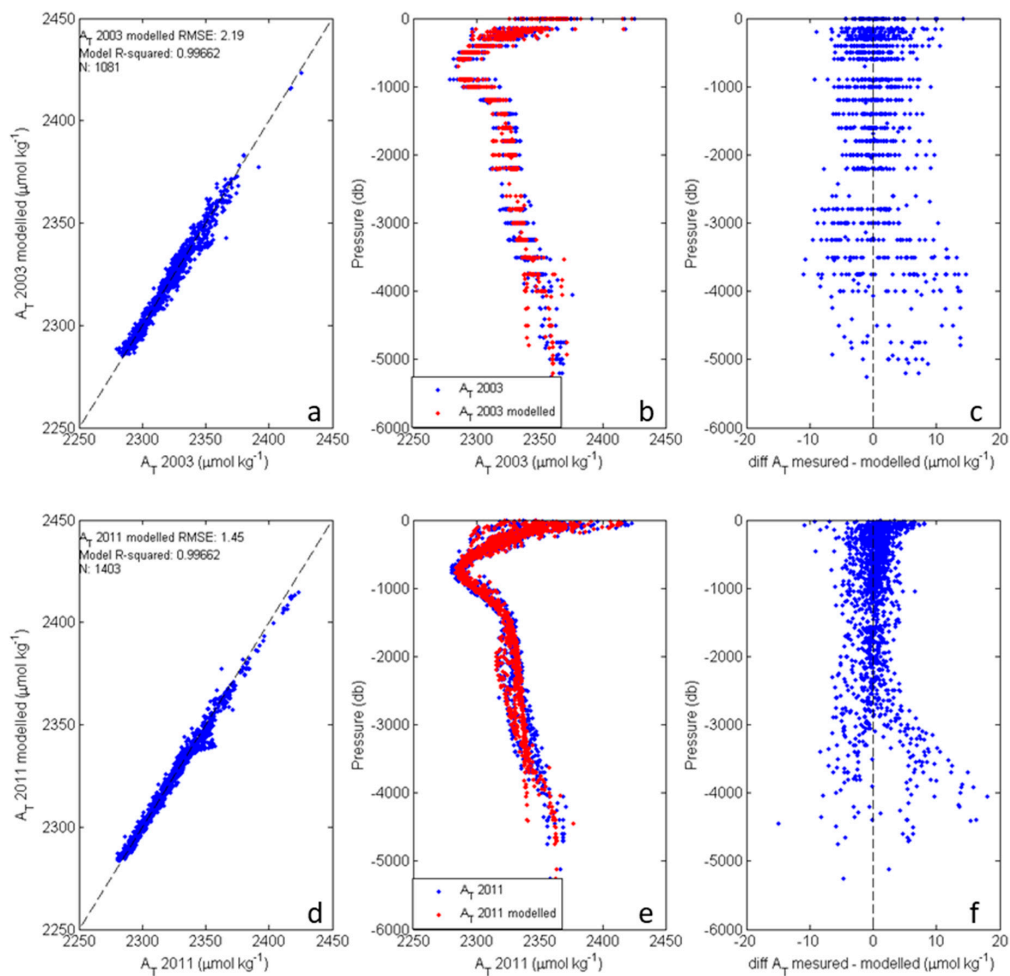


Figure 5. A_T model results considering the A10 section of 2003 (a–c) and 2011 (d–f); measured vs. modeled A_T (a,d), including the RMSE of the model equation, measured vs. modeled r^2 , and number of measurements (N); measured (blue dots) and modeled (red dots) vertical profiles (b,e); vertical profile of the difference between measured and modeled A_T (c,f). The A_T and A_T -differences units are $\mu\text{mol kg}^{-1}$.

3.3. Anthropogenic Carbon Content

We present the $C_{\text{ant-TrOCA}}$ because it indicates the C_{ant} content in the water column in all sections and eddies at their sample times (Figure 6). For the A10 cruises, the $C_{\text{ant-TrOCA}}$ was estimated using the measured concentrations and not the modeled values because they were used to develop the biogeochemical models. In addition, the differences between $\Delta C_{\text{ant-TrOCA}}$ and ΔC_T for the cruise years (Figure 7) clearly indicate that the TrOCA method could reliably identify the C_{ant} content. This dissimilarity could be due to the existing interannual variability of thermohaline properties, because the TrOCA method considers the physical structure of the water column (i.e., A_T , S and θ) and not only the C_T content. Moreover, the A_T is not affected by C_{ant} e.g., [59,60], so it can perfectly indicate the physical variation among years, because it is a parameter related to salinity [61]. This is an important point because we focus on the Agulhas eddies, which are mesoscale structures with significant hydrographical differences between their interior and surrounding waters e.g., [62]. Because we consider the C_{ant} concentrations at a large latitudinal range (22 °S–35 °S), these values reflect the large hydrographic differences in temperature and salinity fields (as observed by comparing the panels of Figures 2 and 3). Additionally, the error propagation equations e.g., [4,5,53,63] was used to determine the precision of the $C_{\text{ant-TrOCA}}$ method. To perform this analysis, we used the physical parameter measurement (θ , S) uncertainties together with the C_T/A_T estimation uncertainties, achieving values

ranging from 2.82 to 3.83 $\mu\text{mol kg}^{-1}$ for the application of 2011 and 2003 C_T/A_T precision, respectively. Compared with the precision of C_T (1.39 and 1.66 $\mu\text{mol kg}^{-1}$ for 2011 and 2003, respectively), these estimates allowed us to conclude that they are of the same order of magnitude and are also smaller than the previous reports from other C_{ant} methods (e.g., $\sim 5\text{--}6 \mu\text{mol kg}^{-1}$ for TrOCA [4,5,63] and $\sim 10 \mu\text{mol kg}^{-1}$ for ΔC^* [64]).

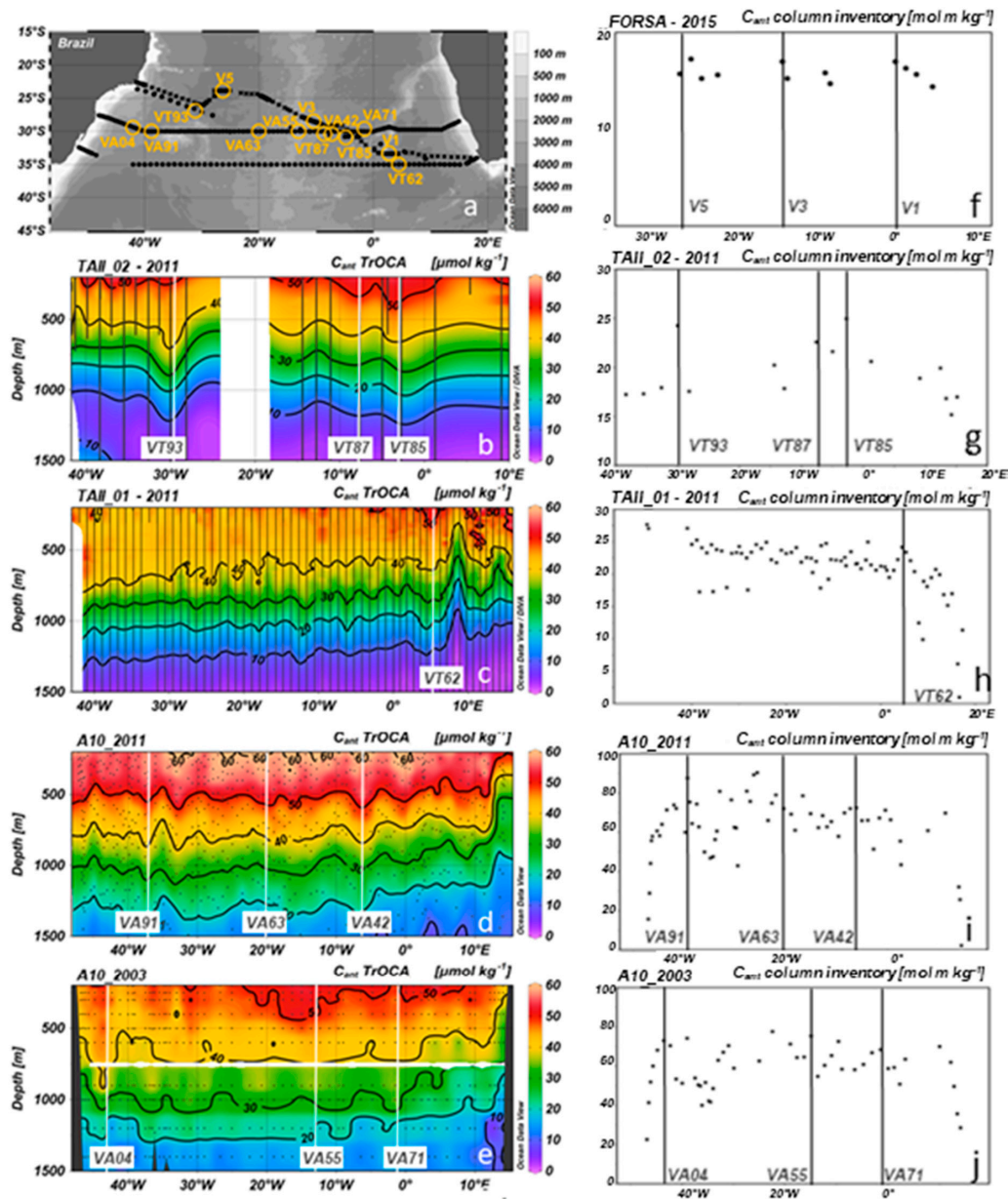


Figure 6. (a) Map of the cruise sections and sampled eddies. For a complete description of this map, please see Figure 1. (b–e) anthropogenic carbon ($C_{\text{ant-TrOCA}} \mu\text{mol kg}^{-1}$) content along the cruise sections: (b) TAIL_02-2011 section, (c) TAIL_01-2011 section, (d) A10_2011 section, (e) A10_2003 section. The continuous gray lines or gray dots indicate the position of CTD stations. The sampled eddies are indicated by a continuous white line; (f–j) anthropogenic carbon ($C_{\text{ant-TrOCA}} \text{mol m kg}^{-1}$) inventory along the water column; (f) FORSA-2015 section, (g) TAIL_02-2011 section, (h) TAIL_01-2011 section, (i) A10_2011 section, (j) A10_2003 section. The column inventory was determined by integrating the C_{ant} from 200 m to 500 m for the FORSA cruise and from 200 m to 1500 m for the other cruises. The sampled eddies are indicated by a continuous black line.

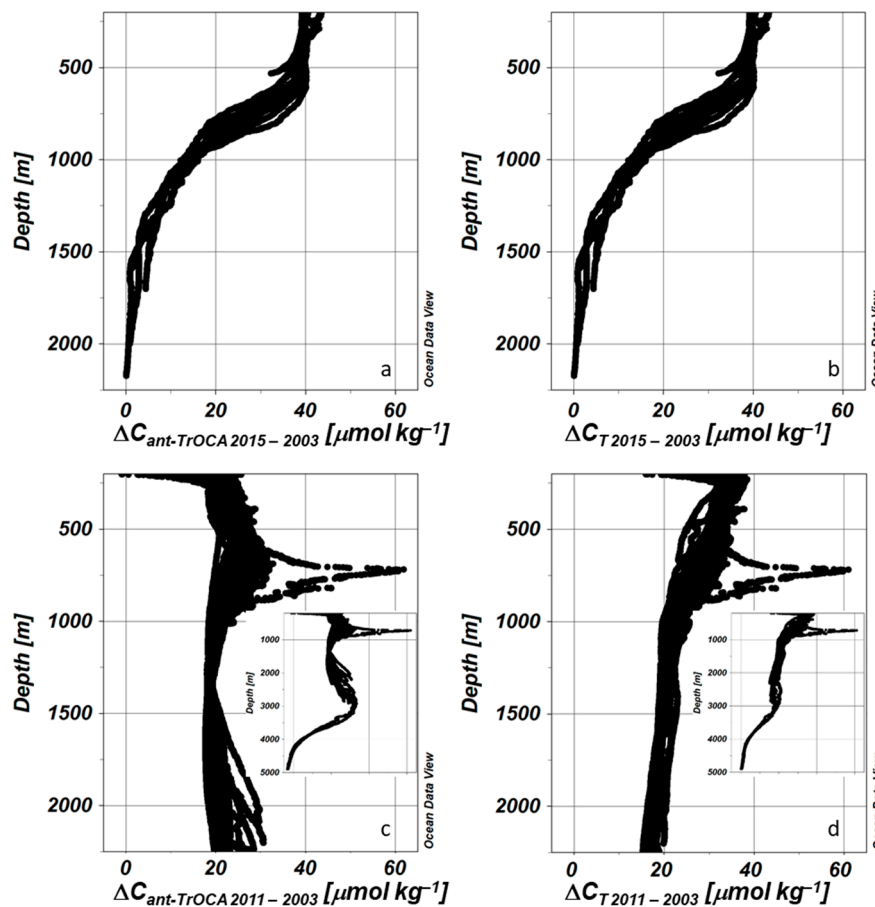


Figure 7. Vertical profiles of $\Delta C_{\text{ant-TrOCA}}$ (left panels) and ΔC_T (right panels); (a,b) FORSA cruise and (c,d) TAII cruise, where c and d include an inset panel denoting the entire water column depth below the surface mixed layer (200 m).

3.4. Characteristics and Physical-Chemical Structure of the Agulhas Eddies

Investigation of the Agulhas eddies was not the focus in three of four cruises studied in this work (i.e., in four of the five sections). As a consequence, certain eddies were not necessarily sampled close to their centers but only crossed at their borders (i.e., VA55, VA63, VT85, and VT87). Thus, the sections of temperature, salinity and C_{ant} of each of these eddies do not always show a typical eddy profile. However, at least a minor signal of an eddy profile can be observed in all eddy sections, apart from the SLA used in their identification. Accordingly, a typical thermostad and/or halostad was observed in the sections of those structures. We present the $C_{\text{ant-TrOCA}}$ profile of each eddy and the surrounding waters in Figure 8. Comparing the C_{ant} content (\pm standard deviation) inside and outside the eddies, this value was significantly higher ($23\% \pm 14\%$) inside all the structures than the value at the same depth in the surrounding waters. A general overview of this difference can be observed in the entire cruise sections (Figure 6), and a more detailed view of the inside–outside C_{ant} sections focused on each of the sampled eddies (Figures 8 and 9). Considering the inside–outside difference at 500 m depth, the mean C_{ant} inside was $18\% \pm 12\%$ higher than that outside and reached $29\% \pm 15\%$ at 1000 m depth (Figure 9).

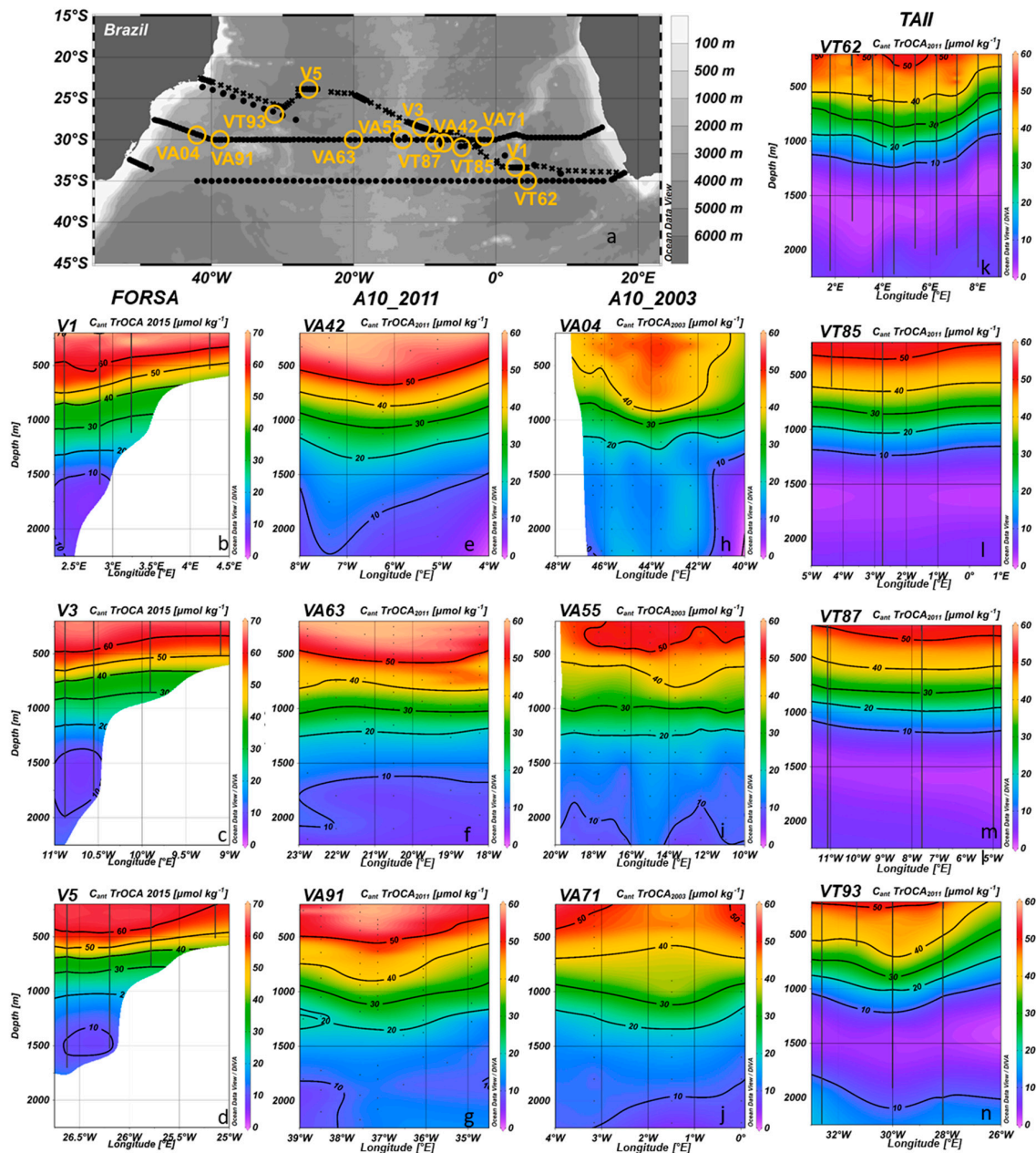


Figure 8. (a) Map of the cruise sections and sampled eddies. For a complete description of this map, please see Figure 1. (b–n) Section of the anthropogenic carbon ($C_{ant-TrOCA}$ $\mu\text{mol kg}^{-1}$) content in the studied eddies; (b–d) V1, V3, and V5, sampled in the FORSA cruise (the white portion of these maps corresponds to nonsampled depths); (e–g) VA42, VA63, and VA91, sampled in the A10_2011 cruise; (h–j) VA04, VA55, and VA71, sampled in the A10_2003 cruise; (k–n) VT62 (TAIL_01 section), VT85 (TAIL_02 section), VT78 (TAIL_02 section), and VT93 (TAIL_02 section), sampled in the TAIL cruise. The continuous gray lines or gray dots indicate the position of CTD stations.

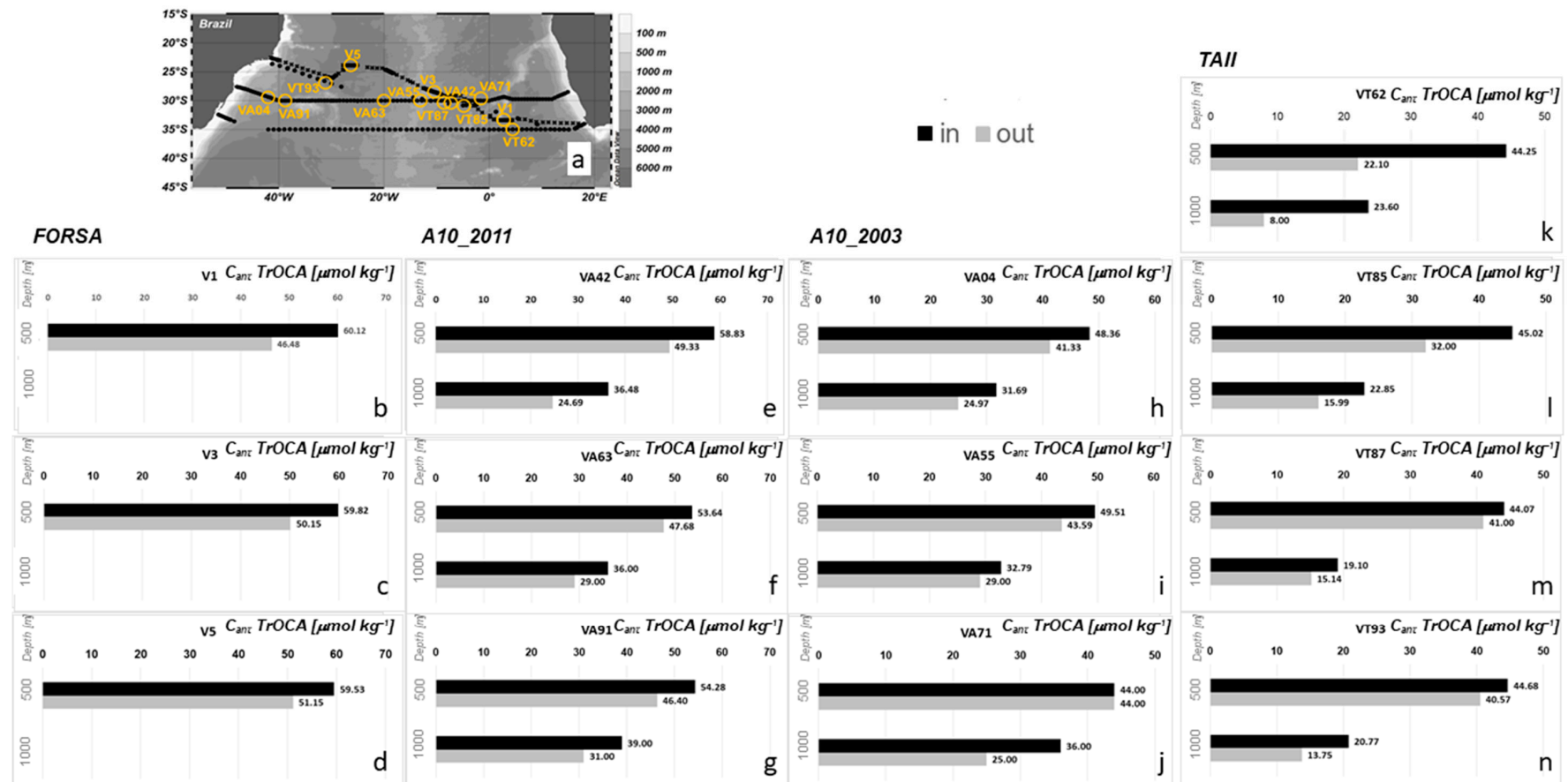


Figure 9. (a) Map of the cruise sections and sampled eddies. For a complete description of this map, please see Figure 1; (b–n) inside-outside eddy anthropogenic carbon ($C_{ant-TrOCA}$ $\mu\text{mol kg}^{-1}$) content at 500 m and 1000 m depth; (b–d) V1, V3, and V5, sampled in the FORSA cruise (the white part at 1000 m correspond to non-sampled depths outside of these eddies); (e–g) VA42, VA63, and VA91, sampled in the A10_2011 cruise; (h–j) VA04, VA55, and VA71, sampled in the A10_2003 cruise; (k–n) VT62 (TAIL_01 section), VT85 (TAIL_02 section), VT87 (TAIL_02 section), and VT93 (TAIL_02 section), sampled in the TAIL cruise.

The radius and age of each studied eddy, with consideration of (i) the sampled day and (ii) the life history, are included in Table 1, which indicates that the eddies were sampled at different stages of their lives. We did not observe a relation between the C_{ant} content according to their respective age, radius in the sampled day, or the sampled basin (Eastern/Western). However, we observed certain relatively old eddies (VA04, VA91, and VT93) near the Brazilian coast, which are, therefore, prone to merge with the Brazilian Current and impact the coastal/shelf ecosystems [65].

4. Discussion

4.1. Polynomial Models for Carbonate System Parameters

The polynomial models introduced in this study were able to correctly represent C_T and A_T with GOA-ON climate precision (i.e., estimated within an uncertainty of approximately $2 \mu\text{mol kg}^{-1}$ in measurements of C_T and A_T) [57], because the achieved RMSE values were smaller than $1.66 \mu\text{mol kg}^{-1}$ for C_T and $2.19 \mu\text{mol kg}^{-1}$ for A_T (Figures 3 and 4). Additionally, the results obtained using the polynomial models developed in this work presented a smaller RMSE than those observed for previous model studies e.g., [66]. For A_T , for example, the polynomial models introduced here presented a RMSE that was reduced by a factor of 2 compared to the RMSE reported by Carter et al. [66] when using only θ and S : 2.19 and $1.45 \mu\text{mol kg}^{-1}$ (this study—2003 and 2011, respectively) versus $4.4 \mu\text{mol kg}^{-1}$ [66]. The same result was observed when we compared our results with those of Goyet et al. [50] for both A_T and C_T . These differences could be related to the fact that these authors [50,66] were considering global oceans (i.e., larger scales) in their studies. The C_T RMSE determined in this study are in good agreement with the results reported by Goyet & Davis [58], who presented an uncertainty of $2 \mu\text{mol kg}^{-1}$ versus 1.66 and $1.39 \mu\text{mol kg}^{-1}$ (2003 and 2011, respectively) in their work.

In addition, the uncertainties observed in the models developed in this study are similar to the reported precision of direct carbonate parameter measurements e.g., [35,59] and have the same order of magnitude indicated in the guide of best practices for CO_2 measurements [44] using the recommended equipment and analysis. Furthermore, the GOA-ON reinforces the importance of the construction of biogeochemical databases with climate precision as good as what we have achieved [57]. Thus, these polynomial models are considered robust for C_T and A_T reconstruction in the South Atlantic basin and can contribute to filling the spatiotemporal gaps and allow reconstruction of marine carbonate system parameters with small uncertainties in the South Atlantic Ocean e.g., [67].

4.2. Anthropogenic Carbon Content in the South Atlantic Ocean

Comparing our C_{ant} estimates with the recent study of Gruber et al. [7], we note that our results were relatively higher than theirs. One main explanation for this difference is related to the C_{ant} methods. This type of difference is normally expected. These differences could also be related to the fact that the previous studies researched the C_{ant} uptake of an early period between 1994 and 2007 (13 years), whereas we investigated the uptake between 2003 and 2011 (8 years) and from 2003 to 2015 (12 years). Additionally, we performed another type of investigation, which was our main focus, i.e., a C_{ant} estimate for the entire industrial period. For the subtropical South Atlantic Ocean, Gruber et al. [7] found a range from 14 to $16 \mu\text{mol kg}^{-1}$ corresponding to the central layer (neutral density of 26.60 kg m^{-3} , $\sim 400 \text{ m}$; subtropical mode waters layer), whereas we found values ranging from 18 to $35 \mu\text{mol kg}^{-1}$ (30 to $40 \mu\text{mol kg}^{-1}$) for the period of 2003 to 2011 in the TAI01 longitudinal section (2011 and 2015 in the FORSA Southeast–Northwest section) at the same layer. As expected, the central layer corresponding to the Southeast–Northwest section is more significantly affected by the C_{ant} . Previous studies [4,5] have reported that the central waters of the Western South Atlantic Ocean are more significantly affected by the C_{ant} penetration than the waters corresponding to the layers above and below, which is reflected in the faster acidification rate of the SACW [4,5].

Looking at the intermediate layer (neutral density of 27.40 kg m^{-3} , $\sim 1000 \text{ m}$; AAIIW layer in the South Atlantic Ocean), the same authors found a range that varies from 5 to $8 \mu\text{mol kg}^{-1}$, whereas

we found values ranging from 15 to 22 $\mu\text{mol kg}^{-1}$ (13 to 18 $\mu\text{mol kg}^{-1}$) for the period of 2003 to 2011 in the TAII_01 longitudinal section (2011 to 2015 in the FORSA Southeast-Northwest section) at the same layer. The slightly higher values of the TAII_01 longitudinal section can be justified by the fact that this sampling was performed along 35 °S, which is closer to the Antarctic Intermediate Water formation region.

Comparing our study with previous work that used the same methodology in the South Atlantic Ocean [4,5], the findings related to the C_{ant} content in the water column since the industrial revolution are in agreement. For the both SACW and AAIW, the results observed in this work are inside the range observed for the shelf-break region of the Brazilian coast [4] as well as for the Argentine Patagonian zone [5].

Additionally, we aimed to compare the C_{ant} content estimated by the TrOCA method between cruise years ($\Delta C_{\text{ant-TrOCA 2011-2003}}$) and a simple C_T difference between cruise years ($\Delta C_T 2011-2003$) at different cruise sections. Thus, we compared the results for the FORSA Southeast-Northwest section (Figure 7a,b) and for the TAII_01 longitudinal section (Figure 7c,d; i.e., one comparison between Figure 7a,b and another between Figure 7c,d). With respect to method comparison, we found that the difference is small, indicating that the TrOCA method could reliably identify the C_{ant} content. The C_{ant} amount found in this peak, approximately 800 m (observed in plots c and d), was observed near the South Brazilian coast, a region that was sampled only in the TAII cruise and not in the FORSA cruise. As indicated by other studies e.g., [4,5], the central layer of this region is more significantly affected by C_{ant} penetration than the layers below and above. Thus, we believe that this difference is reasonable.

4.3. Role Played by the Agulhas Eddies in Anthropogenic Carbon Transport in the South Atlantic Ocean

Considering that the Agulhas eddies can intensify the CO_2 uptake at the sea surface compared to the surrounding waters [34], more C_{ant} can penetrate into the water column through the mode water formation processes. Because SACW is composed of several varieties of South Atlantic mode waters [20,33] and receive a considerable input of Indian mode waters [20], the propagation of the Agulhas eddies within the South Atlantic Ocean could be one of the key processes responsible for the rapid acidification levels reported for the central waters of this basin [3–5]. This hypothesis is proven by the greater amounts of C_{ant} found inside the eddies than in their surrounding waters (Figures 8 and 9). On average, the C_{ant} content is 18% (29%) higher in the waters inside the eddy at 500 m (1000 m) than outside at the same depth (Figure 9).

It is important to reiterate that each eddy has its own physical characteristics, leading to different intensities on their physical forces. The larger the eddy diameter is after its formation, the greater its expected lifetime. As shown in Table 1, the VA04 eddy is the largest structure used in this study, with a radius of approximately 130 km on its sampling day and a mean radius during its lifetime of approximately 111 km. These physical spatial differences mean that specific eddies have particularities and make only one third of them capable of reaching the Western boundary of the South Atlantic Ocean [68,69]. Reinforcing the most important landmarks for the eddy lifetimes, one portion of the Agulhas eddies can die while crossing the Walvis Ridge, while another portion can die while crossing the Mid-Atlantic Ridge. Additionally, these eddies can suffer splitting and merging processes during their trajectories, as we observed for i) V5 in our previous study [34], in which we identified and interaction between V4 and V5 and V5 and V6, and for ii) VA91, which was formed during the splitting of a 925 days old eddy (Table 1). These interactions between eddies are more common when considering the Agulhas evolved eddies (V5 and VA91, for example), which are structures observed on the Western basin of the South Atlantic Ocean after crossing the Mid-Atlantic Ridge [34].

Thus, the Agulhas eddies (i) intensify the CO_2 uptake at the sea surface, as shown by Orselli et al. [34]; (ii) can strengthen the formation processes of the mode waters by increasing the heat flux [18,33]; (iii) contain more C_{ant} than their surrounding waters, as suggested by Woosley et al. [70] and also observed in this study; and (iv) can also carry water masses sourced in the Indian Ocean e.g., [28]. These facts indicate that these mesoscale structures could be one of the key processes influencing the

South Atlantic Ocean acidification state through transport of both natural and anthropogenic CO₂. It is interesting to note that a recent study by Gruber et al. [7] showed that the waters of the subtropical gyre of the South Atlantic Ocean are facing an anomalous increase in the C_{ant} inventory. These observations correspond to the water column content integrated from the surface to 3000 m depth, which is the region under the influence of the Agulhas eddies.

Moreover, in more recent studies, Laxenaire et al. [68] and Guerra et al. [69] observed the physical interaction between some Agulhas eddies and the Brazil Current. Guerra et al. [69] found that over 23 years, one third of the identified Agulhas eddies released in the retroflexion zone reached the Western boundary of the South Atlantic Ocean, with an impact on sea surface temperature (SST), sea surface salinity (SSS), and heat content in the South and Southeast Brazilian coast e.g., [71]. These changes in the SST of the Western boundary led to modifications in the precipitation regime, fluvial discharges, and hydrological cycle, thus affecting the Brazilian coast [1,72,73]. Castellanos et al. [74] verified that an increase in the Agulhas leakage influences the precipitation regime and latent heat flux on the Brazilian coast. Additionally, these eddies can cause intensification of the subtropical gyre [3,74] and can also modify the way in which the El Niño Southern Oscillation impacts the entire South America due to atmospheric teleconnections [1,72,73].

Changes in marine life and biogeochemical cycles are also expected [1]. In the first study of the ocean acidification state in the Brazilian margins, Carvalho-Borges et al. [4] observed an acidification rate of -0.0017 yr^{-1} in the SACW. These authors found that the central and intermediate layers of the Brazilian coastal region are experiencing an acidification rate of the same magnitude as that of the Argentinean Patagonia (-0.0018 yr^{-1}), which is the other coastal region influenced by southward transport along the Southeast South Atlantic Ocean [5]. However, Carvalho-Borges et al. [4] reinforced that this -0.0017 yr^{-1} value could be underestimated, indicating that the SACW presented in the southwest Atlantic Ocean could be suffering even greater acidification changes than those reported in the central gyre of the South Atlantic Ocean. Previously, Woosley et al. [70] suggested that the Agulhas eddies can carry up to 20% more C_{ant} than the surrounding waters, which is reinforced by this study ($\geq 23\%$). Some variations of the observed inside-outside differences could be related to the position of the eddy sampling because certain structures were sampled in their centers, and others were sampled closer to their borders.

Previous studies report that the Western basin of the South Atlantic Ocean could be acidified faster than its Eastern basin due to the stronger ventilation processes e.g., [35], or cross-shelf carbon transport e.g., [4]. We demonstrate in this work that the Agulhas eddies often play a key role in the acidification state of the central waters of the South Atlantic Ocean through the transport of 23% more C_{ant} than their surrounding waters. This excess of CO₂ reaching the Brazilian coast can also have an influence on sensitive marine ecosystems (e.g., coral reefs, rhodolith beds, and continental shelf areas) along the Western South Atlantic Ocean region, which have ecological and economical importance and are considered nonrenewable resources [1,4,65].

5. Summary and Conclusions

This research focused on the influence of Agulhas eddies on C_{ant} transport through the South Atlantic Ocean and their impact on ocean acidification. We used in situ data from three zonal and two Southeast–Northwest transects obtained during three cruises conducted in the spring of 2003 and 2011 and one in the winter of 2015. During these surveys, 13 Agulhas eddies were sampled with CTD stations. We modeled the carbonate parameters in locations where they were not directly measured in the cruises using the polynomial models introduced in this work, which were considered robust in C_T and A_T reconstruction. Additionally, we estimated the C_{ant} content in the water column. The Agulhas eddies have a stronger uptake ability than their surrounding waters, thus increasing the atmospheric CO₂ sink [34]. A typical Agulhas eddy can take up $-2.12 \text{ kg CO}_2 \text{ d}^{-1}$, leading to a $-2.08 \text{ t CO}_2 \text{ lifetime}^{-1}$ [34]. In this study, we also showed that the Agulhas eddies contain up to 29% more C_{ant} than their surrounding waters, which could be influenced by the mode water formation processes.

Because mode waters compose the SACW e.g., [20,32], which currently acidifies faster than the surface and intermediate layers of the South Atlantic Ocean [3–6], we concluded that the Agulhas eddies can act as a trigger for the acidification state of the central water layer of the South Atlantic Ocean via the uptake and consequent transport of large amounts of C_{ant} . Furthermore, recent evidence, such as the interaction between the Agulhas eddies and the Brazil Current [68,69], the contribution of Indian Ocean mode waters observed in the South Atlantic Ocean [20], and the increasing Agulhas leakage [29], highlights the need for additional investigation of the impact of eddies on South Atlantic Ocean acidification. In this study, we focus on the importance of Agulhas eddy dynamics in South Atlantic Ocean biogeochemistry, which is an interesting and novel research topic still under development.

Future studies should focus on other ocean processes and quantification of the Agulhas eddies' impacts on SACW acidification, because the SACW is experiencing intense acidification changes that could have severe impacts on Brazilian coastal ecosystems. These studies should also investigate the global importance of Agulhas eddies in biogeochemistry, because they play an important role in the subtropical gyre of the South Atlantic Ocean and Atlantic meridional overturning circulation [21,71]. Thus, a natural outcome of the results presented in this work is to implement high-resolution process-oriented numerical modeling experiments, including downscaling, which are lacking in current investigations [1,75]. Additionally, we suggest model studies focusing on the impacts of climate change on Agulhas leakage and eddy release, because these phenomena are associated with wind system modifications [29]. Future studies should also focus on its consequences of Agulhas leakage and eddy release on marine organisms and ecosystems.

Author Contributions: I.B.M.O. conducted the data analysis and modeling elements of this study as her PhD project. C.G. acted as the main supervisor for I.B.M.O. in conducting this work and as an expert on carbonate system data and modeling. R.K. acted as a second supervisor for I.B.M.O. in proposing the study and as an expert on carbonate system and water masses. J.L.L.d.A. acted as a third supervisor for I.B.M.O. and as an Agulhas-eddy expert. M.A. contributed as an eddy expert and as P.I. of the FORSA cruise. F.G. conducted the satellite data and AVISO product processing. F.T. contributed as an expert in anthropogenic carbon calculations. C.A.E.G. was the main coordinator for the Brazilian research cruises and was responsible for supplying the TAI and FORSA cruise opportunities for the observations. All authors contributed to the interpretation of results and/or to the writing of the paper.

Funding: This study offers a contribution to the activities of the Brazilian High Latitude Oceanography Group (GOAL) and the Brazilian Ocean Acidification Network (BrOA; www.broa.furg.br). The TAI and FORSA projects were sponsored by the Brazilian National Council for Scientific and Technological Development (CNPq) and Brazilian Improving Coordination of Higher Education Personnel (CAPES), with logistics supported by the Ministry of Science, Technology, Innovation, and Communication (MCTIC), the Brazilian Ministerial Secretary for the Resources of the Sea (SECIRM), and the Brazilian Navy. FORSA was also sponsored by the Brazilian Coastal Monitoring System (SiMCosta). This study also contributes to the project “Estudos Avançados de Médias e Altas Latitudes” (CAPES grant n° 23038.001421/2014-30). I. B. M. Orselli acknowledges CAPES/CMAR2 for her Ph.D. funding (CAPES process n°. 23038.001421/2014-30 and BEX 0077/17-8). R. Kerr acknowledges the CNPq researcher grants n° 302604/2015-4 and 304937/2018-5. M. Araujo is grateful for the support of the Brazilian Research Network on Global Climate Change-Rede CLIMA (FINEP grants 01.13.0353-00).

Acknowledgments: The authors thank all the researchers and students from LEOC/FURG and LOFEC/UFPE for their contributions to cruise planning and sampling, as well as researchers from IMAGES_ESPACE-DEV/UPVD for discussions and suggestions. The authors also thank the crew of the Brazilian vessels RV NHo Cruzeiro do Sul and RV NPqHo Vital de Oliveira for their logistical assistance. Because this work used the Mesoscale Eddy Trajectory Atlas product, the authors thank its producers, supporters, collaborators and distributors: SSALTO/DUACS, CNES, Oregon State University, NASA and AVISO. We also thank for the availability of the CLIVAR/WOCE Repeat Hydrography Section A10 data. The authors thank the editors and three reviewers for their comments and suggestions, which have significantly improved the manuscript.

Conflicts of Interest: The authors declare that they have no conflicts of interest. The funders had no role in the design of the study; in the collection, analyses, or interpretation of data; in the writing of the manuscript, or in the decision to publish the results.

References

1. Campos, E.J.D.; França, C.A.S.; Rodrigues, R.R.; Muelbert, J.H. Inter-relações entre o Atlântico Sul, plataforma continental e regiões costeiras do sul e do sudeste do Brasil. In *Ciência das Mudanças Climáticas e sua Interdisciplinaridade*; Ambrizzi, T., Jacobi, P.R., Dutra, L.M.M., Eds.; Annablume Editora: São Paulo, Brazil, 2015; ISBN 978-85-391-0714-8.
2. Takahashi, T.; Sutherland, S.C.; Wanninkhof, R.; Sweeney, C.; Feely, R.A.; Chipman, D.W.; Hales, B.; Friederich, G.; Chavez, F.; Sabine, C.; et al. Climatological mean and decadal change in surface ocean pCO₂, and net sea-air CO₂ flux over the global oceans. *Deep-Sea Res. II* **2009**, *56*, 554–557. [[CrossRef](#)]
3. Salt, L.A.; Heuven, S.M.; Claus, M.E.; Jones, E.M.; Baar, H.J. Rapid acidification of mode and intermediate waters in the southwestern Atlantic Ocean. *Biogeosciences* **2015**, *12*, 1387–1401. [[CrossRef](#)]
4. De Carvalho-Borges, M.; Orselli, I.B.M.; de Carvalho Ferreira, M.L.; Kerr, R. Seawater acidification and anthropogenic carbon distribution on continental shelf and slope of the western South Atlantic Ocean. *J. Mar. Syst.* **2018**. [[CrossRef](#)]
5. Orselli, I.B.M.; Kerr, R.; Ito, R.G.; Tavano, V.M.; Mendes, C.R.B.; Garcia, C.A.E. How fast is the Patagonian shelf-break acidifying? *J. Mar. Syst.* **2018**, *178*, 1–14. [[CrossRef](#)]
6. Kitidis, V.; Brown, I.; Hardman-Mountford, N.; Lefèvre, N. Surface ocean carbon dioxide during the Atlantic Meridional Transect (1995–2013): Evidence of ocean acidification. *Prog. Oceanogr.* **2017**, *158*, 65–75. [[CrossRef](#)]
7. Gruber, N.; Clement, D.; Carter, B.R.; Feely, R.A.; van Heuven, S.; Hoppema, M.; Ishii, M.; Key, M.R.; Kozyr, A.; Lauvset, S.K.; et al. The oceanic sink for anthropogenic CO₂ from 1994 to 2007. *Science* **2019**, *363*, 1193–1199. [[CrossRef](#)] [[PubMed](#)]
8. Howes, E.L.; Joos, F.; Eakin, M.; Gattuso, J.-P. *The Oceans 2015 Initiative, Part I: An Updated Synthesis of the Observed and Projected Impacts of Climate Change on Physical and Biological Processes in the Oceans*; Studies N°02/15; IDDRI: Paris, France, 2015; p. 52. ISSN 2258-7535.
9. Pardo, P.C.; Pérez, F.F.; Khatiwala, S.; Ríos, A.F. Anthropogenic CO₂ estimates in the Southern Ocean: Storage partitioning in the different water masses. *Prog. Oceanogr.* **2014**, *120*, 230–242. [[CrossRef](#)]
10. Sabine, C.L.; Feely, R.A.; Gruber, N.; Key, R.M.; Lee, K.; Bullister, J.L.; Wanninkhof, R.; Wong, C.S.; Wallace, D.W.; Tilbrook, B.; et al. The Ocean Sink for Anthropogenic CO₂. *Science* **2004**, *305*, 367–371. [[CrossRef](#)]
11. Tanhua, T.; Hoppema, M.; Jones, E.M.; Stöven, T.; Hauck, J.; Dávila, M.G.; Santana-Casiano, M.; Álvarez, M.; Strass, V.H. Temporal changes in ventilation and the carbonate system in the Atlantic sector of the Southern Ocean. *Deep-Sea Res. II* **2016**. [[CrossRef](#)]
12. Cox, P.M.; Betts, R.A.; Jones, C.D.; Spall, S.A.; Totterdell, I.J. Acceleration of global warming due to carbon-cycle feedbacks in a coupled climate model. *Nature* **2000**, *408*, 184–187. [[CrossRef](#)]
13. Touratier, F.; Goyet, C.; Houpert, L.; de Madron, X.D.; Lefèvre, D.; Stabholz, M.; Guglielmi, V. Role of deep convection on anthropogenic CO₂ sequestration in the Gulf of Lions (northwestern Mediterranean Sea). *Deep-Sea Res. I* **2016**, *113*, 33–48. [[CrossRef](#)]
14. Orsi, A.H.; Johnson, G.C.; Bullister, J.L. Circulation, mixing and production of Antarctic bottom water. *Prog. Oceanogr.* **1999**, *43*, 55–109. [[CrossRef](#)]
15. Rintoul, S. *The Southern Ocean in the Earth System*; Smithsonian Institution Scholarly Press: Washington, DC, USA, 2011. [[CrossRef](#)]
16. Talley, L.; Pickard, G.; Emery, W.; Swift, J. *Descriptive Physical Oceanography: An Introduction*; Elsevier: Boston, MA, USA, 2011.
17. Emery, W.J. Water types and water masses. In *Ocean Circulation*; Elsevier: Amsterdam, The Netherlands, 2003; pp. 1556–1567. ISBN 978-0-12-391851-2.
18. Hanawa, K.; Talley, L.D. Mode Waters. In *Ocean Circulation and Climate: Observing and Modelling the Global Ocean*; Siedle, G., Church, J., Gould, J., Eds.; Academic: San Diego, CA, USA; London, UK, 2001; pp. 373–386. ISBN 0-12-641351-7.
19. Van Aken, H.M.; van Veldhoven, A.K.; Veth, C.; De Ruijter, W.P.M.; van Leeuwen, P.J.; Drijfhout, S.S.; Whittle, C.P.; Rouault, M. Observations of a young Agulhas ring, Astrid, during MARE in March 2000. *Deep-Sea Res. II* **2003**, *50*, 167–195. [[CrossRef](#)]
20. Souza, A.G.Q.; Kerr, R.; Azevedo, J.L.L. On the influence of Subtropical Mode Water on the South Atlantic Ocean. *J. Mar. Syst.* **2018**, *185*, 13–24. [[CrossRef](#)]

21. Beal, L.M. A Time Series of Agulhas Undercurrent Transport. *J. Phys. Oceanogr.* **2009**, *39*, 2436–2450. [[CrossRef](#)]
22. Biastoch, A.; Durgadoo, J.V.; Morrison, A.K.; van Sebille, E.; Weijer, W.; Griffies, S.M. Atlantic multi-decadal oscillation covaries with Agulhas leakage. *Nat. Commun.* **2015**, *6*, 10082. [[CrossRef](#)]
23. Stramma, L.; England, M. On the Water masses and mean circulation of the South Atlantic Ocean. *J. Geophys. Res.* **1999**, *104*, 20863–20883. [[CrossRef](#)]
24. Ferreira, M.L.; Kerr, R. Source water distribution and quantification of North Atlantic Deep Water and Antarctic Bottom Water in the Atlantic Ocean. *Prog. Oceanogr.* **2017**, *153*, 66–83. [[CrossRef](#)]
25. Robinson, A.R. *Eddies in Marine Science*; Springer: Berlin, Germany, 1983; 614p.
26. Biastoch, A.; Böning, C.W.; Lutjeharms, J.R.E. Agulhas leakage dynamics affects decadal variability in Atlantic overturning circulation. *Nature* **2008**, *456*, 489–492. [[CrossRef](#)]
27. De Ruijter, W.P.; Biastoch, A.; Drijhout, S.S.; Lutjeharms, J.R.; Matano, R.; Pichevin, T.; van Leeuwen, P.J.; Weijer, W. Dynamics, estimation and impact of South Atlantic interocean exchange. *J. Geophys. Res.* **1999**, *104*, 20885–20910. [[CrossRef](#)]
28. Lutjeharms, J.R.E. *The Agulhas Current*; Springer: Berlin/Heidelberg, Germany, 2006. [[CrossRef](#)]
29. Biastoch, A.; Böning, C.W.; Schwarzkopf, F.U.; Lutjeharms, J.R.E. Increase in Agulhas leakage due to poleward shift of southern hemisphere westerlies. *Nature* **2009**, *462*, 495. [[CrossRef](#)] [[PubMed](#)]
30. Souza, J.M.; de Boyer Montégut, C.; Cabanes, C.; Klein, P. Estimation of the Agulhas ring impacts on meridional heat fluxes and transport using ARGO floats and satellite data. *Geophys. Res. Lett.* **2011**, *38*, L21602. [[CrossRef](#)]
31. Bard, E.; Rickaby, R.E.M. Migration of the subtropical front as a modulator of glacial climate. *Nature* **2009**, *460*, 380–383. [[CrossRef](#)] [[PubMed](#)]
32. Sato, O.T.; Polito, P. Observation of South Atlantic subtropical mode Waters with Argo profiling float data. *J. Geophys. Res. Oceans* **2014**, *119*, 2860–2881. [[CrossRef](#)]
33. Villas Bôas, A.B.; Sato, O.T.; Chaigneau, A.; Castelão, G.P. The signature of mesoscale eddies on the air-sea turbulent heat fluxes in the South Atlantic Ocean. *Geophys. Res. Lett.* **2015**, *42*, 1856–1862. [[CrossRef](#)]
34. Orselli, I.B.M.; Kerr, R.; Azevedo, J.L.L.; Galdino, F.; Araujo, M.; Garcia, C.A.E. The sea-air CO₂ net fluxes in the South Atlantic Ocean and the role played by Agulhas eddies. *Prog. Oceanogr.* **2019**, *170*, 40–52. [[CrossRef](#)]
35. Ríos, A.F.; Álvarez-Salgado, X.A.; Pérez, F.F.; Bingler, L.S.; Aristegui, J.; Mémery, L. Carbon dioxide along WOCE line A14: Water masses characterization and anthropogenic entry. *J. Geophys. Res.* **2003**, *108*, 3123. [[CrossRef](#)]
36. Moreau, S.; Della Penna, A.; Llort, J.; Patel, R.; Langlais, C.; Boyd, P.W.; Matear, R.J.; Phillips, H.E.; Trull, T.W.; Tilbrook, B.; et al. Eddy-induced carbon transport across the Antarctic Circumpolar Current. *Glob. Biogeochem. Cycles* **2017**, *31*, 1368–1386. [[CrossRef](#)]
37. Mata, M.M.; Tavano, V.M.; Garcia, C.A.E. 15 years sailing with the Brazilian High Latitude Oceanography Group (GOAL). *Deep-Sea Res. II* **2018**, *149*, 1–3. [[CrossRef](#)]
38. Lencina-Avila, J.M.; Ito, R.G.; Garcia, C.A.E.; Tavano, V.M. Sea-air carbon dioxide fluxes along 35°s in the Atlantic Ocean and adjacent continental shelves. *Deep-Sea Res. I* **2016**, *115*, 175–187. [[CrossRef](#)]
39. Carvalho, A.C.O.; Mendes, C.R.B.; Kerr, R.; Azevedo, J.L.L.; Galdino, F.; Tavano, V.M. The impact of mesoscale eddies on the phytoplankton community in the South Atlantic Ocean: HPLC-CHEMTAX approach. *Mar. Environ. Res.* **2019**, *144*, 154–165. [[CrossRef](#)] [[PubMed](#)]
40. Uchida, H.; Fukasawa, M.; Murata, A. *WHP P6, A10, I3/I4 REVISIT DATA BOOK Blue Earth Global Expedition 2003 (BEAGLE2003)*; JAMSTEC Publication: Tokyo, Japan, 2005; Volume 1–2.
41. Wanninkhof, R.; Feely, R.; Millero, F.; Carlson, C.; O’Neil Baringer, M.; Macdonald, A.; Johnson, G.; Zhang, J.-Z.; Mordy, C.; Langdon, C.; et al. *Carbon Dioxide, Hydrographic, and Chemical Data Obtained during the R/V Ronald H. Brown in the Atlantic Ocean on CLIVAR Repeat Hydrography Section A10 (September 26–October 31, 2011)*; Carbon Dioxide Information Analysis Center, Oak Ridge National Laboratory, US Department of Energy: Oak Ridge, TN, USA, 2013. [[CrossRef](#)]
42. Chelton, D.B.; Schlax, M.G.; Samelson, R.G. Global observations of nonlinear mesoscale eddies. *Prog. Oceanogr.* **2011**, *91*, 167–216. [[CrossRef](#)]
43. Schlax, M.G.; Chelton, D.B. *The “Growing Method” of Eddy Identification and Tracking in Two and Three Dimensions*; College of Earth, Ocean and Atmospheric Sciences, Oregon State University: Corvallis, OR, USA, 2016.

44. DOE. *Handbook of Methods for Analysis of the Various Parameters of the Carbon Dioxide System in Seawater*; Version 2, ORNL/CDIAC-74; Dickson, A.G., Goyet, C., Eds.; DOE: Washington, DC, USA, 1994.
45. Johnson, K.M.; Dickson, A.G.; Eischeid, G.; Goyet, C.; Guenther, P.; Key, R.M.; Millero, F.J.; Purkerson, D.; Sabine, C.L.; Schottle, R.G.; et al. Coulometric total carbon dioxide analysis for marine studies: Assessment of the quality of total inorganic carbon measurements made during the US Indian Ocean CO₂ survey 1994–1996. *Mar. Chem.* **1998**, *63*, 21–37. [[CrossRef](#)]
46. Goyet, C.; Hacker, S.D. Procedure for calibration of a coulometric system used for total inorganic carbon measurements in seawater. *Mar. Chem.* **1992**, *38*, 37–53. [[CrossRef](#)]
47. Johnson, K.M.; King, A.E.; Sieburth, J.M. Coulometric TCO₂ analyses for marine studies: An introduction. *Mar. Chem.* **1985**, *16*, 61–82. [[CrossRef](#)]
48. Johnson, K.M.; Williams, P.J.; Brandstrom, L.; Sieburth, J.M. Coulometric total carbon analysis for marine studies: Automation and calibration. *Mar. Chem.* **1987**, *21*, 117–133. [[CrossRef](#)]
49. Johnson, K.M. *Operator's Manual: Single-Operator Multiparameter Metabolic Analyzer (SOMMA) for Total Carbon Dioxide (CT) with Coulometric Detection*; Brookhaven National Laboratory: Brookhaven, NY, USA, 1992.
50. Patil, G.P.; Rao, C.R. *Handbook of Statistics. v. 12; Environmental Statistics*: Amsterdam, The Netherlands, 1994; 927p.
51. Goyet, C.; Healy, R.J.; Ryan, J.P. *Global Distribution of Total Inorganic Carbon and Total Alkalinity below the Deepest Winter Mixed Layer Depths*; ORNL/CDIAC-127, NDP-076; Carbon Dioxide Information Analysis Center, Oak Ridge National Laboratory, U.S. Department of Energy: Oak Ridge, TN, USA, 2000; p. 40.
52. Touratier, F.; Azouzi, L.; Goyet, C. CFC-11, $\Delta C^{14}C$ and 3H tracers as a means to assess anthropogenic CO₂ concentrations in the ocean. *Tellus* **2007**, *59B*, 318–325. [[CrossRef](#)]
53. Touratier, F.; Goyet, C. Definition, properties, and Atlantic Ocean distribution of the new tracer TrOCA. *J. Mar. Syst.* **2004**, *46*, 169–179. [[CrossRef](#)]
54. Touratier, F.; Goyet, C. Applying the new TrOCA approach to assess the distribution of anthropogenic CO₂ in the Atlantic Ocean. *J. Mar. Syst.* **2004**, *46*, 181–197. [[CrossRef](#)]
55. Lutjeharms, J.R.E.; Valentine, H.R. Water types and volumetric considerations of the South-East Atlantic upwelling regime. *Afr. J. Mar. Sci.* **1987**, *5*, 63–71. [[CrossRef](#)]
56. Möller, O.O., Jr.; Piola, A.R.; Freitas, A.C.; Campos, E.J.D. The effects of river discharge and seasonal winds on the shelf off Southwestern South America. *Cont. Shelf Res.* **2008**, *28*, 1607–1624. [[CrossRef](#)]
57. Newton, J.A.; Feely, R.A.; Jewett, E.B.; Williamson, P.; Mathis, J. *Global Ocean Acidification Observing Network (GOA-ON): Requirements and Governance Plan*, 2nd ed. 2015. Available online: http://www.goa-on.org/documents/general/GOA-ON_2nd_edition_final.pdf (accessed on 12 June 2019).
58. Goyet, C.; Davis, D.L. Estimation of TCO₂ concentration throughout the water column. *Deep-Sea Res. I* **1997**, *44*, 859–877. [[CrossRef](#)]
59. Goyet, C.; Ito, R.G.; Touratier, F. Anthropogenic carbon distribution in the eastern South Pacific Ocean. *Biogeosciences* **2009**, *6*, 149–156. [[CrossRef](#)]
60. Goyet, C.; Coatanoan, C.; Eischeid, G.; Amaoka, T.; Okuda, K.; Healy, R.; Tsunogai, S. Spatial variation of total CO₂ and total alkalinity in the northern Indian Ocean: A novel approach for the quantification of anthropogenic CO₂ in seawater. *J. Mar. Res.* **1999**, *57*, 135–163. [[CrossRef](#)]
61. Millero, F.J. The marine inorganic carbon cycle. *Chem. Rev.* **2007**, *107*, 308–341. [[CrossRef](#)]
62. Casanova-Masjoan, M.; Pelegrí, J.L.; Sangrà, P.; Martínez, A.; Grisolia-Santos, D.; Pérez-Hernández, M.D.; Hernández-Guerra, A. Characteristics and evolution of an Agulhas ring. *J. Geophys. Res. Oceans* **2017**, *122*, 7049–7065. [[CrossRef](#)]
63. Kerr, R.; Goyet, C.; Cunha, L.C.; Orselli, I.B.M.; Lencina-Avila, J.M.; Mendes, C.R.B.; Carvalho-Borges, M.; Mata, M.M.; Tavano, V.M. Carbonate system properties in the Gerlache Strait, Northern Antarctic Peninsula (February 2015): II. Anthropogenic CO₂ and Seawater Acidification. *Deep-Sea Res. II* **2018**. [[CrossRef](#)]
64. Gruber, N.; Sarmiento, J.L.; Stocker, T.F. An improved method for detecting anthropogenic CO₂ in the oceans. *Glob. Biogeochem. Cycles* **1996**, *10*, 809–837. [[CrossRef](#)]
65. Kerr, R.; Cunha, L.C.; Kikuchi, R.K.P.; Horta, P.; Ito, R.G.; Muller, M.N.; Orselli, I.B.M.; Lencina-Avila, J.M.; de Orte, M.R.; Sordo, L.; et al. The western South Atlantic Ocean in a high-CO₂ world: Current measurement capabilities and perspectives. *Environ. Manag.* **2016**, *57*, 740–752. [[CrossRef](#)]
66. Carter, B.R.; Feely, R.A.; Williams, N.L.; Dickson, A.G.; Fong, M.B.; Takeshita, Y. Updated methods for global locally interpolated estimation of alkalinity, pH and nitrate. *Limnol. Oceanogr. Methods* **2017**. [[CrossRef](#)]

67. Perretti, A.R.; Albergaria-Barbosa, A.C.R.D.; Kerr, R.; Cunha, L.C.D. Ocean acidification studies and the uncertainties relevance on measurements of marine carbonate system properties. *Braz. J. Oceanogr.* **2018**, *66*, 234–242. [[CrossRef](#)]
68. Laxenaire, R.; Speich, S.; Blanke, B.; Chaigneau, A.; Pegliasco, C.; Stegner, A. Anticyclonic eddies connecting the western boundaries of Indian and Atlantic oceans. *J. Geophys. Res. Oceans* **2018**. [[CrossRef](#)]
69. Guerra, L.A.A.; Paiva, A.M.; Chassignet, E.P. On the translation of Agulhas rings to the western South Atlantic Ocean. *Deep-Sea Res. I* **2018**, *139*, 104–113. [[CrossRef](#)]
70. Woosley, R.J.; Millero, F.; Wanninkhof, R. Rapid Anthropogenic Changes in CO₂ and pH in the Atlantic Ocean: 2003–2014. *Glob. Biogeochem. Cycles* **2016**, *30*, 70–90. [[CrossRef](#)]
71. Lumpkin, R.; Garzoli, S.L. Interannual to Decadal Variability in the Southwestern Atlantic’s Surface Circulation. *J. Geophys. Res. Oceans* **2003**, *116*, C01014. [[CrossRef](#)]
72. Rodrigues, R.R.; Haarsma, R.J.; Campos, E.J.D.; Ambrizzi, T. The impacts of inter-El Nino variability on the Tropical Atlantic and Northeast Brazil climate. *J. Clim.* **2011**, *24*, 3402–3422. [[CrossRef](#)]
73. Rodrigues, R.R.; Campos, E.J.D.; Haarsma, R.J. The Impact of ENSO in the South Atlantic Subtropical Dipole Mode. *J. Clim.* **2015**, *28*, 2692–2705. [[CrossRef](#)]
74. Castellanos, P.; Campos, E.J.D.; Piera, J.; Sato, O.T.; Silva Dias, M.A.F. Impacts of Agulhas Leakage on the Tropical Atlantic Western Boundary Systems. *J. Clim.* **2017**. [[CrossRef](#)]
75. Pereira, J.E.; Wainer, I. A mudança do clima e seus impactos no oceano Atlântico Sul em escala regional. In *Ciência das Mudanças Climáticas e sua Interdisciplinaridade*; Ambrizzi, T., Jacobi, P.R., Dutra, L.M.M., Eds.; Annablume Editora: São Paulo, Brazil, 2015; ISBN 978-85-391-0714-8.



© 2019 by the authors. Licensee MDPI, Basel, Switzerland. This article is an open access article distributed under the terms and conditions of the Creative Commons Attribution (CC BY) license (<http://creativecommons.org/licenses/by/4.0/>).

Chapter VI. Synthesis of the discussion and conclusions

4.1 Synthesis of the discussion and conclusions

This thesis investigated the carbonate system properties on the evolution of the Agulhas eddies along the South Atlantic Ocean, emphasizing their role in the ocean CO₂ sink and C_{ant} transport through their trajectories. It was possible to evaluate that the Agulhas eddies are prone to uptake more CO₂ from the atmosphere than the surrounding waters (see [Orselli et al., 2019a](#)). The CO₂ sink was primarily driven by the ocean temperature effect, which could be counterintuitive because the CO₂ solubility is normally higher when the seawater is cold and less salty, whereas the Agulhas eddies

are anticyclonic structures (i.e., present high-pressure centres, displacing isopycnals downward), thus presenting a typical signature of sea surface warming. However, these mesoscale structures can enhance the vertical mixing and present lower C_T than surrounding waters, further intensifying the CO_2 uptake. According to our investigations, we were ledged to split the eddies into eastern and western basins: *Agulhas true* and *Agulhas evolved* eddies, respectively. Eddies are considered as *Agulhas true* structures when they are in the eastern basin of the South Atlantic Ocean and have been recently released; and are considered as *Agulhas evolved* structures when they are in the western basin of the South Atlantic Ocean and likely interacted with other mesoscales structures, suffering processes of splitting or merging. This criteria to split the eddies worked well regarding their CO_2 sink strengths. We observed that the physical-chemical effects (temperature, salinity and mixing) strengthen the drawdown of CO_2 by the ocean when considering the *Agulhas true* eddies and, as long as they are becoming older, the biological activity starts to contribute to the CO_2 uptake behaviour of the *Agulhas evolved* eddies. This was found to be associated with the nutrient transport along its advection on the South Atlantic, mainly caused by vertical mixing and resulting in a biological response like is expected for the cyclonic eddies. Considering our findings, we agree that it is ambitious to state that exist an expected CO_2 pattern of behaviour (i.e., acting as CO_2 uptake or release regions) for cyclonic and anticyclonic eddies, as it is previously defined or even intuitive. The challenges are due to the intrinsic processes that can act in each eddy-region, but also considering the time of the eddies life. Some areas presenting cyclonic structures can be related to upwelling of old-ventilated and CO_2 -rich waters, behaving as sources of CO_2 to the atmosphere, instead of sink zones. On the other hand, anticyclonic eddies (such as the Agulhas eddies) can be associated to strong vertical mixing or to lower C_T concentrations than surrounding waters, likely acting as CO_2

sinking zones. The latter situation was found in this study, which highlighted that the Agulhas eddies can be likely intensifying the CO₂ uptake in the South Atlantic Ocean (Orselli et al., 2019a).

Additionally, it was observed that the Agulhas eddies carry more C_{ant} in their interior than those concentrations observed at the same depths of their surrounding waters (see Orselli et al., 2019b). This can be due to the higher uptake of CO₂ at sea surface and further incorporation at deeper levels inside the eddies. Also, because Agulhas eddies are anticyclonic structures, they are associated with positive heat flux anomalies, which means that the ocean loses heat to the atmosphere in regions where they occur. Therefore, Agulhas eddies can strengthen the formation processes of the mode waters by increasing the heat flux (e.g., Hanawa & Talley, 2001; Talley et al., 2011; Villas Bôas et al., 2015). Thus, the mode water formation processes could be an important pathway to C_{ant} penetration into the water column. Because subtropical mode waters are main contributors to compose the SACW, which is currently acidifying faster than the surface and intermediate layers of the South Atlantic Ocean (Salt et al., 2015; Carvalho-Borges et al., 2018; Orselli et al., 2018), we concluded that the Agulhas eddies can act as a trigger for the acidification state of the central water layer of the South Atlantic Ocean. This process occurs via the increased CO₂ uptake by the Agulhas eddies (Orselli et al., 2019a) and the consequent transport of large amounts of C_{ant} inside them (Orselli et al., 2019b). Previously, some studies reported that the western basin of the South Atlantic Ocean is experiencing a greater or faster acidification than the eastern basin, which could be due to the stronger ventilation processes (e.g., Ríos et al., 2003) or cross-shelf carbon transport (Carvalho-Borges et al., 2018). With the findings presented here, we can state that the Agulhas eddies contribute to this higher acidification in the western basin of the South Atlantic, since recent studies (Guerra et al., 2018; Laxenaire et al., 2018) observed that

one third of the Agulhas eddies released in the retroflexion zone reached the western boundary of the South Atlantic Ocean and also observed a physical interaction between some Agulhas eddies and the Brazil Current. However, this east-west difference regarding C_{ant} content and acidification is an open question that should be more investigated.

Thus, the proposed hypothesis stated in this PhD thesis was confirmed. This is true because we assessed that Agulhas eddies can intensify the uptake of CO_2 and the C_{ant} transport along the Agulhas Corridor in the South Atlantic, which enhances the acidification of the SACW. Thus, if an intensification of the Agulhas leakage continuing to occur (even due to a southward displacement of the entire gyre, or only of the zero line of the wind stress curl), as it is previously reported by some researchers ([Biaostoch et al., 2009](#); [Beal et al., 2011](#); [Oliveira, 2017](#)), the acidification scenario of the SACW is become more hazardous and worrisome. Additionally, a recent study ([Gruber et al., 2019](#)) demonstrated that the South Atlantic Ocean is undergoing an anomalous increase in the C_{ant} inventory, when compared to the other ocean basins, which increase the expectations of a future scenario of changing the current state of acidification.

Since the Agulhas eddies can interact with the Brazil Current on the western side of the South Atlantic Ocean, an enhanced acidification of the central layers will likely impact the marine ecosystems of the Brazilian coastal regions. Additionally, some recent studies indicate that the ocean acidification can also impact on the micronutrient specification and availability (e.g., [Stockdale et al., 2016](#)). Thus, negatively influencing the Western South Atlantic Ocean region, which have vulnerable and sensitive marine ecosystems (e.g., coral reefs, rhodolith beds) along its coastal margins. Most of them have an ecological and economical importance and are considered non-renewable resources.

This thesis also contributed to the GOA-ON main goals and to the global carbon budget needs. These contributions are related to: i) clarify the spatial distribution of carbonate system parameters in the South Atlantic Ocean; ii) quantify the C_{ant} and how this distribution occurs along the global oceans; iii) improve our understanding of global ocean acidification conditions; iv) improve our understanding of ecosystem responses to ocean acidification; and v) acquire and exchange data and knowledge necessary to optimize modelling for ocean acidification and its impacts. Additionally, considering the models introduced here, we were able to achieve the GOA-ON ‘climate’ requirements for A_T and C_T data (**Table 6.1**), indicating that these parameters can be used to identify anthropogenically-driven changes in hydrographic conditions and carbonate chemistry over multidecadal timescales. For $p\text{CO}_2$, the ‘weather’ requirement was achieved, indicating that the parameter can be used to identify impacts/ecosystem responses on local and immediate carbonate system dynamics.

Table 6. 1. Limits of the uncertainties required for each carbonate system parameter, to achieve the climate and weather conditions (i.e., relative uncertainty of the dissolved carbonate ion calculation of 1% and 10%, respectively), defined by the GOA-ON Requirements and Governance Plan (Newton et al., 2015), including the results from the models introduced in this thesis.

Carbonate system parameter	Climate	Weather	Results of the models developed in this thesis
A_T	0.1% (2 $\mu\text{mol kg}^{-1}$)	0.5% (10 $\mu\text{mol kg}^{-1}$)	1.45 to 2.19 $\mu\text{mol kg}^{-1}$
C_T	0.1% (2 $\mu\text{mol kg}^{-1}$)	0.5% (10 $\mu\text{mol kg}^{-1}$)	1.39 to 1.66 $\mu\text{mol kg}^{-1}$
pH	~0.02% (0.003 pH scale)	~0.14% (0.02 pH scale)	Not included
$p\text{CO}_2$	0.5% (2 μatm)	2.5% (10 μatm)	1.69% (6.74 μatm)

Future works should investigate eddy-resolving models to quantify the Agulhas eddies responsibility on the anomalous increase in the C_{ant} inventory of the South Atlantic Ocean and on the higher acidification of the western margin of this basin. The results presented here are both interesting by shedding a new light on a novel research topic as well as by paving the road for expanding and progressing our understanding of this oceanographic subject. Finally, the development of this thesis contributed to the activities conducted by the following Brazilian networks: Brazilian High Latitude Oceanography Group (GOAL), Brazilian Ocean Acidification Network (BrOA), and Brazilian Research Network on Global Climate Change (Rede CLIMA).

4.2 Síntese da discussão e conclusões

Essa tese investigou as propriedades do sistema carbonato na evolução dos vórtices das Agulhas ao longo do Oceano Atlântico Sul, enfatizando seu papel na captação de CO_2 pelo oceano e no transporte de C_{ant} ao longo de suas trajetórias. Foi possível avaliar que os vórtices das Agulhas são propensos a absorver mais CO_2 da atmosfera do que as águas circundantes (ver [Orselli et al., 2019a](#)). A captação de CO_2 foi impulsionada principalmente pelo efeito da temperatura do oceano, o que pode ser contra-intuitivo, porque a solubilidade do CO_2 é normalmente mais alta quando a água do mar é mais fria e menos salgada, enquanto os vórtices das Agulhas são estruturas anticiclônicas (ou seja, apresentam centros de alta pressão, isopicnais deslocadas para baixo), apresentando assim uma assinatura típica do aquecimento da superfície do mar. No entanto, essas estruturas de mesoescala podem melhorar a mistura vertical e apresentar

menor C_T do que as águas circundantes, intensificando ainda mais a captação de CO_2 . De acordo com nossas investigações, fomos levados a dividir os vórtices em bacias leste e oeste: '*Agulhas verdadeiros*' (*Agulhas true*) e '*Agulhas evoluídos*' (*Agulhas evolved*), respectivamente. Os vórtices são considerados estruturas '*Agulhas verdadeiros*' quando estão na bacia oriental do Oceano Atlântico Sul e foram recentemente liberados; e são consideradas como estruturas '*Agulhas evoluídos*' quando estão na bacia ocidental do Oceano Atlântico Sul e provavelmente interagiram com outras estruturas da mesoescala, sofrendo processos de divisão ou fusão. Este critério para dividir os vórtices funcionou bem em relação às suas forças de captação de CO_2 . Observamos que os efeitos físico-químicos (temperatura, salinidade e mistura) fortalecem a captação de CO_2 pelo oceano ao considerar os vórtices '*Agulhas verdadeiros*' e, à medida que envelhecem, a atividade biológica passa a contribuir para o comportamento de captação de CO_2 dos vórtices '*Agulhas evoluídos*'. Verificou-se que isso está associado ao transporte de nutrientes ao longo de sua advecção no Atlântico Sul, causado principalmente pela mistura vertical e resultando em uma resposta biológica, como é esperado para os vórtices ciclônicos. Considerando nossas descobertas, concordamos que é ambicioso afirmar que existe um padrão esperado de comportamento de CO_2 (i.e., agindo como regiões de captação ou liberação de CO_2) para vórtices ciclônicos e anticiclônicos, conforme definido anteriormente ou mesmo como considerado intuitivamente. Os desafios são devidos aos processos intrínsecos que podem atuar em cada região de vórtices, mas também considerando o tempo da vida da estrutura. Algumas áreas que apresentam estruturas ciclônicas podem estar relacionadas à ressurgência de águas ventiladas e ricas em CO_2 , comportando-se como fontes de CO_2 para a atmosfera, em vez de zonas de absorção. Por outro lado, os vórtices anticiclônicos (como os vórtices das Agulhas) podem estar associados a fortes misturas verticais ou a menores concentrações de C_T do que as águas

circundantes, provavelmente atuando como zonas de captação de CO₂. A última situação foi encontrada neste estudo, que destacou que os vórtices das Agulhas podem provavelmente intensificar a captação de CO₂ no Oceano Atlântico Sul.

Além disso, observou-se que os vórtices das Agulhas carregam mais C_{ant} no interior do que as concentrações observadas nas mesmas profundidades das águas circundantes (ver [Orselli et al., 2019b](#)). Isso pode ser devido à maior captação de CO₂ na superfície do mar e maior incorporação em níveis mais profundos dentro dos vórtices. Além disso, como os vórtices das Agulhas são estruturas anticiclônicas, eles estão associados a anomalias positivas no fluxo de calor, o que significa que o oceano perde calor para a atmosfera nas regiões onde ocorre. Portanto, os vórtices das Agulhas podem fortalecer os processos de formação das águas modais, aumentando o fluxo de calor (e.g., [Hanawa & Talley, 2001](#); [Talley et al., 2011](#); [Villas Bôas et al., 2015](#)). Assim, os processos de formação de água modal poderiam ser um caminho importante para a intrusão de C_{ant} na coluna de água. Como as águas modais subtropicais são os principais contribuintes para compor a SACW, que atualmente acidifica mais rapidamente do que as camadas superficial e intermediária do Oceano Atlântico Sul ([Salt et al., 2015](#); [Carvalho-Borges et al., 2018](#); [Orselli et al., 2018](#)), concluímos que os vórtices das Agulhas podem atuar como um gatilho para o estado de acidificação da camada de água central do Oceano Atlântico Sul. Esse processo ocorre através do aumento da captação de CO₂ pelos vórtices das Agulhas e do consequente transporte de grandes quantidades de C_{ant} dentro deles. Anteriormente, alguns estudos relataram que a bacia ocidental do Oceano Atlântico Sul está experimentando uma acidificação maior ou mais rápida que a bacia oriental, o que pode ser devido a processos de ventilação mais fortes (e.g., [Ríos et al., 2003](#)) ou trocas de carbono através da plataforma continental ([Carvalho-Borges et al., 2018](#)). Com os resultados apresentados aqui, podemos afirmar que os vórtices das Agulhas contribuem

para essa maior acidificação na bacia ocidental do Atlântico Sul, pois estudos recentes (Guerra et al., 2018; Laxenaire et al., 2018) observaram que um terço dos vórtices das Agulhas liberados na zona de retroflexão atingiram a borda oeste do Oceano Atlântico Sul e também observaram uma interação entre alguns vórtices das Agulhas e a Corrente do Brasil. No entanto, essa diferença leste-oeste em relação ao teor de C_{ant} e acidificação é uma questão em aberto que deve ser mais investigada.

Assim, foi confirmada a hipótese proposta na tese de doutorado. Isso é verdade porque avaliamos que os vórtices das Agulhas podem intensificar a captação de CO_2 e o transporte de C_{ant} ao longo do corredor de Agulhas, no Atlântico Sul, o que aumenta a acidificação da SACW. Assim, se uma intensificação do vazamento das Agulhas continuar ocorrendo (tanto devido a um deslocamento para o sul de todo o giro, ou apenas da linha de rotacional nulo do vento), conforme relatado anteriormente por alguns pesquisadores (Biastrich et al., 2009; Beal et al., 2011; Oliveira, 2017), o cenário de acidificação da SACW se tornará mais perigoso e preocupante. Além disso, um estudo recente (Gruber et al., 2019) demonstrou que o Oceano Atlântico Sul está passando por um aumento anômalo no inventário de C_{ant} , quando comparado às demais bacias oceânicas, o que aumenta as expectativas de um cenário futuro de mudança do estado atual de acidificação.

Como os vórtices das Agulhas podem interagir com a Corrente do Brasil no lado oeste do Oceano Atlântico Sul, uma acidificação mais intensa das camadas centrais provavelmente afetará os ecossistemas marinhos das regiões costeiras brasileiras. Além disso, alguns estudos recentes indicam que a acidificação oceânica também pode afetar a especificação e disponibilidade de micronutrientes (e.g., Stockdale et al., 2016). Assim, influenciar negativamente a região Oeste do Oceano Atlântico Sul, que possui ecossistemas marinhos vulneráveis e sensíveis (e.g., recifes de coral, leitos de rodólitos)

ao longo de suas margens costeiras. A maioria deles tem uma importância ecológica e econômica e são considerados recursos não renováveis (Kerr et al., 2016).

Esta tese também contribuiu para os principais objetivos do GOA-ON e para as necessidades do balanço global de carbono. Essas contribuições estão relacionadas a: i) esclarecer a distribuição espacial dos parâmetros do sistema carbonato no Oceano Atlântico Sul; ii) quantificar o C_{ant} e como essa distribuição ocorre ao longo dos oceanos globais; iii) melhorar nossa compreensão das condições globais de acidificação oceânica; iv) melhorar nossa compreensão das respostas dos ecossistemas à acidificação dos oceanos; e v) adquirir e trocar dados e conhecimentos necessários para otimizar a modelagem para a acidificação dos oceanos e seus impactos. Além disso, considerando os modelos aqui apresentados, conseguimos atender aos requisitos de nível ‘clima’ (*‘climate’*) do GOA-ON para dados de A_T e C_T (**Tabela 6.1**), indicando que esses parâmetros podem ser usados para identificar alterações conduzidas por atividade antropogênica nas condições hidrográficas e na química do carbonato em escalas de tempo multidecadais. Para $p\text{CO}_2$, o requisito de ‘tempo’ (*‘weather’*) foi atingido, indicando que o parâmetro pode ser usado para identificar impactos / respostas do ecossistema na dinâmica local e imediata do sistema de carbonatos.

Tabela 6.1. Limites das incertezas exigidas para cada parâmetro do sistema de carbonato, para alcançar as condições clima e tempo (i.e., incerteza relativa do cálculo do íon carbonato dissolvido de 1% e 10%, respectivamente), definido pelo Plano de Governança do GOA-ON (Newton et al., 2015), incluindo os resultados dos modelos introduzidos nesta tese.

Parâmetro do sistema de carbonato	Clima	Tempo	Resultados dos modelos desenvolvidos nesta tese
A_T	0.1% (2 $\mu\text{mol kg}^{-1}$)	0.5% (10 $\mu\text{mol kg}^{-1}$)	1.45 a 2.19 ($\mu\text{mol kg}^{-1}$)

C_T	0.1% (2 $\mu\text{mol kg}^{-1}$)	0.5% (10 $\mu\text{mol kg}^{-1}$)	1.39 a 1.66 ($\mu\text{mol kg}^{-1}$)
pH	$\sim 0.02\%$ (0.003 pH scale)	$\sim 0.14\%$ (0.02 pH scale)	Não incluído
$p\text{CO}_2$	0.5% (2 μatm)	2.5% (10 μatm)	1.69% (6.74 μatm)

Trabalhos futuros devem investigar modelos de resolução de vórtices para quantificar a responsabilidade dos vórtices das Agulhas no aumento anômalo do inventário C_{ant} do Oceano Atlântico Sul e na maior acidificação da margem oeste desta bacia. Os resultados apresentados aqui são interessantes pois lançam uma nova luz sobre um novo tópico de pesquisa, bem como pavimentando o caminho para expandir e progredir nossa compreensão desse assunto oceanográfico. Finalmente, o desenvolvimento desta tese contribuiu para as atividades conduzidas pelas seguintes redes brasileiras: Grupo Brasileiro de Oceanografia de Alta Latitude (GOAL), Rede Brasileira de Acidificação Oceânica (BrOA) e Rede Brasileira de Pesquisa sobre Mudança Global do Clima (Rede CLIMA).

4.3 Synthèse de la discussion et conclusions

Cette thèse a étudié les propriétés du système des carbonates lors de l'évolution des tourbillons des Aiguilles le long de l'océan Atlantique Sud, en soulignant leur rôle dans l'absorption du CO₂ par l'océan et le transport de C_{ant} à travers leurs trajectoires. Il a été possible d'évaluer que les tourbillons des Aiguilles sont susceptibles d'absorber plus de CO₂ atmosphérique que les eaux environnantes (voir [Orselli et al., 2019a](#)). L'absorption du CO₂ a été principalement entraîné par l'effet de la température de l'océan, ce qui pourrait être contre-intuitif car la solubilité du CO₂ est normalement plus élevée lorsque l'eau de mer est froide et moins salée, tandis que les tourbillons des Aiguilles sont des structures anticycloniques (i.e., présentent des centres à haute pression, déplaçant des isopycnaux vers le bas), présentant ainsi une signature typique du réchauffement de la surface de la mer. Cependant, ces structures à mésoéchelle

peuvent améliorer le mélange vertical et présenter une C_T plus faible que les eaux environnantes, intensifiant davantage l'absorption de CO_2 . Selon nos recherches, nous avons été amenés à diviser les tourbillons en bassins est et ouest : '*vraies Aiguilles*' ('*Agulhas true*') et '*Aiguilles évoluées*' ('*Agulhas evolved*'), respectivement. Les tourbillons sont considérés comme des structures '*vraies Aiguilles*' lorsqu'ils se trouvent dans le bassin oriental de l'océan Atlantique Sud et ont été récemment relâchés ; et sont considérés comme des structures '*Aiguilles évoluées*' lorsqu'ils se trouvent dans le bassin ouest de l'océan Atlantique Sud et interagissent probablement avec d'autres structures à mésoéchelle, subissant des processus de division ou de fusion. Ce critère pour diviser les tourbillons a bien fonctionné en ce qui concerne la résistance de leur puits de CO_2 . Nous avons observé que les effets physico-chimiques (température, salinité et mélange) renforcent l'absorption du CO_2 par l'océan lorsque l'on considère les '*vraies Aiguilles*' et, tant qu'ils vieillissent, l'activité biologique commence à contribuer au comportement d'absorption du CO_2 des '*Aiguilles évoluées*'. Cela s'est avéré être associé au transport des nutriments le long de son advection dans l'Atlantique Sud, principalement causé par un mélange vertical et entraînant une réponse biologique comme celle attendue pour les tourbillons cycloniques. Compte tenu de nos résultats, nous convenons qu'il est ambitieux d'affirmer qu'il existe un modèle de comportement attendu du CO_2 (i.e., agissant comme des régions d'absorption ou de libération du CO_2) pour les tourbillons cycloniques et anticycloniques, tel qu'il est précédemment défini ou même intuitif. Les défis sont dus aux processus intrinsèques qui peuvent agir dans chaque région des tourbillons, mais aussi en considérant le temps de la vie des tourbillons. Certaines zones présentant des structures cycloniques peuvent être liées à la remontée des eaux ventilées et riches en CO_2 , se comportant comme des sources de CO_2 pour l'atmosphère, au lieu de zones de puits. D'un autre côté, les tourbillons anticycloniques (comme les tourbillons des

Aiguilles) peuvent être associés à un fort mélange vertical ou à des concentrations de C_T plus faibles que les eaux environnantes, agissant probablement comme des zones d'absorption du CO_2 . Cette dernière situation a été trouvée dans cette étude, qui a souligné que les tourbillons des Aiguilles peuvent probablement intensifier l'absorption du CO_2 dans l'océan Atlantique Sud.

De plus, il a été observé que les tourbillons des Aiguilles transportent plus de C_{ant} à l'intérieur que les concentrations observées aux mêmes profondeurs des eaux environnantes (voir [Orselli et al., 2019b](#)). Cela peut être dû à une absorption plus élevée de CO_2 à la surface de la mer et à une incorporation plus poussée à des niveaux plus profonds à l'intérieur des tourbillons. De plus, comme les tourbillons des Aiguilles sont des structures anticycloniques, ils sont associés à des anomalies de flux de chaleur positives, ce qui signifie que l'océan perd de la chaleur dans l'atmosphère dans les régions où il se produit. Par conséquent, les tourbillons des Aiguilles peuvent renforcer les processus de formation des eaux modale en augmentant le flux de chaleur (e.g., [Hanawa & Talley, 2001](#); [Talley et al., 2011](#); [Villas Bôas et al., 2015](#)). Ainsi, les processus de formation d'eau modale pourraient être une voie importante vers la pénétration de C_{ant} dans la colonne d'eau. Parce que les masses d'eau subtropicales sont les principaux contributeurs à la composition de la SACW, qui s'acidifie actuellement plus rapidement que la surface et les couches intermédiaires de l'océan Atlantique Sud ([Salt et al., 2015](#); [Carvalho-Borges et al., 2018](#); [Orselli et al., 2018](#)), nous avons conclu que les tourbillons des Aiguilles peuvent agir comme déclencheur de l'état d'acidification de la couche centrale de l'eau de l'océan Atlantique Sud. Ce processus se produit via l'augmentation de l'absorption du CO_2 par les tourbillons des Aiguilles et le transport conséquent de grandes quantités de C_{ant} à l'intérieur. Précédemment, certaines études ont rapporté que le bassin occidental de l'océan Atlantique Sud connaît une acidification plus grande ou plus rapide

que le bassin oriental, ce qui pourrait être dû aux processus de ventilation plus forts (e.g., [Ríos et al., 2003](#)) ou aux transports transfrontaliers du carbone ([Carvalho-Borges et al., 2018](#)). Avec les résultats présentés ici, nous pouvons affirmer que les tourbillons des Aiguilles contribuent à cette acidification plus élevée dans le bassin ouest de l'Atlantique Sud, car des études récentes ([Guerra et al., 2018](#); [Laxenaire et al., 2018](#)) ont observé qu'un tiers des tourbillons des Aiguilles libérés dans la zone de réflexion ont atteint la limite ouest de l'océan Atlantique Sud. De plus, ils ont également observé une interaction physique entre certains tourbillons des Aiguilles et le courant du Brésil. Cependant, cette différence est-ouest concernant la concentration en C_{ant} et l'acidification est une question ouverte qui devrait être étudiée plus en détail.

Ainsi, l'hypothèse proposée dans cette thèse a été confirmée. Nous avons déterminé que les tourbillons des Aiguilles peuvent intensifier l'absorption du CO_2 et le transport du C_{ant} le long du corridor des Aiguilles dans l'Atlantique Sud, ce qui intensifie l'acidification de la SACW. Ainsi, si une intensification du prolongement des tourbillons des Aiguilles continue de se produire (en raison d'un déplacement vers le sud de l'ensemble du gyre, ou uniquement de la ligne zéro de la boucle de contrainte du vent), comme cela a été précédemment rapporté par certains chercheurs ([Biaostoch et al., 2009](#); [Beal et al., 2011](#); [Oliveira, 2017](#)), le scénario d'acidification du SACW devient plus dangereux et inquiétant. De plus, une étude récente ([Gruber et al., 2019](#)) a démontré que l'océan Atlantique Sud subit une augmentation anormale de l'inventaire de C_{ant} , par rapport aux autres bassins océaniques, ce qui augmente les attentes d'un scénario futur de changement de l'état actuel d'acidification.

Étant donné que les tourbillons des Aiguilles peuvent interagir avec le courant du Brésil du côté ouest de l'océan Atlantique Sud, une acidification accrue des couches centrales aura probablement un impact sur les écosystèmes marins des régions côtières

brésiliennes. De plus, certaines études récentes indiquent que l'acidification des océans peut également avoir un impact sur la spéciation et la disponibilité des micronutriments (e.g., Stockdale et al., 2016). Ainsi, influençant négativement la région ouest de l'océan Atlantique Sud, qui a des écosystèmes marins vulnérables et sensibles (e.g., des récifs coralliens, des lits de rhodolithes) le long de ses marges côtières. La plupart d'entre elles ont une importance écologique et économique et sont considérées comme des ressources non renouvelables.

Cette thèse a également contribué aux principaux objectifs du GOA-ON et aux besoins du budget carbone mondial. Ces contributions sont liées à: i) clarifier la distribution spatiale des paramètres du système carbonaté dans l'océan Atlantique Sud; ii) quantifier le C_{ant} et comment cette distribution se produit le long des océans mondiaux; iii) améliorer notre compréhension des conditions mondiales d'acidification des océans; iv) améliorer notre compréhension des réponses des écosystèmes à l'acidification des océans; et v) acquérir et échanger les données et les connaissances nécessaires pour optimiser la modélisation de l'acidification des océans et de ses impacts. De plus, compte tenu des modèles présentés ici, nous avons été en mesure de satisfaire aux exigences GOA-ON en matière de 'climat' ('*climate*') pour les données A_T et C_T (**Tableau 6.1**), indiquant que ces paramètres peuvent être utilisés pour identifier les changements d'origine anthropique des conditions hydrographiques et de la chimie des carbonates sur des échelles de temps pluri-décennales. Pour le $p\text{CO}_2$, l'exigence 'temps' ('*weather*') a été atteinte, ce qui indique que le paramètre peut être utilisé pour identifier les impacts / réponses de l'écosystème sur la dynamique locale et immédiate du système du carbone.

Tableau 6. 1. Limites des incertitudes requises pour chaque paramètre du système carbonaté, pour atteindre les conditions ‘climat’ et ‘temps’ (i.e., incertitude relative du calcul des ions carbonates dissous de 1% et 10%, respectivement), définies par le GOA-ON Requirements and Governance Plan (Newton et al., 2015), y compris les résultats des modèles présentés dans cette thèse.

Paramètre du système de carbonate	Climat	Temps	Résultats des modèles développés dans cette thèse
A_T	0.1% (2 $\mu\text{mol kg}^{-1}$)	0.5% (10 $\mu\text{mol kg}^{-1}$)	1.45 a 2.19 ($\mu\text{mol kg}^{-1}$)
C_T	0.1% (2 $\mu\text{mol kg}^{-1}$)	0.5% (10 $\mu\text{mol kg}^{-1}$)	1.39 a 1.66 ($\mu\text{mol kg}^{-1}$)
pH	~0.02% (0.003 pH scale)	~0.14% (0.02 pH scale)	Non inclus
$p\text{CO}_2$	0.5% (2 μatm)	2.5% (10 μatm)	1.69% (6.74 μatm)

Les travaux futurs devraient étudier des modèles de résolution des tourbillons pour quantifier la responsabilité des tourbillons des Aiguilles sur l'augmentation anormale de l'inventaire C_{ant} de l'océan Atlantique Sud et sur l'acidification plus élevée de la marge ouest de ce bassin. Les résultats présentés ici sont à la fois intéressants en apportant un éclairage nouveau sur un nouveau sujet de recherche ainsi qu'en ouvrant la voie à l'expansion et à la progression de notre compréhension de ce sujet océanographique. Enfin, le développement de cette thèse a contribué aux activités menées par les réseaux brésiliens suivants : Groupe océanographique brésilien de haute latitude (GOAL), Réseau brésilien d'acidification des océans (BrOA) et Réseau brésilien de recherche sur le changement climatique mondial (Rede CLIMA).

Chapter VII. Associated/related production

Different activities were conducted during the PhD period, including the PhD program requirements such as giving and attending classes, and other that were developed independently of the program, the associated production. The last included different activities that are briefly described in this chapter.

7.1. Scientific collaborations

As a researcher of GOAL and BrOA, I could collaborate with the development of the following studies:

7.1.1. MSc. dissertation conducted by Mariah de Carvalho-Borges

Seawater acidification and anthropogenic carbon distribution in the continental shelf-break of the Western South Atlantic Ocean. Mariah de Carvalho-Borges, **Iole B. M. Orselli**, Rodrigo Kerr and Maria L. C. Ferreira (2018). Journal of Marine Systems. doi.org/10.1016/j.jmarsys.2018.06.008.

7.1.1. PhD thesis conducted by Jannine M. Lencina-Avila

Past and future evolution of the carbonate system in a coastal zone of the northern Antarctic Peninsula. Lencina-Avila, Jannine M.; Goyet, Catherine; Kerr, Rodrigo; **Orselli, Iole B. M.**; Mata, Mauricio M; Touratier, Franck. (2018). Deep Sea Research II. doi.org/10.1016/j.dsr2.2017.10.018

7.1.2. Research activity conducted by Prof. Rodrigo Kerr

Carbonate system properties in the Gerlache Strait, Northern Antarctic Peninsula (February 2015): I. Sea–Air CO₂ fluxes. Rodrigo Kerr, **Iole B.M. Orselli**, Jannine M. Lencina-Avila, Renata T. Eidt, Carlos Rafael B. Mendes, Leticia C. da Cunha, Catherine Goyet, Mauricio M. Mata, Virginia Maria Tavano. (2018). Deep Sea Research II. doi.org/10.1016/j.dsr2.2017.02.008

7.1.3. Research activity conducted by Prof. Rodrigo Kerr

Carbonate system properties in the Gerlache Strait, Northern Antarctic Peninsula (February 2015): II. Anthropogenic CO₂ and Seawater Acidification. Rodrigo Kerr, Catherine Goyet, Leticia C. da Cunha, **Iole B. M. Orselli**, Jannine M. Lencina-Avila,

Carlos Rafael B. Mendes, Mariah de C. Borges, Mauricio M. Mata, Virginia Maria Tavano. (2018). Deep Sea Research II. doi.org/10.1016/j.dsr2.2017.07.007

7.1.4. MSc. dissertation conducted by Thiago Monteiro

Towards an intensified summer CO₂ sink behaviour in the Southern Ocean coastal regions. Thiago Monteiro, Rodrigo Kerr, **Iole B.M. Orselli**, Jannine M. Lencina-Avila. (2020). Progress in Oceanography. doi.org/10.1016/j.pocean.2020.102267

7.1.5. MSc. dissertation conducted by Ciro Cataneo Liutti

Spatiotemporal variability of the seawater CO₂ fugacity on the southwestern South Atlantic Ocean. Ciro Cataneo Liutti, Rodrigo Kerr, **Iole B.M. Orselli**, Rosane Gonçalves Ito, Carlos Alberto Eiras Garcia. Under review. Continental Shelf Research.

7.1.6. MSc. dissertation conducted by Juan Camilo Torres-Lasso

Interannual variability of the ocean acidification state and anthropogenic CO₂ in the Bransfield Strait, Northern Antarctica Peninsula. Juan Camilo Torres-Lasso, Rodrigo Kerr, Jannine Marquez Lencina-Avila, **Iole Beatriz Marques Orselli**, Mariah de Carvalho-Borges, Catherine Goyet, Mauricio M. Mata. Under review. Journal of Marine Systems.

7.2. Undergraduate student co-supervision

During 2017-2018, Julia Kalid Mansur conducted her undergraduate research and developed her monography studying the Patos Lagoon Estuary. Her work was entitled Reconstruction of the carbonate system on the Patos Lagoon Estuary, Rio Grande do Sul, Brazil, and was conducted under the supervision of Rodrigo Kerr and **Iole B. M. Orselli**. Her defence was on November 23rd, 2018.

7.3. Training course on CO₂ measurements

In order to spread the knowledge of the CO₂ autonomous measuring system GO-8050, I organized a training course on the system mounting, operation, troubleshooting and data analysis. The course was conducted between July 23rd and 25th, 2019, and included theoretical and practical activities. The agenda is included below (Fig. 6.1)



The CARBON Team
Laboratório de Estudos dos Oceanos e Clima

Propósito

- Habilitar os participantes do curso a montar, operar e processar os resultados do equipamento de CO₂ (GO-8050);
- Difundir conhecimento entre os membros da equipe;

1º Treinamento GO-8050 CARBON Team

Instrutora: Iole Orselli CEOCEAN – Instituto de Oceanografia – FURG

24 de julho, quarta-feira

9h00 – Atividade 3: prática 2

- Operação do equipamento.

Health break (15 min) durante a manhã.

12h00 – Almoço (livre)

13h30 – Atividade 4: prática 3

- Dúvidas sobre o funcionamento do equipamento.
- Desmontagem e cuidados.

Health break (15 min) durante a tarde.

25 de julho, quinta-feira

9h00 – Atividade 5: processamento de dados 1

- Correção da fração molar de CO₂ pelos padrões.

Health break (15 min) durante a manhã.

12h00 – Almoço (livre)

13h30 – Atividade 6: processamento de dados 2

- Cálculos da pressão parcial de CO₂.
- Cálculos dos fluxos líquidos de CO₂ entre oceano e atmosfera.

Health break (15 min) durante a tarde.

16h00 – Síntese e encerramento

7.4. Conferences

7.4.1. 4th International Symposium on the Ocean in a High-CO₂ World

This conference was held in Hobart, Australia, between 3rd and 6th May, 2016. I presented five studies conducted by our research group, being one about my master dissertation (1st below), one about an undergrad student that I supervised (2nd below) and the others about other collaborations.

1) Anthropogenic carbon distribution and ocean acidification state in the Patagonian shelf break region; **Iole B. M. Orselli**, Rodrigo Kerr, Rosane G. Ito, Virgínia M. Tavano and Carlos A. E. Garcia.

2) CO₂ net fluxes along south and southeast Brazilian continental shelf and slope; Ana G. Correa, **Iole B. M. Orselli**, Rodrigo Kerr

3) Spatial variability of CO₂ fluxes in the Gerlache Strait, Antarctica, during austral summer 2015; Eidt, Renata T., Kerr, Rodrigo, **Orselli, Iole B. M.**

4) Spatial variation of total alkalinity and total dissolved inorganic carbon along the Brazilian continental shelf-break and slope: preliminary results; Mariah Borges, **Iole Orselli**, Rodrigo Kerr

5) Surface total alkalinity, salinity and temperature: a study case in the Southwestern Atlantic Ocean; Leticia Cotrim da Cunha, Cintia Albuquerque, Rodrigo Kerr, **Iole Orselli**.

7.4.2. 3rd GOA-ON Science Workshop

This conference was held in Hobart, Australia, between 8th and 10th May, 2016. I had the opportunity to take part in the discussions regarding the next steps on the ocean acidification studies and met some great researchers.

7.4.3. 1st LAOCA meeting

This conference was held in Buenos Aires, Argentina, in 2017. I submitted some results of my PhD to the 1st meeting of LAOCA, entitled “*The role of Agulhas eddies on air-sea CO₂ exchanges in the South Atlantic Ocean*” (Orselli, Iole B.M.; Kerr, Rodrigo; Azevedo, José L. Lima; Garcia, Carlos Alberto E.; Araujo, Moacyr), which was presented by Rodrigo Kerr.

7.4.4. 4th GOA-ON Science Workshop

This conference was held in Hangzhou, China, between 14th and 17th April, 2019. I presented part of my PhD results, in a study named “*Effect of Agulhas eddies on absorption and transport of anthropogenic carbon in the South Atlantic Ocean*” (Orselli, Iole B.M.; Goyet, Catherine; Kerr, Rodrigo; Azevedo, José L. Lima; Araujo, Moacyr; Galdino, Felipe; Touratier, Frank; Garcia, Carlos Alberto E.).

7.4.5. SOLAS Open Science Conference

This conference was held in Sapporo, Japan, between 21st and 25th April, 2019. The presented study was entitled “*Satellite-derived carbon dioxide partial pressure along Agulhas eddies trajectories*” (Orselli, Iole B.M.; Galdino, Felipe; Azevedo, José L. Lima; Kerr, Rodrigo; Goyet, Catherine).

7.4.6. Ocean Sciences Meeting

Apart from those conferences I have already participated, I am also going to attend the Ocean Sciences Meeting, that is taking place in San Diego, California, between 16th and 21st February, 2020.

7.5.Relevant courses

Along the PhD period I had the opportunity to participate in some international courses. They were the following:

7.5.1. SOLAS Sumer School

This summer school took place in the Institut d'Études Scientifiques de Cargèse, Corse, France, between July 24th and August 3rd, 2018.

7.5.2. SatCO₂

This course took place in Hangzhou, China, 13th April, 2019.

7.5.3. Instrumenting our ocean for better observation: a training course on a suite of biogeochemical sensors

This summer school took place in the Sven Lovén Centre for Marine Sciences, University of Gothenburg, Kristineberg, Sweden, between July 10th and 19th, 2019 and was promoted by IOCCP and BONUS INTEGRAL.

7.6. Received grants

To participate in those conferences and courses, I have applied to some grants and fellowships. I was contemplated with grants from: CAPES, CNPq, IOCCP, BONUS INTEGRAL, IAEA.

7.7. Ship-based fieldwork

7.7.1. NAUTILUS

With the Brazilian group (GOAL), I took part of the NAUTILUS research team in three Antarctic cruises: 2016, 2017 and 2019. The cruises were conducted in the Northern Antarctic Peninsula.

7.7.2. AtlantOs

With a German group from GEOMAR, I took part of the AtlantOs research team in the Meteor-M133 cruise “**Ocean Observation – from sensor to knowledge**”. The cruise was conducted between December 15th, 2016 and January 13th, 2017. It was a South Atlantic crossing, from Cape Town – South Africa to Port Stanley – Falklands.

7.8. Relevant laboratory activities

7.8.1. Implementation of A_T methodology

In November 2016, I was invited to go to the State University of Rio de Janeiro by Prof. Dr. Letícia Cotrim da Cunha, to help on the implementation of open cell A_T analysis in her laboratory *Laboratório de Geoquímica Orgânica Marinha (LAGOM)*. I also implemented this methodology in the LEOC laboratory, where I am based,

7.8.2. Open cell AT analysis of an inter-university collaboration

I participated with Prof. Dr. Rodrigo Kerr in the analysis of A_T samples for a collaboration with the Santa Catarina Federal University. The samples were from an experiment conducted by Prof. Dr. Paulo Horta.

7.8.3. International intercalibration of carbonate system analysis.

I was responsible to conduct the analysis of the samples acquired for the international intercalibration exercise of carbonate system analysis (2017).

Chapter VIII. References

1. Angel-Benavides, I. M., Pilo, G. S., Dias, F. B. & Garcia, C. A. E. (2016). Influência dos Vórtices de Mesoescala na Concentração de Clorofila da Confluência Brasil-Malvinas: Mecanismos Inferidos por Sensoriamento Remoto. *Brazilian Journal of Aquatic Science and Technology*, 20(1), 10-20.
2. Arrhenius, S., 1896. On the influence of carbonic acid in the air upon the temperature of the ground. *Philosophic Magazine and Journal of Science, Series 5*, Vol. 41, pp.237276
3. Azevedo, J. L. L. & Mata, M. M. (2010). O mecanismo de autopropulsão de vórtices oceânicos: uma revisão. *Revista Brasileira de Geofísica*, 28 (3), 153-172
4. Bakker, D.C.E., Pfeil, B., Landa, C.S., Metzl, N., O'Brien, K.M., Olsen, A., et al. (2016). A multi-decade record of high-quality fCO₂ data in version 3 of the Surface Ocean CO₂ Atlas (SOCAT). *Earth System Science Data*, 8, 383–413. <http://dx.doi.org/10.5194/essd-8383-2016>.

5. Balch, W.M. and P.E. Utgoff (2009), Potential interactions among ocean acidification, coccolithophores, and the optical properties of seawater. *Oceanography*, 22(4), 146–159
6. Bard, E. & Rickaby, R. E. M. Migration of the subtropical front as a modulator of glacial climate. *Nature*, 2009, 460, 380–383. <http://doi.org/10.1038/nature08189>
7. Beal, L. M. (2009). A Time Series of Agulhas Undercurrent Transport. *Journal of Physical Oceanography*, 39, 2436-2450.
8. Beal, L. M., De Ruijter, W. P. M., Biastoch, A., Zahn, R. & SCOR/WCRP/IAPSO Working Group 136. (2011). On the role of the Agulhas system in ocean circulation and climate. *Nature*, 492, 429-436. doi:10.1038/nature09983
9. Biastoch, A. & Krauss, W. (1999). The role of mesoscale eddies in the source regions of the Agulhas current. *Journal of Physical Oceanography*, 29, 2303-2317.
10. Biastoch, A., Böning, C.W. & Lutjeharms, J. R. E. (2008). Agulhas leakage dynamics affects decadal variability in Atlantic overturning circulation. *Nature*, 456, 489–492, <http://doi.org/10.1038/nature07426>.
11. Biastoch, A., Böning, C. W., Swarzkopf, F. U. & Lutjeharms, J. R. E. (2009). Increase in Agulhas leakage due to poleward shift of southern hemisphere westerlies. *Nature*, 462, 495–498. <http://doi.org/10.1038/nature08519>
12. Biastoch, A., Durgadoo, J. V., Morrison, A. K., van Sebille, E., Weijer, W. & Griffies, S. M., 2015. Atlantic multi-decadal oscillation covaries with Agulhas leakage. *Nature Communications*, 6, 10082. <http://doi.org/10.1038/ncomms10082>
13. Broecker, W.S. & Peng, T.-H. (1982). *Tracers in the Sea*. Lamont-Doherty Geological Observatory, Palisades, NY. 690p.
14. Cai, W.-J. (2003). Riverine inorganic carbon flux and rate of biological uptake in the Mississippi River plume. *Geophysical Research Letters*, 30(2), 1032. <http://doi.org/10.1029/2002GL016312>.
15. Campos, E.J.D., França, C.A.S, Rodrigues, R.R., Muelbert, J.H. Inter-relações entre o Atlântico Sul, plataforma continental e regiões costeiras do sul e do sudeste do Brasil. In: *Ciência das mudanças climáticas e sua interdisciplinaridade*;

- Ambrizzi, T., Jacobi, P.R. & Dutra, L.M.M., Eds. (2015); ISBN: 978-85-391-0714-8.
16. Carvalho-Borges, M., Orselli, I. B. M., Ferreira, M. L. de Carvalho & Kerr, R. (2018). Seawater acidification and anthropogenic carbon distribution on continental shelf and slope of the western South Atlantic Ocean. *Journal of Marine Systems*. <https://doi.org/10.1016/j.jmarsys.2018.06.008>
 17. Carvalho, A.C.O, Mendes, C.R.B, Kerr, R., Azevedo, J.L.L, Galdino, F., Tavano, V.M. The impact of mesoscale eddies on the phytoplankton community in the South Atlantic Ocean: HPLC-CHEMTAX approach. *Mar Environ Res*, v. 144, p. 154-165, 2019. <https://doi.org/10.1016/j.marenvres.2018.12.003>
 18. Carter, B.R., Feely, R.A., Williams, N.L., Dickson, A.G., Fong, M.B., & Takeshita, Y. Updated methods for global locally interpolated estimation of alkalinity, pH and nitrate. *Limnol Oceanogr Methods*, 2017, 00. <http://doi.org/10.1002/lom3.10232>
 19. Casanova-Masjoan, M., Pelegrí, J. L., Sangrà, P., Martínez, A., Grisolia-Santos, D., Pérez-Hernández, M. D. & Hernández-Guerra, A. (2017). Characteristics and evolution of an Agulhas ring. *Journal of Geophysical Research: Oceans*, 122. <http://doi.org/10.1002/2017JC012969>
 20. Castellanos, P., Campos, E.J.D., Piera, J., Sato, O.T. & Silva Dias, M.A.F. Impacts of Agulhas Leakage on the Tropical Atlantic Western Boundary Systems. *J Climate*, 2017, <http://doi.org/10.1175/JCLI-D-15-0878.s1>
 21. Chelton, D.B., Schlax, M.G. & Samelson, R.G. (2011). Global observations of nonlinear mesoscale eddies. *Progress in Oceanography*, 91 (2), 167-216. <http://doi.org/10.1016/j.pocean.2011.01.002>
 22. Chelton & Schlax, 2016. *Mesoscale Eddies in Altimeter Observations of SSH Database*. <http://wombat.coas.oregonstate.edu/eddies>
 23. Chen, C.-T. A. & Borges, A. V. (2009). Reconciling opposing views on carbon cycling in the coastal ocean: Continental shelves as sinks and near-shore ecosystems as sources of atmospheric CO₂. *Deep-Sea Research II*, 56, 578–590.
 24. Chen, F., Cai, W-J, Benitez-Nelson, C. & Wang, Y. (2007). Sea surface pCO₂-SST relationships across a cold-core cyclonic eddy: Implications for

- understanding regional variability and air-sea gas exchange. *Geophysical Research Letters*, 34, L10603. <http://doi.org/10.1029/2006GL028058>
25. Ciais, P., Sabine, C., Bala, G., Bopp, L., Brovkin, V., Canadell, J., et al. (2013). Carbon and Other Biogeochemical Cycles. In Stocker, T.F., Qin, G.-K., Plattner, M., Tignor, S.K. Allen, J. Boschung, et al. (Eds.), *Climate Change 2013: The Physical Science Basis. Contribution of Working Group I to the Fifth Assessment Report of the Intergovernmental Panel on Climate Change*. Cambridge University Press, Cambridge, United Kingdom and New York, NY, USA.
 26. Cox, P. M., Betts, R. A., Jones, C. D., Spall, S. A., Totterdell, I. J. (2000). Acceleration of global warming due to carbon-cycle feedbacks in a coupled climate model. *Nature*, 408, 184-187.
 27. Denman, K. L., Brasseur, G., Chidthaisong, A., Ciais, P., Cox, P. M., Dickinson, R. E., et al. (2007). Couplings Between Changes in the Climate System and Biogeochemistry, In Solomon, S., Qin, D., Manning, M., Chen, Z., Marquis, M., Averyt, K.B., et al. (Eds.), *Climate Change 2007: The Physical Science Basis. Contribution of Working Group I to the Fourth Assessment Report of the Intergovernmental Panel on Climate Change*. Cambridge University Press, Cambridge, United Kingdom and New York, NY, USA, 499–587.
 28. de Ruijter, W. P. M., Biastoch, A., Drijfhout, S. S., Lutjeharms, J. R. E., Matano, R. P., Pichevinet, T. al. (1999). Dynamics, estimation and impact of South Atlantic interocean exchange. *Journal of Geophysical Research*, 104, 20885–20910. <http://doi.org/10.1029/1998JC900099>
 29. DOE. Handbook of Methods for Analysis of the Various Parameters of the Carbon Dioxide System in Seawater; version 2, Dickson, A.G., & Goyet, C. Eds., ORNL/CDIAC-74, 1994
 30. Doney, S.C., Fabry, V.J., Feely, R.A., Kleypas, J.A., (2009). Ocean acidification: the other CO₂ problem. *Ann Rev Mar Sci* 1:169-1923
 31. Dickson, A. G., Afghan, J.D., Anderson, G.C., (2003). Reference materials for oceanic CO₂ analysis: a method for the certification of total alkalinity. *Marine Chemistry*, Vol. 80.
 32. Dickson A. G., Sabine C. L. & Christian J. R. (2007). Guide to best practices for ocean CO₂ measurements. PICES Special Publication 3:1-191

33. Dufois, F., Hardman-Mountford, N. J., Greenwoog, J., Richardson, A. J., Feng, M. & Matear, R. J. (2016). Anticyclonic eddies are more productive than cyclonic eddies in subtropical gyres because of winter mixing. *Science Advances*, 2(5), e1600282. <http://doi.org/10.1126/sciadv.1600282>
34. Eden, C. & Dietze, H. (2009). Effects of mesoscale eddy/ wind interactions on biological new production and eddy kinetic energy. *Journal of Geophysical Research*, 114(C5), C05023–C05023. <http://doi.org/10.1029/2008JC005129>
35. Emery, W.J. (2003). Water types and water masses. In: *Ocean Circulation*, Elsevier. 1556–1567. ISBN: 978-0-12-391851-2
36. Fay, A. R. & G. A. McKinley (2013), Global trends in surface ocean pCO₂ from in situ data. *Global Biogeochemical Cycles*, 27, 541–557. <http://doi.org/10.1002/gbc.20051>.
37. Fay, A. R. & McKinley, G. A. (2017). Correlations of surface ocean pCO₂ to satellite chlorophyll on monthly to interannual timescales. *Global Biogeochemical Cycles*, 31, 436–455. <http://doi.org/10.1002/2016GB005563>
38. Feely, R. A., Sabine, C. L., Takahashi, T. & Wanninkhof, R. (2001), Uptake and storage of carbon dioxide in the ocean: The global CO₂ survey. *Oceanography*, 14(4), 18–32.
39. Ferreira, M. L. & Kerr, R. Source water distribution and quantification of North Atlantic Deep Water and Antarctic Bottom Water in the Atlantic Ocean. *Prog Oceanogr*, 2017, Vol. 153, pp. 66-83. doi: 10.1016/j.pocean.2017.04.0037
40. Fleming, P. J. & Wallace, J. J. (1986). How not to lie with statistics: the correct way to summarize benchmark results. *Communications of the ACM*, 29 (3), 218–221. <http://doi.org/10.1145/5666.5673>
41. Flierl, G. R. (1979). A simple model for a structure of warm and cold core rings. *Journal of Geophysical Research*, 84 (C2), 781-785.
42. Frankignoulle, M. & Borges, A. V. (2001). European continental shelf as a significant sink for atmospheric carbon dioxide. *Global Biogeochemical Cycles*, 15(3), 569–576. <http://doi.org/10.1029/2000GB001307>
43. Frenger, I., Gruber, N., Knutti, R. & Münnich, M. (2013). Imprint of Southern Ocean eddies on winds, clouds and rainfall. *Nature Geoscience*, 6(8), 608–612.

44. Garcia, C. A. E., Garcia, V. M. T. & McClain, C. R. (2005). Evaluation of SeaWiFS chlorophyll algorithms in the Southwestern Atlantic and Southern Oceans. *Remote Sensing of Environment*, 95, 125 – 137.
45. Giannini, M. F. C., Garcia, C. A. E., Garcia, V. M. T. & Ciotti, A. M. (2013). Effects of low-salinity and high-turbidity waters on empirical ocean colour algorithms: An example for Southwestern Atlantic waters. *Continental Shelf Research*, 59, 84–96.
46. Gordon, A. L., Weiss, R. F., Smethie Jr., W. M. & Warner, M. J. (1992). Thermocline and intermediate water communication between the South Atlantic and Indian Oceans. *Journal of Geophysical Research*, 97, 7223-7240. <http://doi.org/10.1029/92JC00485>
47. Gordon, A. L. (2003). Oceanography: The brawniest retroflexion. *Nature*, 421, 904-805. <http://doi.org/10.1038/421904a>
48. *GO-8050 Instruction Manual, General Oceanic®. 2007. Automated Flowing pCO2 Measuring System.* General Oceanics Inc
49. Goyet, C. & Hacker, S. D. Procedure for calibration of a coulometric system used for total inorganic carbon measurements in seawater, *Mar Chem*, 1992, 38, 37-53
50. Goyet, C. & Davis, D. L. Estimation of TCO₂ concentration throughout the water column. *Deep-Sea Res I*, 1997, 44(5), 859-877
51. Goyet, C., Healy, R. J. & Ryan, J. P. Global distribution of total inorganic carbon and total alkalinity below the deepest winter mixed layer depths. ORNL/CDIAC-127, NDP-076. Carbon Dioxide Information Analysis Center, Oak Ridge National Laboratory, U.S. Department of Energy, Oak Ridge, Tennessee, 2000; 40 pp.
52. Goyet, C, Ito, R.G. & Touratier, F. Anthropogenic carbon distribution in the eastern South Pacific Ocean. *Biogeosciences*, 2009, Vol. 6, pp. 149–156. <https://doi.org/10.5194/bg-6-149-2009>
53. Goyet, C. Coatanoan, C., Eischeid, G., Amaoka, T., Okuda, K., Healy, R. & Tsunogai, S. Spatial variation of total CO₂ and total alkalinity in the northern Indian Ocean: A novel approach for the quantification of anthropogenic CO₂ in seawater, *J Mar Res*, 1999, Vol. 57, N. 1, p. 135-163. <http://doi.org/10.1357/002224099765038599>

54. Gruber, N, Sarmiento, J.L. & Stocker, T.F. An improved method for detecting anthropogenic CO₂ in the oceans. *Global Biogeochem Cy*, 1996, Vol. 10, 4, 809-837. <https://doi.org/10.1029/96GB01608>
55. Gruber, N., Clement, D., Carter, B.R., Feely, R.A., van Heuven, S., Hoppema, M., Ishii, M., Key, M.R., Kozyr, A., Lauvset, S.K., Lo Monaco, C., Mathis, J.T., Murata, A., Olsen, A., Perez, F.F., Sabine, C.L., Tanhua, T. & Wanninkhof, R. The oceanic sink for anthropogenic CO₂ from 1994 to 2007. *Science*, (2019), 363, 1193–1199.
56. Guerra, L.A.A., Paiva, A.M. & Chassignet, E.P. On the translation of Agulhas rings to the western South Atlantic Ocean. *Deep-Sea Res I*, 2018, 139, 104-113. <https://doi.org/10.1016/j.dsr.2018.08.005>
57. Hales, B., Strutton, P. G., Saraceno, M., Letelier, R., Takahashi, T., Feely, R. A., et al. (2012). Satellite-based prediction of pCO₂ in coastal waters of the eastern North Pacific. *Progress in Oceanography*, 103, 1–15. <http://doi.org/10.1016/j.pocean.2012.03.001>
58. Hanawa, K. & Talley, L.D. Mode Waters. In: *Ocean circulation and climate: observing and Modelling the Global Ocean*. Siedle, G., Church, J., Gould, J., Eds.; San Diego, Calif. London: Academic, 2001; 373-386. ISBN 0-12-641351-7
59. Howes, E. L., Joos, F., Eakin, M., Gattuso, J.-P. The Oceans 2015 Initiative, Part I: An updated synthesis of the observed and projected impacts of climate change on physical and biological processes in the oceans, Studies N°02/15, IDDRI, Paris, France, 2015; 52 pp. ISSN 2258-7535
60. Iida, Y., Kojima, A., Takatani, Y., Nakano, T., Sugimoto, H., Midorikawa, T. & Ishii, M. (2015). Trends in pCO₂ and sea–air CO₂ flux over the global open oceans for the last two decades. *Journal of Oceanography*, 71(6), 637–661. <http://doi.org/10.1007/s10872-015-0306-4>
61. Ishii, M., Kosugi, N., Sasano, D., Saito, S., Midorikawa, T. & Inoue, H. Y. (2011). Ocean acidification off the south coast of Japan: a result from time series observations of CO₂ parameters from 1994 to 2008. *Journal of Geophysical Research*, 116(C06022). <http://doi.org/10.1029/2010JC006831>
62. IPCC, 2007. Climate Change 2007: The Physical Science Basis. Cambridge University Press, Cambridge, United Kingdom and New York, NY, USA.

63. IPCC, 2013: Summary for Policymakers. In: Climate Change 2013: The Physical Science Basis. Cambridge University Press, Cambridge, United Kingdom and New York, NY, USA.
64. Ito, R. G., Schneider, B. & Thomas, H. (2005). Distribution of surface fCO₂ and air-sea fluxes in the Southwestern subtropical Atlantic and adjacent continental shelf. *Journal of Marine Systems*, 56, 227–242.
65. Ito, R. G., Garcia, C. A. E. & Tavano, V. M. (2016). Net sea-air CO₂ fluxes and modelled pCO₂ in the southwestern subtropical Atlantic continental shelf during spring 2010 and summer 2011. *Continental Shelf Research*, 119, 68-84.
66. Jahne, B. H. G. & W. Dietrich (1987). Measurement of the diffusion coefficients of sparingly soluble gases in water. *Journal of Geophysical Research*, 92, 10767–76. <http://doi.org/10.1029/JC092iC10p10767>
67. Jiang, L.-Q., Cai, W.-J., Wanninkhof, R., Wang, Y. & Lüger, H. (2008), Air-sea CO₂ fluxes on the U.S. South Atlantic Bight: Spatial and seasonal variability. *Journal of Geophysical Research*, 113(C07019). <http://doi.org/10.1029/2007JC004366>
68. Johnson, K. M., King, A. E., & Sieburth, J. McN. Coulometric TCO₂ analyses for marine studies: An introduction. *Mar Chem*, 1985, 16, pp. 61-82. [https://doi.org/10.1016/0304-4203\(85\)90028-3](https://doi.org/10.1016/0304-4203(85)90028-3)
69. Johnson, K. M., Williams, P.J., Brandstrom, L., & Sieburth, J. McN. Coulometric total carbon analysis for marine studies: Automation and calibration. *Mar Chem*, 1987, 21, pp. 117-33.
70. Johnson, K. M. Operator's Manual: Single-Operator Multiparameter Metabolic Analyzer (SOMMA) for Total Carbon Dioxide (CT) with Coulometric Detection, Brookhaven National Laboratory, Brookhaven, N.Y., 1992.
71. Johnson, K.M., Dickson, A.G., Eiseid, G., Goyet, C., Guenther, P., Key, R.M., Millero, F. J., Purkerson, D., Sabine, C.L., Schottle, R.G., Wallace, D.W.R., Wilke, R.J. & Winn, C.D. Coulometric total carbon dioxide analysis for marine studies: assessment of the quality of total inorganic carbon measurements made during the US Indian Ocean CO₂ survey 1994-1996, *Mar Chem*, 1998, 63, 21-37. [http://doi.org/10.1016/s0304-4203\(98\)00048-6](http://doi.org/10.1016/s0304-4203(98)00048-6)

72. Jones, E. M., Hoppema, M., Strass, V., Hauck, J., Salt, L., Ossebaar, S., et al. (2017). Mesoscale features create hotspots of carbon uptake in the Antarctic Circumpolar Current. *Deep-Sea Research II*, 138, 39–51. <http://doi.org/10.1016/j.dsr2.2015.10.006>
73. Kahru, M., Mitchell, B. G., Gille, S. T., Hewes, C. D. & Holm-Hansen, O. (2007). Eddies enhance biological production in the Weddell-Scotia Confluence of the Southern Ocean. *Geophysical Research Letters*, 34, L14603. <http://doi.org/10.1029/2007GL030430>
74. Kerr, R., Cunha, L. C., Kikuchi, R. K. P., Horta, P., Ito, R. G., Muller, M. N., Orselli, I. B. M., Lencina-Avila, J. M., de Orte, M. R., Sordo, L., Pinheiro, B., Bonou, F. K., Shubert, N., Bergstrom, E., Copertino, M. S. The western South Atlantic Ocean in a high-CO₂ world: current measurement capabilities and perspectives. *Environ Manage*, 2016, Vol. 57, pp. 740–752. <http://doi.org/10.1007/s00267-015-0630-x>
75. Kerr, R., Goyet, C., Cunha, L.C., Orselli, I.B.M., Lencina-Avila, J.M, Mendes, C. R. B., Carvalho-Borges, M., Mata, M. M., Tavano, V.M. Carbonate system properties in the Gerlache Strait, Northern Antarctic Peninsula (February 2015): II. Anthropogenic CO₂ and Seawater Acidification. *Deep-Sea Res II*, 2018, <http://doi.org/10.1016/j.dsr2.2017.07.007>
76. Khatiwala, S., Tanhua, T., Mikaloff Fletcher, S., et al., 2013. Global ocean storage of anthropogenic carbon. *Biogeosciences*, 10.
77. Kitidis, V., Brown, I., Hardman-Mountford, N. & Lefèvre, N. (2017). Surface ocean carbon dioxide during the Atlantic Meridional Transect (1995-2013): evidence of ocean acidification. *Progress in Oceanography*, 158, 65-75. <https://doi.org/10.1016/j.pocean.2016.08.005>
78. Landschützer, P., Gruber, N., Haumann, F.A., Rödenbeck, C., Bakker, D.C., Van Heuven, S., et al. (2015). The reinvigoration of the Southern Ocean carbon sink. *Science*, 349 (6253), 1221–1224.
79. Laruelle, G. G., Dürr, H. H., Lauerwald, R., Hartmann, J., Slomp, C. P., Goossens, N. & Regnier, P. A. G. (2013). Global multi-scale segmentation of continental and coastal waters from the watersheds to the continental margins. *Hydrology and Earth System Sciences*, 17, 2029–2051.

80. Laruelle, G. G., Lauerwald, R., Pfeil, B. & Regnier, P. (2014). Regionalized global budget of the CO₂ exchange at the air-water interface in continental shelf seas. *Global Biogeochemical Cycles*, 28 (11), 1199-1214. <http://doi.org/10.1002/2014GB004832>
81. Laruelle, G.G., Lauerwald, R., Rotschi, J., Raymond, A., Hartmann, J. & Regnier, P. (2015). Seasonal response of air–water CO₂ exchange along the land–ocean aquatic continuum of the northeast North American coast. *Biogeosciences*, 12:1447–1458. <http://doi.org/10.5194/bg12-1447-2015>.
82. Laxenaire, R., Speich, S., Blanke, B., Chaigneau, A., Pegliasco, C., Stegner, A. Anticyclonic eddies connecting the western boundaries of Indian and Atlantic oceans. *J Geophys Res Oceans*, 2018, <http://doi.org/10.1029/2018JC014270>
83. Le Quéré, C., Peters, G. P., Andres, R. J., et al., 2013. Global Carbon Budget 2013. Earth System Science Data, Vol. 6.
84. Le Quéré, C., Moriarty, R., Andrew, R. M., Peters, G. P., Ciais, P., Friedlingstein, P., et al. (2015). Global carbon budget 2014. *Earth System Science Data*, 7, 47–85.
85. Le Quéré, C., Moriarty, R., Andrew, R.M., Canadell, J.G., Sitch, S., Korsbakken, P., et al. (2016). Global Carbon Budget 2016. *Earth System Science Data*, 8, 605–649.
86. Lefèvre, N. & Moore, G. F. (2000). Distribution of the CO₂ partial pressure along an Atlantic meridional transect. *Progress in Oceanography*, 45. 401–413.
87. Lehahn, Y., d'Ovidio, F., Lévy, M., Amitai, Y. & Heifetz, E. (2011). Long range transport of a quasi isolated chlorophyll patch by an Agulhas ring. *Geophysical Research Letters*, 38, L16610, doi:10.1029/2011GL048588
88. L16610 1 o f 6
89. Lencina-Avila, J.M., Ito, R. G., Garcia, C. A. E. & Tavano, V. M. (2016). Sea-air carbon dioxide fluxes along 35°s in the Atlantic Ocean and adjacent continental shelves. *Deep-Sea Research I*, 115, 175-187. <http://dx.doi.org/10.1016/j.dsr.2016.06.004>
90. *LI-7000 CO₂/H₂O analyser Instruction Manual*. 2007, LI-COR, Inc

91. Lovenduski, N. S., Gruber, N. & Doney, S. C. (2008). Toward a mechanistic understanding of the decadal trends in the Southern Ocean carbon sink, *Global Biogeochemical Cycles*, 22(3), GB3016. <http://doi.org/10.1029/2007GB003139>
92. Lumpkin, R. & Garzoli, S. L. Interannual to Decadal Variability in the Southwestern Atlantic's Surface Circulation. *J Geophys Res Oceans*, 2003, Vol. 116, C01014, <http://doi.org/10.1029/2010JC006285>.
93. Lutjeharms, J. R. E. (2006). *The Agulhas Current*. Springer. Berlin Heidelberg. <http://doi.org/10.1007/3-540-37212-1>
94. Lutjeharms, J.R.E. & Valentine, H.R. Water types and volumetric considerations of the South-East Atlantic upwelling regime. *Afr J Mar Sci*, 1987, 5,1, 63-71, <http://doi.org/10.2989/025776187784522487>
95. Martin, A. P. & Richards, K. J. (2001). Mechanisms for vertical nutrient transport within a North Atlantic mesoscale eddy. *Deep-Sea Research II*, 48, 757-773.
96. Mata, M.M.; Tavano, V.M., Garcia, C.A.E. 15 years sailing with the Brazilian High Latitude Oceanography Group (GOAL). *Deep-Sea Res II*, 2018, v. 149, p. 1-3, 2018. <https://doi.org/10.1016/j.dsr2.2018.05.007>McGillicuddy, D. J. (2016). Mechanisms of Physical-Biological-Biogeochemical Interaction at the Oceanic Mesoscale. *Annual Review of Marine Science*, 8, 125-159. <https://doi.org/10.1146/annurev-marine-010814-015606>
97. McKinley, G. A., Fay, A. R., Takahashi, T. & N. Metzl (2011). Convergence of atmospheric and North Atlantic carbon dioxide trends on multidecadal timescales, *Nature Geosciences*, 4(9), 606–610.
98. McKinley, G. A., Fay, A. R., Lovenduski, N. & Pilcher, D. J. (2017). Natural variability and anthropogenic trends in the ocean carbon sink, *Annual Review of Marine Science*, 9, 125-150. <http://doi.org/10.1146/annurev-marine-010816-060529>
99. McKinley, G. A., Follows, M.J. & Marshall, J. (2004). Mechanisms of air-sea CO₂ flux variability in the equatorial Pacific and the North Atlantic. *Global Biogeochemical Cycles*, 18(2), GB2011. <http://doi.org/10.1029/2003GB002179>.
100. McMinn, A., Müller, M. N., Martin, A., Ryan, K. G., 2014. The Response of Antarctic Sea Ice Algae to Changes in pH and CO₂. *PLoS ONE*, Vol. 9(1).

101. Millero, F. J. The marine inorganic carbon cycle. *Chem Rev*, 2007; Vol. 107, pp. 308-341. <http://doi.org/10.1021/cr0503557>
102. Möller, O. O. Jr., Piola, A. R., Freitas, A. C. & Campos, E.J.D. (2008). The effects of river discharge and seasonal winds on the shelf off Southeastern South America. *Continental Shelf Research*, 28, 1607–1624.
103. Moreau, S., Penna, A. D., Llort, J., Patel, R., Langlais, C., Boyd, P. W., et al. (2017). Eddy-induced carbon transport across the Antarctic Circumpolar Current. *Global Biogeochemical Cycles*, 31(9), 1368-1386. <http://doi.org/10.1002/2017GB005669>
104. Newton, J. A., Feely, R. A., Jewett, E. B., Williamson, P. & Mathis, J. *Global Ocean Acidification Observing Network (GOA-ON): Requirements and Governance Plan*. 2nd. 2015; Available from: <https://www.iaea.org/ocean-acidification/page.php?page=2200>.
105. O'Brien, T. D., Lorenzoni, L., Isensee, K. & Valdés, L. (2017). *What are Marine Ecological Time Series telling us about the ocean? A status report*. Edition: IOC/2017/TS129. Publisher: IOC-UNESCO.
106. Oliveira, F. M. (2017). *Changes in the South Atlantic Subtropical Gyre circulation from the 20th into the 21st century*. 10.11606/D.21.2018.tde-09042018-125458
107. Orselli, I.B.M., Kerr, R., Ito, R.G., Tavano, V. M., Mendes, C. R. B. & Garcia, C. A. E. How fast is the Patagonian shelf-break acidifying? *J Marine Syst*, 2018, 178, 1–14. <https://doi.org/10.1016/j.jmarsys.2017.10.007>
108. Orselli, I.B.M., Kerr, R., Azevedo, J.L.L., Galdino, F, Araujo M & Garcia C.A.E. The sea-air CO₂ net fluxes in the South Atlantic Ocean and the role played by Agulhas eddies. *Prog Oceanogr*, 2019a, 170, 40–52. <https://doi.org/10.1016/j.pocean.2018.10.006>
109. Orselli, I.B.M., Goyet, C., Kerr, R., Azevedo, J.L.L., Araujo, M., Galdino, F, Touratier, F. & Garcia C.A.E., 2019b. The Effect of Agulhas Eddies on Absorption and Transport of Anthropogenic Carbon in the South Atlantic Ocean. *Climate*, 7, 84; doi:10.3390/cli7060084

110. Orsi, A. H., Johnson, G. C. & Bullister, J. L. (1999). Circulation, mixing and production of Antarctic bottom water. *Progress in Oceanography*, 43, 55–109. [http://doi.org/10.1016/S0079-6611\(99\)00004-X](http://doi.org/10.1016/S0079-6611(99)00004-X).
111. Padin, X. A., Vázquez-Rodríguez, M., Castañol, M., Velo, A., Alonso-Pérez, F., Gago, J., et al. (2010). Air-sea CO₂ fluxes in the Atlantic as measured during boreal spring and autumn. *Biogeosciences*, 7, 1587–1606.
112. Pal, S. K. (1998). *Statistics for Geoscientists: Techniques and Applications*. ISBN 81-7022-712-1. New Delhi, India.
113. Pardo, P. C., Pérez, F. F., Khatiwala, S. & Ríos, A. F. (2014). Anthropogenic CO₂ estimates in the Southern Ocean: Storage partitioning in the different water masses *Progress in Oceanography*, 120, 230–242. <http://doi.org/10.1016/j.pocean.2013.09.005>
114. Patil, G.P. & Rao, C.R. 1994. *Handbook of statistics*. v. 12: Environmental statistics. 927 p.
115. Pereira, J.E. & Wainer, I. A mudança do clima e seus impactos no oceano Atlântico Sul em escala regional. In: *Ciência das mudanças climáticas e sua interdisciplinaridade*; Ambrizzi, T., Jacobi, P.R. & Dutra, L.M.M., Eds. 2015; ISBN: 978-85-391-0714-8.
116. Perretti, A. R., Albergaria-Barbosa, A. C. R. D., Kerr, R., & Cunha, L. C. D. Ocean acidification studies and the uncertainties relevance on measurements of marine carbonate system properties. *Braz J Oceanogr*, 2018, 66(2), 234-242. <http://dx.doi.org/10.1590/s1679-87592018000706602>
117. Peterson, R. G. & Stramma, L. (1991). Upper-level circulation in the South Atlantic ocean, *Progress in Oceanography*, 2(6), 1-73.
118. Pierrot, D., Neil, C., Sullivan, K., Castle, R., Wanninkhof, R., Lüger, H., et al. (2009). Recommendations for autonomous underway pCO₂ measuring systems and data-reduction routines. *Deep-Sea Research II*, 56, 512–522.
119. Rintoul, S, 2011. *The southern ocean in the earth system*. Smithsonian Institution Scholarly Press, Washington.
120. Ríos, A. F., Álvarez-Salgado, X. A., Pérez, F. F., Bingler, L. S., Arístegui, J. & Mémery, L. (2003). Carbon dioxide along WOCE line A14: Water masses

- characterization and anthropogenic entry. *Journal of Geophysical Research*, 108(C4), 3123. <http://doi.org/10.1029/2000JC000366>.
121. Robinson, Allan R. *Eddies in Marine Science*. Springer. Verlag, 1983, 614p.
122. Rodrigues, R.R., Haarsma, R.J., Campos, E.J.D. & Ambrizzi, T. The impacts of inter-El Nino variability on the Tropical Atlantic and Northeast Brazil climate. *J Climate*, 2011, Vol. 24, pp. 3402-3422, <http://doi.org/10.1175/2011JCLI3983.1>.
123. Rodrigues, R. R., Campos, E.J.D. & Haarsma, R.J. The Impact of ENSO in the South Atlantic Subtropical Dipole Mode. *J Climate*, 2015, Vol. 28, pp. 2692-2705, <http://doi.org/10.1175/JCLI-D-14-00483.1>.
124. Rost, B. & Riebesell, U. (2004). Coccolithophores and the biological pump: responses to environmental changes. In Thierstein, H. R. & Young, J. R. (Eds) *Coccolithophores: from molecular processes to global impact*. Berlin. Springer, 99-125.
125. Sabine, C. L., Feely, R. A., Gruber, N., Key, R. M, Lee, K., Bullister, J. L. et al. (2004). The Ocean Sink for Anthropogenic CO₂. *Science*, 305 (5682), 367–371.
126. Sarmiento, J. L. & Gruber, N. (2006). *Ocean Biogeochemical Dynamics*. Princeton, Woodstock: Princeton University Press. ISBN: 9780691017075.
127. Salt, L. A., van Heuven, S. M. A. C., Claus, M. E., et al. (2015). Rapid acidification of mode and intermediate waters in the southwestern Atlantic Ocean. *Biogeosciences*, 12, 1387–1401.
128. Sato, O. T. & Polito, P. Observation of South Atlantic subtropical mode Waters with Argo profiling float data. *J Geophys Res Oceans*, 2014, 119, 2860–2881. <http://doi.org/10.1002/2013JC009438>
129. Schlitzer, R. (2016) *Ocean Data View*, <http://odv.awi.de>.
130. Schlax, M.G. & Chelton, D.B. (2016). *The “Growing Method” of Eddy Identification and Tracking in Two and Three Dimensions*. College of Earth, Ocean and Atmospheric Sciences, Oregon State University, Corvallis, Oregon, July 8, 2016
131. Schuster, U., Watson, A. J., Bates, N. R., Corbiere, A., Gonzalez-Davila, M., Metzl, N., et al. (2009), Trends in North Atlantic sea-surface fCO₂ from 1990 to

2006. *Deep-Sea Research II*, 56(8), 620–629.
<http://doi.org/10.1016/j.dsr2.2008.12.011>
132. Schuster, U., McKinley, G. A., Bates, N., Chevallier, F., Doney, S. C., Fayet, A. R., al. (2013). Na Assessment of the Atlantic and Arctic sea-air CO₂ fluxes, 1990–2009. *Biogeosciences*, 10, 607–627. <http://doi.org/10.5194/bg-10-607-2013>.
133. Signorini, S. R., Mannino, A., Najjar Jr., R. G., Friedrichs, M. A. M., Cai, W.-J., Salisbury, J., et al. (2013), Surface ocean pCO₂ seasonality and sea-air CO₂ flux estimates for the North American east coast, *Journal of Geophysical Research Oceans*, 118, 5439–5460. <http://doi.org/10.1002/jgrc.20369>
134. Song, H. J. M., Munro, D. R., Dutkiewicz, S., Sweeney, C., McGillicuddy, D. J. & Hausmann, U. (2016), Mesoscale modulation of air-sea CO₂ flux in Drake Passage, *Journal of Geophysical Research Oceans*, 121, 6635–6649. <http://doi.org/10.1002/2016JC011714>.
135. Souza, J. M. A. C., Boyer Montegut, C. de, Cabanes, C. & Klein, P. (2011). Estimation of the Agulhas ring impacts on meridional heat fluxes and transport using ARGO floats and satellite data. *Geophysical Research Letters*, 38, L21602. <http://doi.org/10.1029/2011GL049359>.
136. Souza, A. G. Q., Kerr, R. & Azevedo, J. L. L. (2018). On the influence of Subtropical Mode Water on the South Atlantic Ocean. *Journal of Marine Systems*, 185, 13-24. <https://doi.org/10.1016/j.jmarsys.2018.04.006>
137. Stockdale, A., Tipping, E., Lofts, S., Mortimer, Robert J. G. (2016). Effect of Ocean Acidification on Organic and Inorganic Speciation of Trace Metals. *Environ. Sci. Technol.*, 50, 1906–1913. DOI:10.1021/acs.est.5b05624
138. Stramma, L. & England, M. On the Water masses and mean circulation of the South Atlantic Ocean. *J Geophys Res*, 1999, 104, C9, 20863-20883. <http://doi.org/10.1029/1999JC900139>
139. Sutherland, S. C, Newberger, T., Takahashi, T. & Sweeney, C. (2015). *Report of underway pCO₂ measurements in surface waters and the atmosphere during August 2015 R/V Nathaniel B. Palmer Cruise 15/8*. Lamont-Doherty Earth Observatory of Columbia University. Palisades, NY 10964. 1 December 2015
140. Tanhua, T., Hoppema, M., Jones, E. M., Stöven, T., Hauck, J., Dávila, M. G., Santana-Casiano, M., Álvarez, M., Strass, V. H. Temporal changes in ventilation

- and the carbonate system in the Atlantic sector of the Southern Ocean. *Deep-Sea Res II*, 2016, <http://dx.doi.org/10.1016/j.dsr2.2016.10.004>.
141. Takahashi, T., Feely, R. A., Weiss, R., Wanninkhof, R. H., Chipman, D. W., Sutherland, S. C. & Takahashi, T. T. (1997). Global air-sea flux of CO₂: an estimate based on measurements of sea-air pCO₂ difference. *Proceedings of the National Academy of Sciences*, 94, 8292–8299.
 142. Takahashi, T., Sutherland, S. C., Sweeney, C., Poisson, A., Metzl, N., Tilbrook, B., et al. (2002). Global sea-air CO₂ flux based on climatological surface ocean pCO₂, and seasonal biological and temperature effects. *Deep-Sea Research II*, 49, 1601–1622. [http://dx.doi.org/10.1016/S0967-0645\(02\)00003-6](http://dx.doi.org/10.1016/S0967-0645(02)00003-6)
 143. Takahashi, T., Sutherland, S. C., Wanninkhof, R., Sweeney, C., Feely, R. A., Chipman, D. W., et al. (2009). Climatological mean and decadal change in surface ocean pCO₂, and net sea-air CO₂ flux over the global oceans. *Deep-Sea Research II*, 56, 554–557.
 144. Talley, L., Pickard, G., Emery, W. & Swift, J. (2011). *Descriptive physical oceanography: an introduction*. Elsevier, Boston.
 145. Tans, P. P., Fung, I. Y., & Takahashi, T. (1990). Observational constraints on the global atmospheric CO₂ budget. *Science*, 247, 1431–1438.
 146. Tilburg, C. E., Subrahmanyam, B. & O'Brien, J. J. (2002). Ocean color variability in the Tasman Sea. *Geophysical Research Letters*, 29(10), 1487. <http://doi.org/10.1029/2001GL014071>
 147. Touratier, F., Goyet, C. Definition, properties, and Atlantic Ocean distribution of the new tracer TrOCA. *J Marine Syst*, 2004a., Vol. 46, pp. 169–179. <https://doi.org/10.1016/j.jmarsys.2003.11.016>
 148. Touratier, F., Goyet, C. Applying the new TrOCA approach to assess the distribution of anthropogenic CO₂ in the Atlantic Ocean. *J Marine Syst*, 2004b, Vol.46, pp. 181–197. <https://doi.org/10.1016/j.jmarsys.2003.11.020>
 149. Touratier, F., Azouzi, L. & Goyet, C. CFC-11, $\Delta C^{14}C$ and 3H tracers as a means to assess anthropogenic CO₂ concentrations in the ocean. *Tellus*, 2007, 59B, pp. 318–325. <http://doi.org/10.1111/j.1600-0889.2006.00247.x>

150. Touratier, F., Goyet, C., Houpert, L., et al. Role of deep convection on anthropogenic CO₂ sequestration in the Gulf of Lions (northwestern Mediterranean Sea). *Deep-Sea Res I*, 2016, 113, 33–48. <https://doi.org/10.1016/j.dsr.2016.04.003>
151. Uchida, H., Fukasawa, M. & Murata, A. (2005). *WHP P6, A10, I3/I4 Revisit Data Book Blue Earth Global Expedition 2003 (BEAGLE2003)*, 1, 2. JAMSTEC Publication.
152. *Using CO₂ and H₂O scrubbers with LI-COR gas analyser*. LI-COR, Inc
153. van Aken, H.M., van Veldhoven, A.K., Veth, C., De Ruijter, W.P.M., van Leeuwen, P.J., Drijfhout, S.S., Whittle, C.P. & Rouault, M. Observations of a young Agulhas ring, Astrid, during MARE in March 2000. *Deep-Sea Res II*, 2003, 50(1), 167–195. [http://doi.org/10.1016/S0967-0645\(02\)00383-1](http://doi.org/10.1016/S0967-0645(02)00383-1).
154. Villas Bôas, A.B, Sato, O. T., Chaigneau, A. & Castelão, G.P. (2015). The signature of mesoscale eddies on the air-sea turbulent heat fluxes in the South Atlantic Ocean. *Geophysical Research Letters*, 42(6), 1856–1862, <http://doi.org/10.1002/2015GL063105>.
155. Zeng, J., Nojiri, Y., Landschützer, P., Telszewski, M. & Nakaoka, S. (2014) A global surface ocean fCO₂ climatology based on a feed-forward neural network. *Journal of Atmospheric and Oceanic Technology*, 31, 1838–1849.
156. Wang, Z. A., Wanninkhof, R., Cai, W-J., Byrne, R. H., Hu, X., Peng, T-H. & Huang, W-J. (2013). The marine inorganic carbon system along the Gulf of Mexico and Atlantic coasts of the United States: Insights from a transregional coastal carbon study. *Limnology and Oceanography*, 58(1), 325–342.
157. Wang, X., Murtugudde, R., Hackert, E., Wang, J. & Beauchamp, J. (2015). Seasonal to decadal variations of sea surface pCO₂ and sea-air CO₂ flux in the equatorial oceans over 1984–2013: A basin-scale comparison of the Pacific and Atlantic Oceans. *Global Biogeochemical Cycles*, 29, 597–609. <http://doi.org/10.1002/2014GB005031>.
158. Wanninkhof, R. (1992). Relationship between wind speed and gas exchange over the ocean. *Journal of Geophysical Research*, 97(C5), 7373–7382. <http://doi.org/10.1029/92JC00188>

159. Wanninkhof, R. (2014). Relationship between wind speed and gas exchange over the ocean revisited. *Limnology and Oceanography Methods*, 12 (6), 351–362. <http://doi.org/10.4319/lom.2014.12.351>
160. Wanninkhof, R. & Castle, R. (2013). *Underway measurements of surface partial pressure of CO₂ during the R/V Ronald H. Brown in the Atlantic Ocean on CLIVAR Repeat Hydrography Section A10 (September 26 - October 31, 2011)*. Carbon Dioxide Information Analysis Center, Oak Ridge National Laboratory, US Department of Energy, Oak Ridge, Tennessee. http://doi.org/10.3334/CDIAC/OTG.CLIVAR_A10_2011_UW
161. Wanninkhof, R., Feely, F., Millero, C., Carlson, M., O’Neil Baringer, A., Macdonald, G., Johnson, J.-Z., Zhang, C., Mordy, C., Langdon, J., Bullister, P., Schlosser, W., Jenkins, A., Foreman, A., Coppola, A., McNichol & R. Key. *Carbon Dioxide, Hydrographic, and Chemical Data Obtained During the R/V Ronald H. Brown in the Atlantic Ocean on CLIVAR Repeat Hydrography Section A10 (September 26 - October 31, 2011)*. http://cdiac.ornl.gov/ftp/oceans/CLIVAR/A10_2011/. Carbon Dioxide Information Analysis Center, Oak Ridge National Laboratory, US Department of Energy, Oak Ridge, Tennessee, 2013; doi: 10.3334/CDIAC/OTG.CLIVAR_A10_2011
162. Weiss, R.F. (1974). Carbon dioxide in water and seawater: the solubility of a non-ideal gas. *Marine Chemistry*, 2, 203–215.
163. Weiss, R. F. & Price, B. A. (1980). Nitrous oxide solubility in water and seawater. *Marine Chemistry*, 8, 347-359.
164. Woosley, R. J., Millero, F. & Wanninkhof, R. (2016). Rapid Anthropogenic Changes in CO₂ and pH in the Atlantic Ocean: 2003-2014. *Global Biogeochemical Cycles*, 30, 70–90. <http://doi.org/10.1002/2015GB005248>.